

Electrocatalysis at Liquid/Liquid Interfaces

THÈSE N° 4620 (2010)

PRÉSENTÉE LE 8 MARS 2010

À LA FACULTÉ SCIENCES DE BASE
LABORATOIRE D'ÉLECTROCHIMIE PHYSIQUE ET ANALYTIQUE
PROGRAMME DOCTORAL EN CHIMIE ET GÉNIE CHIMIQUE

ÉCOLE POLYTECHNIQUE FÉDÉRALE DE LAUSANNE

POUR L'OBTENTION DU GRADE DE DOCTEUR ÈS SCIENCES

PAR

Raheleh Partovi NIA

acceptée sur proposition du jury:

Prof. C. Comninellis, président du jury

Prof. H. Girault, directeur de thèse

Dr J.-M. Barbe, rapporteur

Prof. J.-E. Moser, rapporteur

Prof. Z. Samec, rapporteur



ÉCOLE POLYTECHNIQUE
FÉDÉRALE DE LAUSANNE

Suisse
2010

Dedication

This thesis is dedicated to *my husband (Reza)* and wonderful *parents (Hassan and Seddigheh)* who have raised me to be the person I am today. You have been with me every step of the way. Thank you for all the unconditional love, guidance, and support that you have always given me. Thank you for everything. I love you.

Acknowledgements

I would like to thank Professor Hubert H. Girault for the opportunity he has given to me by receiving me in his group of research, and for the interest and the benevolence that he devoted to me during all the course of this thesis work. His ideas and guidance have been invaluable and this let me discover the hazards of scientific research. I must also express my gratitude to Dr. Bin Su for his great help and advice during this project. I would like to give special thanks to Manuel Alejandro Mendez Agudelo for his help in the course of my thesis and devoting time to read my thesis.

My sincere gratitude also goes to other past and present members of analytical and physical chemistry team, Imren Hatay, Mélanie Abonnenc, Mohammad Hojeij, Fei Li, Michel Prudent, Fernando Cortes Salazar, Jean-Marc Busnel, Christophe Roussel, Nathalie Younan, Astrid Johana Olaya Avendano, Niels Lion for their help, discussions and encouragement.

I would like to thank the Dr. Claude P. Gros for synthesizing the porphyrins. I wish to thank Valérie Devaud for her support on techniques and experiments. I am also thankful to Maria Szuman, secretaries of LEPA, for her help not only on administrative affairs during my Ph.D study. All my colleagues in LEPA deserve thanks for the innumerable things I have learned from them and the kind help they provided.

Special thanks go to my PhD defence committee: Prof.C.Comninellis, Prof. Z.Samec, Prof. J-M.Barbe, Prof. J-E.Moser, for devoting time and effort to review my thesis.

I wish to express my deepest appreciation to my husband Reza Khazaei for his support, accompanying and patience and his help to pass the difficult moments. I would like to give my best thanks to my parents who have always supported and encouraged me in all the decisions.

I am greatly indebted to my brother, Vahid for his outstanding advice, both in a scientific and a non-scientific way. I would also like to thank my sister, Elaheh for her unique sense of humor. Special thanks to my parents in law for their kindness and support.

Many thanks to my brother and sister in law for their friendship and all the good times we had. I would like to thank Sierro family, in particular Jean-Michel and Elisabeth and Nicole for joyful time I spent with them and their kind in Switzerland.

I want to thank all of my friends who helped me especially; I want to thank Bibi Maryam Mousavi for sharing my sorrows and laughter together.

Résumé

Le présent travail de thèse est consacré à l'étude de la réduction de l'oxygène à l'interface entre deux solutions électrolytiques immiscibles (ITIES), et catalysée par différents types de porphyrines. Des approches à la fois électrochimiques et spectrophotométriques ont été utilisées afin de caractériser les mécanismes de transfert à ces interfaces.

La réduction de l'oxygène et l'oxydation du décaméthylferrocène (DMFc) en phase organique (1,2-DCE), ainsi que la production de peroxyde d'hydrogène (H_2O_2) en phase aqueuse, ont été étudiées et sont basées sur la réaction contrôlée par un ion commun à l'interface entre deux phases.

La stabilité du DMFc et $DMFc^+$ au cours de la réaction, à l'interface entre les deux phases, a été mise en évidence par spectrométrie de masse en mesurant la phase 1,2-DCE. Des simulations numériques basées sur la théorie de la fonctionnelle de la densité (Density function theory, DFT) ont été menées afin de définir un chemin réactionnel.

L'effet catalytique du 5,10,15,20-tetraphénylporphyrinatocobalt(II) [Co(tpp)], 2,3,7,8,12,13,17,18-Octaethyl-porphine cobalt(II) (CoOEP) ainsi que de deux porphyrines « base libre », 5,10,15,20-meso-tetraphénylporphyrin (H_2TPP) et 2,3,7,8,12,13,17,18-octaethyl-21H,23H-porphyrin (H_2OEP), a été étudié à l'interface polarisée eau|1,2-DCE afin de réduire l'oxygène en présence de donneur d'électrons (*i.e.* des dérivés du ferrocène) et à différents pH. La catalyse de la réduction d'oxygène à cette interface en fonction de la différence de potentiel appliquée est suivie par voltamétrie cyclique. En effet, les donneurs d'électrons en phase organiques se combinent aux protons en phase aqueuse pour réduire l'oxygène. Le signal observé correspond au transfert d'électrons couplé aux protons (proton-coupled electron transfer, *PCET*) qui a été confirmé par l'inhibition du courant et donc de la réaction en l'absence d'un catalyseur ou d'oxygène.

Les catalyseurs, [Co(tpp)] and CoOEP, sont similaires aux porphyrines conventionnelles le cobalt, en activant l'oxygène par coordination lors de la formation de la structure superoxide. L'avantage majeur du présent système est la capacité est de contrôler avec précision le transfert de protons de la phase aqueuse à la phase organique et donc le transfert couplé d'électrons, notamment grâce contrôle du potentiel Galvani interfacial.

Le transfert assisté de protons utilisant deux porphyrines “base libre” telles que le H₂TPP et H₂OEP a été étudié à l’interface eau|1,2-DCE. La formation de di-acid H₄TPP²⁺ et H₄OEP²⁺, liée à la double protonation de H₂TPP et H₂OEP au niveau des nitrogènes tertiaires dans le cycle, a été observée à l’interface par voltamétrie du transfert d’ions ainsi que par spectroscopie en UV visible. De plus, les dérivés neutres et ionisés de H₂TPP ont été déterminés dans le “diagramme de partition ionique” pour illustrer les diverses contributions de H₂TPP.

Mots-Clés: Réduction de l’oxygène, porphyrine cobalt, porphyrine base-libre, Ferrocène, liquide|liquide, interface.

Abstract

This thesis is devoted to the study of oxygen reduction reaction catalysed by porphyrins at the interface between two immiscible electrolyte solutions (ITIES). Electrochemical and spectrophotometric techniques are introduced to these interfaces in order to gather more information about the transfer mechanism.

Furthermore, the reduction of oxygen and the oxidation of decamethylferrocene (DMFc) in 1,2-DCE and production of hydrogen peroxide (H_2O_2) in the aqueous phase, on the basis of the two-phase reaction controlled by a common ion are investigated. Mass spectrometric measurements were carried out for the 1,2-DCE phase before and after two-phase reaction with an aqueous phase containing acid to indicate the stability of DMFc and the DMFc^+ over the course of the two-phase reaction. Density function theory (DFT) computations have been performed based on developed a reaction pathway.

Catalytic effect of 5,10,15,20-tetraphenylporphyrinatocobalt(II) [Co(tpp)], 2,3,7,8,12,13,17,18-Octaethyl-porphyrin cobalt(II) (CoOEP) and two free-base porphyrins 5,10,15,20-meso-tetraphenylporphyrin (H_2TPP) and 2,3,7,8,12,13,17,18-octaethyl-21H,23H-porphyrin (H_2OEP) have been investigated as a catalyst for a two electron reduction of O_2 in presence of an electron donor at various pH values at the polarized water|1,2-DCE interface. Using voltammetry, it is possible to drive this catalytic reduction at the interface as a function of the applied potential difference, where aqueous protons and organic electron donors combine to reduce O_2 . The signal observed corresponds to a proton-coupled electron transfer (PCET) reaction, as no current and no reaction can be observed in the absence of either catalyst, acid or O_2 . [Co(tpp)] and CoOEP catalysis work like conventional cobalt porphyrins, activating O_2 via coordination by the formation of a superoxide structure. The advantages of the present system is that, by controlling the interfacial potential difference, the proton transfer from water to 1,2-DCE can be accurately controlled. Accordingly, the driving force for proton-coupled electron transfer reactions is also effectively harnessed.

Assisted proton transfer (APT) reactions were studied across the water|1,2-DCE interface facilitated by two free-base porphyrins such as H_2TPP and H_2OEP .

At a water|1,2-DCE interface, the interfacial formation of di-acid $\text{H}_4\text{TPP}^{2+}$ and $\text{H}_4\text{OEP}^{2+}$ are observed by ion-transfer voltammetry and UV-Visible spectroscopy, due to the double protonation of H_2TPP and H_2OEP at the tertiary nitrogens in the ring. Additionally, "Ionic

Partition Diagram” of neutral and ionisable H₂TPP compounds is plotted to illustrate the various contributions of H₂TPP.

Keywords: Oxygen Reduction; Cobalt Porphyrin; Free–Base; Ferrocene; Liquid|Liquid Interface

Abbreviations

Abbreviation	Description
1,2-DCE	1,2-dichloroethane
TPAs ⁺	Tetraphenylarsonium cation
TPB ⁻	Tetraphenylborate anion
TBA ⁺	Tetrabutylammonium cation
NB	Nitrobenzene
TAA ⁺	Tetraalkylammonium cation
Ach ⁺	Acetylcholine cation
TCNQ	7,7,8,8-tetracyanoquinodimethane
DPPE	Dipalmitoyl phosphatidyl choline
OEP	Octaethylporphyrin
TPP	Tetraphenylporphyrin
MPc	Metal phthalocyanines
CoP	Cobalt porphyrin
Py	Pyridyl
MT(PCP)P	Meso tetrakis [2,2]paracyclophanyl metalloporphyrin
DMFc	Decamethylferrocene
FMN	Flavin mononucleotid
CQH ₂	Tetrachlorohydroquinone
C ₆₀ ⁻	Fullerene monoanion
H ₂ TPP	5,10,15,20-tetraphenyl-21H,23H-porphyrin
H ₂ OEP	2,3,7,8,12,13,17,18-octaethyl-21H,23H-porphyrin

Abbreviations

[Co(tpp)]	5,10,15,20 meso-tetraphenyl porphyrin cobalt(II)
CoOEP	2,3,7,8,12,13,17,18-Octaethyl-21H,23H-porphyrin cobalt(II)
TMA	Tetramethylammonium
TEA	Tetraethylammonium
TBA	Tetrabutylammonium
BA	Bis(triphenylphosphoranylidene)ammonium
TPBCl	Tetrakis(4-chlorophenyl) borate
TB	Tetrakis(pentafluorophenyl)- borate
DFc	1,1'-dimethylferrocene
Fc	Ferrocene
ZnTPP	5,10,15,20 meso-tetraphenyl porphyrin zinc
NHE	Normal hydrogen electrode
Cp	Cyclopentadienyl ring
H ₂ OETPP	Octaethyltetraphenylporphyrin
H ₂ DPP	Dodecaphenylporphyrin
TFA	Trifluoroacetic acid
B	Mono-base
TATB	Tetraphenylarsenium tetraphenylborate
Ox or O	Oxidized form of redox couple
Red or R	Reduced form of redox couple
CT	Charge transfer
ET	Electron transfer
IT	Ion transfer
EC	Electrochemical reaction

Abbreviations

C	Chemical reaction
CV	Cyclic voltammetry
ACT	Aqueous Complexation followed by Transfer
TIC	Transfer by Interfacial Complexation
TOC	Transfer followed by Organic Complexation
TID	Transfer by Interfacial Decomplexation
pzc	potential of zero charge
SHE	Standard hydrogen electrode
UV-Visible	Ultra Violet-Visible
SECM	Scanning Electrochemical Microscopy
MEMED	Microelectrochemical measurements at expanding droplet
NMR	Nuclear Magnetic Resonance
MCD	Magnetic circular dichroism
ESR	Electron spin resonance
PDT	Photodynamic therapy
BNCT	Boron neutron capture therapy
FC	Fuel cell
ORR	Oxygen reduction reaction
PEMFC	Polymer electrolyte membrane fuel cell
Nafion	Nf
SCE	Standard calomel electrode
CE	Counter electrode
RE	Reference electrode
GC	Glassy carbon electrode
RDE	Rotating disk electrode

Abbreviations

RRDE	Rotating ring-disk electrode
APT	Assisted proton transfer
PCET	Proton-coupled electron transfer
MS	Mass spectrometer
ATP	Adenosine triphosphate
ITIES	Interface between two immiscible electrolyte solution
UME	Ultra microelectrode
A	Acceptor
D	Donor
M	Metal

Glossary of symbols

Symbol Description

ϕ	Galvani potential	[V]
a_i	Activity of i	[-]
ϕ_i	Potential drop across the inner layer	[V]
$\Delta_o^w \phi$	Interfacial (Galvani) potential difference	[V]
$\Delta_o^w \phi_{et}^0$	Standard electron transfer potential	[V]
$\Delta_o^w \phi_{et}^{0'}$	Formal electron transfer potential	[V]
ΔG_{tr}^0	Standard Gibbs transfer energy	[J mol ⁻¹]
$\Delta G_{tr,i}$	Gibbs energy of ion transfer	[J mol ⁻¹]
ΔG_{IS}	Gibbs energy for ion-solvent interaction	[J mol ⁻¹]
C_{diff}	Differential capacitance	[F]
C	Interfacial capacitance	[F]
C_{dl}	Double-layer capacitance	[F]
c	Concentration	[M]
μ_i^α	Chemical potential of i in phase α	[J mol ⁻¹]
μ^0	Standard chemical potential	[J mol ⁻¹]
$\tilde{\mu}$	Electrochemical potential	[J mol ⁻¹]
Z_f	Faradaic impedance	[Ω]
z	Charge number	[-]
E^0	Standard electrode potential	[V]
E	Amplitude of the potential modulation	[V]
e	Elementary charge	[C]
I_{re}	Real part of current magnitude	[A]
I_{im}	Imaginary part of current magnitude	[A]
I_{SC}	Cathodic steady-state current	[A]
I_{SA}	Anodic steady-state current	[A]
j	Current density	[A cm ⁻²]
I_{SS}	Steady-state current	[A]
R	Resistance	[Ω]
R_s	Solution resistance	[Ω]

Glossary of symbols

R	Universal gas constant	[J K ⁻¹ mol ⁻¹]
r	Molecular radius	[m]
ϵ_0	Vacuum permittivity	[C ² J ⁻¹ M ⁻¹]
ϵ_r	Relative permittivity	[-]
n	Number of electrons transferred	[-]
N_A	Avogadro constant	[mol ⁻¹]
F	Faraday constant	[C mol ⁻¹]
K_a	Acid dissociation constant	[M]
γ	Activity coefficient	[-]
T	Temperature	[K]
t	Time	[s]
D	Diffusion coefficient	[cm ² s ⁻¹]
ω	Frequency	[s ⁻¹]
λ_{\max}	Maximum wavelength	[nm]
λ	Wavelength	[nm]
ν	Scan rate	[V s ⁻¹]
w	Water	[-]
o	Organic	[-]
A	Absorbance	[-]
δ	Diffusion layer thickness	[m]
P^0	Standard partition coefficient	[-]
a	Radius of the tip	[m]
V	Volume	[L or dm ³]

Table of Contents

	Page
Dedications	
Acknowledgements.....	i
Résumé	ii
Abstract	iv
Abbreviations.....	vi
Glossary of Symbols.....	x

Chapter 1- Introduction

1.1 Electrochemistry at liquid liquid interfaces.....	1
1.2 Review of electrochemical studies at liquid liquid interfaces.....	1
1.3 Interfacial structure and electrical double layers.....	3
1.4 Thermodynamics of the liquid liquid interface.....	7
1.4.1 Physical meaning of the interfacial potential difference.....	7
1.4.2 Nernst equation at ITIES.....	7
1.5 Polarisation of liquid interfaces.....	11
1.5.1 Ideally non-polarisable ITIES.....	11
1.5.2 Ideally polarisable ITIES.....	12
1.5.3 Potential window.....	13
1.6 Charge transfer process at ITIES.....	14
1.6.1 Simple ion transfer at ITIES.....	14
1.6.2 Facilitated ion transfer at ITIES.....	17
1.6.3 Electron transfer.....	19
1.7 Applications of liquid liquid interface.....	21
1.7.1 Analytical applications.....	21
1.7.2 Biological, physiological and pharmaceutical applications.....	22
1.8 General review on porphyrins.....	25
1.8.1 Introduction to porphyrins.....	25
1.8.2 Fundamental properties of porphyrins.....	27
1.8.3 Electrochemistry of porphyrins.....	31
1.8.4 Applications of porphyrins.....	33
1.9 References.....	35

Chapter 2- Introduction to electrocatalysis of oxygen reduction

2.1 Oxygen reduction catalysis for future energy resource.....	45
2.2 Oxygen reduction.....	45
2.2.1 Reaction pathway.....	45
2.2.2 The Redox mechanism.....	48
2.2.3 Molecular oxygen interaction with metal sites.....	49
2.3 Fuel cell: reduction of O ₂	50

2.4 Metal catalysts.....	51
2.4.1 Pt catalyst.....	51
2.4.2 Macrocyclic metal complexes (phthalocyanines and porphyrins).....	54
2.4.2.1 Metallo-phthalocyanines.....	54
2.4.2.2 Metallo-porphyrins.....	55
2.4.2.3 Cofacial metallocomplexes.....	57
2.5 Oxygen reduction at liquid liquid interfaces.....	59
2.6 References.....	61

Chapter 3-Experimental and Instrumentation

3.1 Chemicals.....	64
3.1.1 Salts.....	65
3.1.2 Solvents.....	65
3.1.3 Porphyrin products.....	65
3.1.4 Others.....	65
3.1.5 Synthesis of organic supporting electrolytes.....	65
3.2 Methodology for determination of bulk redox potentials.....	66
3.3 Referenc electrodes.....	67
3.4 The four electrode potentiostate.....	67
3.5 The electrochemical cell.....	67
3.6 Cyclic voltammetry and potential window at liquid liquid interfaces.....	68
3.7 Differential capacitance measurements.....	70
3.8 Two-phase reaction controlled by a common ion	72
3.9 Mass spectrometric measurements.....	73
3.10 References.....	74

Chapter 4-Hydrogen peroxide generation by decamethylferrocene in biphasic system

4.1 Introduction.....	76
4.2 UV-Visible spectroscopic measurements.....	78
4.3 Calculation of the Galvani potential difference across the liquid liquid interface.....	82
4.4 Standard redox potentials of O ₂ /H ⁺ reduction reactions in 1,2-DCE.....	84
4.4.1 General case.....	84
4.4.2 $\left[E_{\text{O}_2/\text{O}_2^{\bullet-}}^0 \right]_{\text{SHE}}^{\text{w}}$	85
4.4.4 $\left[E_{\text{O}_2/\text{H}_2\text{O}_2}^0 \right]_{\text{SHE}}^{\text{DCE}}$, $\left[E_{\text{O}_2/\text{H}_2\text{O}}^0 \right]_{\text{SHE}}^{\text{DCE}}$ and $\left[E_{\text{H}_2\text{O}_2/\text{H}_2\text{O}}^0 \right]_{\text{SHE}}^{\text{DCE}}$	87
4.5 Cyclic voltammetric measurements at a platinum microdisc electrode.....	88
4.6 Titrating the aqueous phases with sodium iodide (NaI).....	90
4.7 Proton transfer by DMFc.....	92
4.8 Oxygen reduction in aerobic conditions.....	95
4.9 DMFc partition and Signal II.....	96
4.10 Mechanisms.....	99
4.1 Conclusions.....	101
4.11 References.....	102

Chapter 5-Proton Pump for oxygen reduction catalyzed by 5,10,15,20-tetraphenylporphyrinatocobalt(II)

5.1 Introduction.....	104
5.2 Electrochemical measurements.....	106
5.3 Shake flask experiments with Fc, DFc and DMFc.....	110
5.4 Mechanisms.....	114
5.5 Conclusions.....	116
5.6 References.....	117

Chapter 6- Cobalt(II) Octaethylporphyrin catalysis for dioxygen reduction at liquid | liquid interfaces

6.1 Introduction.....	119
6.2 Interfacial electron transfer.....	120
6.3 Two-phase reactions controlled by common ion.....	124
6.4 CoOEP catalyzed oxygen reduction by Fc.....	127
6.5 CoOEP catalyzed oxygen reduction by DMFc.....	131
6.6 Mechanism.....	133
6.7 Conclusions.....	134
6.8 References.....	136

Chapter 7-Assisted proton transfer by free-base porphyrin at polarized interface

7.1 Introduction.....	138
7.2 Visible absorption spectroscopic titration of H ₂ TPP with trifluoroacetic acid	139
7.3 Proton transfer across the water 1,2-DCE interface.....	141
7.3.1 Shake flask experiment.....	141
7.3.2 Voltammetric behaviour.....	142
7.4 Mechanism of H ⁺ ion transfer facilitated by H ₂ TPP.....	145
7.5 Ionic partition diagram.....	146
7.5.1 The case of a lipophilic monobasic compound.....	147
7.5.2 Calculation of the boundary lines.....	149
7.5.2.1 Partition equilibria between the two phases.....	149
7.5.2.2 Equilibria in the aqueous phase.....	152
7.5.2.3 Equilibria in the organic phase.....	153
7.5.3 Born solvation model.....	155
7.6 H ₂ TPP catalyzed oxygen reduction by DMFc.....	159
7.7 Conclusions.....	164
7.8 References.....	166

Chapter 8-Protonation and catalytic role of free-base octaethyl porphyrin for oxygen reduction across the water|1,2-DCE interface

8.1 Introduction.....	169
8.2 Ion-transfer voltammetry.....	170
8.3 Spectrophotometric titration.....	175
8.4 H ₄ OEP ²⁺ catalyzed oxygen reduction by DMFc	177
8.5 Shake flask experiments.....	178

8.6 Mechanisms.....	180
8.7 Conclusions.....	181
8.8 References	182
Chapter 9-Summary.....	183

Curriculum Vitae

Chapter 1

Introduction

This chapter presents an introduction to electrochemistry at liquid|liquid interfaces, which is an important aspect of this thesis. The structure, types and the various charge transfer reactions at the interface are detailed.

1.1 Electrochemistry at liquid | liquid interfaces

Liquid|liquid interfaces, also named the Interface between Two Immiscible Electrolyte Solutions (ITIES) in the electrochemical literature^[1, 2] are formed between two liquid solvents of low (ideally zero) mutual miscibility, each an electrolyte for electrochemical applications. One of these solvents is usually water, and the other is a polar organic solvent with moderate or high dielectric permittivity, such as nitrobenzene (NB) or 1,2-dichloroethane (1,2-DCE). The ITIES is, by nature, a molecular interface characterized by unique electrical, structural and dynamical properties.

Charge transfer processes across the ITIES, including electron and ion transfer, have attracted a great deal of interest for two reasons. First, the biomimetic features of these processes have been a concern for over one century and they are regarded as fundamental steps in vital processes, such as photosynthesis and mitochondrial respiration.^[2] There is a wide range of practical applications of liquid|liquid interfaces in chemistry and industry, including solvent extraction,^[3, 4] phase-transfer catalysis, drug delivery systems,^[5-10] electroanalysis with ion selective electrodes,^[11] artificial photosynthesis and pollutant destruction.^[12, 13]

1.2 Review of electrochemical studies at liquid | liquid interfaces

Studies at liquid|liquid interfaces using electrochemical methods started in 1902, when Nernst and Riesenfeld observed the transfer of ions during the passage of current through water|phenol|water interfaces.^[14] In 1906, Cremer pointed out the analogy between the

water|oil|water system and biological membranes and their surrounding electrolytes.^[15] The interest in ITIES spread to physiologists using ITIES as a model for the investigation of the potential differences and currents observed in biological cells. In 1939, the first theoretical study on ITIES was introduced by Verwey and Niessen,^[16] who presented a physical model of the ITIES as two back-to-back Gouy-Chapman diffuse layers.

The 1970s, this field witnessed renewed interest for two reasons. A first breakthrough came in the late 1960s when Gavach *et al.* demonstrated that ITIES could be polarized and the Galvani potential difference between the two phases could be used as a driving force for charge transfer reactions.^[17] The concept of polarisability of ITIES, based on the standard Gibbs energy of ion transfer, was later developed by Koryta *et al.*^[18] During the period that followed these pioneering contributions, most of the experimental work was based on controlled current techniques, such as chronopotentiometry. But due to a lack of knowledge of the interfacial structure and associated potential drop across interfaces, progress in electrochemistry at liquid|liquid interfaces was rather slow. The second breakthrough came in 1977 when Samec *et al.* introduced the four-electrode potentiostat with iR drop compensation by means of a positive feedback loop.^[19-21] This experimental approach opened a new route to use controlled potential techniques including cyclic voltammetry,^[20, 21] chronoamperometry,^[22] current scan polarography,^[23] differential pulse stripping voltammetry,^[24] *ac* voltammetry^[25] and *ac* impedance^[26] to study interfacial charge transfer reactions. In 1986, micrometer-sized ITIES was introduced by Taylor and Girault, by means of supporting the interface at the tip of a pulled glass micropipette.^[27] Later, they developed another method to fabricate micro-ITIES by making a microhole in a thin inert membrane using an UV laser photoablation technique to support the interface.^[28] Compared with the traditional macroscopic ITIES, micro-ITIES minimize problems caused by charging currents and ohmic potential drop, and significantly increase the mass-transfer rate in kinetic measurements. This format has been widely employed in amperometric and potentiometric sensors.^[29-31] In the 1990s, membrane stabilized ITIES^[32-34] and organic polymer membranes incorporating selective ionophores^[35] were also used in the analytical fields as the electrochemical ion sensors. Many new approaches, both computational and experimental,

have been employed to study liquid|liquid interfaces in recent years. Computer calculations using molecular dynamics simulations were introduced by Benjamin to provide information on the structure and dynamics of neat liquid|liquid interfaces.^[36, 37] Studies of interfacial molecular orientation using the technique of surface second harmonic generation,^[38, 39] kinetic studies of interfacial charge transfer processes using both spectro-electrochemical approaches^[40] and scanning electrochemical microscopy,^[41-45] as well as dynamic studies of photo-induced electron transfer,^[46, 47] have also been well developed. Very recently, promising new applications of liquid|liquid interfaces have considered functionalized ITIES with deposited nanoparticles^[48-50] and adsorbed photosensitive reactants,^[51-55] which can be alternative approaches to two-phase electrocatalysis and solar energy conversion, based on the photo-induced electron transfer at liquid|liquid interfaces.

Finally, the level of interest in the ITIES system currently remains high with many more aspects of fields yet to be discovered and with the possible developments of further applications.

1.3 Interfacial structure and electrical double layers

The structure of the liquid|liquid interface becomes more difficult to picture in the presence of electrolytes in the adjacent phases. The first description of the ITIES used a direct transposition of the existing models for solid|liquid systems. Electrical double layers exist at all boundaries between two ionic or electrically conducting liquid phases. In the case of liquid|liquid interfaces, the electrical double layer is an interacting electrical (ionic and dipolar) region involving two extended regions where ionic species are distributed. Traditional electrochemical experiments at liquid|liquid interfaces have contributed much to the understanding of the electrical double layers and interfacial structure. The liquid|liquid interface is an inhomogeneous environment and, consequently, a molecular interface with its own dynamical properties. It is difficult to define an interfacial structure as the time scale becomes a parameter in the definition. Thus, whether the interface is sharp or diffuse is dependent considerably on the timescale. Early work on the structure of liquid|liquid interfaces was limited to the macroscopic level and the liquid|liquid interface was characterized by a modified Verwey-Niessen model,^[16] comprising an ion-free layer of

oriented solvent molecules (inner layer) separating two back-to-back diffuse double layer region, as shown in Figure 1.1.

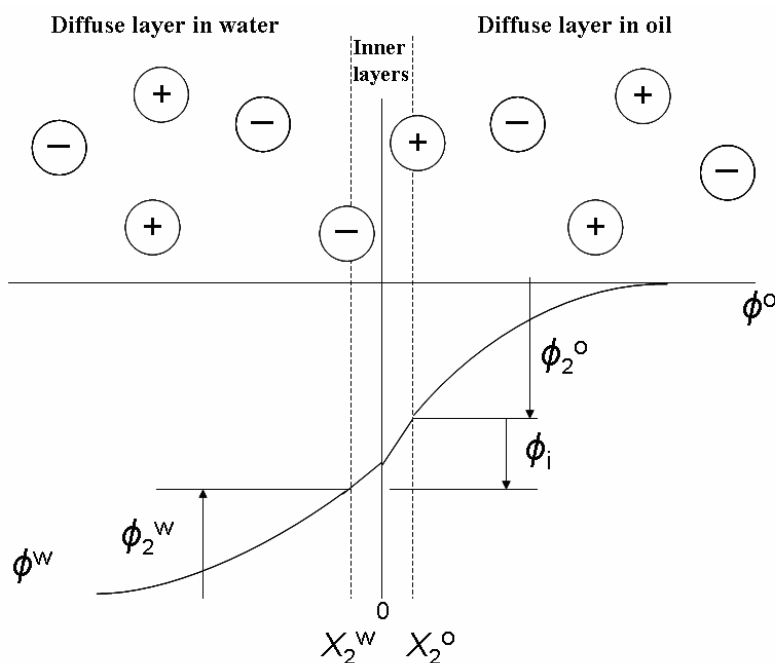


Figure 1.1: Modified Verwey-Niessen model of an ITIES and definition of potential differences involved. Full circles represent point-charge ions X_2^w and X_2^o are the positions of the ions at the planes of closest approach (outer Helmholtz planes) to the hypothetical plane of contact in the water (w) or oil (o) phase, respectively.

Verwey and Niessen represented the interface as two back-to-back diffuse layers, with one phase containing an excess of the positive space charge and the other phase an equal excess of the negative space charge.^[16] The diffuse layers were described in terms of the Gouy-Chapman theory, and the boundary between the two liquids was visualised as a dimensionless geometrical surface separating the two space charge regions. Early surface tension^[56] and capacitance^[26] measurements were found compatible with the Verwey-Niessen model at potentials close to the point of zero charge.

Analysis of the potential dependence of ion transfer kinetics led to formalism similar to the Butler-Volmer equation familiar to electron transfer dynamics on metal electrodes.^[1, 57] Based on these results, Gavach *et al.* proposed a revised model based on the Stern modification of

the Gouy-Chapman theory.^[58] The so-called modified Verwey-Niessen model introduces the concept of an ion-free layer of oriented solvent molecules separating the space charge region. The Galvani potential difference $\Delta_o^w \phi$ between the two phases is split into three contributions. The result of the model is that the interfacial (Galvani) potential difference can be expressed by three contributions:^[59]

$$\Delta_o^w \phi = \phi_2^w - \phi_2^o + \phi_i \quad (1.1)$$

Where ϕ represents the Galvani (or inner) potential of the respective phases, ϕ_2^w and ϕ_2^o are the potential drops across the diffuse layer in the aqueous and organic phases, respectively, and ϕ_i is the potential drop across the inner layer composed of solvent molecules, such as water, with ordered dipoles generating a dipolar contribution, as depicted in Figure 1.1.

Samec *et al.* further proposed that ions could penetrate into the inner layer over some distance.^[60] While, Girault and Schiffrin suggested that the interfacial region was not molecularly sharp,^[61] but consisted of a mixed solvent layer with a continuous variation in the solvent composition. Ions could penetrate the mixed solvent layer owing to interfacial ion pairing with ions of the other phase (see Figure 1.2). The mixed solvent layer model was supported by theoretical calculations for a lattice-gas model of the liquid|liquid interface by Schmickler,^[62] which suggested that the thickness of the inner layer depended on the miscibility of the two solvents. In recent years, it has been possible to study the structure of the liquid|liquid interface in some detail.^[36, 63]

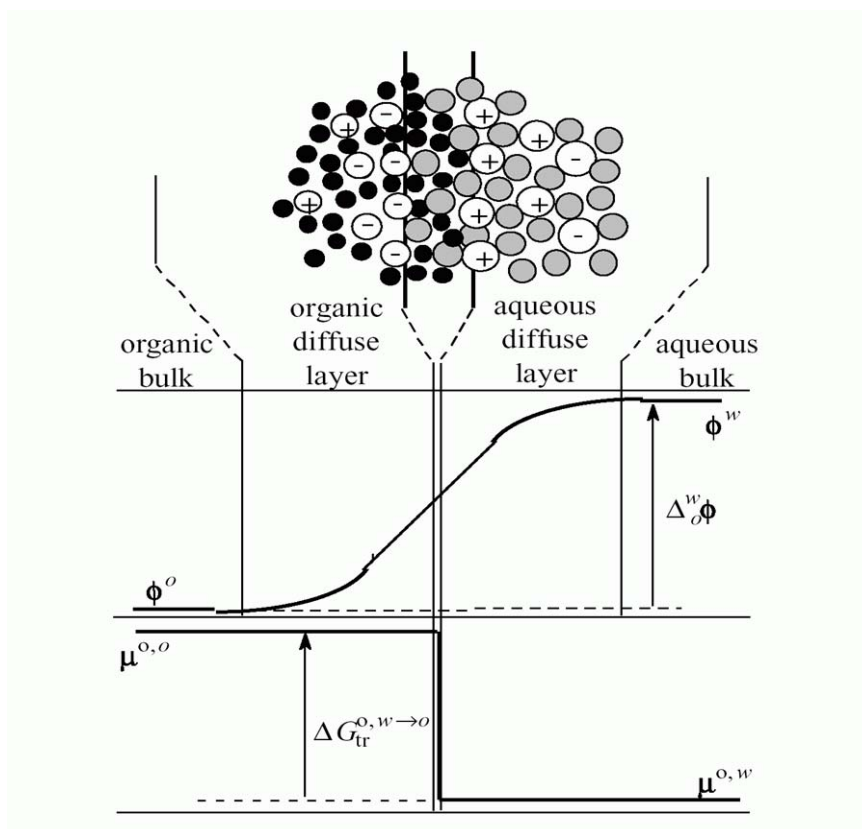


Figure 1.2: Schematic representation of the mixed solvent layer model, the potential distribution across the interfacial region and the evolution of the chemical potential in term of Gibbs energy.

Molecular dynamics computer simulations performed by Benjamin *et al.* have supported the idea that the interface is molecularly sharp but very rough with finger-like distortions due to one solvent penetrating the other on the pico-second time scale.^[64-70] This roughness is dynamic and driven by thermal fluctuations that produce an apparent finite width defining the interfacial region. The transition from one solvent to the other occurs within about 1 nm, *i.e.* a few layers of solvent molecules. On the other hand, the existence of an inner layer of thickness about 1 nm has been verified by neutron reflectivity^[68] and ellipsometry experiments.^[69] Schlossman *et al.* determined the ionic distribution profile at the ITIES using X ray reflectivity.^[71]

1.4 Thermodynamics of the liquid | liquid interface

1.4.1 Physical meaning of the interfacial potential difference

Considering that the interfacial (Galvani) potential difference is a very important parameter for the thermodynamics of liquid|liquid interfaces, the physical meaning of $\Delta_o^w\phi$ is stated briefly in this section. The potential difference at an ITIES is usually assumed to comprise two contributions, from the inner layer and from the diffuse layers. The former arises from the presence of a layer of oriented molecular dipoles, from the ionization of surfactant head groups and from the adsorption of ions present in the environment.^[72] The diffuse layer is formed by dissolved ions from the ambient solution which are attracted to the intrinsically charged interface and the potential difference across it can be as high as 500 mV.^[73, 74] At the potential of zero charge, the potential drop in the compact inner layer has been calculated to be about 5-50 mV.^[64-66, 75, 76] Specific adsorption can substantially elevate the potential difference in the compact layer.^[77] The potential difference across the compact layer of oriented molecular dipoles is almost independent of electrolyte composition, while the potential in the diffuse Gouy-Chapman layer is strongly affected by the ionic strength of the medium.^[77] The sum of the potential drops in both dipole and diffuse layers is referred to as the interfacial potential $\Delta_o^w\phi$.

1.4.2 Nernst equation at ITIES

In the following we will consider two immiscible solvents denoted by the indices "o" and "w", both containing the ionic species "i". The energy required at equilibrium to transfer i from the bulk of solvent w to the bulk of solvent o can be expressed as

$$\Delta G_{tr,i}^{w \rightarrow o} = \tilde{\mu}_i^o - \tilde{\mu}_i^w = 0 \quad (1.2)$$

Where $\tilde{\mu}_i^w$ and $\tilde{\mu}_i^o$ represent the electrochemical potentials, *i.e.* the work required to transfer the ion i from the vacuum into the corresponding phase. The electrochemical potential can be separated into chemical and electrical contributions:

$$\tilde{\mu}_i^\alpha = \mu_i^\alpha + z_i F \phi^\alpha \quad (1.3)$$

$$\mu_i^\alpha = \mu_i^{0,\alpha} + RT \ln a_i^\alpha \quad (1.4)$$

Where z_i is the charge of the ion i , μ_i^α is the chemical potential of i in phase α and ϕ^α is the Galvani potential of the phase α . Combining Equations (1.3) and (1.4), can be written as

$$\tilde{\mu}_i^\alpha = \mu_i^{0,\alpha} + RT \ln a_i^\alpha + z_i F \phi^\alpha \quad (1.5)$$

Thus, with the use of Equations. (1.2) and (1.5), the equilibrium condition of liquid|liquid interfaces results into the following relationship:

$$\mu_i^{0,w} + RT \ln a_i^w + z_i F \phi^w = \mu_i^{0,o} + RT \ln a_i^o + z_i F \phi^o \quad (1.6)$$

From this expression, the standard Gibbs energy of transfer from w to o can be expressed as:

$$\Delta G_{tr,i}^{w \rightarrow o} = \tilde{\mu}_i^o - \tilde{\mu}_i^w = (\mu_i^{0,o} - \mu_i^{0,w}) + RT \ln \left(\frac{a_i^o}{a_i^w} \right) - z_i F \Delta_o^w \phi \quad (1.7)$$

Where $\Delta G_{tr,i}^{w \rightarrow o}$ represents standard Gibbs transfer energy for the ion from the water to the oil phase, $\Delta_o^w \phi = \phi^w - \phi^o$ is the Galvani potential difference between the two phases as a result of the partitioning of the ion i , which is given by Equation (1.8) from Equation (1.7):

$$\Delta_o^w \phi = \frac{\Delta G_{tr,i}^{0,w \rightarrow o}}{z_i F} + \frac{RT}{z_i F} \ln \left(\frac{a_i^o}{a_i^w} \right) \quad (1.8)$$

Where $\Delta G_{tr,i}^{0,w \rightarrow o}$ is the standard molar Gibbs energy of ion transfer from phase w to phase o, which is given by the difference in the standard molar Gibbs energy of ion solvation in the

two phases. Then, the standard potential of transfer for i , $\Delta_o^w \phi_i^0$, can be defined as:

$$\Delta_o^w \phi_i^0 = \frac{\Delta G_{tr,i}^{0,w \rightarrow o}}{z_i F} \quad (1.9)$$

Thus, the Nernst equation for ion transfer across ITIES is:

$$\Delta_o^w \phi = \Delta_o^w \phi_i^0 + \frac{RT}{z_i F} \ln \left(\frac{a_i^o}{a_i^w} \right) \quad (1.10)$$

Equation (1.10) can be expressed in terms of concentration by replacing the standard ion transfer potential by the formal ion transfer potential $\Delta_o^w \phi_i^{0'}$ including the ratio of the activity coefficients (γ):

$$\Delta_o^w \phi = \Delta_o^w \phi_i^{0'} + \frac{RT}{z_i F} \ln \left(\frac{c_i^o}{c_i^w} \right) \quad (1.11)$$

Where

$$\Delta_o^w \phi_i^{0'} = \Delta_o^w \phi_i^0 + \frac{RT}{z_i F} \ln \left(\frac{\gamma_i^o}{\gamma_i^w} \right) \quad (1.12)$$

Similar formalism can be applied to the case of heterogeneous electron transfer between redox couples across the liquid|liquid interface. Consider that the following reaction occurs at the interface:



Where O_1^w and R_2^o are the reactants in the aqueous and organic phases, respectively, and R_1^w and O_2^o are corresponding products in the two phases. At equilibrium, the electrochemical potentials of the reactants and products are equal:^[72]

$$n_2 \tilde{\mu}_{O_1}^w + n_1 \tilde{\mu}_{R_2}^o = n_2 \tilde{\mu}_{R_1}^w + n_1 \tilde{\mu}_{O_2}^o \quad (1.16)$$

Equation (1.16) can be written as

$$n_2 \mu_{R_1}^{0,w} + n_1 \mu_{O_2}^{0,o} - n_1 \mu_{R_2}^{0,o} - n_2 \mu_{O_1}^{0,w} + RT \ln \left(\left(\frac{a_{R_1}^w}{a_{O_1}^w} \right)^{n_2} \left(\frac{a_{O_2}^o}{a_{R_2}^o} \right)^{n_1} \right) + \quad (1.17)$$

$$n_2(z_{R_1} - z_{O_1})F\phi^w + n_1(z_{O_2} - z_{R_2})F\phi^o = 0$$

$$\Delta_o^w \phi = \frac{n_2(\mu_{R_1}^{0,w} - \mu_{O_1}^{0,o}) + n_1(\mu_{O_2}^{0,o} - \mu_{R_2}^{0,o})}{n_1 n_2 F} + \frac{RT}{n_1 n_2 F} \ln \left(\left(\frac{a_{R_1}^w}{a_{O_1}^w} \right)^{n_2} \left(\frac{a_{O_2}^o}{a_{R_2}^o} \right)^{n_1} \right) \quad (1.18)$$

Where $z_{O_1} - z_{R_1} = n_1$ and $z_{O_2} - z_{R_2} = n_2$, *i.e.* the difference of the charges of the reactant and product couples. Introducing the standard chemical potentials into Equation (1.18) yields

$$\Delta_o^w \phi = \Delta_o^w \phi_{et}^0 + \frac{RT}{n_1 n_2 F} \ln \left(\left(\frac{a_{R_1}^w}{a_{O_1}^w} \right)^{n_2} \left(\frac{a_{O_2}^o}{a_{R_2}^o} \right)^{n_1} \right) \quad (1.19)$$

Where the standard electron transfer potential $\Delta_o^w \phi_{et}^0$ is defined as

$$\Delta_o^w \phi_{et}^0 = \frac{n_2(\mu_{R_1}^{0,w} - \mu_{O_1}^{0,o}) + n_1(\mu_{O_2}^{0,o} - \mu_{R_2}^{0,o})}{n_1 n_2 F} \quad (1.20)$$

$$\Delta_o^w \phi_{et}^0 = \frac{n_1 E_{O_2/R_2}^{0,o} - n_2 E_{O_1/R_1}^{0,w}}{n_1 n_2} \quad (1.21)$$

As in the case of ion transfer, the Nernst equation can be expressed in terms of concentrations:

$$\Delta_o^w \phi = \Delta_o^w \phi_{et}^{0'} + \frac{RT}{n_1 n_2 F} \ln \left(\left(\frac{c_{R1}^w}{c_{O1}^w} \right)^{n_2} \left(\frac{c_{O2}^o}{c_{R2}^o} \right)^{n_1} \right) \quad (1.22)$$

1.5 Polarisation of liquid interfaces

$\Delta_o^w \phi$ can be varied in three ways in experiments:^[59] (1) by dissolving a common salt in the two phases; (2) by using a common potential determining ion in the two phases; (3) via an externally applied potential. The first two interfaces are named as ideally non-polarisable interfaces and the third represents ideally polarisable interface.

1.5.1 Ideally non-polarisable ITIES

A non-polarisable ITIES is formed in the presence of common ions in the two phases. The first type of non-polarisable ITIES is that where a single binary electrolyte, A^+B^- , is present in both phases and completely dissociated into a cation A^+ and B^- an anion in each phase, as Equation (1.23):^[72]



Considering that the concentrations of A^+ and B^- are equal in each phase, the interfacial potential difference established at equilibrium is:

$$\Delta_o^w \phi = \frac{\Delta_o^w \phi_A^0 + \Delta_o^w \phi_B^0}{2} + \frac{RT}{F} \ln \left(\frac{\gamma_A^w \gamma_B^o}{\gamma_A^o \gamma_B^w} \right) \quad (1.24)$$

Therefore, the Galvani potential difference across the interface is independent of the electrolyte concentration, and is entirely controlled by the ability of the ions A^+ and B^- to transfer from one phase to the other. The second type of non-polarisable ITIES is formed between the two phases containing only a single common ion C^+ , as Equation (1.25):



In this case, the counter ions D^- and E^- are sufficiently hydrophobic and hydrophilic, respectively, to remain confined in their respective phase, so that C^+ is the unique ion that can transfer across the interface. $\Delta_o^w \phi$ between the two immiscible solvents is determined by the activity ratio of C^+ in two phases, according to the Nernst equation:

$$\Delta_o^w \phi = \Delta_o^w \phi_C^0 + \frac{RT}{F} \ln \left(\frac{a_C^o}{a_C^w} \right) \quad (1.26)$$

In the experiments, $\Delta_o^w \phi$ can be controlled by varying the electrolyte concentrations (*i.e.* the concentrations of C^+) in both phases. Normally, non-polarisable ITIES are commonly used as organic reference electrodes because they can form ion selective electrodes (ISEs) for organic ions.^[72]

1.5.2 Ideally polarisable ITIES

When a system comprises two different electrolytes A_1B_1 and A_2B_2 in phases w and o (Equation (1.27)), it has the properties of an ideally polarisable ITIES.



In this case, the aqueous supporting electrolyte ions A_1^+ and B_1^- are very hydrophilic and organic supporting electrolyte ions A_2^+ and B_2^- are very hydrophobic, *i.e.*,

$$\Delta_o^w \phi_{A_1^+}^0 \gg 0 \text{ and } \Delta_o^w \phi_{B_1^-}^0 \ll 0 \quad (1.28)$$

$$\Delta_o^w \phi_{A_2^+}^0 \ll 0 \text{ and } \Delta_o^w \phi_{B_2^-}^0 \gg 0 \quad (1.29)$$

Under these conditions, $\Delta_o^w \phi$ is controlled by the electrical charge in the interfacial region,

which can be supplied from an external source.

1.5.3 Potential Window

As previously mentioned, no faradaic process occurs at an ideally polarisable interface, since all components of a system are considered having an infinite standard Gibbs energy of transfer (Equations 1.28 and 1.29). As ionic species have finite solubility in any electrolyte phase, ideally polarisable liquid|liquid interface can be defined in a limited potential range. “polarisation range” (Figure 1.3), means the range of potentials controlled by the potentiostat.

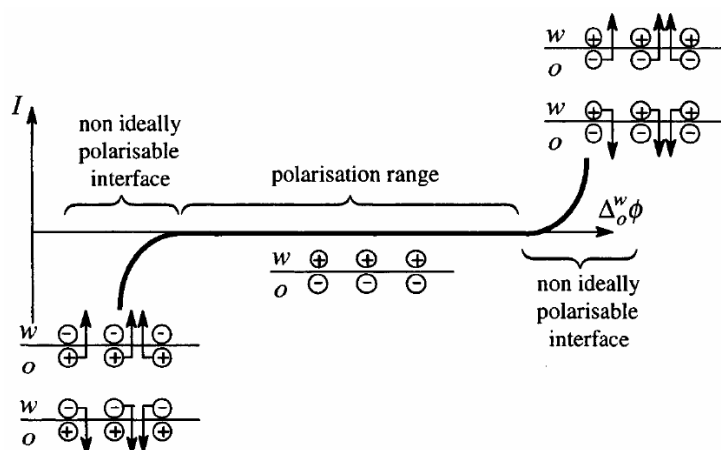


Figure 1.3: Scheme of interfacial processes within the potential window.

When, the applied potential reaches high positive values, the cations A_1^+ or the anions B_2^- gain a sufficient energy to transfer in the adjacent phase. In the same way, very negative potentials supply enough energy for B_1^- or A_2^+ to transfer in the other phase. In both cases, the chemical composition of the adjacent phases is altered by an interfacial faradic current, so that the interface becomes non ideally polarisable. The behaviour of the interface all along the applied range is called “potential window” and is schematically described in Figure 1.3. As in the case of metal|electrolyte interfaces, faradaic transfer processes can be studied under potentiostatic control only within the polarization range. This window can be expanded by using very hydrophobic and hydrophilic supporting electrolytes in the oil and water phase respectively, since this kind of salts require a high energy to transfer into the adjacent phase.

1.6 Charge transfer process at ITIES

Charge transfer reactions are of fundamental importance due to the wide range of applications of these processes in chemistry and biology.^[18] The study is also important at the theoretical level, as the heterogeneous environment is characterised by a number of unique properties that are expected to influence the behaviour of a chemically active system in a way that is significantly different from its behaviour in bulk solution. Here studies of charge transfer reactions at the ITIES have been classified into three groups: ion transfer, facilitated ion transfer, electron transfer.

1.6.1 Simple ion transfer at ITIES

Let us consider the same system as this described by Equation (1.27), with a moderately hydrophilic cation C^+ dissolved in both phases. In absence of any current flow, the partition equilibrium of C^+ gives rise to a potential difference defined by the Nernst equation:

$$\Delta_o^w \phi_{eq} = \Delta_o^w \phi_{C^+}^{0'} + \frac{RT}{z_{C^+} F} \ln \left(\frac{c_{C^+,eq}^o}{c_{C^+,eq}^w} \right) \quad (1.30)$$

The ionic redistribution will generate a current response. Effectively, to restore the electroneutrality of each phase, redox reaction will take place at the counter electrodes present in aqueous and organic solutions. By convention, the current is taken positive for the passage of a positive charge from water to the oil phase. For the cation C^+ , a positive over-potential gives rise to a positive current as the cations transfer across interface from water to organic phase. Conversely, a negative potential perturbation favours the inverse passage resulting in a negative signal. The total voltammetric wave obtained for a reversible cation transfer at a micro-interface is schematically shown in Figure 1.4. In the case of an anion transfer, the inequalities related to the concentration ratio are reversed, resulting in a transfer from water to oil for negative over-potentials and from oil to water for positive over-potentials.

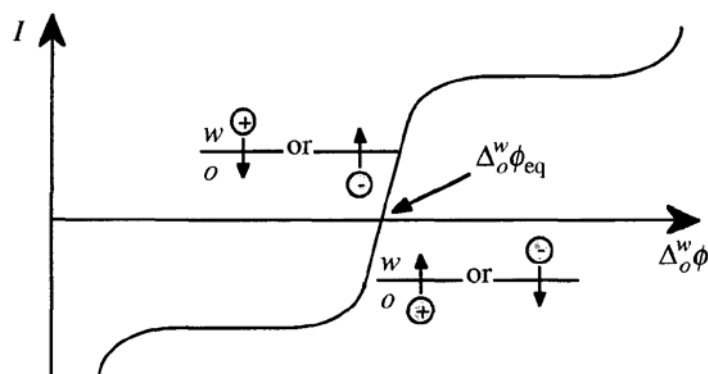


Figure 1.4: Steady state representation of the current evolution for cation or anion transfer.

The standard transfer potential of an ion is not available by direct measurement on the current-potential curves. Effectively, the Galvani potential difference is offset with respect to the potential applied to the reference electrode. This offset arises from the series of liquid|liquid and solid|liquid junctions present in the electrochemical cells. For this reason there has been a permanent interest in the evaluation of the Galvani potential difference.

To establish an ionic scale, many different assumptions have been suggested. the most commonly used approach is “TATB” assumption, which is based on the assumption that the standard Gibbs transfer energies of tetraphenylarsonium (TPAs⁺) cation $\Delta G_{\text{tr,TPAs}^+}^{0,w \rightarrow o}$ and tetraphenylborate (TPB⁻) anion $\Delta G_{\text{tr,TPB}^-}^{0,w \rightarrow o}$ in an arbitrary pair of solvents are equal due to their similar sizes and shapes where the charge is masked under the phenyl groups.^[78, 79] When the standard Gibbs energy of transfer of the salt TPAs⁺TPB⁻ (tetraphenylarsonium tetraphenylborate) is known for an arbitrary pair of solvents, a scale of standard Gibbs transfer energies of ion and standard potential differences can be calculated. Consequently, their solvation energies can be taken as equal in magnitude, resulting in the equality of their Gibbs energies of transfer for any pair of solvents:

$$\Delta G_{\text{tr,TPAs}^+}^{0,w \rightarrow o} = \Delta G_{\text{tr,TPB}^-}^{0,w \rightarrow o} = 1/2 \Delta G_{\text{tr,TPAsTPB}}^{0,w \rightarrow o} \quad (1.31)$$

This assumption does not take into account the fact that the As-C and B-C bond lengths are not equivalent^[80] each having values of 1.92 and 1.63 Å, respectively. Therefore, the cation

and anion will be solvated to different degrees and difference in radii between the two ions may result in different Gibbs energies of transfer. Using this property and assuming that both ions have similar diffusion coefficient (same size), Valent *et al.*^[81] stated that, when TPAsTPB is used as organic supporting electrolyte, the center of symmetry of the current-potential curve corresponds to the zero point of the Galvani potential difference scale. Obviously, the evaluation of the zero point is only valid provided TPAs⁺ and TPB⁻ are the potential window limiting species. Other authors used the TATB assumption to reference the Gibbs energy of ion transfer determined by solubility^[82] or partition^[83] measurements. It should be noticed that standard Gibbs energies of transfer estimated from partition data (Gibbs energies of partition) are related to ion transfer between two mutually saturated solvents, whereas Gibbs transfer energies refer to pure solvents. Nevertheless, these values are equal when the ion of interest is not strongly hydrated^[1], *i.e.* is not present as hydrate in water saturated solvent.

Girault and Schiffirin^[84] proposed another way to define the potential scale by using the potential of zero charge (pzc) as the zero point. The pzc is a readily accessible quantity that may be measured by using a streaming electrolyte electrode^[85, 86] or by plotting electrocapillary curves, the maximum of which corresponds to the pzc.^[87]

Gavach *et al.*^[88] studied the transfer of the tetrabutylammonium cation (TBA⁺) from an aqueous solution of tetrabutylammonium bromide in presence of sodium bromide as the supporting electrolyte to a nitrobenzene (NB) solution containing tetrabutylammonium tetraphenylborate (TBATPB). This pioneering experiment showed that the observed current from water to the NB phase was due to the diffusion controlled transfer of the TBA⁺ cation. Gavach *et al.* also studied the kinetics of the transfer reaction of a series of tetraalkylammonium (TAA⁺) ions (*i.e.* calculation of the standard rate constants) at the water|NB interface.

Samec *et al.* studied the transfer of cesium and picrate ions across water|NB interfaces using cyclic voltammetry employing a four electrode potentiostat. The rapid development of this field allowed a vast accumulation of thermodynamic data *i.e.* determination of Gibbs energies

of simple ion transfer reactions from half wave potential measurements and also kinetic parameters such as charge transfer coefficient and reaction rate constant, obtained using *ac* impedance techniques.^[89] Senda *et al.* extended the kinetic studies of ion transfer reaction to monovalent anions across water|NB interfaces.^[90] The effect of varying the physical properties of one of the solvents on the transfer of acetylcholine (Ach⁺) ion was studied by Girault *et al.* by chrono-coulometry.^[91] Different experimental parameters were also systematically studied including the viscosity and the dielectric constant of the electrolyte phases by means of *ac* impedance techniques at the water|NB interface.^[91, 92]

1.6.2 Facilitated ion transfer at ITIES

The first example of facilitated, or assisted, ion transfer reaction at polarized liquid|liquid interface was reported in 1979 by Koryta who studied the transfer of potassium and sodium ions facilitated by a natural antibiotic and a synthetic ionophore.^[93]

Different assisted ion transfer mechanisms have been studied and published since Koryta reported that the decrease in an ion Gibbs energy of transfer is due to the formation of a complex with a ligand or ionophore.^[5, 93] Since the work of Koryta^[93] extensive studies have been carried out on this type of reaction and numerous publications have appeared covering a wide range of natural or synthetic macromolecule ionophores such as valinomycin^[94-96], tetracycline,^[97] monensin,^[98, 99] nonactin,^[100, 101] nigericin,^[102] DB18C6,^[103-106] hydrophilic crown ethers^[107] and lithium selective ionophore ETH 1810.^[107] Because of the diversity of ligands and metallic cations, a great variety of mechanisms have been reported by several authors and then compiled by Shao *et al.*^[108] The physico-chemical properties of the ligand (partition constant, charge, acid-base activity, *etc.*) as well as its chelating capacity for a given cation (complex formation constants in both phases, and stoichiometry of the formed complexes) determine the nature of the charge transfer process across the liquid|liquid interface.

Most of metal ions were previously unable to be studied because they were too hydrophilic for their transfer to occur within the polarization range. In presence of specific ionophores in the organic phase, the energy necessary to transfer the ion from the water to the oil phase is lowered as a result of the stabilization effect brought by the complexation reaction. The ion

transfer is then observed within the potential window. Considerable effort has been dedicated to explain the mechanisms of facilitated ion transfer reactions. In 1991, a new terminology, which accurately describes the reaction mechanism was introduced. Then four types of reaction mechanisms (Figure 1.5) can be distinguished.^[108]

ACT: Aqueous Complexation followed by Transfer

TIC: Transfer by Interfacial Complexation

TOC: Transfer followed by Organic Complexation

TID: Transfer by Interfacial Decomplexation

ACT mechanism was proposed by Lin *et al.*^[109], who claimed that if a ligand was dissolved in the organic phase, the assisted ion transfer reaction would take place via the diffusion of the ligand from oil to water, followed by complexation in the aqueous phase and transfer of the complexed ion. This mechanism is only viable if the ionophore is also soluble in the aqueous phase. Samec and Papoff^[104] and Kakutani *et al.*^[110], however, concluded that the mechanism was transfer by TIC. This mechanism is favoured by choosing a ratio of concentration such that the ion in the aqueous phase is in excess compared with the concentration of the ligand in the oil phase. In the case of transfer by interfacial complexation (TIC), we have to consider the mass transfer of the different reactants to the interface. The third mechanism, ion transfer followed by complexation in the organic phase (TOC), is the ion transfer equivalent of an electrochemical mechanism in electrode kinetics. This mechanism was favoured in the early days by Koryta^[93]. The symmetric mechanism of a TIC is a transfer by interfacial dissociation (TID). Very large majority of the reactions studied follows a mechanism of transfer by interfacial complexation/decomplexation (TIC/TID mechanism).^[108]

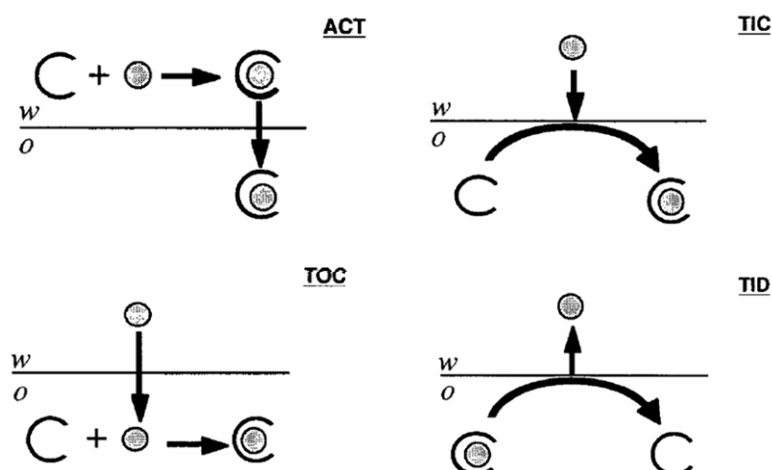


Figure 1.5: Schematic representations of the different reaction pathways for the assisted transfer process.

1.6.3 Electron transfer

Most of the analytical applications deal with transport of ions across the interface, either directly or in some facilitated form using a ligand to adjust the Gibbs energy of transport appropriately to fit into the potential window. However, in addition to ion transport across the ITIES, it is also possible to observe processes involving electron transfer. Electron transfer (*ET*) between redox species confined to two immiscible solvents was first demonstrated more than 20 years ago, and different theoretical treatments for this process have since then appeared.^[13] Such processes typically require one redox system in each of the two phases and then the electron transfer can occur on the interface. The redox couples used were for example ferrocene-ferricinium for the nonaqueous phase and ferri-ferrocyanide in the aqueous phase.^[111] Studies of the thermodynamics and kinetics of the electron transfer across the liquid|liquid interface are the focus problems in interface electrochemistry.^[112-114] It is significant for us to realize and understand many important physiological processes, open the secret of life by exploring *ET* at the liquid|liquid interface and to set up perfect kinetics theory at the liquid|liquid interface.^[115] Heterogeneous *ET* at ITIES is the transfer of an electron from a donor redox species present in one phase to an acceptor redox species in the opposite phase without any additional features as illustrated in Figure 1.6.

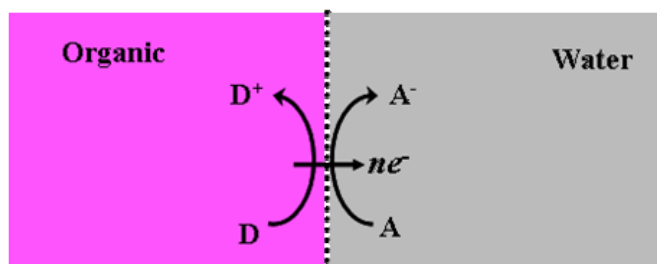


Figure 1.6: Schematic diagram of *ET* reaction across the ITIES. The letters *D* and *A* correspond to donor and acceptor species located in the organic and aqueous phase, respectively.

Detailed investigation of *ET* kinetics using fundamental models has been hindered by primitive understanding of the interfacial structure and potential distribution across the ITIES. The contribution of solvent to the reorganization energy was calculated using models in which interface was represented as a sharp boundary between two dielectrics.^[116] In this model, most of the interfacial potential drop occurred between the reacting redox species across the ITIES. In an alternative approach, the formalism for homogeneous *ET* reactions was extended to the ITIES, with the interface represented as mixed solvent area.^[117] According to this model, the interfacial potential difference had two contributions to the *ET* reaction; changing the *ET* Gibbs energy and the interfacial concentration the reactants. A similar interfacial structure was assumed in a model developed by Schmickler, in which the potential drop between the reactants was small and effectively independent of the applied potential in solutions with high ionic strength.^[118] Senda *et al.* put forward another theory, in which the electrical double layer consisted of an inner layer sandwiched between two diffuse layers on each side of the interface, and the charge transfer reaction occurred at the planes of contact of the inner layer with the two diffuse layers.^[119] Experimental studies have been able to address *ET* kinetics across ITIES only in the last few years, which were able to test some the elements outlined above. Most of the early experimental studies on the potential dependence of *ET* reactions at ITIES were obtained at externally polarised interfaces. Schiffrin and co-workers employed cyclic voltammetry to study interfacial *ET* using the Nicholson method to extract standard rate constants.^[120, 121] In another report, the conventional theory of faradic impedance and Butler-Volmer equation were applied to study

ET and ITIES ^[122] and the measured transfer coefficient was found to be potential, which was attributed to the double-layer effects and to ionic adsorption.

Samec *et al.* found that the rate constant for *ET* between ferrocene in NB and aqueous ferrocyanide was almost potential independent, but the studies were complicated by the transfer of ferrocenium ion from the organic phase to the aqueous phase.^[26] Girault and co-workers studied the *ET* reaction between both 7,7,8,8-tetracyanoquinodimethane (TCNQ) and $\text{Fe}(\text{CN})_6^{4-}$ and 1,1'-dimethylferrocene (DFc) and $\text{Fe}(\text{CN})_6^{3-}$ at a polarised water|1,2-dichloroethane (1,2-DCE) interface using in situ UV-Visible spectroscopy.^[123] They found that the potential dependence of the observed rate constant did not show a purely Butler-Volmer trend. Recent experimental studies used potential drop across the interface. Bard and co-workers have pioneered the scanning electrochemical microscopy (SECM) approach, where the *ET* rate constants were measured without the interferences of *iR* drop and charging current, using ClO_4^- in each phase as a potential determining ion.^[41, 42, 124] Microelectrochemical measurements at expanding droplets (MEMED) method was used by Unwin and co-workers to investigate the *ET* reaction between $\text{Fe}(\text{CN})_6^{4-}$ and TCNQ at the ITIES.^[125]

1.7 Applications of liquid | liquid interface

1.7.1 Analytical applications

Sun and Vanýsek demonstrated that the interface could be used for determination of lead (II) ion by its transport across the interface.^[126] Because lead (II) itself is quite hydrophilic, the transport must be facilitated by a ligand former, such as polyethylene glycol. The class of compounds seeing recent interest, the dendrimers, were also investigated on the liquid | liquid interfaces.^[127] In particular, it was the non-redox active species, poly(propylenimine) and poly(amidoamine), for which transfer across (acidified water)|1,2-DCE interface was a viable electroanalytical technique, since redox voltammetry is not possible. ITIES voltammetry allowed low micromolar detection of dendrimers. It was observed that the electrochemistry depended on the dendrimer family, the generation number, and the experimental pH. ITIES can be also successfully used for liquid | liquid extraction.^[128-130]

Jain *et al.* demonstrated the use of calixarene compound to preconcentrate and transport lanthanum(III) ion.^[131] Transfer of permanganate ion was investigated across the water|NB interface with reported potential transfer, Gibbs energy of transfer, the transfer rate constant and the apparent α coefficient (symmetry factor equivalent in the redox electrochemistry) of this reaction.^[132] The ion transfer in this case is quasi-reversible, because following the permanganate transport into the organic phase a chemical reaction occurs. The kinetic parameters were obtained by cyclic voltammetry and chronopotentiometric techniques. For many applications and even for theoretical calculations dealing with liquid|liquid interface it is necessary to know the diffusion coefficients and the transferring species and also the effective charges of the transferred species. Yuan *et al.* demonstrated how to do this by a chronoamperometric method.^[133] They employed a micropipette electrode. Since the micropipette has a large time constant (due to high resistance and relative large capacitance of the thin glass surrounding the pipette), only measurements at times more than 5 ms were possible. The authors performed finite element simulation to show validity of the experimental data. The facilitated transport is very useful in situation where the ion itself falls outside the potential window of the supporting electrolytes, usually because it is too hydrophilic. To make the ion more oil soluble, complexation with large, usually neutral species is performed. Besides the already mentioned analytical applications^[126] many other determinations with facilitated transport were reported, of which only selected few can be mentioned.^[134-142]

1.7.2 Biological, physiological and pharmaceutical applications

Antibiotics are one class of compounds that have enjoyed particular attention of the analytical work on the liquid|liquid interfaces. The typical function of an antibiotic involves facilitated transport of ions (even though, it is actually the ions, that facilitate the transport of the antibiotics) across a biological membrane. Therefore, antibiotics with appropriate modification will be transported across the ITIES.^[98, 99, 102, 143, 144] It is not without interest that antibiotics can be also synthesized, using a two phase method, on a liquid|liquid interface.^[145, 146] The interface is also a natural site where polar and in particular large

molecules can be absorbed. Phospholipids ^[147], phosphatidylcholine ^[148-151], acetylcholine^[152], cellular protein annexin, and proteins (bovine serum albumin), were all studied.^[153]

Janchenova *et al.* ^[154, 155], studied adsorption and ion pairing interactions of phospholipids on the water|1,2-DCE interface. In particular, they were interested in dipalmitoyl phosphatidyl choline (DPPC) (L- α -lecithin), which appears to have rather complex behavior. Amemiya presented several analytical papers where the property of the liquid|liquid interface was used to detect species of biological importance. He demonstrated how heparin, negatively charged polysaccharide, can be detected on the 1,2-DCE interface.^[156]

The detection requires use of ionophores to accomplish the transfer. One of the more successful ionophores was octadecyl trimethylammonium ion (present as its bromide salt). He used protamines as a model species to demonstrate, first time ever, voltammetric observation of phase transfer of biological polyions at water|NB interfaces.^[157] The smooth, unrestrained liquid|liquid interface is of great advantage in the X-ray studies on ITIES and it is certainly of some advantage in electroanalytical applications where the surface area is that of the geometrical area. However, in applications where large surface area is needed, such as in phase transfer catalysis or in the use for energy applications in possible solar cells, ^[46, 47, 51, 157-159] the limited surface area is a problem. Girault *et al.* demonstrated that increase in surface area can be performed when a 3-dimensional ITIES experiment is performed on vitreous carbon.^[160]

An interesting nanotechnology procedure using liquid|liquid interfaces was demonstrated by Glaser *et al.* ^[161] where the hexane|water interface was used to align forming particles in a manner that a particle sphere consisting from two different materials, one on each side, is formed. These particles were formed from simultaneous growth of Au and Fe₃O₄. At least theoretically Kornyshev *et al.* suggested a principle of operation of a molecular device on ITIES that could transform the energy of light into repetitive mechanical motion.^[162]

When Nernst postulated the thermodynamic basis for electrode equilibrium potential, leading to what is known now as the Nernst equation, he also carried out with Riesenfeld experiments

at liquid|liquid interfaces.^[163] However, early work on liquid interfaces was mostly non-electrochemical, focusing on extraction processes, salting-out in ion solvent extraction, measurements of physical properties such as interfacial tension, and physiological studies on model membranes.^[164-169] Systematic electrochemical treatment did not begin until the late 1970's when Koryta *et al.* demonstrated that the liquid|liquid interface lends itself to the same formalism as a solution|metal interface and that similar, if not identical, experimental methodology could be used.^[170] This led soon to development of various electrochemical techniques to study the liquid|liquid interface, including, among others, studies of the solvent dropping interface,^[101, 171-174] cyclic voltammetry,^[101] impedance measurements,^[175-178] drop pressure method,^[179] Galvanostatic pulse method^[180, 181] stripping voltammetry and voltfluorometry,^[182-185] and transport across a microinterface^[28, 186, 187]. Electron transfer and photoinduced electron transfer have been also observed on ITIES or theoretically treated^[46, 47, 117, 120, 124, 188, 189], as well as electrochemical catalysis^[190, 191] adsorption^[150, 157, 192, 193] and electrodeposition.^[194-205] Newer techniques have been more recently applied to ITIES, such as the quartz crystal microbalance^[206] and scanning electrochemical microscopy on liquid|liquid interfaces.^[41, 42, 152, 207, 208] Although the field of liquid|liquid electrochemistry is still relatively new, more scientists are finding its results or methodology relevant and important to their own work.^[209] Recent efforts have led to many practical applications in analytical chemistry and electrochemistry.^[12, 210] Charge transport across an interface between two immiscible ionically conductive media is very important both in naturally occurring systems and in designed applications. Examples include ion transport across biological membranes^[157, 211] drug delivery,^[212] behavior of ion-selective electrodes with liquid membranes and similar sensors^[213], extraction processes in oil recovery^[214] or nuclear waste reclamation and recovery^[215], phase transfer catalysis in organic synthesis^[216], pharmacology^[217-219], and many applications in electroanalytical chemistry,^[12, 219-223] applied or developmental. Fundamentally, the interface is equivalent to one side of a membrane of an ion selective electrode and thus these studies usually draw on the work of ITIES as well. Microinterfaces are another useful analytical tool, one already used to build sensors^[224] or to be used in the scanning pipette electrochemical microscopy^[225-227] or in other analytical detection schemes.^[136, 186, 228, 229] Ionic liquids which recently gained popularity in chemistry

research also show promise for applications in the ITIES work.^[230-233] Studies of charge transport, not only ion but also electron, across the liquid|liquid interface are often interpreted in terms of molecular or ionic ordering at the interface. Both computer simulations and analytic theories aiming to understand these electrochemical studies predict or assume very often existence of molecular ordering at the interface.^[209, 234] However, there are few techniques that are capable to probe directly this interface on the molecular length scale. Such techniques include surface second harmonic generation^[38, 235-240], total internal reflection spectroscopy^[241-243], *ac* potential modulation spectroscopy^[46, 239] vibrational sum-frequency spectroscopy^[244], and time-resolved quasi-elastic light scattering^[245], as well as neutron reflectivity.^[246-248] To answer fundamental questions about the structure and transport across this interface on the molecular length scale a method using X-ray surface scattering was developed.^[71, 249-252] This X-ray method provides information on interfacial molecular ordering on the sub-nanometer length scale that is complementary to that provided by the electrochemical and optical techniques.

1.8 General review on porphyrins

1.8.1 Introduction to porphyrins

The word porphyrins stems from the ancient Greek word *porphura*, which was used to describe the colour purple. Indeed all neutrally occurring and synthetic porphyrins are deeply coloured compounds. The porphyrin macrocycle is an aromatic system consisting of four “pyrrole-type” rings joined by four methine (meso) carbons (Figure 1.7).

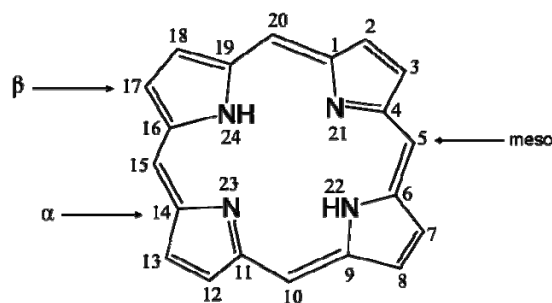


Figure 1.7: Structure of porphyrin and IUPAC numbering system.

Although a porphyrin ring has a total of 22- π electrons, only 18 of them participate in any one

of the several delocalization pathways. The delocalised aromatic character of porphyrins, which results from extensive conjugation (Figure 1.8), accounts for the one of the most striking features of these chromophores, namely their intense colour.

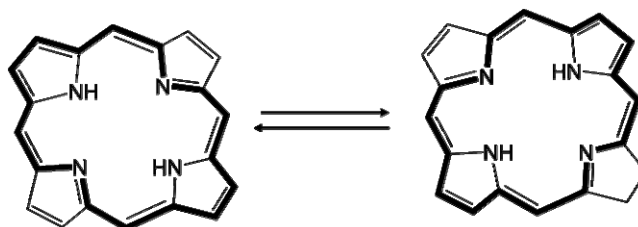


Figure 1.8: Delocalised 18 π -electron conjugation pathway and tautomerism of porphyrins.

In order to simplify the IUPAC numbering system in Figure 1.7, carbons 1, 4, 6, 9, 11, 14, 16 and 19 are referred to as the α positions and carbons 2, 3, 7, 8, 12, 13, 17 and 18 as the β positions and carbons 5, 10, 15 and 20 as the meso positions.^[253] The two inner NH groups (22, 24 or 21, 23) lose proton under basic conditions in order to form a dianionic species. Such a porphyrins dianion is able to coordinate almost every metal within its cavity to form a metalloporphyrin. This incorporation may result in the distortion of the planar macrocycle in order to maximise the binding strength towards the metal fragment.^[253]

Different types of groups or side chains can be attached to the β carbons of the pyrrole rings or the methine carbons (meso) which is the basis of the versatile structures of porphyrins. The metal complexes of porphyrin ligands (metalloporphyrins) are a large class of coordination compounds which can be found in many biological systems in nature. For instance, chlorophylls which are involved in the photosynthesis of green plants are magnesium chlorins. Chlorins are porphyrin derivatives with one pyrrole ring reduced. Hemoproteins, which play important functions in oxygen transport and storage in human bodies, contain an iron-porphyrin moiety. The chemistry of porphyrins has been a subject of extensive multidisciplinary research for several decades.^[254]

Porphyrins containing alkyl substituents at the β -pyrrole positions are commonly referred to as etio-type porphyrins. The most common naturally occurring etio-type porphyrin is

protoporphyrin IX which is a moiety of many hemoproteins.^[255] Octaethylporphyrin (OEP) is the most common synthesized etio-type porphyrin. Those porphyrins having substituents only at the four methine bridges are known as meso-type porphyrins. The four substituents are most commonly derivatives of benzene or pyridine. Tetraphenylporphyrin (TPP) is the most common one of this type which is easily synthesized, but it does not occur naturally.

1.8.2 Fundamental properties of porphyrins

Porphyrins and related compounds, which have been the subject of intense interest since the early 19th century, have attracted scientists from many areas due to their immense biological importance and their fascinating physical, chemical, and spectroscopic properties.^[256, 257] By varying the choice of the metal center, the bonding and characteristics of the metalloporphyrin may be critically affected. This diversity is one reason why metalloporphyrins have found many applications in modern life, such as magnetic materials,^[258] photoconductive materials, non-linear optical materials.^{[259],[260]} In order to evaluate the applications of MPs, it is necessary to understand the electronic structure and photophysical properties. To interpret their various electronic states, optical absorption spectra and luminescence properties, Martin Gouterman first proposed a four-orbital model in the 1960s and it remains an effective model for explaining the absorption spectra of porphyrins.^[260] This model is depicted in Figure 1.9 and it illustrates the electronic density distributions in the orbitals. The a_{1u} and a_{2u} orbitals are HOMOs and the two LUMOs are identified as $eg(\pi^*)$. As seen in the Figure 1.9, the HOMO a_{2u} orbital is mainly localized on the pyrrolic nitrogen and meso-carbon atoms while HOMO-1 a_{1u} has contribution mainly from the α and β atoms. The LUMOs are delocalized on the porphyrin ring. For a molecule with D_{4h} symmetry, the $eg(\pi^*)$ orbitals are strictly degenerate whereas the two a orbitals are nearly degenerate.^[261]

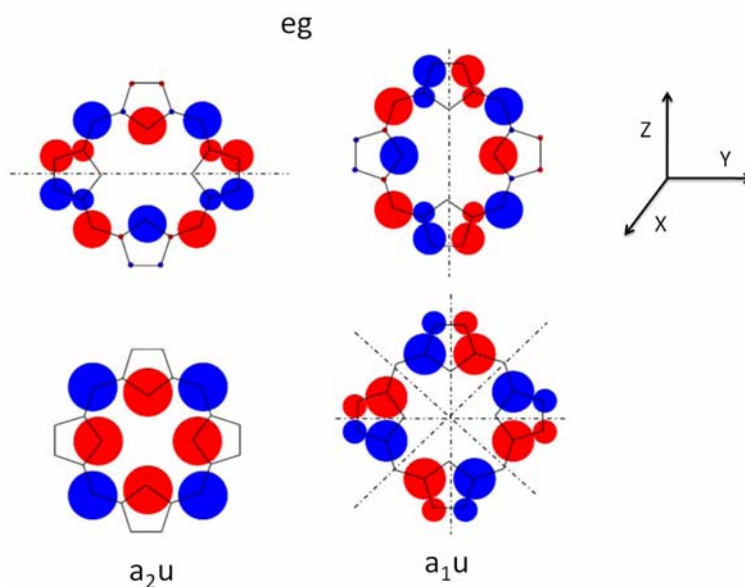


Figure 1.9: Porphyrin HOMOs (bottom) and LUMOs(top); Electron densities are shown in red and blue.

In the visible absorption spectra, porphyrins usually show an intense Soret band^[262] at around 400 nm, which results from the delocalized cyclic electronic pathway of porphyrins. Several weaker absorption bands between 450 nm and 800 nm, which are responsible for the rich color of porphyrins, are also observed and known as Q bands. Metalloporphyrins all have characteristic absorption bands in the UV-Visible region. These bands are thought to arise mainly from the $\pi \rightarrow \pi^*$ transitions due to the π -electrons of the porphyrin ring.^[260] The ring centered oxidation and metal-centered oxidation usually give rise to distinctly different electronic spectral changes.^[263] If the oxidation process is porphyrin-ring centered, the Soret band will usually blue shift, and its intensity is reduced considerably; the Q-bands will usually shift and decrease in intensity leading to a broad feature in the visible region. On the other hand, if the oxidation process is metal-centered, there is no major loss of intensity of the Soret band, but the peak position will shift. The two Q-bands are retained (with or without change in position).^[263]

Figure 1.11 describes the schematic diagram showing the possible transitions of metalloporphyrins. The absorption bands arise from transition between two HOMOs and two LUMOs ($\pi \rightarrow \pi^*$). Accordingly the lowest singlet excited configurations are $^1(a_1u, eg)$ and $^1(a_2u, eg)$ both having the E_u character. The Q bands are the result of the transition dipoles

nearly canceling each other out, resulting in a weaker absorption band. The higher energy B band transition results from a linear combination of the two transitions adding the transition dipoles and it is intense.^[264]

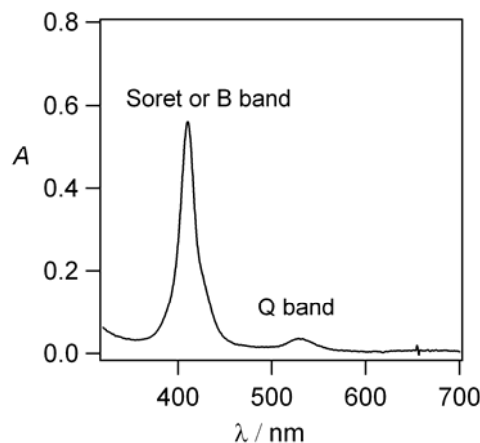


Figure 1.10: A typical absorption spectrum of a metalloporphyrin.

The four orbital model has been very effective in explaining the effects of various substituents, central metal ions and extraneous ligands.^[265] As shown in Figure 1.9, molecular orbital theory calculations of the porphine core have shown that the a_{1u} orbital has nodes at the pyrrole nitrogens and it cannot directly interact with metal. It also has nodes at the meso-carbons and is not expected to be influenced by meso substitution. In contrast, the a_{2u} orbital should be strongly affected by meso substituents. On the other hand the a_{2u} orbital puts less charge at the β carbons of the pyrrole rings than a_{1u} orbital does. Less electronegative metals shift a_{2u} to higher energy and more electronegative metals stabilize a_{2u} . Hypso porphyrins show blue shifts of the absorption spectra compared to regular porphyrins. If the metal possesses filled d orbitals, $d\pi$ electron donation from the dxz and d_{yz} orbitals to the empty $eg-\pi^*$ -orbitals of the porphyrin may occur, raising the $eg-\pi^*$ orbitals and lowering the $d\pi$ orbitals which have become bonding (metal to ring π back bonding, Figure 1.11). As a result the energy gap between the LUMO and HOMO will increase showing the hypsochromic shift.

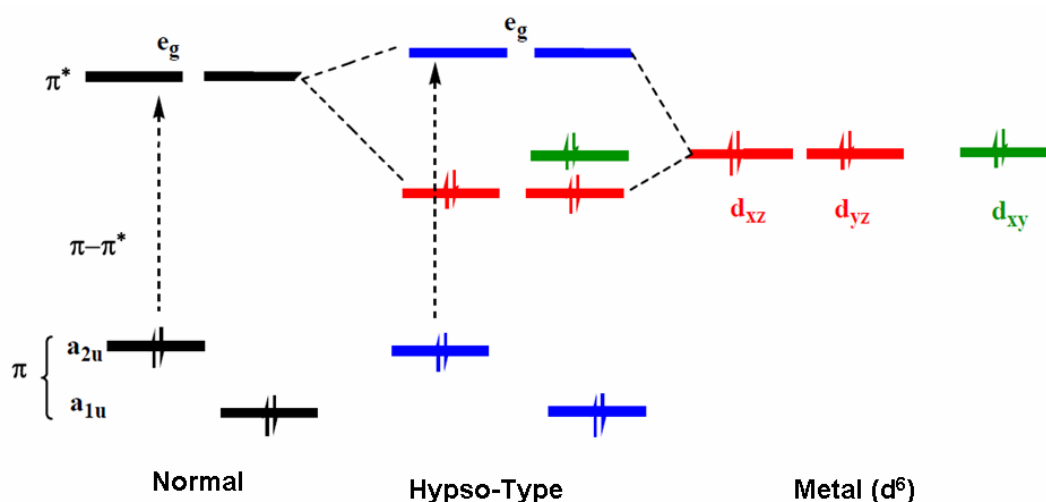


Figure 1.11: Origin of the hypsochromic shift of the Q band.

The porphyrin ring is generally stable under strongly acidic and basic conditions. Strong bases, such as alkoxides can remove the two protons ($pK_a \sim 16$) on the inner nitrogen atoms of porphyrin to form a dianion. On the other hand, the two free pyrroline nitrogen atoms ($pK_b \sim 9$) can be easily protonated with acids such as trifluoroacetic acid, to form a dication. The inner protons can also be replaced by a metal. Various types of metals (e.g., Zn, Cu, Ni, Sn) can be inserted into the porphyrin cavity by using various metal salts.^[266] Demetalation of metalloporphyrins can usually be achieved by the treatment with acids, and different types of acids are required. Alkylation of the pyrroline nitrogen atoms can also be achieved in a similar way to protonation and metalation.^[267] Aromatic compounds such as porphyrins used to be assumed to be planar. The X-ray structures of simple porphyrins showed the ring to be planar, recently, there have been tremendous numbers of nonplanar porphyrins reported in the literature.^[268, 269] Nonplanar porphyrins have intriguing physical and biological properties due to the distortion of the porphyrin ring. Many different factors such as metalation, peripheral substitutions, alkylation of the pyrroline nitrogen atoms, and even protonation, can distort the nominally planar structure of the porphyrin macrocycle.

1.8.3 Electrochemistry of porphyrins

The redox behavior of porphyrins has been extensively investigated because of its relevance to many biological processes. Several studies in this area have been published in the literature.^[257, 270] Most of the research has been carried out in nonaqueous media. Generally, metalloporphyrins may be oxidized or reduced at three discrete sites. In nonaqueous media, free base porphyrins (porphyrins without a central metal) and metalloporphyrins with 'inactive' metals (eg Zn(II), Mg(II)) usually undergo two successive reversible one-electron oxidations, leading to the formation of corresponding π -cation radicals and dication, and two successive reversible one electron reductions, yielding the π -cation radicals and dianions, respectively. Metal centered electron transfer reactions are also observed for a number of metalloporphyrins containing electroactive metals (e.g. Mn(III), Fe(III), Ni(II), Co(II)).^[257]

Various techniques have been employed to investigate the electrochemical behavior of porphyrins. In the 1960s and early 1970s, traditional electrochemical techniques such as polarography, cyclic voltammetry and rotating-disk voltammetry had been used mainly to study the electrode reactions of metalloporphyrin complexes.^[257] Several 'rules' regarding the electrochemistry of metalloporphyrins have been proposed from these early works. For example, when measuring the redox potentials of a series of metallo-octaethylporphyrins, Fuhrhop and co-workers concluded that for almost all complexes the potential difference between the first oxidation to form a cation radical and the first reduction to form an anion radical was a constant, $\Delta E = 2.25 \pm 0.15 \text{ V}$.^[271] In addition, the difference in potential between the first and second reductions was $0.42 \pm 0.05 \text{ V}$, and the potential difference between the first and the second oxidation was $0.29 \pm 0.05 \text{ V}$. Similar results were observed for complexes of tetraphenylporphyrins.^[271] These simple rules have been used to distinguish between the ring-centered and metal-centered redox types.^[272] Unfortunately, there are a number of exceptions to these simple rules, and many of these seem to involve the biologically important complexes of iron, manganese and cobalt porphyrins.^[273-275] An important subject in the electrochemistry of metalloporphyrins is the assignment of the redox sites within porphyrins. For a metalloporphyrin containing an electroactive metal, the electron-transfer processes might be either porphyrin-ring centered or metal-centered. Both types of reaction have been found in biochemical processes in nature. For instance, for iron porphyrins, the Fe(II)/Fe(III) redox couple is involved in many biological processes such as oxygen binding of hemoglobins and

electron transport reactions facilitated by cytochromes.^[276, 277] The versatile roles of the iron in these naturally occurring systems reflect the great influence of the porphyrins ligands on the redox properties of the central metals. The transfer of electrons to or from the porphyrin ring, on the other hand, is also important in natural processes. Magnesium chlorin π -cation radicals have been proposed as intermediates in the photosynthesis processes of all green plants^[278], and ferryl protoporphyrin IX π -cation radicals are found as intermediates in the enzymatic cycles of several peroxidases and catalases.^[279] While voltammetry measurements can usually give useful information about the redox sites^[271], in some cases the simple inspection of a voltammetric wave does not allow unambiguous identification of the electron transfer site within the complex. For instance, it is known that oxidation of Fe(III) porphyrins under different conditions may result in either loss of an electron from the porphyrin ring to give a π -cation radical,^[280] or in loss of an electron from the iron, to produce hypervalent Fe(IV) species.^[281] Felton and co-workers^[282, 283] assigned the one-electron oxidation products of both Fe(III)TPPClO₄ and Fe(III)OEPClO₄ as Fe(IV) species based on irregularities of the half-wave potentials. However, formation of Fe(III)-cation radicals from these processes were confirmed by Phillippi and Goff,^[284, 285] on the basis of magnetic-susceptibility measurements and NMR studies. An assumption which has been frequently forwarded in support of identifying metal-centered oxidation against ligand-centered oxidation is that the half-wave potential for the oxidation of the porphyrin ring should be independent of the axial coordination of the central metal, whereas the metal oxidation potential should vary largely with the axial ligand.^[257] As to the validity of this assumption, Hinman and Pavelich pointed out that this argument holds only where the overall charge of the complex remains unchanged on varying the axial ligand(s).^[286] The half-wave potential for oxidation of the porphyrin ring in Zn(II)TPP shifts by up to about 300 mV on complexation with anions, while very little potential shift is observed on complexation with uncharged ligands. Therefore great caution must be exerted in ascribing unusual features of the voltammetry of metalloporphyrins which involve electrochemically active metals and spectroscopic techniques should be employed to further investigate these redox processes. Since products of these two types of reactions are usually spectroscopically distinct, some suitable spectroscopic methods could be able to distinguish them. Electronic spectroscopy has

been employed intensively to identify the site of oxidation/reduction in metalloporphyrins. Apart from electronic spectroscopy, several other spectroscopic methods have also been explored to identify the site of the redox process. These methods include NMR,^[287] magnetic circular dichroism (MCD),^[288] vibrational spectroscopy, and ESR spectroscopy. The first two methods are less frequently used. The application of vibrational spectroscopy in metalloporphyrins has been of particular interest in recent years.

1.8.4 Applications of porphyrins

As mentioned above, porphyrins and related tetrapyrrolic compounds occur widely in nature and play important roles in various biological processes. For example, heme (Figure 1.12), the iron(II) protoporphyrin-IX complex, is the prosthetic group in hemoglobins and myoglobins, which are responsible for oxygen transportation in red blood cells and oxygen storage in living tissue. In addition to the vital roles these compounds play in biological systems, porphyrins, especially numerous synthetic porphyrins, have also found applications outside the modeling and mimicking of natural systems. For example, they have found applications in molecular sensors, molecular recognition, photodynamic therapy, boron neutron capture therapy, virus destruction, DNA cleavage, data storage, nonlinear optics and electrochromism. Due to their wide applications, the synthesis of porphyrins and their assemblies has become a very attractive research area.^[257, 289] Due to their selective localization in tumor cells, synthetic tetrapyrrole pigments have tremendous applications in PDT (photodynamic therapy) and BNCT (boron neutron capture therapy).^[290] PDT and BNCT are both binary cancer therapies and their side effects are limited. PDT involves the irradiation of a photosensitizer with light of a specific wavelength, which is absorbed by the photosensitizer and subsequently causes the excitation of the photosensitizer to its excited singlet state, then through intersystem crossing, to reach to its excited triplet state.

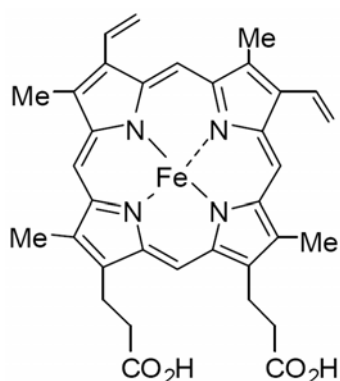


Figure 1.12: Structure of iron(II) protoporphyrin-IX complex.

The resulting excitation energy is absorbed by the triplet ground state of dioxygen (found in all living cells) and the highly toxic singlet dioxygen ($^1\text{O}_2$) is generated; this kills the tumor cells. BNCT involves the capture of thermal neutrons by boron-10 nuclei, which have been selectively delivered to tumor cells. The captured neutron releases $\text{Li}^{[268]}$ and $\text{He}^{[262]}$ nuclei with kinetic energy. These two particles are extremely cytotoxic but can only travel a distance of about one cell diameter in tissues, thus it can selectively kill the tumor cell containing it. Porphyrins and metalloporphyrins are also ideal model compounds for studying light harvesting, energy and electron transfer, and multielectron redox catalysis.^[257, 291] Porphyrin-based multiporphyrin arrays and molecular wires have received much interest. In these model systems, it is important to know how individual molecules within arrays communicate with each other. So far, factors such as distance, orientation and geometry have been recognized to be important factors to control this intercommunication.^[289]

1.9 References

- [1] H. H. Girault, D. J. Schiffrin, *Electroanalytical Chemistry, Vol. 15*, New York, **1989**.
- [2] W. Z. Nernst, *Journal of Physical Chemistry* **1892**, 137.
- [3] H. Freiser, *Chemical Reviews* **1988**, 88, 611.
- [4] P. R. Danesi, D. Chiarizia, *Critical Reviews in Analytical Chemistry* **1980**, 10, 1.
- [5] K. Arai, F. Kusu, K. Takamura, *Liquid-Liquid Interfaces: Theory and Methods*, CRC Press, Boca Raton, **1996**.
- [6] G. Steyaert, G. Lisa, P. Gaillard, G. Boss, F. Reymond, H. H. Girault, P. A. Carrupt, B. Testa, *Journal of the Chemical Society - Faraday Transactions* **1997**, 93, 401.
- [7] F. Reymond, G. Steyaert, P. A. Carrupt, B. Testa, H. Girault, *Journal of the American Chemical Society* **1996**, 118, 11951.
- [8] F. Reymond, P. A. Carrupt, B. Testa, H. H. Girault, *Chemistry - A European Journal* **1999**, 5, 39.
- [9] T. Ohkouchi, T. Kakutani, M. Senda, *Bioelectrochemistry and Bioenergetics* **1991**, 25, 71.
- [10] H. Alemn, *Pure and Applied Chemistry* **2004**, 76, 697.
- [11] M. Senda, Y. Yamamoto, *Liquid-Liquid Interfaces: Theory and Methods*, CRC Press, Boca Raton, **1996**.
- [12] F. Reymond, D. Fermin, H. J. Lee, H. H. Girault, *Electrochimica Acta* **2000**, 45, 2647.
- [13] D. J. Fermin, R. Lahtinen, *Liquid Interfaces in Chemical, Biological and Pharmaceutical Applications, Vol. 95*, New York, **2001**.
- [14] W. Nernst, E. H. Riesenfeld, *Annals of Physics* **1902**, 8, 600.
- [15] M. Z. Cremer, *Journal of Biology* **1906**, 47, 562.
- [16] E. J. W. Verwey, K. F. Niessen, *Philosophical Magazine* **1939**, 28, 435.
- [17] C. Gavach, Mlodnicka, J. Gustalla, *Les Comptes rendus de l'Académie des sciences* **1968**, C266, 1196.
- [18] J. Koryta, P. Vanysek, M. Brezina, *Journal of Electroanalytical Chemistry* **1977**, 75, 211.
- [19] Z. Samec, V. Marecek, J. Koryta, M. W. Khalil, *Journal of Electroanalytical Chemistry* **1977**, 83, 393.
- [20] Z. Samec, V. Marecek, J. Weber, *Journal of Electroanalytical Chemistry* **1978**, 96, 245.
- [21] Z. Samec, V. Marecek, J. Weber, *Journal of Electroanalytical Chemistry* **1979**, 103, 11.
- [22] T. Kakutani, T. Osakai, M. Senda, *Bulletin of the Chemical Society of Japan* **1983**, 56, 991.
- [23] D. Homolka, V. Marecek, *Journal of Electroanalytical Chemistry* **1980**, 112, 91.
- [24] Z. Samec, D. Homolka, V. Marecek, *Journal of Electroanalytical Chemistry* **1982**, 135, 265.
- [25] B. Hundhammer, T. Solomon, H. Alemu, *Journal of Electroanalytical Chemistry* **1983**, 149, 179.
- [26] Z. Samec, V. Marecek, D. Homolka, *Journal of Electroanalytical Chemistry* **1981**, 126, 121.
- [27] G. Taylor, H. H. J. Girault, *Journal of Electroanalytical Chemistry* **1986**, 208, 179.
- [28] J. A. Campbell, H. H. Girault, *Journal of Electroanalytical Chemistry* **1989**, 266, 465.
- [29] F. Silva, M. J. Sousa, C. M. Pereira, *Electrochimica Acta* **1997**, 42, 3095.
- [30] M. D. Osborne, H. H. Girault, *Electroanalysis* **1995**, 7, 714.
- [31] M. D. Osborne, H. H. Girault, *Mikrochimica Acta* **1995**, 117, 175.

- [32] S. Wilke, *Analytica Chimica Acta* **1994**, 295, 165.
- [33] B. Hundhammer, T. Solomon, T. Zerihun, M. Abegaz, A. Bekele, M. Graichen, *Journal of Electroanalytical Chemistry* **1994**, 371, 1.
- [34] S. Wilke, H. Franzke, H. Muller, *Analytica Chimica Acta* **1992**, 268, 285.
- [35] S. Sawada, H. Torii, T. Osakai, T. Kimoto, *Analytical Chemistry* **1998**, 70, 4286.
- [36] I. Benjamin, *Annual Review of Physical Chemistry* **1997**, 48, 407.
- [37] I. Benjamin, *Chemical Reviews* **1996**, 96, 1449.
- [38] J. C. Conboy, G. L. Richmond, *Journal of Physical Chemistry B* **1997**, 101, 983.
- [39] R. R. Naujok, H. J. Paul, R. M. Corn, *Journal of Physical Chemistry* **1996**, 100.
- [40] Z. Ding, D. J. Fermin, P. F. Brevet, H. H. Girault, *Journal of Electroanalytical Chemistry* **1998**, 458, 139.
- [41] C. Wei, A. J. Bard, M. V. Mirkin, *Journal of Physical Chemistry* **1995**, 99, 16033.
- [42] M. Tsionsky, A. J. Bard, M. V. Mirkin, *Journal of Physical Chemistry* **1996**, 100, 17881.
- [43] S. Amemiya, A. J. Bard, *Analytical Chemistry* **2000**, 72, 4940.
- [44] Y. Shao, T. W. Zerda, *Journal of Physical Chemistry B* **1998**, 102, 3387.
- [45] A. L. Barker, P. R. Unwin, S. Amemiya, J. Zhou, A. J. Bard, *Journal of Physical Chemistry B* **1999**, 103, 7260.
- [46] D. J. Fermin, Z. Ding, H. D. Duong, P. F. Brevet, H. H. Girault, *Journal of Physical Chemistry B* **1998**, 102, 10334.
- [47] D. J. Fermin, H. D. Duong, Z. Ding, P. F. Brevet, H. H. Girault, *Physical Chemistry Chemical Physics* **1999**, 1, 1461.
- [48] C. Johans, R. Lahtinen, K. Kontturi, D. J. Schiffrin, *Journal of Electroanalytical Chemistry* **2000**, 488, 99.
- [49] M. Platt, R. A. W. Dryfe, E. P. L. Roberts, *Chemical Communications* **2002**, 2324.
- [50] J. Guo, T. Tokimoto, R. Othman, P. R. Unwin, *Electrochemistry Communications* **2003**, 5, 1005.
- [51] D. J. Fermin, H. D. Duong, Z. Ding, P. F. Brevet, H. H. Girault, *Journal of the American Chemical Society* **1999**, 121, 10203.
- [52] H. Jensen, J. J. Kakkassery, H. Nagatani, D. J. Fermin, H. H. Girault, *Journal of the American Chemical Society* **2000**, 122, 10943.
- [53] N. Eugster, D. J. Fermin, H. H. Girault, *Journal of Physical Chemistry B* **2002**, 106, 3428.
- [54] N. Eugster, H. Jensen, D. J. Fermin, H. H. Girault, *Journal of electroanalytical chemistry* **2003**, 560, 143.
- [55] B. Su, N. Eugster, H. H. Girault, *Journal of the American Chemical Society* **2005**, 127, 10760.
- [56] M. Gros, S. Gromb, C. Gavach, *Journal of Electroanalytical Chemistry* **1978**, 89, 29.
- [57] H. H. Girault, *In Modern Aspects of Electrochemistry, Vol. 25*, Plenum Press, New York, **1993**.
- [58] C. Gavach, P. Seta, B. D'Epenoux, *Journal of Electroanalytical Chemistry* **1977**, 83, 225.
- [59] S. X. Guo, P. R. Unwin, A. L. Whitworth, J. Zhang, *Progress in Reaction Kinetics and Mechanism Vol. 29*, **2004**.
- [60] Z. Samec, V. Marecek, D. Homolka, *Journal of Electroanalytical Chemistry* **1985**, 187, 31.

- [61] H. H. Girault, D. J. Schiffrin, *Journal of Electroanalytical Chemistry* **1983**, 150, 43.
- [62] W. Schmickler, *In Liquid Interfaces in Chemical, Biological and Pharmaceutical Applications, Vol. 95*, New York, **2001**.
- [63] W. Schmickler, *Journal Electroanalytical Chemistry* **1997**, 426, 5.
- [64] I. Benjamin, *Journal of Chemical Physics* **1992**, 96, 577.
- [65] I. Benjamin, *Journal of Chemical Physics* **1992**, 97, 1432.
- [66] I. Benjamin, *Journal of Chemical Physics* **1994**, 180, 287.
- [67] D. Michael, I. Benjamin, *Journal of Physical Chemistry* **1995**, 99, 1530.
- [68] J. Strutwolf, A. L. Barker, M. Gonsalves, D. J. Caruana, P. R. Unwin, D. E. Williams, J. R. P. Webster, *Journal of Electroanalytical Chemistry* **2000**, 483, 163.
- [69] R. D. Webster, D. Beaglehole, *Physical Chemistry Chemical Physics* **2000**, 2, 5660.
- [70] K. B. Eisenthal, *Chemical Reviews* **1996**, 96, 1343.
- [71] G. Luo, S. Malkova, J. Yoon, D. G. Schultz, B. Lin, M. Meron, I. Benjamin, P. Vanssek, M. L. Schlossman, *Journal of Electroanalytical Chemistry* **2006**, 593, 142.
- [72] A. G. Volkov, D. W. Deamer, *Liquid-Liquid Interface: Theory and Method*, CRC Press, Boca Raton FL, **1995**.
- [73] M. Tomic, N. Kallay, *Journal of Physical Chemistry* **1992**, 96, 3874.
- [74] A. M. Carmona-Ribeiro, B. R. Midmore, *Journal of Physical Chemistry* **1992**, 96, 3542.
- [75] J. C. Franklin, D. S. Cafiso, *Biophysical Journal* **1993**, 64, A297.
- [76] A. Maitra, T. K. Jain, Z. Shervani, *Colloids and Surfaces* **1990**, 47, 255.
- [77] D. J. Schiffrin, M. R. Calde, M. C. Wiles, *Journal of Electrochemistry Society* **1986**, 133, C134.
- [78] A. J. Parker, *Electrochimica Acta* **1976**, 21, 671.
- [79] E. Grunwald, G. Baughman, G. Kohnstam, *Journal of American Chemical Society* **1960**, 82, 5801.
- [80] Y. Shao, A. A. Stewart, H. H. Girault, *Journal of the Chemical Society, Faraday Transactions* **1991**, 87, 2593.
- [81] O. Valent, J. Koryta, M. Panoch, *Journal of Electroanalytical Chemistry* **1987**, 226, 21.
- [82] M. H. Abraham, A. F. D. De Namor, *Journal of the Chemical Society, Faraday Transactions 1: Physical Chemistry in Condensed Phases* **1976**, 72, 955.
- [83] J. Czapkiewicz, B. Czapkiewicz-Tutaj, *Journal of the Chemical Society* **1980**, 76, 1663.
- [84] H. H. J. Girault, D. J. Schiffrin, *Electrochimica Acta* **1986**, 31, 1341.
- [85] H. H. J. Girault, D. J. Schiffrin, *Journal of Electroanalytical Chemistry* **1984**, 161, 415.
- [86] Z. Koczorowski, I. Paleska, J. Kotowski, *Journal of Electroanalytical Chemistry* **1987**, 235, 287.
- [87] Z. Samec, V. Marecek, *The interface structure and electrochemical processes at the boundary between two immiscible liquids*, Springer-verlag Berlin **1987**.
- [88] C. Gavach, F. Henry, *Journal of Electroanalytical Chemistry* **1974**, 54, 361.
- [89] T. Wandlowski, V. Marecek, K. Holub, Z. Samec, *Journal of Physical Chemistry* **1989**, 93, 8204.
- [90] T. Kakiuchi, J. Noguchi, M. Senda, *Journal of Electroanalytical Chemistry* **1992**, 327, 63.
- [91] Y. Shao, J. A. Campbell, H. H. Girault, *Journal of Electroanalytical Chemistry* **1991**, 300, 415.
- [92] T. Kakiuchi, Y. Teranishi, *Journal of Electroanalytical Chemistry* **1995**, 396, 401.
- [93] J. Koryta, *Electrochimica Acta* **1979**, 24, 293.
- [94] V. J. Cunnane, D. J. Schiffrin, M. Fleischmann, G. Geblewicz, D. Williams, *Journal of Electroanalytical Chemistry* **1988**, 243, 455.

- [95] J. Koryta, Y. N. Kozlov, M. Skalicky, *Journal of Electroanalytical Chemistry* **1987**, 234, 355.
- [96] P. Vanysek, W. Ruth, J. Koryta, *Journal of Electroanalytical Chemistry* **1983**, 148, 117.
- [97] N. Kozlov Yu, J. Koryta, *Analytical Letters* **1983**, 16, 255.
- [98] J. Koryta, G. Du, W. Ruth, P. Vanysek, *Faraday Discussions of the Chemical Society* **1984**, 77, 209.
- [99] V. Marecek, H. Janchenova, M. Brezina, M. Betti, *Analytica Chimica Acta* **1991**, 244, 15.
- [100] A. Hofmanova, L. Q. Hung, W. Khalil, *Journal of Electroanalytical Chemistry* **1982**, 135, 257.
- [101] D. Homolka, L. Q. Hung, A. Hofmanova, M. W. Khalil, J. Koryta, V. Marecek, Z. Samec, S. K. Sen, P. Vanysek, J. Weber, M. BÅ™mezina, M. Janda, I. Stibor, *Analytical Chemistry* **1980**, 52, 1606.
- [102] A. Sabela, J. Koryta, O. Valent, *Journal of Electroanalytical Chemistry* **1986**, 204, 267.
- [103] P. D. Beattie, A. Delay, H. H. Girault, *Electrochimica Acta* **1995**, 40, 2961.
- [104] Z. Samec, P. Papoff, *Analytical Chemistry* **1990**, 62, 1010.
- [105] J. A. Campbell, A. A. Stewart, H. H. Girault, *Journal of the Chemical Society, Faraday Transactions 1: Physical Chemistry in Condensed Phases* **1989**, 85, 843.
- [106] E. Makrlík, L. Q. Hung, A. Hofmanova, *Electrochimica Acta* **1983**, 28, 847.
- [107] Y. Kudo, Y. Takeda, H. Matsuda, *Journal of Electroanalytical Chemistry* **1995**, 396, 333.
- [108] Y. Shao, M. D. Osborne, H. H. Girault, *Journal of Electroanalytical Chemistry* **1991**, 318, 101.
- [109] S. Lin, Z. Zhao, H. Freiser, *Journal Electroanalytical Chemistry* **1986**, 210, 137.
- [110] T. Kakutani, Y. Nishinor, T. Osakai, M. Senda, *Bulletin of the Chemical Society of Japan* **1986**, 59, 781.
- [111] J. Hanzlík, Z. Samec, J. Hovorka, *Journal of Electroanalytical Chemistry* **1987**, 216, 303.
- [112] J. Koryta, *Electrochimica Acta* **1984**, 29, 445.
- [113] J. Koryta, *Electrochimica Acta* **1988**, 33, 189.
- [114] Z. Samec, V. Marecek, J. Weber, D. Homolka, *Journal of Electroanalytical Chemistry* **1981**, 126, 105.
- [115] M. Senda, T. Kakiuchi, T. Osaka, *Electrochimica Acta* **1991**, 36, 253.
- [116] R. A. Marcus, *Journal of Physical Chemistry* **1990**, 94, 1050.
- [117] H. H. J. Girault, D. J. Schiffrin, *Journal of Electroanalytical Chemistry* **1988**, 244, 15.
- [118] W. Schmickler, *liquid interfaces* **1997**, 428, 123.
- [119] M. Senda, *Electrochimica Acta* **1995**, 40, 2993.
- [120] G. Geblewicz, D. J. Schiffrin, *Journal of Electroanalytical Chemistry* **1988**, 244, 27.
- [121] V. J. Cunnane, D. J. Schiffrin, C. Beltran, G. Geblewicz, T. Solomon, *Journal of Electroanalytical Chemistry* **1988**, 247, 203.
- [122] Y. Cheng, D. J. Schiffrin, *Journal of the Chemical Society* **1993**, 89, 199.
- [123] Z. Ding, D. J. Fermin, P. F. Brevet, H. H. Girault, *Journal of Electroanalytical Chemistry* **1998**, 458, 139.
- [124] T. Solomon, A. J. Bard, *Journal of Physical Chemistry* **1995**, 99, 17487.
- [125] J. Zhang, P. R. Unwin, *Journal of Physical Chemistry B* **2000**, 104, 2341.
- [126] Z. Sun, P. Vanysek, *Analytica Chimica Acta* **1990**, 228, 241.

- [127] A. Berduque, M. D. Scanlon, C. J. Collins, D. W. M. Arrigan, *Langmuir* **2007**, *23*, 7356.
- [128] B. L. Rivas, S. Villegas, B. Ruf, I. M. Peric, *Journal of the Chilean Chemical Society* **2007**, *52*, 1164.
- [129] A. Oliva, A. Molinari, C. Avila, M. F. Flores, *Journal of the Chilean Chemical Society* **2006**, *51*, 865.
- [130] C. Gomez G, C. Von Plessing R, C. G. Godoy M, R. Reinbach H, R. Godoy, *Journal of the Chilean Chemical Society* **2005**, *50*, 479.
- [131] V. K. Jain, S. G. Pillap, H. C. Mandal, *Journal of the Chilean Chemical Society* **2007**, *52*, 1177.
- [132] H. Heli, M. Shamsipur, M. F. Mousavi, *Polish Journal of Chemistry* **2006**, *80*, 313.
- [133] Y. Yuan, L. Wang, S. Amemiya, *Analytical Chemistry* **2004**, *76*, 5570.
- [134] M. H. M. Cacote, C. M. Pereira, L. Tomaszewski, H. H. Girault, F. Silva, *Electrochimica Acta* **2004**, *49*, 263.
- [135] Y. Shao, M. V. Mirkin, *Analytical Chemistry* **1998**, *70*, 3155.
- [136] R. Zazpe, C. Hibert, J. O'Brien, Y. H. Lanyon, D. W. M. Arrigan, *Lab on a Chip - Miniaturisation for Chemistry and Biology* **2007**, *7*, 1732.
- [137] P. O'Dwyer, V. J. Cunnane, *Journal Electroanalytical Chemistry* **2005**, *581*, 16.
- [138] G. Pieruz, P. Grassia, R. A. W. Dryfe, *Desalination* **2004**, *167*, 417.
- [139] B. Kralj, R. A. W. Dryfe, *Journal Electroanalytical Chemistry* **2003**, *560*, 127.
- [140] D. Zhan, Y. Xiao, Y. Yuan, Y. He, B. Wu, Y. Shao, *Journal of Electroanalytical Chemistry* **2003**, *553*, 43.
- [141] Y. Yatziv, I. Turyan, D. Mandler, *Journal of the American Chemical Society* **2002**, *124*, 5618.
- [142] Y. Kitatsuji, Z. Yoshida, H. Kudo, S. Kihara, *Journal of Electroanalytical Chemistry* **2002**, *520*, 133.
- [143] J. Koryta, W. Ruth, P. Vanysek, A. Hofmanova, *Analytical Letters* **1983**, *15*, 1685.
- [144] G. Du, J. Koryta, W. Ruth, P. Vanysek, *Journal of Electroanalytical Chemistry* **1983**, *159*, 413.
- [145] A. Illanes, L. Wilson, O. Corrotea, L. Tavernini, F. Zamorano, C. Aguirre, *Journal of Molecular Catalysis B: Enzymatic* **2007**, *47*, 72.
- [146] C. Aguirre, P. Opazo, M. Venegas, R. Riveros, A. Illanes, *Process Biochemistry* **2006**, *41*, 1924.
- [147] Z. Samec, A. Trojanek, P. Krtil, *Faraday Discussions* **2005**, *129*, 301.
- [148] T. Kakiuchi, T. Kondo, M. Kotani, M. Senda, *Langmuir* **1992**, *8*, 169.
- [149] H. H. J. Girault, D. J. Schiffrin, *Journal of Electroanalytical Chemistry* **1984**, *179*, 277.
- [150] Z. Samec, A. Trojanek, H. H. Girault, *Electrochemistry Communications* **2003**, *5*, 98.
- [151] T. Kakiuchi, M. Kotani, J. Noguchi, M. Nakanishi, M. Senda, *Journal of Colloid And Interface Science* **1992**, *149*, 279.
- [152] R. Gulaboski, C. M. Pereira, M. N. D. S. Cordeiro, I. Bogeski, E. Ferreira, D. Ribeiro, M. Chirea, A. F. Silva, *Journal of Physical Chemistry B* **2005**, *109*, 12549.
- [153] E. Bitto, M. Li, A. M. Tikhonov, M. L. Schlossman, W. Cho, *Biochemistry* **2000**, *39*, 13469.
- [154] H. Janchenova, A. Lhotsky, K. Stulik, V. Marecek, *Journal of Electroanalytical Chemistry* **2007**, *601*, 101.
- [155] H. Janchenova, K. Stulik, V. Marecek, *Journal of Electroanalytical Chemistry* **2007**, *604*, 109.
- [156] J. Guo, Y. Yuan, S. Amemiya, *Analytical Chemistry* **2005**, *77*, 5711.

- [157] S. Amemiya, X. Yang, T. L. Wazenegger, *Journal of the American Chemical Society* **2003**, *125*, 11832.
- [158] D. J. Fermin, Z. Ding, H. D. Duong, P. F. Brevet, H. H. Girault, *Chemical Communications* **1998**, 1125.
- [159] D. J. Fermin, H. D. Duong, Z. Ding, P. F. Brevet, H. H. Girault, *Electrochemistry Communications* **1999**, *1*, 29.
- [160] S. Tan, M. Hojeij, B. Su, G. Meriguet, N. Eugster, H. H. Girault, *Journal of Electroanalytical Chemistry* **2007**, *604*, 65.
- [161] N. Glaser, D. J. Adams, A. Boker, G. Krausch, *Langmuir* **2006**, *22*, 5227.
- [162] L. Rudd, D. J. Lee, A. A. Kornyshev, *Journal of Physics Condensed Matter* **2007**, *19*.
- [163] W. Nernst, E. H. Riesenfeld, *Annals of Physics* **1902**, *8*, 600.
- [164] P. Bothorel, C. Lussan, *Comptes rendus hebdomadaires des seances de academic des science; Sciences naturelles* **1968**, 266, 2492.
- [165] W. D. Harkins, E. C. Humphery, *The Journal of the American Chemical Society* **1916**, *38*, 228.
- [166] E. K. Fischer, W. D. Harkins, *Journal of Physical Chemistry* **1932**, *36*, 98.
- [167] R. P. Bell, *Journal of Physical Chemistry* **1928**, *32*, 882.
- [168] J. H. Mathews, A. J. Stamm, *Journal of the American Chemical Society* **1924**, *46*, 1071.
- [169] W. D. Harkins, E. C. Humphery, *The Journal of the American Chemical Society* **1916**, *38*, 236.
- [170] J. Koryta, P. Vanysek, M. Brezina, *Journal of Electroanalytical Chemistry* **1976**, *67*, 263.
- [171] J. Koryta, P. Vanysek, M. Brezina, *Journal of Electroanalytical Chemistry* **1977**, *75*, 211.
- [172] P. Vanysek, *Journal of Electroanalytical Chemistry* **1981**, *121*, 149.
- [173] J. Koryta, M. Brezina, A. Hofmanova, D. Homolka, L. Q. Hung, W. Khalil, V. Marecek, Z. Samec, S. K. Sen, P. Vanysek, J. Weber, *Journal of Electroanalytical Chemistry* **1980**, *116*, 61.
- [174] P. Vanysek, M. Behrendt, *Journal of Electroanalytical Chemistry* **1981**, *130*, 287.
- [175] Z. Samec, V. Marecek, D. Homolka, *Journal of Electroanalytical Chemistry* **1981**, *126*, 121.
- [176] T. Wandlowski, S. Racinsky, V. Marecek, Z. Samec, *Journal of Electroanalytical Chemistry* **1987**, *227*, 281.
- [177] T. Wandlowski, V. Marecek, Z. Samec, *Journal of Electroanalytical Chemistry* **1988**, *242*, 277.
- [178] P. Vanysek, I. C. Hernandez, J. Xu, *Microchemical Journal* **1990**, *41*, 327.
- [179] J. D. Reid, O. R. Melroy, R. P. Buck, *Journal of Electroanalytical Chemistry* **1983**, *147*, 71.
- [180] V. Marecek, Z. Samec, *Analytica Chimica Acta* **1983**, *151*, 265.
- [181] V. Marecek, Z. Samec, *Journal of Electroanalytical Chemistry* **1983**, *149*, 185.
- [182] T. Kakiuchi, Y. Takasu, *Analytical Chemistry* **1994**, *66*, 1853.
- [183] T. Kakiuchi, Y. Takasu, *Journal of Electroanalytical Chemistry* **1994**, *365*, 293.
- [184] T. Kakiuchi, Y. Takasu, *Journal of Electroanalytical Chemistry* **1995**, *381*, 5.
- [185] H. Nagatani, S. Suzuki, D. J. Fermin, H. H. Girault, K. Nakatani, *Analytical and Bioanalytical Chemistry* **2006**, *386*, 633.
- [186] A. A. Stewart, G. Taylor, H. H. Girault, J. McAleer, *Journal of Electroanalytical*

- Chemistry* **1990**, 296, 491.
- [187] Y. Shao, H. H. Girault, *Journal of Electroanalytical Chemistry* **1992**, 334, 203.
- [188] V. Sladkov, V. Guillou, S. Peulon, M. L'Her, *nitrobenzene and water* **2004**, 573, 129.
- [189] R. A. Marcus, *Journal of Physical Chemistry* **1990**, 94, 7742.
- [190] R. M. Lahtinen, D. J. Fermin, H. Jensen, K. Kontturi, H. H. Girault, *Electrochemistry Communications* **2000**, 2, 230.
- [191] Y. Shao, M. V. Mirkin, J. F. Rusling, *Journal of Physical Chemistry B* **1997**, 101, 3202.
- [192] N. Rogiers, W. Eugster, M. Furger, R. Siegwolf, *Theoretical and Applied Climatology* **2005**, 80, 187.
- [193] R. R. Naujok, D. A. Higgins, D. G. Hanken, R. M. Com, *Journal of the Chemical Society, Faraday Transactions* **1995**, 91, 1411.
- [194] A. Trojanek, J. Langmaier, Z. Samec, *Journal of Electroanalytical Chemistry* **2007**, 599, 160.
- [195] M. Vignali, R. Edwards, V. J. Cunnane, *Journal of Electroanalytical Chemistry* **2006**, 592, 37.
- [196] C. Johans, R. Lahtinen, K. Kontturi, D. J. Schiffrin, *Journal Electroanalytical Chemistry* **2000**, 488, 99.
- [197] Y. Luan, M. An, G. Lu, *Applied Surface Science* **2006**, 253, 459.
- [198] M. Vignali, R. A. H. Edwards, M. Serantoni, V. J. Cunnane, *Journal of Electroanalytical Chemistry* **2006**, 591, 59.
- [199] V. Mirceski, R. Gulaboski, *Journal of Physical Chemistry B* **2006**, 110, 2812.
- [200] V. Mirceski, *Electrochemistry Communications* **2006**, 8, 123.
- [201] I. Turyan, M. Etienne, D. Mandler, W. Schuhmann, *Electroanalysis* **2005**, 17, 538.
- [202] E. Tada, Y. Oishi, H. Kaneko, *Electrochemical and Solid-State Letters* **2005**, 8, C26.
- [203] A. Eftekhari, *Journal of Electroanalytical Chemistry* **2004**, 227, 331.
- [204] E. Tada, H. Kaneko, *Chemistry Letters* **2000**, 1306.
- [205] M. Guainazzi, G. Silvestri, G. Serravalle, *Journal of the Chemical Society, Chemical Communications* **1975**, 200.
- [206] P. Vanysek, L. A. Delia, *Electroanalysis* **2006**, 18, 371.
- [207] T. Solomon, A. J. Bard, *Analytical Chemistry* **1995**, 67, 2787.
- [208] Y. Selzer, D. Mandler, *Journal of Electroanalytical Chemistry* **1996**, 409, 15.
- [209] A. G. Volkov, D. W. Deamer, *Liquid-Liquid Interfaces: Theory and Methods*, **1996**.
- [210] P. Vanysek, *Analytical Chemistry* **1990**, 62, 827A.
- [211] T. Spataru, N. Spataru, N. Bonciocat, C. Luca, *Bioelectrochemistry* **2004**, 62, 67.
- [212] A. Malkia, P. Liljeroth, A. K. Kontturi, K. Kontturi, *Journal of Physical Chemistry B* **2001**, 105, 10884.
- [213] S. A. Dassie, A. M. Baruzzi, *Journal Electroanalytical Chemistry* **2000**, 492, 94.
- [214] M. J. Tupy, H. W. Blanch, C. J. Radke, *Industrial and Engineering Chemistry Research* **1998**, 37, 3159.
- [215] J. Plesek, B. Gruner, S. Hermanek, J. Baca, V. Marecek, J. Janchenova, A. Lhotsky, K. Holub, P. Selucky, J. Rais, I. Cisarova, J. Slavsky, *Polyhedron* **2002**, 21, 975.
- [216] C. Forssten, J. Strutwolf, D. E. Williams, *Electrochemistry Communications* **2001**, 3, 619.
- [217] R. Gulaboski, M. N. D. S. Cordeiro, N. Milhazes, J. Garrido, F. Borges, M. Jorge, C. M. Pereira, I. Bogeski, A. H. Morales, B. Naumoski, A. F. Silva, *Analytical Biochemistry* **2007**, 361, 236.
- [218] L. Basaez, I. Peric, C. Aguirre, P. Vanysek, *Boletin de la Sociedad Chilena de Quimica* **2001**, 46, 203.

- [219] H. Alemu, *Pure and Applied Chemistry* **2004**, 76, 697.
- [220] F. Reymond, H. J. Lee, J. S. Rossier, L. Tomaszewski, R. Ferrigno, C. M. Pereira, H. H. Girault, *Chimia* **1999**, 53, 103.
- [221] J. Koryta, *Selective electrode reviews* **1991**, 13, 133.
- [222] B. Liu, M. V. Mirkin, *Electroanalysis* **2000**, 12, 1433.
- [223] Z. Samec, E. Samcova, H. H. Girault, *Talanta* **2004**, 63, 21.
- [224] B. J. Seddon, Y. Shao, J. Fost, H. H. Giraults, *Electrochimica Acta* **1994**, 39, 783.
- [225] D. Zhan, X. Li, W. Zhan, F. R. F. Fan, A. J. Bard, *Analytical Chemistry* **2007**, 79, 5225.
- [226] D. A. Walsh, J. L. Fernandez, J. Mauzeroll, A. J. Bard, *Analytical Chemistry* **2005**, 77, 5182.
- [227] P. Sun, Z. Zhang, Z. Gao, Y. Shao, *Angewandte Chemie - International Edition* **2002**, 41, 3445.
- [228] Q. Qian, G. S. Wilson, K. Bowman-James, *Electroanalysis* **2004**, 16, 1343.
- [229] Q. Qian, G. S. Wilson, K. Bowman-James, H. H. Girault, *Analytical Chemistry* **2001**, 73, 497.
- [230] J. Langmaier, Z. Samec, *Electrochemistry Communications* **2007**, 9, 2633.
- [231] R. Ishimatsu, N. Nishi, T. Kakiuchi, *Langmuir* **2007**, 23, 7608.
- [232] R. Ishimatsu, N. Nishi, T. Kakiuchi, *Chemistry Letters* **2007**, 36, 1166.
- [233] T. Kakiuchi, *Analytical Chemistry* **2007**, 79, 6443.
- [234] W. Schmickler, *Interfacial Electrochemistry*, Oxford University Press, New York, **1996**.
- [235] J. Zhang, C. J. Sleving, L. Murtomaki, K. Kontturi, D. E. Williams, P. R. Unwin, *Langmuir* **2001**, 17, 821.
- [236] K. L. Kott, D. A. Higgins, R. J. McMahon, R. M. Corn, *Journal of the American Chemical Society* **1993**, 115, 5342.
- [237] D. A. Higgins, R. M. Corn, *Journal of Physical Chemistry* **1993**, 97, 489.
- [238] D. A. Higgins, R. R. Naujok, R. M. Corn, *Chemical Physics Letters* **1993**, 213, 485.
- [239] H. Nagatani, A. Piron, P. F. Brevet, D. J. Fermin, H. H. Girault, *Analytical Chemistry* **2002**, 18, 6647.
- [240] J. C. Conboy, G. L. Richmond, *Electrochimica Acta* **1995**, 40, 2881.
- [241] S. Ishizaka, N. Kitamura, *Bulletin of the Chemical Society of Japan* **2001**, 74, 1983.
- [242] J. M. Perera, G. W. Stevens, F. Grieser, *Colloids and Surfaces A: Physicochemical and Engineering Aspects* **1995**, 95, 185.
- [243] J. C. Conboy, J. L. Daschbach, G. L. Richmond, *Journal of Physical Chemistry* **1994**, 98, 9688.
- [244] D. S. Walker, M. G. Brown, C. L. McFearin, G. L. Richmond, *Journal of Physical Chemistry B* **2004**, 108, 2111.
- [245] H. Yui, Y. Ikezoe, T. Sawada, *Analytical Sciences* **2004**, 20, 1501.
- [246] J. Strutwolf, A. L. Barker, M. Gonsalves, D. J. Caruana, P. R. Unwin, D. E. Williams, J. R. P. Webster, *Journal Electroanalytical Chemistry* **2000**, 483, 163.
- [247] A. Zarbakhsh, A. Querol, J. Bowers, M. Yaseen, J. R. Lu, J. R. P. Webster, *Langmuir* **2005**, 21, 11704.
- [248] A. Zarbakhsh, A. Querol, J. Bowers, J. R. P. Webster, *Faraday Discussions* **2005**, 129, 155.
- [249] G. Luo, S. Malkova, S. V. Pingali, D. G. Schultz, B. Lin, M. Meron, I. Benjamin, P. Vanysek, M. L. Schlossman, *Journal of Physical Chemistry B* **2006**, 110, 4527.

- [250] G. Luo, S. Malkova, S. V. Pingali, D. G. Schultz, B. Lin, M. Meron, T. J. Graber, J. Gebhardt, P. Vanysek, M. L. Schlossman, *Electrochemistry Communications* **2005**, 7, 627.
- [251] G. Luo, S. Malkova, S. V. Pingali, D. G. Schultz, B. Lin, M. Meron, T. J. Graber, J. Gebhardt, P. Vanysek, M. L. Schlossman, *Faraday Discussions* **2005**, 129, 23.
- [252] G. Luo, S. Malkova, J. Yoon, D. G. Schultz, B. Lin, M. Meron, I. Benjamin, P. Van $\frac{1}{2}$ sek, M. L. Schlossman, *Science* **2006**, 311, 216.
- [253] R. Bonnett, *The porphyrins, Vol. 1*, Academic Press, New York, **1978**.
- [254] D. Dolphin, *The Porphyrins, Vol. 1-7*, Academic Press, New York, **1978**.
- [255] Q. H. Gibson, *The Porphyrins, Vol. 5*, Academic Press, New York, **1978**.
- [256] K. M. Smith, *Porphyrins and Metalloporphyrins*, Elsevier, Amsterdam, **1975**.
- [257] K. M. Kadish, *Inorganic Chemistry, Vol. 34*, **1986**, 435
- [258] A. R. Harutyunyan, *Chemical Physics Letters* **1995**, 246, 615.
- [259] M. K. Casstevens, M. Samoc, J. Pflieger, P. N. Prasad, *The Journal of Chemical Physics* **1990**, 92, 2019.
- [260] M. Gouterman, *The Porphyrins, Vol. 3*, Academic Press, New York, **1978**.
- [261] K. Kalyanasundaram, *Photochemistry of Polypyridine and Porphirin Complexes*, Academic Press, London, **1992**.
- [262] J. L. Soret, *Comptes Rendus* **1883**, 97, 1267.
- [263] S. J. Chantrell, C. A. McAuliffe, R. W. Munn, A. C. Pratt, *Coordination Chemistry Reviews* **1975**, 16, 259.
- [264] K. S. Suslick, R. A. Watson, *New Journal of Chemistry* **1992**, 16, 633.
- [265] K. Kalyanasundaram, *Photochemistry of Polypyridine and Porphirin Complexes*, Academic Press, London, **1992**.
- [266] W. Buchler J, *Porphyrins and Metalloporphyrins*, Elsevier, Amsterdam, **1975**.
- [267] D. K. Lavalley, *The Chemistry and Biochemistry of N-Substituted Porphyrins*, VCH Publishers: Weinheim, **1987**.
- [268] Y. Song, R. E. Haddad, S. L. Jia, S. Hok, M. M. Olmstead, D. J. Nurco, N. E. Schore, J. Zhang, J. G. Ma, K. M. Smith, S. Gazeau, J. Pycaut, J. C. Marchon, C. J. Medforth, J. A. Shelnut, *Journal of the American Chemical Society* **2005**, 127, 1179.
- [269] J. L. Retsek, C. M. Drain, C. Kirmaier, D. J. Nurco, C. J. Medforth, K. M. Smith, I. V. Sazanovich, V. S. Chirvony, J. Fajer, D. Holten, *Journal of the American Chemical Society* **2003**, 125, 9787.
- [270] R. H. Felton, *The Porphyrins, Vol. 5*, Academic Press, New York, **1978**.
- [271] J. H. Fuhrhop, K. M. Kadish, D. G. Davis, *Journal of the American Chemical Society* **1973**, 95, 5140.
- [272] R. H. Felton, N. T. Yu, D. C. O'Shea, J. A. Shelnut, *Journal of the American Chemical Society* **1974**, 96, 3675.
- [273] K. M. Kadish, M. M. Morrison, *Inorganic Chemistry* **1976**, 15, 980.
- [274] K. M. Kadish, M. M. Morrison, *Bioinorganic Chemistry* **1977**, 7, 107.
- [275] F. A. Walker, D. Beroiz, K. M. Kadish, *Journal of the American Chemical Society* **1976**, 98, 3484.
- [276] L. Latos-Grazynski, R. J. Cheng, G. N. La Mar, A. L. Batch, *Journal of the American Chemical Society* **1982**, 104, 5992.
- [277] O. H. W. Kao, J. H. Wang, *Biochemistry* **1965**, 4, 342.
- [278] W. W. Parson, B. Ke, *Photosynthesis: Energy Conversion by Plants and Bacteria*, Academic Press, New York, **1983**.
- [279] H. B. Dunford, J. S. Stillman, *Coordination Chemistry Reviews* **1976**, 19, 187.
- [280] A. L. Balch, G. N. La Mar, L. Latos-Grazynski, M. W. Renner, V. Thanabal, *Journal of*

- the American Chemical Society* **1985**, 107, 3003.
- [281] J. T. Groves, R. Quinn, T. J. McMurry, M. Nakamura, G. Lang, B. Boso, *Journal of the American Chemical Society* **1985**, 107, 354.
- [282] R. H. Felton, G. S. Owen, D. Dolphin, J. Fajer, *Journal of the American Chemical Society* **1971**, 93, 6332.
- [283] R. H. Felton, G. S. Owen, D. Dolphin, A. Forman, D. C. Borg, J. Fajer, *Annals of the New York Academy of Sciences* **1973**, 206, 504.
- [284] M. A. Phillippi, H. M. Goff, *Journal of the American Chemical Society* **1979**, 101, 7641.
- [285] M. A. Phillippi, H. M. Goff, *Journal of the American Chemical Society* **1982**, 104, 6026.
- [286] A. S. Hinman, B. J. Pavelich, *Journal of Electroanalytical Chemistry* **1989**, 269, 53.
- [287] A. Wolberg, J. Manassen, *Journal of the American Chemical Society* **1970**, 92, 2982.
- [288] D. Kim, L. A. Miller, G. Rakhit, T. G. Spiro, *Journal of Physical Chemistry* **1986**, 90, 3320.
- [289] K. M. Kadish, K. M. Smith, R. Guilard, *The Porphyrin Handbook, Vol. 1-3*, Academic press, **2000**.
- [290] I. B. Sivaev, D. Gabel, D. J. Wohrle, **2001**, 5, 767.
- [291] J. P. Collman, P. S. Wagenknecht, J. E. Hutchison, *Angewandte Chemie - International Edition in English* **1994**, 33, 1537.

Chapter 2

Introduction to electrocatalysis of oxygen reduction

2.1 Oxygen reduction catalysis for future energy resource

The tremendous consumption of fossil fuels emitting carbon dioxide (CO₂) is a serious factor contributing to the green-house effect. It is important to recognize that global warming is closely related to energy resources, and further, that the main energy resource, oil, could be exhausted by the mid-21st century. Consequently, the need to create renewable energy resources free of environmental pollution is urgent. For example, wind power plants and solar cells are attracting attention as candidates to create renewable energy in the near future. It is important that any new energy resource be compatible with the energy cycle on the earth. The main energy cycles, both of living things and fossil fuels, are supported by photosynthesis that utilizes solar energy. In this sense, artificial photosynthesis, which aims at creating energy resource from solar energy and water, is a promising candidate.^[1-4] In addition to the artificial photosynthesis, a fuel cell (FC) is expected to be one of the most promising energy resources in the next generation. In an FC electric energy can be obtained from chemical energy (fuel), such as H₂, methanol from carbon dioxide, natural gas, or gasoline. Hydrogen fuelled proton exchange membrane fuel cells have demonstrated great promise as future source of energy due to their high conversion efficiency, lower temperature of operation and lack of greenhouse emissions.

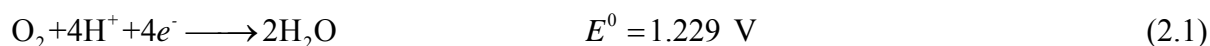
2.2 Oxygen reduction

2.2.1 Reaction pathway

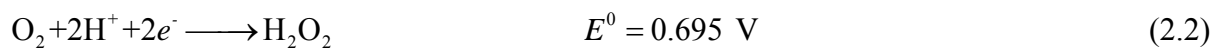
Oxygen reduction reaction (ORR) process includes several individual reactions depending on the electrode material (Scheme 2.1). For electrochemical catalytic ORR analysis, two general processes can take place; each containing few discrete steps. One is production of water through a direct four-electron pathway, and the other is production of hydrogen peroxide

through a two-electron pathway. The desired feature for a successful ORR catalyst would reduce oxygen molecules to water through the four-electron route. Incomplete reduction of oxygen to hydrogen peroxide not only leads to low energy conversion efficiency, but also produces this reactive intermediate that can further convert to harmful free radical species.

Direct four electron pathway



Peroxide pathway



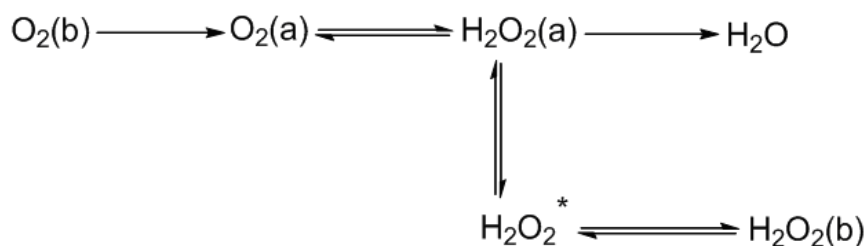
Which can be followed by



Or by the decomposition reaction

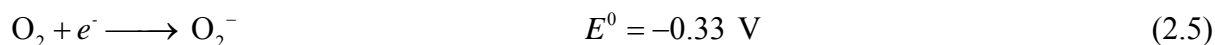


In general the following over-all scheme is given for this reaction:^[1, 2]

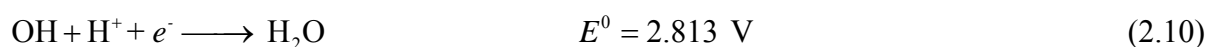
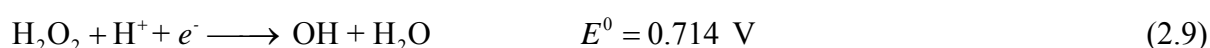
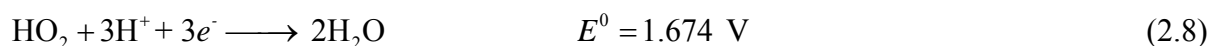
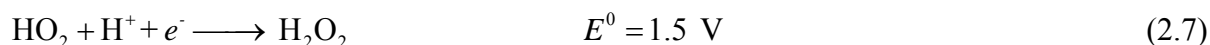


Scheme 2.1: The reaction pathway for oxygen reduction reaction

In which indicates a,* and b mean adsorbed species, vicinity of the electrode and bulk respectively. The reduction following the peroxide pathway (2.2) can, if reaction (2.3) also 100% efficiently happens, of course give the same result as the direct four electron pathway will be governed by the equilibrium between the adsorbed H_2O_2 and the $H_2O_2^*$ and the rate of hydrogen peroxide reduction. If hydrogen peroxide is reduced before it is desorbed no difference will be noticed with the four electron pathway. However, any hydrogen peroxide that will come into solution will be corrosive towards the carbon support material and the metal chelate. In the absence of adsorption effects the following intermediate steps can occur; The formation of the superoxide-ion



And

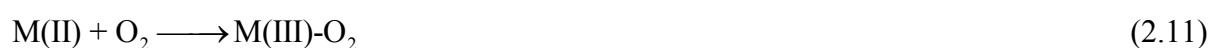


The standard potentials are values vs the normal hydrogen electrode (NHE) at 25°C.^[3] The oxygen molecule has a bond strength corresponding to $\Delta H_f^0 = -498.7 \text{ kJ mole}^{-1}$.^[4] Compared with the C-C bond ($-160 \text{ kJ mole}^{-1}$), it is clear that O-O bond breaking is a major problem and that reduction process must be activated. In case of the superoxide-ion, the O-O bond strength is considerably lowered to approximately $-350 \text{ kJ mole}^{-1}$.^[4] The formation of the superoxide-ion O_2^- is considered to be the rate determining step^[5, 6] in the oxygen reduction and

specially this step is catalysed if oxygen accepting sites are present on the electrode surface. A multi-electron transfer is kinetically slow as it requires many steps, which suggests that a highly efficient and active catalyst site is required, and Pt and its colloidal particles are the most active and efficient catalysts for both O₂ reductions.^[7, 8] Till now Pt has been found to be the best electrocatalyst for the oxygen reduction reaction (ORR) due to higher electrocatalytic activity and stability. But the limitation is due to high costs incurred. In recent years lot of emphasis has been put on Pt alloy catalysts because of even higher activity and lower cost as compared to Pt catalysts.^[9, 10] However, the activity of a Pt catalyst often changes with the preparation method, because the activity strongly depends on the particle size and effective area of the catalyst. Since it is important to use efficient and stable catalysts for energy conversion, the application of such an unstable catalyst to the energy supply system is not desired. Pt is a rare, precious material, so that it is highly desirable to design and develop a new catalyst system to replace Pt, especially by means of molecular catalysts.

2.2.2 The redox mechanism

Oxygen binding involves binding with the d-orbitals of the central metal-ion and is of course influenced by the electron density on the metal center. The mechanism of the oxygen reduction, forming hydrogen peroxide, is commonly supposed to follow the redox pathway (acid medium).^[11]



Or, with minor difference,^[12]



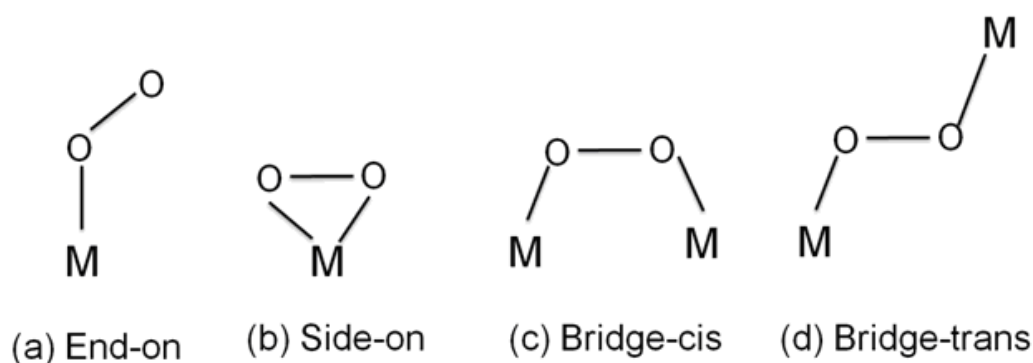


In which the M(II) is the oxygen accepting site. If such a redox-mechanism is involved, the $\text{M}^{\text{III}}/\text{M}^{\text{II}}$ redox transition will be determining for the activity. The redox potential depends on the type of central metal ion, and will be influenced by an eventual fifth ligand (*e.g.* carbon surface group), and by the nature of the ligand, including side-chains.^[12] Here the redox transition of the iron chelates is too cathodic for high activity (too stable Fe^{III}) whereas the cobalt chelates have transitions at too high potentials for optimal activity (too stable Co^{II}). Such a Volcano relation between the redox potential and the electrocatalytic activity has also been found for other reactions, as, for example, the oxidation of hydrazine and cysteine.^[13] A study of different phthalocyanines (Pcs) revealed that the high electron density on the cobalt center, the higher is the observed catalytic activity for the oxygen reduction.^[14] The redox mechanism requires the stability of the 3+ and 2+ oxidation state of a metal, needed for oxygen activation, in the potential region of interests for the oxygen reduction. It has been found that Co and Fe porphyrins are active as long as the 3+ oxidation state is possible at given potential.^[15] Although in most cases the M(II) site is assumed to be the oxygen-accepting site (2.11)^[16] and $\text{M}^{\text{III}}/\text{M}^{\text{II}}$ transition is thought govern the reaction (2.11-2.16).

2.2.3 Molecular oxygen interaction with metal sites

In the case of M-N_4 chelates, the interaction between the metal and the nitrogen can be described as a σ -coordination of nitrogen lone pairs towards the metal and a π -back donation between metal $d\pi$ -orbitals with nitrogen $p\pi$ -orbitals.^[13] The mixing between the $d\pi$ orbitals on the metal and the p orbitals on the nitrogen provide a mechanism for back-bonding charge transfer from the metal to the ring, diminishing the electron density at the metal. The coordination around the metal ion gives rise to splitting of the d-orbital energy levels. The smaller the ring size, and consequently the shorter the metal nitrogen distances, the larger the ligand field effect (the phthalocyanine ring is larger than the porphyrin ring).^[13]

Various adsorption configurations of oxygen on metal sites given in Scheme 2.2. Different models, Zagal *et al.*^[17] postulated that the rupture of O-O bond leads to formation of water when oxygen interacts simultaneously with two active sites on the electrode surface (in the case of cofacial porphyrins). This favourable adopted oxygen-catalyst interaction is called ‘bridge cis’ illustrated in Scheme 2.2. Other single site interactions lead to two electron transfer resulting in formation of hydrogen peroxide and they are ‘end-on, side-on and bridge-trans’ (Scheme 2.2). Since degree of oxygen reduction completeness depends on the interaction of oxygen with the catalytic site, it is therefore expected that an adduct formed upon such an interaction should be long-lived. It follows also that the interaction is more likely to be successful when there is a high concentration of catalyst on the electrode surface.



Scheme 2.2: Different configurations adopted by molecular oxygen upon interaction with metal sites.

2.3 Fuel cell: reduction of O₂

Among FCs, the polymer electrolyte membrane fuel cell (PEMFC) shown schematically in Figure 2.1, has been considered to be the most promising candidate as a new energy resource, since PEMFC is expected to achieve a high power efficiency in a compact size.^[7] In this scheme, (1) H₂ is oxidized into H⁺ on the anode, (2) The H⁺ is then transported to the cathode through a H⁺ conducting polymer electrolyte membrane such as Nafion (Nf) and (3) O₂ is reduced via a multi-electron transfer. Both the basic science and the technology of catalytic O₂ reduction has received much attention in the last three decades. The O₂ reduction must be coupled with a H⁺ supply from the anode. As a strategy for fabricating O₂ an efficient FC

cathode, the investigation of O₂ reduction by a molecular catalyst should essentially be carried out using a H⁺ exchangeable polymer membrane with a high O₂ permeability.

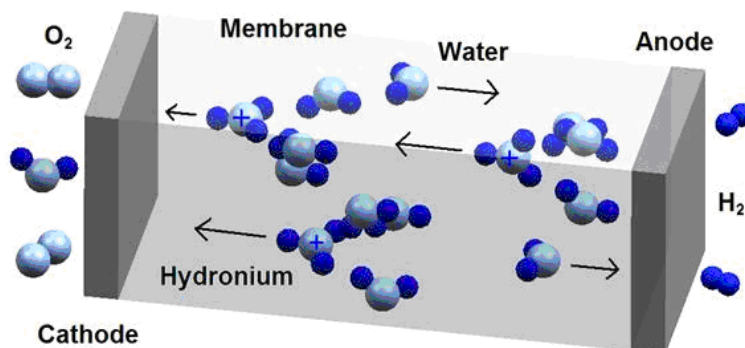


Figure 2.1: Schematic illustration of PEMFC.

2.4 Metal catalysts

Although great efforts to design and develop new active catalysts have been made, there have been few examples of efficient molecule-based catalyst capable of four-electron reduction of O₂. The pioneering molecular catalysts of macrocyclic metal complexes (phthalocyanines, porphyrins, etc.)^[18-21] are still insufficient as far as both activity and stability concerned, so that the improvement of the catalysis performance is still a continuous research subject. Molecular catalysts for O₂ reduction will be described compared with metal catalysts.

2.4.1 Pt catalyst

Fuel cells are widely considered to be a sustainable energy conversion system and are a key technology for the development of a hydrogen economy. Low-temperature fuel cells have been undergoing rapid development for mobile applications and in particular for the transport sector. Platinum is commonly used as anode and cathode catalyst in low-temperature fuel cells. The cost of platinum, however, and the limited world supply are significant barriers to the widespread use of these types of fuel cells. To reduce the cost of the fuel cells, one of the important challenges is the development of platinum-free catalysts or catalysts with a lower content of Pt.

Platinum is used as an electrocatalyst for oxygen reduction in phosphoric acid fuel cells and proton exchange membrane fuel cells. Because catalysis is a surface effect, the catalyst needs to have the highest possible surface area. So, the active phase is dispersed on a conductive support such as high surface area carbon powders. But because of the elevated price and limited resources, Pt cannot be used for large-scale applications and alternative materials are needed. In addition, platinum used as anode material, at room or moderate temperatures is readily poisoned by carbon monoxide, present in the reformat gas used as H₂ carrier. Moreover, Pt alone does not present satisfactory activity for the oxygen reduction reaction (ORR) when used as cathode material. For all these reasons, binary and ternary Pt-based catalysts and nonplatinum-based catalysts have been tested as electrode materials for low temperature fuel cells.^[8, 22, 23] In the early 1990s, several binary Pt alloy systems such as PtNi, PtCo, and PtCr in small-scale fuel cells investigated to characterize kinetic parameters complemented by several X-ray techniques to examine lattice parameters, stability, and the nature of surface species.^[24, 25] It has been observed that the base-metal elements smaller than Pt, when alloyed with Pt, enter the crystal structure through substitution and cause a lattice contraction. The increasing electrocatalytic activity of the Pt-alloys (such as PtCr, PtV, PtTi, PtW, PtAl, PtAg) show a strong correlation with a decrease in interatomic or nearest-neighbor distance between Pt atoms.^[26] This effect has been attributed to the smaller Pt–Pt bond distances resulting in more favorable sites that enhance the dissociative adsorption of oxygen. There have been several attempts made to hypothesize the or at least draw strong correlations between the enhanced activity of Pt-alloys over Pt that may be broadly classified as structural factors, inhibition by anion adsorption, electronic factors, and surface sensitive factors.

Although Pt catalysis is old, it remains the current catalyst most capable of an efficient four-electron transfer reduction of O₂ into H₂O. Nafion (Nf) composed of a hydrophobic region based on the perfluorocarbon polymer backbone, and a hydrophilic region based on sulfonic acid side chain,^[27] is a typical proton-conductive membrane used in PEMFC. A catalyst system composed of Pt and Nf is a typical model as the FC cathode to reduce O₂. The Nf enhances the stability and dispersibility of Pt particles, showing a reproducible electrochemistry when used as an electrode-coated material.^[28] Pt microparticles deposited in a Nf membrane were oxidized to the PtO species under anodic conditions (> 0.5V vs. SCE),

and it was found that the oxide surface catalyzed the two-electron reduction of O_2 into H_2O_2 . However, when PtO was reduced to Pt by applying the potential of (0 V vs. SCE) prior to O_2 reduction, no formation of H_2O_2 occurred, but four-electron reduction of O_2 proceeded on the 'pure' Pt surface. The schematic illustration of the O_2 reduction at the PtO-covered Pt particles is shown in Figure 2.2.

It is important to elucidate the characteristics of the electrode (and/or catalyst)/membrane interface to establish an efficient PEMFC cathode. As for this, catalytic O_2 reduction at Pt black embedded in a Nf membrane was studied.^[29] An O_2 reduction at the interface between a Nf membrane and electrochemically oxidized glassy carbon electrode (GC) was also studied.^[30] The design and development of electrode (and/or catalyst)/membrane interface composed of a kinetically efficient catalyst and a highly adjustable site of O_2 will be one of key subjects to establish a practical FC cathode.

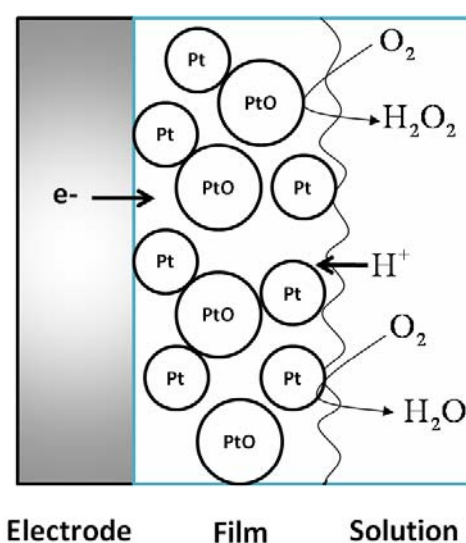


Figure 2.2: Schematic view of mechanism of dioxygen reduction at PtO covered Pt particle-deposited GC electrodes.

Okada *et al.* have exhibited that a small amount of impurity cation (Li^+ , Na^+ , K^+ , Ca^{2+} , Fe^{3+} , Ni^{2+} and Cu^{2+}) remarkably influences the O_2 reduction kinetics at a Pt/Nf interface.^[31] The kinetic current for charge transfer of O_2 reduction was found to decrease about 40 , 60% when compared with that for a pure membrane. Such suppression by impurity cations was not

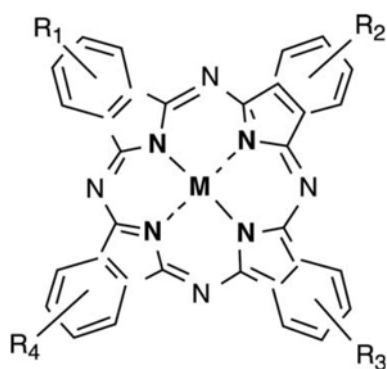
observed at Pt/electrolyte solution interface. They ascribed such a specific event at Pt/Nf interface to a modification of electronic double layer, originating from a reorientation of the polymer network (change of polymer flexibility) in the presence of the impurity. A highly dispersed Pt/WO₃/C was applied to O₂ reduction, for comparison with a Pt/C system.^[32] Although WO₃ is an acid resistant oxide, the partially dissolved species from the oxide acts as a homogeneous catalyst to decompose H₂O₂ in an O₂ reduction process, consequently leading to higher activity with Pt/WO₃/C than with Pt/C. Dissolution and diffusion of the WO₃ into bulk electrolyte can be suppressed by a Nf coating on the Pt/WO₃/C.

2.4.2 Macrocyclic metal complexes catalysts (phthalocyanines and porphyrins)

Research into ORR catalysts based on non-noble metals began in 1964, when Jasinski found that cobalt phthalocyanine was an active catalyst for the reduction of oxygen^[33] and has greatly proliferated since. Soon after Jasinski's finding, catalysts were prepared by adsorbing similar FeN₄ and CoN₄ macrocycles on a carbonaceous support and pyrolyzing the resulting material in an inert atmosphere^[34]. Then, a major breakthrough was achieved when it was demonstrated that these often-expensive macrocycles could be substituted by individual N and Co precursors.^[35] This approach was followed by several groups.

2.4.2.1 Metallo-phthalocyanines

Metal phthalocyanines (MPc) and their sulfonated derivatives (MTsPc), where the central metal is often Co and Fe (the chemical structures are shown in Scheme 2.3), have been known as pioneering molecule based catalysts for O₂ reduction. The effectiveness of these complexes has been discussed in terms of a molecular orbital theory.^[36] The cobalt(II) phthalocyanine tetrasulfonic acid (CoPcs) work as a two-electron reduction catalyst yielding H₂O₂, while FePcs are capable of four-electron reduction of O₂ into H₂O, although the catalysis features change with the degree of the overpotentials applied, as well as the pH conditions employed.^[31, 37, 38]

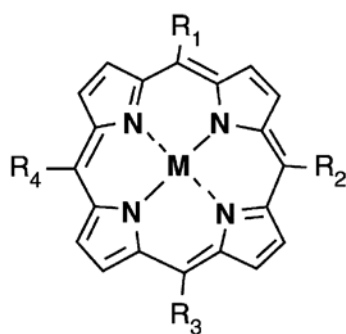


Scheme 2.3: Chemical structures of metal phthalocyanine.

Especially when applying low overpotentials for FePc, the four electron reduction is attributed to dimeric species formation on a rough electrode surface.^[38, 39] However, in these phthalocyanine catalyst systems, it has been recognized that a mono-layered deposition of the complex (i.e. the electrode/catalyst interface) is the most effective for the catalysis (when a thick-layered MPc was deposited onto the electrode, only a small fraction was effective).^[40] The extremely poor electron conductivity of MPcs has seriously obstructed the developments of a new and efficient catalyst system. In order to overcome the inefficient electroactivity, a conductive organic polymer was employed as a matrix.

2.4.2.2 Metallo-porphyrins

Co porphyrin (CoP) and its derivatives (see Scheme 2.4) have often exhibited two-electron reduction catalysis for O₂. Anson *et al.* have shown that coordination of Ru(NH₃)₅³⁺ to the pyridyl (Py) sites in cobalt tetrapyrridylporphyrin (CoP(Py)₄) adsorbed on an electrode converts the catalysis performance from two-electron to four-electron reduction (selectivity of H₂O formation was over 90% below +0.2 V vs. SCE).^[41] The four-electron reduction of O₂ by the simplest Co porphine adsorbed on an electrode was found to take place on applying an unusually positive potential of ~ +0.5 V, although H₂O₂ formation also occurred at relatively low potentials.^[42] It was likely that the H₂O formation originates from a dimer complex, cofacially orientated through Van der Waals interaction. However, since most part of the ‘cofacial structure’ changed into a monomeric species after the catalytic O₂ reduction, the selectivity for H₂O formation remarkably decreased from >90 to ~35% .



Scheme 2.4: Chemical structures of metal porphyrin.

When gold electrode coated with the β -cyclodextrin film containing cobalt porphyrin, H_2O_2 is the only product from O_2 , probably because the formation of a dimeric structure that be responsible for a four-electron transfer reduction of O_2 is suppressed, due to the formation of a supramolecular complex between the cyclodextrin polymer and the porphyrin. The Co ‘Picket Fence’ Porphyrin (cobalt 5,10,15,20-tetrakis(pivalamidophenyl) porphyrin) has been applied to O_2 reduction system.^[43] The ‘Pickets’ appended on one side of porphyrin ring results in unusually high affinity for O_2 in the presence of an axial base (such as 1-methylimidazole). However, the existence of the ‘Picket’ causes hindrance of its catalysis towards O_2 reduction, most probably due to the difficulty of dimeric formation ($\text{Co-O}_2\text{-Co}$). Hematoporphyrin IX and Protoporphyrin IX were efficiently immobilized on a cellulose/ titanium (IV) oxide composite fiber surface by the reaction of $-\text{COOH}$ group on the porphyrin with TiO_2 , presumably by forming the $-\text{COO-Ti}$ chemical bond.^[44] Each complex acts as a catalyst for two electron transfer reduction of O_2 , indicating that it is difficult to achieve efficient four-electron reduction in mono-molecularly orientated system. New catalyst films of meso-tetrakis [2,2]-paracyclophanyl metalloporphyrin complexes (MT(PCP)P) with Mn(II), Fe(II), Ni(II), and Co(II) were synthesized by oxidative electropolymerization of cyclophanyl groups in EtCl_2 .^[45] Each MT(PCP)P exhibited efficient catalytic performance for the four-electron O_2 reduction in both acidic and basic media, most probably due to transannular interaction between porphyrin core and cyclophane. Murray *et al.* have reported electrocatalytic O_2 reduction using amino-, pyrrole-, and hydroxy-substituted tetraphenyl metallo-porphyrins.^[46]

2.4.2.3 Cofacial metallocomplexes

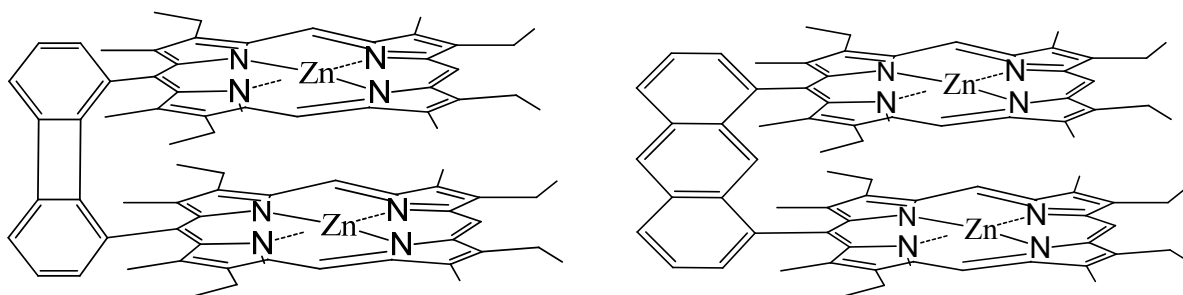
Cofacial bis(metallo)porphyrins (Scheme 2.5) were initially prepared to study the interaction between closely lying electroactive centers such as in the case of cytochromes,^[47, 48] to obtain multi-electron transfer,^[49] or to find new catalysts for the reduction of small substrate molecule such as O₂.^[50]

Catalytic activity in these systems can be easily detected with cyclic voltammetry (CV) or rotating disk electrode voltammetry (RDE).^[51, 52] In the case of CV, a comparison of the current-voltage curves obtained for the substrate with a bare electrode and with an electrode modified with the cofacial bis(metallo)porphyrin will suffice to demonstrate catalytic activity. Higher current density and a decrease in the substrate overpotential when using the modified electrode are reliable indicators that the cofacial complex catalyzes the reduction or the oxidation of the substrate.^[50] RDE is also very useful in that it provides more information about the kinetics of the catalytic process. In addition, rotating ring-disk electrode (RRDE) voltammetric experiments^[52] help to gain insight into the electrochemical nature of the intermediary and final products of the catalytic reaction.

This method study the number of the electrons donated to O₂. In studying oxygen reduction mediated by porphyrins, the technique of rotating ring-disk voltammetry, which permits the quantitative measurement of hydrogen peroxide production and allows discrimination between the formation of such peroxide as an intermediate or merely as a minor side product. The porphyrin to be tested as a reduction catalyst is applied to the graphite disk by irreversible adsorption from a dilute solution.^[53] As the assembly is rotated, fresh, oxygen-saturated electrolyte is drawn vertically toward the disk surface and ejected radially across the disk and ring. The disk potential is controlled by a potentiostat and the (disk) current-potential profile records the oxygen reduction process. At the same time, the ring is held at a potential (+1.4 V) where any hydrogen peroxide reaching it is rapidly oxidized to dioxygen but no other electrode reactions proceed. The ring current response thus monitors hydrogen peroxide production, and the ratio of disk to ring currents, normalized for the collection efficiency, of the ring, defines the relative contributions of the four-electron and two-electron reduction processes. Moreover, possible contributions to the disk current arising from subsequent reactions of H₂O₂ (reduction to water or disproportionation to water and dioxygen) may be

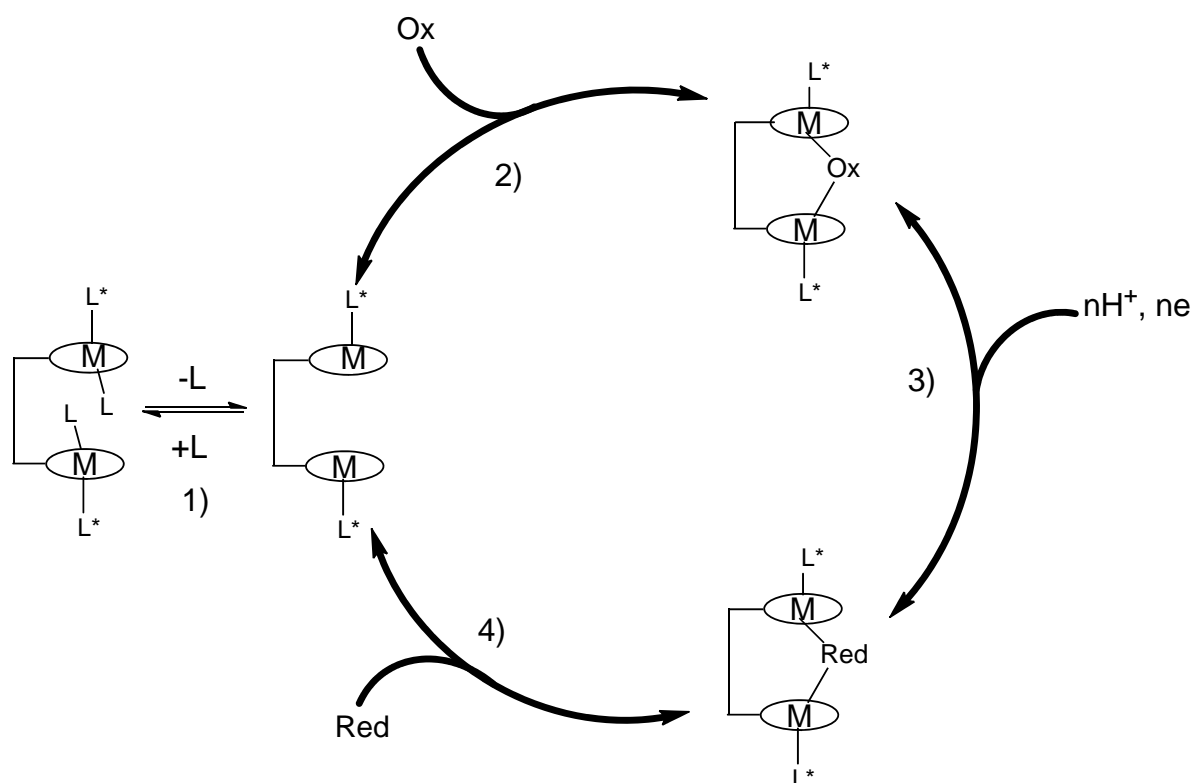
evaluated by examining the dependence of the current ratio on electrode rotation rates. At higher rotation rates, H_2O_2 is removed from the disk surface before further reaction can take place, resulting in an increased ring current and decreased disk current. Invariance of the current ratio with rotation rate indicates the H_2O_2 is formed only as a parallel product in dioxygen reduction, not as an intermediate.^[54]

Electrochemical studies of cofacial porphyrins led to the conclusion that the rigidity and length of the spacer or linker between the two porphyrin units play a major role in how good a catalyst the cofacial complex is. If the spacer is too flexible, the two porphyrins do not adopt a face-to-face configuration.^[55] Indeed, X-ray data revealed that the two units are laterally shifted with respect to each other to maximize π — π overlap. If the two porphyrin units are too tightly linked to each other, the geometry of the cavity where the binding of the substrate occurs is not flexible enough to accommodate the structural changes that will take place during the catalytic process



Scheme 2.5: Examples of cofacial bis(metallo)porphyrins.

If the linker is too long, communication between the two chromophores is absent. Anthracene and biphenylene linkers optimize this length/ rigidity compromise.^[56] A proposed overall catalytic process is schematically represented in Scheme 2.6.



Scheme 2.6: Cofacial bis(metallo)porphyrins as electrocatalysts. 1) Formation of the active site; 2) and 4) substrate binding or product release; 3) multielectron transfer. L^* .bulky ligand blocking the outer coordination sites (solvent molecule or imidazole, for example); L .smaller ligand that can be displaced by the substrate.

The latter case exemplifies the use of electrochemistry as an effector of supramolecular events and as a detection technique. The substrate binding, which allows for the catalytic activity is controlled by the redox state of the substrate. The release of the product, on the other hand, from the cofacial bis(metallo)porphyrin is also redox-controlled.

2.5 Oxygen reduction at liquid | liquid interfaces

Oxygen reduction catalyzed by porphyrins is of great interest in fields as diverse as biology, photosynthesis and electrocatalysis.^[57, 58] In nature, oxygen reduction occurs at soft interfaces, namely biomembranes that provide both a physical separation of the reactants and products,

and an electrochemical driving force resulting from the membrane electrical potential difference. Electrochemistry at liquid|liquid interfaces is a new type of bio-inspired electrochemistry. Indeed, ITIES also provide a physical separation of the reactants and products and the polarization of this soft interface provides an electrochemical control for different charge transfer reactions such as ion transfer, assisted ion transfer such as acid-base reactions involving an interfacial protonation or heterogeneous electron transfer reactions between an hydrophilic and a lipophilic redox couple.^[59-61] The interface between two immiscible electrolyte solutions is formed between two solvents of a low mutual miscibility, such as water and 1,2-DCE, each containing an electrolyte. This type of electrochemistry without a solid working electrode provides a suitable model for investigating heterogeneous processes occurring in biological systems such as oxygen reduction reactions within aerobic living organisms. Oxygen reduction at the ITIES has been studied by using various lipophilic electron donors, decamethylferrocene (DMFc),^[62-67] reduced flavin mononucleotide (FMN),^[68] tetrachloroquinone (CQH₂)^[69] and fullerene monoanion (C₆₀⁻).^[70] In the case of DMFc, the oxygen reduction produces H₂O₂, as evidenced by two-phase reactions^[65] and *in-situ* detection of H₂O₂ using scanning electrochemical microscopy.^[66] Furthermore, the catalytic effect of various porphyrin compounds including cobalt tetraphenylporphyrin^[64, 67] on the oxygen reduction by DMFc at the water|1,2-DCE interface has also been investigated. The interfacial reduction of oxygen catalyzed by a metalloporphyrin, *e.g.* Co(II) porphine has been reported. Recently the catalytic effect of the protonated forms of 5,10,15,20-tetraphenyl-21H,23H-porphine (H₂TPP)^[71] and metalloporphyrin, *e.g.* Co(II) porphine^[72] on the oxygen reduction at the polarized water|1,2-DCE interface has been reported.

2.6 References

- [1] K. L. Hsueh, D. T. Chin, S. Srinivasan, *Journal of Electroanalytical Chemistry* **1983**, 153, 79.
- [2] H. S. Wroblowa, P. Yen Chi, G. Razumney, *Journal of Electroanalytical Chemistry* **1976**, 69, 195.
- [3] J. P. Hoare, *Standard potentials at aqueous solutions* **1985**.
- [4] F. V. D. Brink, W. Visscher, E. Barendrecht, *Recueil des Travaux Chimiques des Pays-Bas* **1980**, 99, 253.
- [5] E. Yeager, *Electrochimica Acta* **1984**, 29, 1527.
- [6] V. Mohan Rao, H. Manohar, *Inorganic and Nuclear Chemistry Letters* **1980**, 16, 499.
- [7] Kinoshita.K, *Electrochemical oxygen technology*, Wiley, New York, **1992**.
- [8] J. Kiwi, M. Gratzel, *Journal of the American Chemical Society* **1979**, 101, 7214.
- [9] H. A. Gasteiger, S. S. Kocha, B. Sompalli, F. T. Wagner, *Applied Catalysis B: Environmental* **2005**, 56, 9.
- [10] M. Teliska, V. S. Murthi, S. Mukerjee, D. E. Ramaker, *Journal of the Electrochemical Society* **2005**, 152, A2159.
- [11] F. Beck, *Journal of Applied Electrochemistry* **1977**, 7, 239.
- [12] J. A. R. van Veen, J. F. van Baar, C. J. Kroese, J. G. F. Coolegem, N. de Wit, H. A. Colijn, *Berichte der Bunsengesellschaft/Physical Chemistry Chemical Physics* **1981**, 85, 693.
- [13] J. H. Zagal, *Coordination Chemistry Reviews* **1992**, 119, 89.
- [14] J. Zagal, M. Paez, A. A. Tanaka, J. R. dos Santos Jr, C. A. Linkous, *Journal of Electroanalytical Chemistry* **1992**, 339, 13.
- [15] E. Theodoridou, A. D. Jannakoudakis, P. D. Jannakoudakis, S. Antoniadou, J. O. Besenhard, **1992**, 22, 733.
- [16] C. Hinnen, F. Coowar, M. Savy, *Journal of Electroanalytical Chemistry* **1989**, 264, 167.
- [17] J. H. Zagal, M. A. Paez, J. F. Silva, *N4-macrocyclic metal complexes*, Springer, New York, **2006**.
- [18] J. P. Randin, *Electrochimica Acta* **1974**, 19, 83.
- [19] A. J. Appleby, J. Fleisch, M. Savy, *Journal of Catalysis* **1976**, 44, 281.
- [20] F. Beck, *Journal of Applied Electrochemistry* **1977**, 7, 239.
- [21] J. Zagal, P. Bindra, E. Yeager, *Journal of the Electrochemical Society* **1980**, 127, 1506.
- [22] M. Yagi, M. Kaneko, *Chemical Reviews* **2001**, 101, 21.
- [23] A. Fujishima, K. Honda, *Nature* **1972**, 238, 37.
- [24] S. Mukerjee, S. Srinivasan, *Journal of Electroanalytical Chemistry* **1993**, 357, 201.
- [25] S. Mukerjee, S. Srinivasan, M. P. Soriaga, *Journal of Electrochemical Society* **1995**, 142, 1409.
- [26] V. Jalan, E. J. Taylor, *Journal of Electrochemical Society* **1983**, 130, 2299.
- [27] Lowry.S, Mauritz.K, *Journal of American Chemical Society* **1980**, 102, 4065.
- [28] C. R. Martin, I. Rubinstein, A. J. Bard, *Journal of the American Chemical Society* **1982**, 104, 4817.
- [29] J. Premkumar, R. Ramaraj, *Journal of Solid State Electrochemistry* **1997**, 1, 172.
- [30] H. M. Saffarian, R. Srinivasan, D. Chu, S. Gilman, *Journal of the Electrochemical Society* **2001**, 148, A559.

- [31] J. Maruyama, I. Abe, *Journal of Electroanalytical Chemistry* **2002**, 527, 65.
- [32] T. Okada, Y. Ayato, H. Satou, M. Yuasa, I. Sekine, *Journal of Physical Chemistry B* **2001**, 105, 6980.
- [33] R. Jasinski, *Nature* **1964**, 201, 1212.
- [34] J. P. Dodelet, J. H. Zagal, F. Bedioui, *N4-Macrocyclic Metal Complexes*, Springer, New York **2006**.
- [35] S. Gupta, D. Tryk, I. Bae, W. Aldred, E. Yeager, *Journal of Applied Electrochemistry* **1989**, 19, 19.
- [36] Z. Sun, H. C. Chiu, A. C. C. Tseung, *Electrochemical and Solid-State Letters* **2001**, 4, E9.
- [37] J. Zagal, M. Paez, A. A. Tanaka, J. R. dos Santos, C. A. Linkous, *Journal of Electroanalytical Chemistry* **1992**, 339, 13.
- [38] A. Van Der Putten, A. Elzing, W. Visscher, E. Barendrecht, *Journal of Electroanalytical Chemistry* **1986**, 214, 523.
- [39] A. Elzing, A. Van Der Putten, W. Visscher, E. Barendrecht, *Journal of Electroanalytical Chemistry* **1987**, 233, 99.
- [40] A. Elzing, A. van der Putten, W. Visscher, E. Barendrecht, *Journal of Electroanalytical Chemistry* **1986**, 200, 313.
- [41] B. Steiger, C. Shi, F. C. Anson, *Inorganic Chemistry* **1993**, 32, 2107.
- [42] C. Shi, B. Steiger, M. Yuasa, F. C. Anson, *Inorganic Chemistry* **1997**, 36, 4294.
- [43] B. Steiger, F. C. Anson, *Inorganic Chemistry* **2000**, 39, 4579.
- [44] S. L. P. Dias, Y. Gushikem, E. S. Ribeiro, E. V. Benvenuti, *Journal of Electroanalytical Chemistry* **2002**, 523, 64.
- [45] J. E. Bennett, A. Burewicz, D. E. Wheeler, I. Eliezer, L. Czuchajowski, T. Malinski, *Inorganica Chimica Acta* **1998**, 271, 167.
- [46] A. Bettelheim, B. A. White, S. A. Raybuck, R. W. Murray, *Inorganic Chemistry* **1987**, 26, 1009.
- [47] Shwartz.F, Gouterman.M, Muljiani.Z, Dolphin.D, *Bioinorganic.Chemistry* **1972**, 2, 1.
- [48] Ogoshi.H, Sugimoto.H, Yoshida.Z, *Tetrahedron Letters* **1977**, 2, 169.
- [49] Collman.J.P, Denisevich.P, Konai.Y, Marrocco.M, Koval.C, Anson.F.C, *Journal of the American Chemical Society* **1980**, 102, 6027.
- [50] Collman.J.P, Wagenknecht.P, Hutchison.J, *Angewandte Chemie* **1994**, 106, 1620.
- [51] L. Mest.Y, Her.M.L, Hendricks.N.H, Kim.K, Collman.J.P, *Inorganic Chemistry* **1992**, 31, 835.
- [52] Thirsk.H.R, Harrison.J.A, *Guide to the Study of Electrode Kinetics*, Academic Press, New York, **1972**.
- [53] A. P. Brown, C. Koval, F. C. Anson, *Journal of Electroanalytical Chemistry* **1976**, 72, 379.
- [54] A. Damjanovic, M. A. Genshaw, J. O'M Bockris, *The Journal of Chemical Physics* **1966**, 45, 4057.
- [55] Fillers.J, Ravichandran.K, Abdalmuhdi.I, Tulinsky.A, K.Chang.C, *Journal of the American Chemical Society* **1986**, 108, 417.
- [56] Collman.J.P, Hutchison.J.E, Lopez.M.A, Guillard.R, *Journal of the American Chemical Society* **1992**, 114, 8066.
- [57] R. Boulatov, *N4-Macrocyclic Metal Complexes, Vol. 1*, Springer, New York, **2006**.

- [58] J. H. Zagal, M. A. Paez, J. F. Silva, *N4-Macrocyclic Metal Complexes, Vol. 2*, Springer, New York, **2006**.
- [59] F. Reymond, D. Fermin, H. J. Lee, H. H. Girault, *Electrochimica Acta* **2000**, *45*, 2647.
- [60] H. H. Girault, *Modern Aspects of Electrochemistry, Vol. 25*, **1993**.
- [61] A. G. Volkov, D. W. Deamer, Editors, *Liquid-Liquid Interfaces: Theory and Methods*, **1996**.
- [62] V. J. Cunnane, G. Geblewicz, D. J. Schiffrin, *Electrochimica Acta* **1995**, *40*, 3005.
- [63] A. Trojanek, J. Langmaier, Z. Samec, *Electrochemistry Communications* **2006**, *8*, 475.
- [64] A. Trojanek, V. Marecek, H. Janchenova, Z. Samec, *Electrochemistry Communications* **2007**, *9*, 2185.
- [65] B. Su, R. P. Nia, F. Li, M. Hojeij, M. Prudent, C. Corminboeuf, Z. Samec, H. H. Girault, *Angewandte Chemie - International Edition* **2008**, *47*, 4675.
- [66] F. Li, B. Su, F. C. Salazar, R. P. Nia, H. H. Girault, *Electrochemistry Communications* **2009**, *11*, 473.
- [67] R. Partovi-Nia, B. Su, F. Li, C. P. Gros, J. M. Barbe, Z. Samec, H. H. Girault, *Chemistry - A European Journal* **2009**, *15*, 2335.
- [68] M. Suzuki, M. Matsui, S. Kihara, *Journal of Electroanalytical Chemistry* **1997**, *438*, 147.
- [69] H. Ohde, K. Maeda, Y. Yoshida, S. Kihara, *Journal of Electroanalytical Chemistry* **2000**, *483*, 108.
- [70] P. Liljeroth, B. M. Quinn, K. Kontturi, *Langmuir* **2003**, *19*, 5121.
- [71] A. Trojanek, J. Langmaier, B. Su, H. H. Girault, Z. Samec, *Electrochemistry Communications* **2009**.
- [72] I. Hatay, B. Su, F. Li, M. A. Mendez, T. Khoury, C. P. Gros, J. M. Barbe, M. Ersoz, Z. Samec, H. H. Girault, *Journal of the American Chemical Society* **2009**, *131*, 13453.

Chapter 3

Experimental and Instrumentation

3.1 Chemicals

All reagents and solvents are of analytical grade ($\geq 98\%$ purity) and are used without further purification.

3.1.1 Salts

Sodium iodide (NaI)- Fluka

Lithium chloride (LiCl)- Fluka

Lithium sulfate (Li_2SO_4)-Fluka

Tetramethylammonium chloride (TMACl)- Fluka

Tetraethylammonium chloride (TEACl)- Fluka

Tetraethylammonium perchlorate (TEAClO_4)-Fluka

Tetrabutylammonium chloride (TBACl)- Fluka

Tetrabutylammonium perchlorate (TBAClO_4)-Fluka

Bis(triphenylphosphoranylidene)ammonium chloride (BACl)- Fluka

Potassium tetrakis(4-chlorophenyl) chloride (KTPBCl)- Fluka

Lithium tetrakis(pentafluorophenyl)- borate (LiTB)- Boulder Scientific Company

3.1.2 Solvents

Water (H₂O)-Milli-Q reagent water system (Millipore Milli-Q185)

1,2-dichloroethane (1,2-DCE)-Fluka

Methanol (MeOH)-Fluka

3.1.3 Porphyrin products

Free-base 5,10,15,20-meso-tetraphenylporphyrin (H₂TPP)^[1], Free-base 2,3,7,8,12,13,17,18-octaethyl-21H,23Hporphyrin (H₂OEP)^[2, 3], 5,10,15,20 meso-tetraphenyl porphyrin cobalt(II) [Co(tpp)]^[4] and 2,3,7,8,12,13,17,18-Octaethyl-porphyrin cobalt(II) (CoOEP) were synthesized following the typical procedures.^[5, 6]

3.1.4 Others

Sulfuric acid (H₂SO₄) -Sigma–Aldrich

1,1'-dimethylferrocene (DMFc)- Sigma–Aldrich

Ferrocene (Fc)-Sigma–Aldrich

Hydrochloric acid (HCl, 32%)-Merck

Starch (from potatoes)-Fluka

Decamethylferrocene (DMFc)- Alfa Aesar

3.1.5 Synthesis of organic supporting electrolytes

TMATPBCl, BATB and TMATB were prepared by metathesis of equimolar quantities of the corresponding salts dissolved in a 2:1 mixture of methanol:water. Both solutions are gently mixed together and the resulting precipitate is filtered, washed with water and dried under vacuum. The salt is then re-crystallised in acetone and dried under vacuum before use.

3.2 Methodology for determination of bulk redox potentials

The redox system ferrocenium/ferrocene (Fc^+/Fc) has been proposed as a suitable internal standard for reference potential calibration in organic media. Such suitability lies in extrathermodynamic assumption that the activity of a univalent large symmetrical ion, with charge buried, is the same as activity of uncharged molecule of the same size and structure in all the solvents.^[7] Use of the Fc^+/Fc couple as an internal standard demands the observation of reversible electrochemistry in the investigated medium. Since only a form is required to be added in the solution, voltammetry has been extensively employed for ascertaining the reversibility of the system as well as to determine the standard (formal) reference potential of the redox couple. The redox potential of porphyrins was determined with 3-electrode system, reference electrode (Ag wire) working electrode (Pt microelectrode) counter electrode (Pt wire). The potential scale was referenced to the formal redox potential of ferrocene (Fc) $\left[E_{\text{Fc}^+/\text{Fc}}^{\circ, 1, 2\text{-DCE}} \right]_{\text{SHE}} = 0.64 \text{ V}$ as an internal reference. We employ this value as a reference potential for the redox species in the same medium. The formal redox potentials of the porphyrins were obtained from cyclic voltammetry in 1,2-DCE on a 10 μm diameter Pt microelectrode at 25 mVs^{-1} . In all cases, the voltammetric responses described a well-defined sigmoidal curve. Formal potential of the porphyrins evaluated from cyclic voltammetric peak potentials recorded 5mM BATB in dry 1,2-DCE purged with argon (Ar). Diffusion coefficient (D) of porphyrins was calculated from Randles-Sevcik equation. Diffusion coefficient derived from the Equation (3.1)

$$i = 4nFDca \quad (3.1)$$

Where i is the steady state current, n is the electron transfer number, F (96485 c/mol) is the Faraday constant, D is the diffusion coefficient, c is the concentration and a is the radius of the tip UME (ultramicroelectrode) (10 μm , Pt). One example of the Voltammetric redox and diffusion coefficients is summerized in Table 3.1

Table 3.1: Data refer to 50 μM of porphyrin with 5mM BATB supporting electrolyte in dry 1,2-DCE a 20mVs^{-1}

Concentration (50 μM)	E_1 vs SHE / V	E_2 vs SHE / V	E_3 vs SHE / V	D / cm^2s^{-1}
ZnTPP	0.30	0.61	—	3×10^{-6}

3.3 Reference electrodes

The two types of reference electrodes used are Ag/AgCl and Ag/Ag₂SO₄. These are prepared by connecting the silver wire and a counter electrode to the positive and negative terminals, respectively, of a 1.5 V potential difference. Both wires are subsequently placed in an aqueous solution of NaCl plus a small amount of HCl or Li₂SO₄ plus amount of H₂SO₄. The resultant current flow produced a layer of the insoluble silver salt on the silver wire.

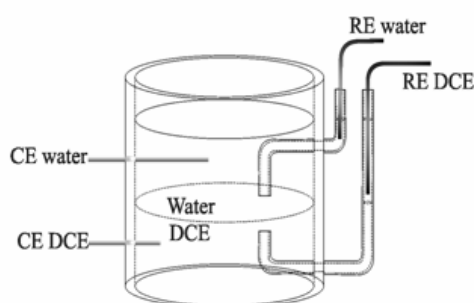
3.4 The four electrode potentiostat

The possibility to apply a constant polarisation by means of a four-electrode potentiostat has led to considerable advances in the field of liquid|liquid interfaces. Indeed, many experimental results on the electrical double layer or heterogeneous charge transfer across the liquid|liquid boundary were obtained at polarisable interfaces, the polarisability allowing to externally control the electrical state of the interface. The thermodynamic state of these interfaces is generally controlled by electrochemical polarisation using a 4-electrode system.^[8-10] The 4-electrode potentiostat features two reference electrodes measuring the potential in each phase, as well as two counter electrodes supplying the current. The reference electrodes are usually placed inside Luggin capillaries located close to the interface in order to minimise the solution resistance.^[11]

3.5 The electrochemical cell

The electrochemical cell used in cyclic voltammetry and capacitance is a homemade cylindrical glass vessel with a geometrical area of 1.53 cm^2 as pictured in Scheme 3.1. For all cyclic voltammetry electrochemical experiments Autolab PGSTAT 30 potentiostat (Metrohm, Switzerland) is used. The interface is polarised by means of the two reference electrodes RE_{water} and RE_{DCE} and the current is measured via the two platinum counter

electrodes CE_{water} and CE_{DCE} . The interface is situated between two Luggin capillaries to minimise the influence of the ohmic resistance in the solution. In order to ensure that a constant potential drop is established at the reference electrode|liquid interfaces, the aqueous phase and the organic reference electrolyte solution contain ions common to the electrodes, in general chloride or sulfate. The counter electrodes are platinum wires. Polarizable ITIES are formed when the aqueous electrolyte is very hydrophilic and the organic salt very hydrophobic. The range of polarisation potentials (the potential window) is limited by the transfer of ions constituting the supporting electrolyte.



Scheme 3.1: Schematic representation of the four electrode glass cell.

3.6 Cyclic voltammetry and potential window at liquid|liquid interfaces

Cyclic voltammetry was first successfully applied to liquid|liquid interfaces by Samec *et al.*^[12], who investigated the reversible ion transfer of tetraalkylammonium ions. It is now a widely used technique for the study of charge transfer reactions across these molecular interfaces. The cyclic voltammogram and capacitance-potential curve in Figure 3.1 show the potential window associated with the electrochemical cell. The interface can be considered polarizable within the limits -0.4 to 0.4 V. Outside this range the current rises as the ions constituting the supporting electrolytes are transferred. In order to determine the standard Gibbs energies of charge transfer and to estimate the Galvani potential difference across the water|organic interface of interest, it is necessary to use an extrathermodynamic assumption to define the energy scale. The commonly used “TATB” assumption states that tetraphenylarsonium (TPAs^+) and tetraphenylborate (TPB^-) have an identical standard transfer

energy at the water|1,2-DCE interface.^[13] On the basis of this assumption, the formal ion transfer potential of tetramethylammonium cation (TMA^+) at the water|1,2-DCE interface is estimated as 0.160 V.^[14] The voltammetric response in Figure 3.1 (a) shows the current rise associated with the transfer of Li^+ and TB^- at positive potentials and SO_4^{2-} or BA^+ at negative potentials. The quality of polarisability of liquid|liquid interfaces is far behind that of electrode|solution interfaces, both in terms of the magnitude of residual current density and the width of the potential window.^[15]

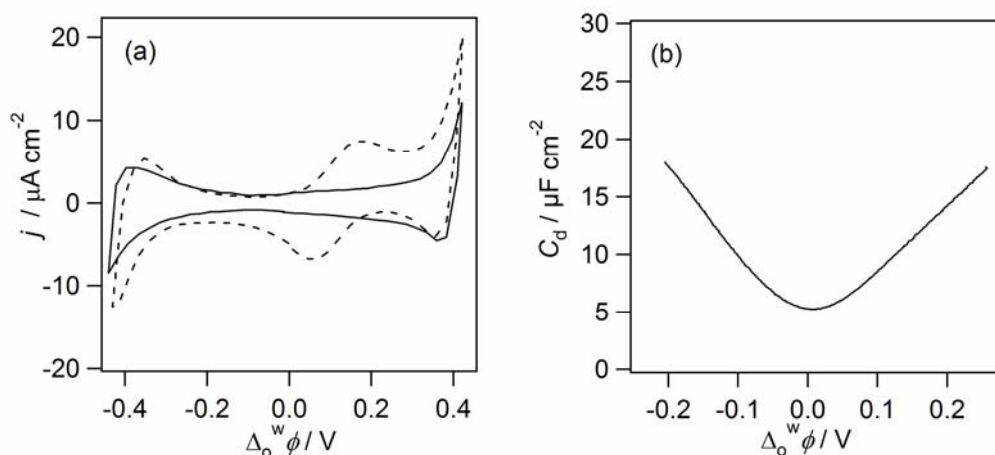
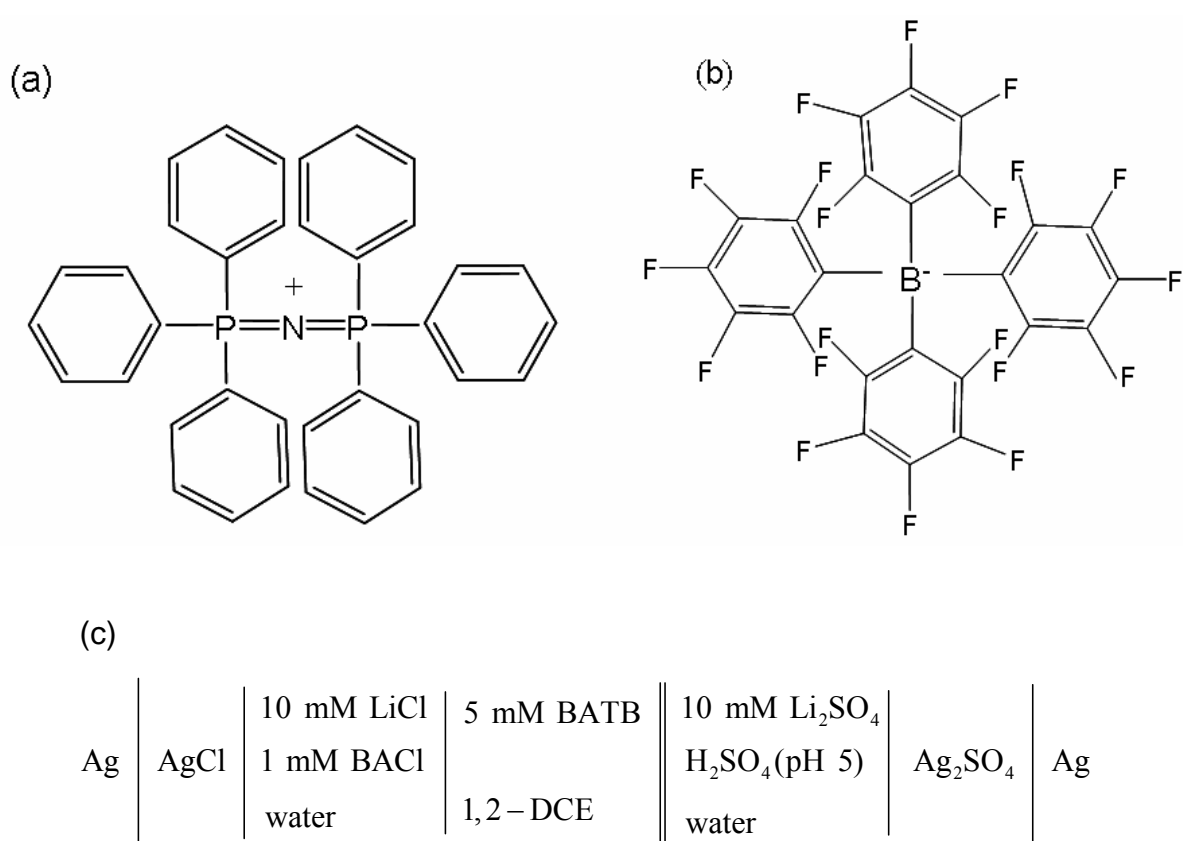


Figure 3.1: (a) Cyclic voltammogram in the absence (full line) or in the presence (dashed line) of TMA^+ (b) and capacitance-potential curve at the water/1,2-DCE interface. (c) the cell composition was as in Figure 3.2.

Several salts can be used as aqueous or organic electrolytes, yielding various potential windows. With 1,2-DCE as an organic solvent, a potential range spanning over about 0.8 V is obtained when the electrolytes Li_2SO_4 and BATB (Scheme 3.2 (c)) are used in the water and organic phases respectively. These salts have been used in this work for most experiments, unless specified otherwise. A schematic representation of the blank cell, in the absence of reagents, is displayed in Scheme 3.2 (c).

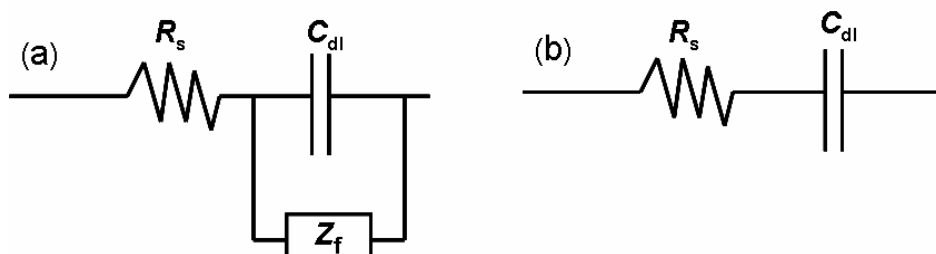


Scheme 3.2: (a) Molecular structures of the organic ions bis(triphenylphosphoranylidene) ammonium (BA^+) (b) and tetrakis(pentafluorophenyl)borate (TB^-) (c) schematic representation of the blank electrochemical cell.

3.7 Differential capacitance measurements

Differential capacitance is an important characteristic parameter of electrochemical interfaces [16]. It provides an accurate measure of the excess charge at an electrode surface [17-19] and contains detailed information about microscopic properties of the electrode interface. [20-24] Most traditional differential capacitance techniques use phase-selective *ac* voltammetry [17, 18, 25-29] where a sinusoidal perturbation voltage at a fixed frequency is superimposed on the *dc* voltage of cyclic voltammetry (CV); the in-phase and quadrature components of the resulting *ac* current are measured as functions of the *dc* voltage and the measured parameters are converted to (voltage dependent) C_{diff} . If these measurements are performed at more than one *ac* frequencies, then the *dc* voltage scan of CV is repeated every time the frequency is changed. [17, 18, 25, 26] This approach only is practical for systems held in “long-term” stationary state that provide identical surface conditions in repetitive CV cycles and

throughout the time (at least several minutes in most cases) necessary to complete the multiple dc scans. Scheme 3.3 shows equivalent circuit for the interface between two immiscible electrolyte solutions, C is the capacity of the interface, Z_f the faradaic impedance and R_s the solution resistance between the tips of Luggin capillaries.^[9,30] Capacitance measurements at liquid|liquid interfaces are a particular case of admittance measurements, where the frequency dependent current response is monitored as a function of the Galvani potential difference between the two phases.^[31] In the absence of heterogeneous charge transfer reactions ($Z_f = 0$) the system can be modelled by a resistance and capacitance in series.^[32, 33]



Scheme 3.3: Equivalent circuit for capacitance measurements in the presence (a) and absence (b) of heterogeneous charge transfer.

Under perturbation by a small sine signal at a given frequency.^[34]

$$e = E \sin(\omega t) \tag{3.2}$$

Where E is the amplitude of the potential modulation and ω the frequency, the admittance of this circuit is:

$$Y = \frac{1}{R_s + \frac{1}{i\omega C}} = \frac{R_s(\omega C)^2 - i\omega C}{1 + (\omega R_s C)^2} \tag{3.3}$$

And the current magnitude is:

$$I = E \cdot \frac{R_s(\omega C)^2 + i\omega C}{1 + (\omega R_s C)^2} \quad (3.4)$$

With the real and imaginary parts:

$$I_{re} = E \cdot \frac{R_s(\omega C)^2}{1 + (\omega R_s C)^2} \quad (3.5)$$

$$I_{im} = E \cdot \frac{\omega C}{1 + (\omega R_s C)^2} \quad (3.6)$$

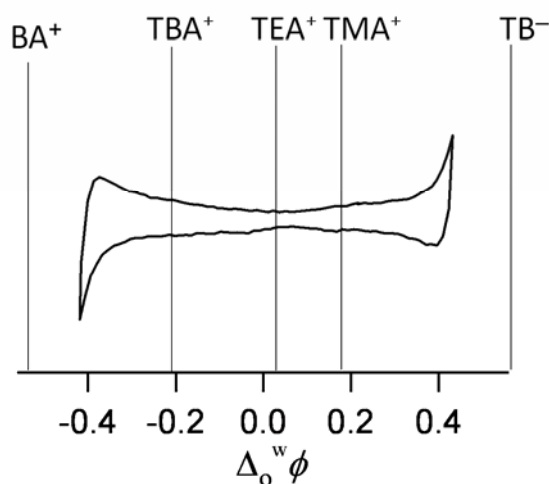
Hence the interfacial capacitance can be calculated as:

$$C = \frac{I_{re}^2 + I_{im}^2}{\omega E I_{im}} \quad (3.7)$$

In the presence of adsorbates, the interfacial capacitance is affected by the additional charge or changes in the dielectric properties at the interface.^[11] Capacitance-potential curves such as the one in Figure 3.1 (b) measured by applying Equation (3.7) at various frequencies. Capacitance measurements can provide a qualitative evidence of the adsorption of charged species at the liquid|liquid interface.

3.8 Two-phase reactions controlled by a common ion

The interface polarization can be controlled by the distribution of ions, for example by dissolving a hydrophilic and a lipophilic salt featuring a common ion (either cation or anion) in water and in the organic solution respectively. In this way, the Galvani potential difference across the interface is given by the Nernst equation for the distribution of this common ion and the interface is polarized but non-polarizable. As illustrated in Scheme 3.4, the Galvani potential difference across the interface can be varied by employing different common ions. This method allows a chemical control of the Galvani potential difference without supplying an external voltage. The Galvani potential difference across the water|1,2-DCE interface calculated for different common ions in Chapter 4.



Scheme 3.4: Illustration of the interface polarization by various common ions at the water/1,2-DCE interface.

Two-phase reactions were performed in small glass flasks with a volume of 10 ml. A flask was filled first with equal volume solution containing reactants, followed by the addition of 2 ml of aqueous solution containing 10 mM HCl/5 mM H₂SO₄. The salts of the common ion, were added in the same concentration to the aqueous and 1,2-DCE phases, respectively. After stirring and further waiting for the clear separation of two phases, the aqueous and organic solutions were isolated from each other. The organic phase was directly subjected to the UV-visible spectroscopic measurement (Ocean Optical CHEM 2000 spectrophotometer, quartz cuvette with a path length 10 mm), while the aqueous phase was first treated by excess NaI (equivalent to 0.1 M) prior to the UV-visible spectroscopic measurement.

3.9 Mass spectrometric measurements

Mass analysis was carried out on LCT time of flight mass spectrometer combining with an electrospray ionization source (Micromass, Manchester, UK), also in positive ionization mode. The MS power supply was set at 3.0 kV. The ion optics parameters were set in order to maximize the signal.

3.10 References

- [1] C. D. Dorough, J. R. Miller, F. M. Hunnekens, *Journal of American Chemical Society* **1951**, 73, 4315.
- [2] D. H. R. Barton, S. Z. Zard, *Journal of the Chemical Society, Chemical Communications* **1985**, 1098.
- [3] N. Ono, H. Kawamura, M. Bougauchi, K. Maruyama, *Tetrahedron* **1990**, 46, 7483.
- [4] K. M. Smith, K. M. Kadish, *The Porphyrin Handbook, Vol. 1*, Academic Press, New York, **2000**.
- [5] K. M. Kadish, K. M. Smith, R. Guilard, Eds, *The Porphyrin Handbook, Vol. 3*, Academic Press, New York, **2000**.
- [6] P. Hambright, eds, K. M. Kadish, K. M. Smith, R. Guilard, in *The Porphyrin Handbook*, **2000**.
- [7] O. Popovych, R. Tomkins, *Nonaqueous solution chemistry*, Wiley, New York, **1981**.
- [8] Z. Samec, V. Marecek, J. Weber, *Journal of Electroanalytical Chemistry* **1979**, 100, 841.
- [9] Z. Samec, *Chemical Reviews* **1988**, 88, 617.
- [10] C. Gavach, F. Henry, *Journal of Electroanalytical Chemistry* **1974**, 54, 361.
- [11] Z. Samec, V. Marecek, D. Homolka, *Faraday Discussions of the Chemical Society* **1984**, 77, 197.
- [12] Z. Samec, V. Marecek, J. Weber, *J. Electroanal. Chem* **1979**, 100, 841.
- [13] A. J. Parker, *Electrochimica Acta* **1976**, 21, 671.
- [14] M. H. Abraham, A. F. D. De Namor, *Journal of the Chemical Society, Faraday Transactions 1: Physical Chemistry in Condensed Phases* **1976**, 72, 955.
- [15] Z. Samec, T. Kakiuchi, *In Advances in Electrochemical Science and Engineering Vol. 4*, **1995**.
- [16] W. Schmickler, *Chemical Reviews* **1996**, 96, 3177.
- [17] G. Nagy, D. Roy, *Langmuir* **1995**, 11, 711.
- [18] T. D. Hewitt, R. Gao, D. Roy, *Surface Science* **1993**, 291, 233.
- [19] G. Beltramo, E. Santos, *Journal of Electroanalytical Chemistry* **2003**, 556, 127.
- [20] K. Lust, E. Lust, *Journal of Electroanalytical Chemistry* **2003**, 552, 129.
- [21] V. D. Jovic, B. M. Jovic, *Journal of Electroanalytical Chemistry* **2003**, 541, 13.
- [22] V. D. Jovic, B. M. Jovic, *Journal of Electroanalytical Chemistry* **2003**, 541, 1.
- [23] T. Pajkossy, T. Wandlowski, D. M. Kolb, *Journal of Electroanalytical Chemistry* **1996**, 414, 209.
- [24] J. W. Halley, *Electrochimica Acta* **1996**, 41, 2229.
- [25] R. Gao, T. D. Hewitt, D. Roy, *Journal of Physics and Chemistry of Solids* **1993**, 54, 685.
- [26] D. A. Harrington, *Journal of Electroanalytical Chemistry* **1993**, 355, 21.
- [27] A. Chen, J. Lipkowski, *Journal of Physical Chemistry B* **1999**, 103, 682.
- [28] M. Sluyters-Rebach, J. H. Sluyters, *A.J. Bard (Ed), Electroanalytical Chemistry, Vol. 4*, New York, **1970**.
- [29] B. E. Conway, J. Barber, S. Morin, *Electrochimica Acta* **1998**, 44, 1109.
- [30] A. Muthukrishnan, M. V. Sangaranarayanan, *Journal of Colloid and Interface Science* **2006**, 296, 624.
- [31] N. Eugster, PhD thesis, EPFL (Lausanne), **2004**.
- [32] A. G. Volkov, D. W. Deamer, D. L. Tanelian, V. S. Markin, *Progress in Surface Science* **1996**, 53, 1.

- [33] C. M. Pettit, P. C. Goonetilleke, D. Roy, *Journal of Electroanalytical Chemistry* **2006**, 589, 219.
- [34] B.Su, PhD thesis, EPFL (Lausanne), **2006**.

Chapter 4

Hydrogen peroxide generation by decamethylferrocene in biphasic system

4.1 Introduction

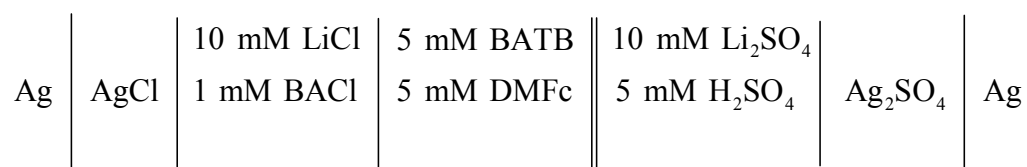
Electrochemical polarization of ITIES can be used to drive electron transfer and ion transfer reactions, but also to control adsorption phenomena. Hence, such interfaces have been considered as suitable models for investigating heterogeneous reactions occurring in biological systems, which are in many cases ion-coupled electron transfer reactions. Within aerobic living organisms, proton-coupled oxygen reduction consumes protons on one side of the biomembrane to generate a transmembrane proton gradient, leading to a transmembrane potential difference to drive the synthesis of adenosine triphosphate (ATP) for life activities.^[1]

The reduction of molecular oxygen (O_2) is a technologically important research topic, particularly in the context of a hydrogen economy. The O_2 reduction reaction (ORR) can proceed by a direct four-electron reduction to produce water or a two-electron reduction to give hydrogen peroxide, with the former pathway being highly desirable for fuel cell applications. The development of fuel cells for the combined production of electricity and hydrogen peroxide (H_2O_2) has been proposed recently.^[2-4] H_2O_2 is an industrially important product that is used on a scale of about three million metric tons per year worldwide. Its production is currently based almost exclusively on the anthraquinone hydrogenation and oxidation process.^[5] Many alternative routes have also been developed, one of which is the electrochemical cathodic reduction of O_2 ^[5-7] in the presence of molecular electrocatalysts such as cobalt tetraphenylporphyrin,^[8-10] cobalt porphine,^[11] free base tetraphenylporphyrin^[12] and anthraquinones.^[13-18] In this Chapter, we present an electrochemical method for producing H_2O_2 at a soft molecular interface and some thermodynamic considerations of O_2 reduction by DMFc at the water|1,2-DCE interface. We chose the ORR by ferrocene derivatives, a reaction that has been known for many years, to illustrate this principle.^[19-21] The main

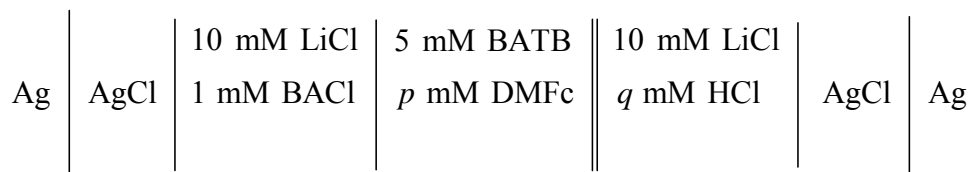
advantage of the present biphasic system is that the ORR can be stopped at the formation of H_2O_2 , which can be directly extracted into the aqueous phase during the reaction. H_2O_2 is a strong oxidant that readily oxidizes ferrocene derivatives, which usually leads to the absence of H_2O_2 in the final products of the homogeneous oxidation of ferrocene derivatives by O_2 .^[21] A reaction mechanism similar to an *EC* type reaction at the conventional electrode|solution interface is proposed, in which a proton transfer assisted by DMFc across the water|1,2-DCE interface is equivalent to the electrochemical step giving rise to a measurable current signal and the following irreversible oxygen reduction reaction represents the chemical step. The two steps are coupled at the interface, with protons supplied by the aqueous phase and electrons provided by DMFc in 1,2-DCE. The standard redox potentials of O_2 reduction calculated on the basis of a thermodynamic cycle also suggests that the O_2 reduction is largely favored in 1,2-DCE.

When an interface is formed between Li_2SO_4 and bis(triphenylphosphoranylidene) ammonium tetrakis(pentafluorophenyl)-borate (BATB) as the hydrophilic and lipophilic electrolytes, respectively, in water and 1,2-DCE results in a potential window from -0.5 to 0.4 V, as shown by the dotted line in Figure 4.1. This window is determined by the transfer of Li^+ and SO_4^{2-} ions from water to 1,2-DCE at positive and negative potentials respectively, since BA^+ and TB^- ions are too lipophilic to transfer first. If an ion having a medium lipophilicity, for example decamethylferrocenium ($DMFc^+$) in 1,2-DCE, is present it will transfer within the above potential window, and this transfer can be monitored by cyclic voltammetry, as shown by the full line in Figure 4.1. The electrochemical cells is depicted as follows:

Cell 1



Cell 2



Alternatively, the interface polarization can be controlled by the distribution of ions, for example by dissolving a hydrophilic and a lipophilic salt featuring a common ion in water and in the organic solution, respectively. In this way, the Galvani potential difference across the interface is given by the Nernst equation for the distribution of this common ion.

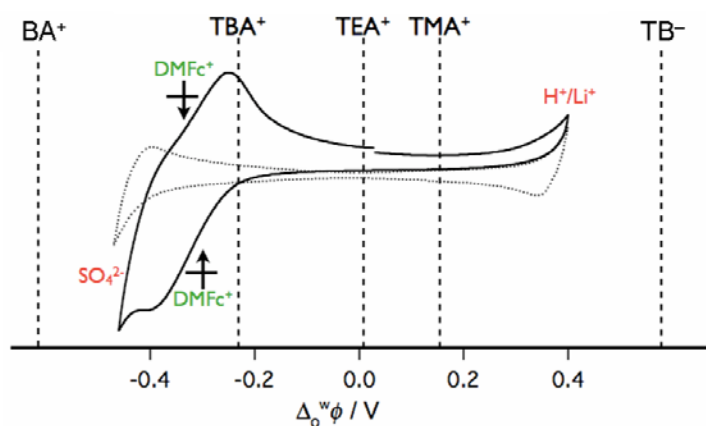


Figure 4.1: Polarization of a water/1,2-DCE interface by various common ions. The dotted and full lines show the potential window and transfer of DMFc^+ due to polarization by external voltages, respectively.

As illustrated in Figure 4.1, the Galvani potential difference across the interface can be varied by employing different common ions. This method allows a chemical control of the Galvani potential difference without supplying an external voltage.

4.2 UV-Visible spectroscopic measurements

Figure 4.2 (a) illustrates an equal-volume (2:2 mL), two-phase reaction under static conditions using TB^- as the common ion. The Galvani potential difference across the water|1,2-DCE interface is fixed at potentials 0.53 V.^[22] A fresh solution of 5 mM DMFc in 1,2-DCE is yellow. After 1 h in contact with 10 mM Li_2SO_4 , the 1,2-DCE phase turns green, thus

indicating the oxidation of DMFc to DMFc^+ , whereas the aqueous phase remains colorless. The two phases were then separated and the UV-Visible spectrum of the 1,2-DCE solution measured. As can be seen in Figure 4.2 (b) this solution shows an absorption band due to the DMFc^+ cation ($\lambda_{\text{max}}=779 \text{ nm}$) whereas the absorption peak for DMFc ($\lambda_{\text{max}}=425 \text{ nm}$) has disappeared and has been replaced by a very large absorbance in the UV range.

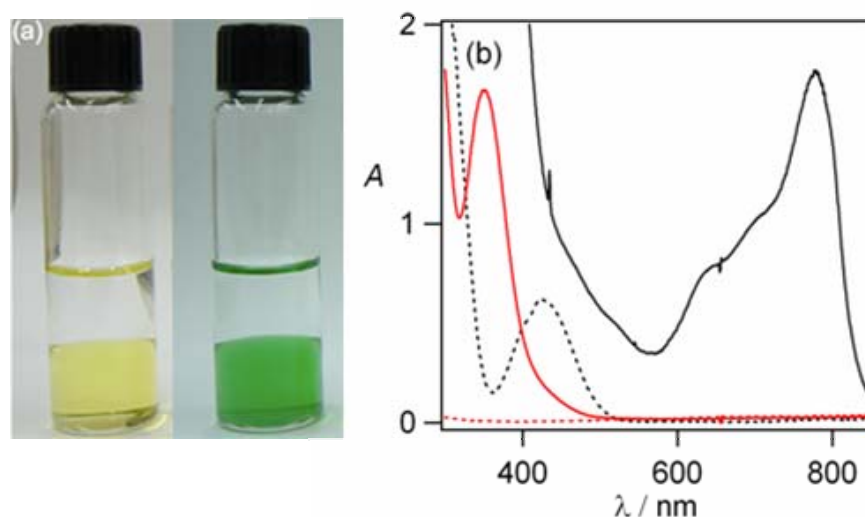


Figure 4.2: (a) Two-phase reaction controlled by TB^- ions at the beginning (left) and after 1 h (right). (b) UV-Visible spectra of the 1,2-DCE phase (black full line) and the water phase before (red dotted line) and after (red full line) treatment with 0.1M NaI after 1 h of the two-phase reaction; the spectrum of freshly prepared 5 mM DMFc (black full line) is also included for comparison.

Figure 4.3 illustrates the influence of the Galvani potential difference on this two-phase reaction when employing different common ions. The Galvani potential difference at the water|1,2-DCE interface is set at 0.53, 0.160, -0.074, -0.23, and -0.75 V by the ions TB^- , TMA^+ , TEA^+ , TBA^+ and BA^+ ,^[22] respectively, as shown in Figure 4.1. It is clear from the colour change in Figure 4.3, as well as the UV-Visible spectra (Figure 4.4), that the reaction rate follows the order $\text{TB}^- > \text{TMA}^+ > \text{TEA}^+ > \text{TBA}^+ > \text{BA}^+$. The reaction is very fast when TB^- is used as the common ion. The colour change of the 1,2-DCE solution from yellow to green starts immediately at the interfacial region upon contact of the aqueous solution with the 1,2-DCE solution, thereby indicating that the O_2 reduction by DMFc occurs at the interface.

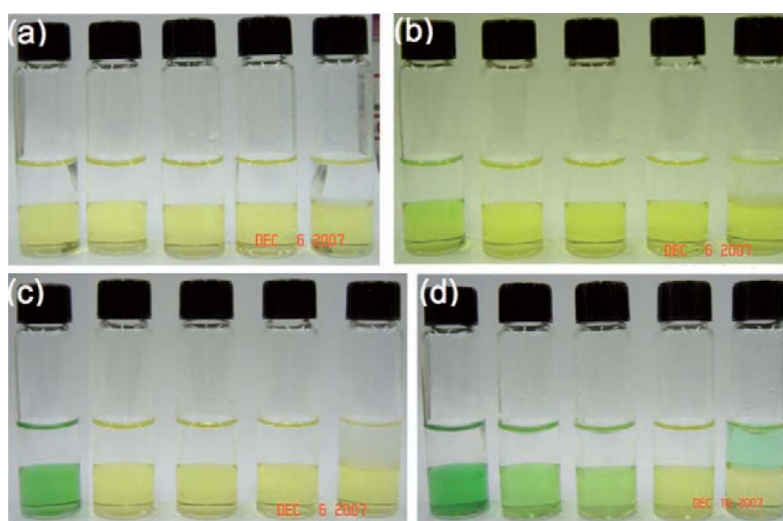


Figure 4.3: Two-phase reaction controlled by different common ions (TB^- , TMA^+ , TEA^+ , TBA^+ , and BA^+ from left to right; 5 mM in both phases) after a) 0 min, b) 62 min, c) 17.5 h, and d) 102 h.

When TMA^+ and TEA^+ are used as the common ion, however, the green colour of the 1,2-DCE phase can only be seen after more than 10 h, and in the case of TBA^+ the 1,2-DCE phase remains yellow after 102 h and only a weak absorption band at $\lambda_{\max}=779$ nm can be seen in the UV-Visible spectrum. In contrast, the 1,2-DCE phase remains yellow after 102 h with BA^+ as the common ion but the aqueous phase is slightly green. Absorption measurements show that the appearance of an absorption band at $\lambda_{\max}=779$ nm in the UV-Visible spectrum of the aqueous phase is concomitant with a decrease of the absorbance of DMFc in the 1,2-DCE phase ($\lambda_{\max}=425$ nm); only a negligible absorbance is observed for the $DMFc^+$ ion in the 1,2-DCE phase. This suggests that the $DMFc^+$ ion formed in the BA^+ controlled experiment is transferred from 1,2-DCE to water, which coincides with the illustration shown in Figure 4.1 and 4.3 clearly shows the influence of the Galvani potential difference on this biphasic reaction, which reflects the potential dependence of either the proton partition or the heterogeneous O_2 reduction, or both. A control experiment using 5 mM H_2SO_4 and 5 mM LiTB in water with 0.5 mM DMFc and 5 mM BATB in 1,2-DCE was carried out to elucidate the stoichiometry of the reaction.

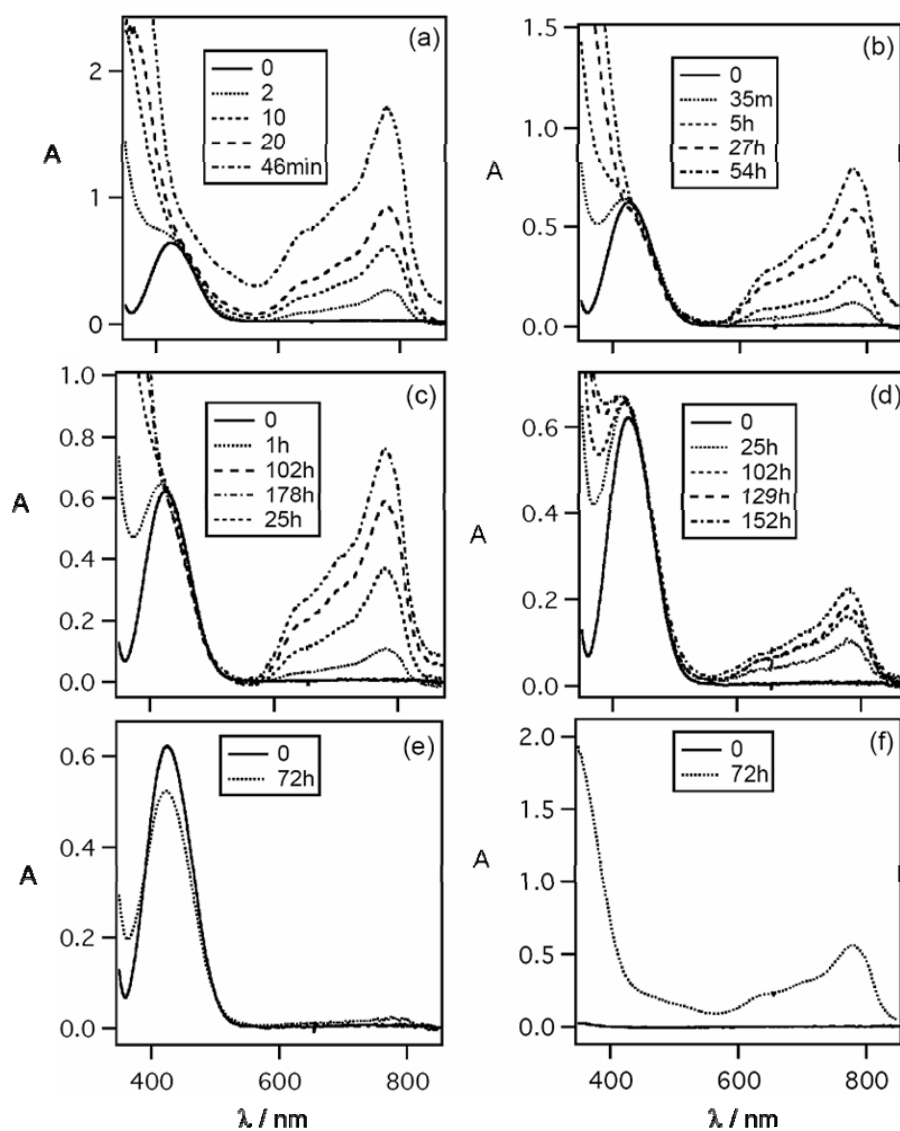


Figure 4.4: UV-Visible absorption spectra of the 1,2-DCE phase in the course of two-phase reaction controlled by various common ions: TB^- (a), TMA^+ (b), TEA^+ (c), TBA^+ (d), BA^+ (e). (f) the UV-Visible absorption spectra of the aqueous phase before and after 72 hours of two-phase reaction using BA^+ as the common ion. The spectra (a)-(e) were recorded in the quartz cuvette filling with 0.7 ml 1,2-DCE solution on the bottom and 0.7 ml aqueous solution on the top. The cuvette was covered by a Teflon cap and further sealed by Teflon tape in the course of measurement.

4.3 Calculation of the Galvani potential difference across the liquid|liquid interface

As shown in spectroscopic measurements, two-phase reactions were performed, where the Galvani potential difference across the liquid|liquid interface was controlled by the distribution of all the ions between the two phases. In order to calculate this potential, we first considered the Nernst equation for the different ionic species i present in the system:

$$\Delta_o^w \phi = \Delta_o^w \phi_{tr,i}^{0,w \rightarrow o} + \frac{RT}{z_i F} \ln \frac{c_i^o}{c_i^w} \quad (4.1)$$

At the same time, the mass balance for the different species is considered:

$$\frac{V_o}{V_w} c_{i, \text{initial}}^o + c_{i, \text{initial}}^w = \frac{V_o}{V_w} c_i^o + c_i^w \quad (4.2)$$

$$c_{i, \text{total}}^w = c_i^o + c_i^w \quad (4.3)$$

Where $c_{i, \text{initial}}^o$ and $c_{i, \text{initial}}^w$ stand for the concentrations of i initially added in the organic and aqueous phases, respectively. The concentrations at the equilibrium are denoted as c_i^o and c_i^w .^[23-25] In our particular case, the volume ratio between the organic and the aqueous phase V_o/V_w was always unitary, ergo it will be no further considered. On the other hand, the calculations are always performed assuming equilibrium conditions; therefore the mass balance equilibrium concentrations correspond to those involved in the Nernst equation for the ion transfer process. Additionally, the electroneutrality condition must be fulfilled and reads:

$$\sum_i^j z_i c_i^w = 0 \quad (4.4)$$

$$c_i^o = c_i^w \left(1 + \exp \left(\frac{F}{RT} (\Delta_o^w \phi - \Delta_o^w \phi_{tr,i}^{0,w \rightarrow o}) \right) \right) \quad (4.5)$$

Which after being combined with Equations. (4.1) and (4.3) finally yields

$$\sum_i^j z_i \frac{c_{i,\text{total}}}{1 + \exp\left[\frac{F}{RT}(\Delta_o^w \phi - \Delta_o^w \phi_{tr,i}^{0,w \rightarrow o})\right]} = 0 \quad (4.6)$$

Thus, after solving Equation (4.4), the potential drop across the interface can be obtained. Nonetheless, prior knowledge of the standard ion transfer potential is required for all the ionic species. Taking this into account, the formal standard ion transfer potentials of BA^+ was assumed to be 60 mV more negative than that of Cl^- . Analogously, this value for TB^- was taken as 60 mV more positive than that of Li^+ . This assumption is quite reasonable since it is found experimentally in repetition cyclic voltammograms that the potential window is limited by the transfer of Li^+ and Cl^- in its positive and negative edges, respectively. The Galvani potential difference between the two phases resulting from the distribution of all the ions is dominated by the partition of the common ion, here TB^- anion as an example. With such a choice of electrolyte, this distribution Galvani potential difference can be calculated knowing the respective Gibbs energy of transfer of the different ionic species and is found to be equal to 0.54 V. At equilibrium the acid HTB is extracted in the organic phase at a concentration of 3.57 mM, as shown in Table 4.1. After a short stirring of the reaction flask, the two phases were separated from each other and were analyzed. Finally, from the potential value calculated, the concentrations for all the ions in both phases become accesible after applying Equations (4.1) and (4.2), as shown in Tables 4.1.

Table 4.1: Calculated equilibrium concentrations after contact with 5 mM BATB in 1,2-DCE with 10 mM HCl and 5 mM LiTB in water.

	c_{H^+}/mM	$c_{\text{BA}^+}/\text{mM}$	$c_{\text{TB}^-}/\text{mM}$	$c_{\text{Li}^+}/\text{mM}$	$c_{\text{Cl}^-}/\text{mM}$
Water	6.42	2.02e-21	0.052	3.63	10.00
1,2-DCE	3.57	5	9.94	3.58	3.02e-18

The Galvani potential difference across the water|1,2-DCE interface calculated for different common ions in Table 4.2

Table 4.2: Calculated Galvani potential difference of different common ions at water/1,2-DCE (5 mM H_2SO_4 use for acidic media).

Ion	Counterion (w)	Counterion (o)	$\Delta_o^w \phi^0$ (V)
TB^-	Li^+	BA^+	0.53
TMA^+	Cl^-	$TPBCl^-$	0.160
TEA^+	Cl^-	ClO_4^-	-0.074
TBA^+	Cl^-	ClO_4^-	-0.23
BA^+	Cl^-	TB^-	-0.753

4.4 Standard redox potentials of O_2/H^+ reduction reactions in 1,2-DCE

4.4.1 General case

The redox potentials of various O_2 reduction reactions in water have been very well known, whereas those of in organic media have not. Hence, the standard redox potential of various O_2 reduction reactions in 1,2-DCE with respect to the Standard Hydrogen Electrode (SHE) were estimated on the basis of thermodynamic considerations as summarized in Table 4.3. First, let us consider a general redox reaction:



The standard redox potentials for the redox couple O/R in the aqueous phase and organic phase with respect to SHE are defined as:^[26]

$$\left[E_{\text{O/R}}^0 \right]_{\text{SHE}}^{\text{w}} = \left[\left(\mu_{\text{O}}^{0,\text{w}} - \mu_{\text{R}}^{0,\text{w}} \right) - n \left(\mu_{\text{H}^+}^{0,\text{w}} - \frac{1}{2} \mu_{\text{H}_2}^0 \right) \right] / nF \quad (4.8)$$

$$\left[E_{\text{O/R}}^0 \right]_{\text{SHE}}^{\text{o}} = \left[\left(\mu_{\text{O}}^{0,\text{o}} - \mu_{\text{R}}^{0,\text{o}} \right) - n \left(\mu_{\text{H}^+}^{0,\text{w}} - \frac{1}{2} \mu_{\text{H}_2}^0 \right) \right] / nF \quad (4.9)$$

Where $\mu_{\text{O}}^{0,\text{s}}$ (s = o or w) and $\mu_{\text{R}}^{0,\text{s}}$ (s = o or w) denote the standard chemical potentials of O and R, respectively. $\mu_{\text{H}^+}^{0,\text{w}}$ and $\mu_{\text{H}_2}^0$ represent the standard chemical potentials of proton in water and of hydrogen in gas phase. From Equations (4.8) and (4.9) we can get:

$$\begin{aligned} \left[E_{\text{O/R}}^0 \right]_{\text{SHE}}^{\text{o}} &= \left[E_{\text{O/R}}^0 \right]_{\text{SHE}}^{\text{w}} + \left[\left(\mu_{\text{O}}^{0,\text{o}} - \mu_{\text{O}}^{0,\text{w}} \right) - \left(\mu_{\text{R}}^{0,\text{o}} - \mu_{\text{R}}^{0,\text{w}} \right) \right] / nF \\ &= \left[E_{\text{O/R}}^0 \right]_{\text{SHE}}^{\text{w}} + \left(\Delta G_{\text{tr,O}}^{0,\text{w} \rightarrow \text{o}} - \Delta G_{\text{tr,R}}^{0,\text{w} \rightarrow \text{o}} \right) / nF \end{aligned} \quad (4.10)$$

Where $\Delta G_{\text{tr,O}}^{0,\text{w} \rightarrow \text{o}}$ and $\Delta G_{\text{tr,R}}^{0,\text{w} \rightarrow \text{o}}$ denote the standard Gibbs energy of transferring O and R from water to organic phase, respectively. Equation (4.10) tells that the work needed to reduce O to R in an organic phase can be equivalent to the sum of the work needed to reduce O to R in water and the work needed to transfer both O and R from water to the organic phase. As reported previously, a series of redox potentials of ferrocene derivatives, such as $\left[E_{\text{DMFc}^+/\text{DMFc}}^0 \right]_{\text{SHE}}^{\text{o}} = 0.07 \text{ V}$ in 1,2-DCE, have been estimated with respect to that of ferrocene.^[27] Moreover, in the case of proton reduction reaction in 1,2-DCE, its standard redox potential corresponds to the Gibbs transfer energy of proton across the water|1,2-DCE interface expressed in the voltage scale, that is 0.55 V.^[26]

4.4.2 $\left[E_{\text{O}_2/\text{O}_2^{\bullet-}}^0 \right]_{\text{SHE}}^{\text{w}}$

In the case of superoxide formation in a solution:



The standard redox potentials for the redox couple $\text{O}_2/\text{O}_2^{\bullet-}$ in the aqueous (s = w) and organic (s = o) phase with respect to SHE are:

$$\left[E_{\text{O}_2/\text{O}_2^-}^0 \right]_{\text{SHE}}^{\text{w}} = \left[\left(\mu_{\text{O}_2}^0 - \mu_{\text{O}_2^-}^{0,\text{w}} \right) - \left(\mu_{\text{H}^+}^{0,\text{w}} - \frac{1}{2} \mu_{\text{H}_2}^0 \right) \right] / F \quad (4.12)$$

$$\left[E_{\text{O}_2/\text{O}_2^-}^0 \right]_{\text{SHE}}^{\text{o}} = \left[\left(\mu_{\text{O}_2}^0 - \mu_{\text{O}_2^-}^{0,\text{o}} \right) - \left(\mu_{\text{H}^+}^{0,\text{w}} - \frac{1}{2} \mu_{\text{H}_2}^0 \right) \right] / F \quad (4.13)$$

Where $\mu_{\text{O}_2}^{0,\text{s}}$ (s = o or w) and $\mu_{\text{O}_2^-}^{0,\text{s}}$ (s = o or w) denote the standard chemical potentials of O_2 and O_2^- , respectively. $\mu_{\text{H}^+}^{0,\text{w}}$ and $\mu_{\text{H}_2}^0$ represent the standard chemical potentials of proton in water and of hydrogen in gas phase. Arranging Equations (4.12) and (4.13) leads to:

$$\left[E_{\text{O}_2/\text{O}_2^-}^0 \right]_{\text{SHE}}^{\text{o}} = \left[E_{\text{O}_2/\text{O}_2^-}^0 \right]_{\text{SHE}}^{\text{w}} + \left(\mu_{\text{O}_2^-}^{0,\text{w}} - \mu_{\text{O}_2^-}^{0,\text{o}} \right) / F = \left[E_{\text{O}_2/\text{O}_2^-}^0 \right]_{\text{SHE}}^{\text{w}} - \Delta G_{\text{tr}, \text{O}_2^-}^{0,\text{w} \rightarrow \text{o}} / F \quad (4.14)$$

The Gibbs energy of transfer of O_2^- can be calculated knowing that the respective solubility of oxygen in water and 1,2-DCE are $2.5 \times 10^{-4} \text{ mol dm}^{-3}$ [28] and $1.39 \times 10^{-3} \text{ mol dm}^{-3}$ [29] respectively. The standard Gibbs energy of transfer of molecular oxygen from water to 1,2-DCE is then $-4.25 \text{ kJ mol}^{-1}$. On the basis of the Born solvation model, we can calculate the Gibbs energy of transfer of the superoxide anion with calculate the Gibbs energy of transfer of the superoxide anion with

$$\Delta G_{\text{tr}, \text{O}_2^-}^{0,\text{w} \rightarrow \text{o}} = \Delta G_{\text{tr}, \text{O}_2}^{0,\text{w} \rightarrow \text{o}} + \frac{F^2}{8\pi\epsilon_0 r_{\text{O}_2}} \left(\frac{1}{\epsilon^{\text{o}}} - \frac{1}{\epsilon^{\text{w}}} \right) \quad (4.15)$$

Which yields assuming that the radius of molecular oxygen is equal to the bond length (120pm) a value of 46.3 kJ mol^{-1} . With $\left[E_{\text{O}_2/\text{O}_2^-}^0 \right]_{\text{SHE}}^{\text{w}} = -0.330 \text{ V}$, one obtain $\left[E_{\text{O}_2/\text{O}_2^-}^0 \right]_{\text{SHE}}^{\text{DCE}} \approx -0.81 \text{ V}$ in 1,2-DCE.

4.4.3 $\left[E_{\text{O}_2/\text{H}_2\text{O}_2}^0 \right]_{\text{SHE}}^{\text{DCE}}$, $\left[E_{\text{O}_2/\text{H}_2\text{O}}^0 \right]_{\text{SHE}}^{\text{DCE}}$ and $\left[E_{\text{H}_2\text{O}_2/\text{H}_2\text{O}}^0 \right]_{\text{SHE}}^{\text{DCE}}$

In the case of two-electron two-proton reduction of O_2 to H_2O_2 in a solution as expressed below:



The standard redox potentials for the redox couple $\text{O}_2/\text{H}_2\text{O}_2$ in the aqueous ($\text{s} = \text{w}$) and organic ($\text{s} = \text{o}$) phase are:

$$\left[E_{\text{O}_2/\text{H}_2\text{O}_2}^0 \right]_{\text{SHE}}^{\text{w}} = \left[\left(\mu_{\text{O}_2}^0 + 2\mu_{\text{H}^+}^{0,\text{w}} - \mu_{\text{H}_2\text{O}_2}^{0,\text{w}} \right) - 2 \left(\mu_{\text{H}^+}^{0,\text{w}} - \frac{1}{2} \mu_{\text{H}_2}^0 \right) \right] / 2F \quad (4.17)$$

$$\left[E_{\text{O}_2/\text{H}_2\text{O}_2}^0 \right]_{\text{SHE}}^{\text{o}} = \left[\left(\mu_{\text{O}_2}^0 + 2\mu_{\text{H}^+}^{0,\text{o}} - \mu_{\text{H}_2\text{O}_2}^{0,\text{o}} \right) - 2 \left(\mu_{\text{H}^+}^{0,\text{w}} - \frac{1}{2} \mu_{\text{H}_2}^0 \right) \right] / 2F \quad (4.18)$$

Thus we get:

$$\begin{aligned} \left[E_{\text{O}_2/\text{H}_2\text{O}_2}^0 \right]_{\text{SHE}}^{\text{o}} &= \left[E_{\text{O}_2/\text{H}_2\text{O}_2}^0 \right]_{\text{SHE}}^{\text{w}} + \left[\left(\mu_{\text{H}_2\text{O}_2}^{0,\text{w}} - \mu_{\text{H}_2\text{O}_2}^{0,\text{o}} \right) - 2 \left(\mu_{\text{H}^+}^{0,\text{w}} - \mu_{\text{H}^+}^{0,\text{o}} \right) \right] / 2F \\ &= \left[E_{\text{O}_2/\text{H}_2\text{O}_2}^0 \right]_{\text{SHE}}^{\text{w}} - \left(\Delta G_{\text{tr}, \text{H}_2\text{O}_2}^{0, \text{w} \rightarrow \text{o}} - 2\Delta G_{\text{tr}, \text{H}^+}^{0, \text{w} \rightarrow \text{o}} \right) / 2F \end{aligned} \quad (4.19)$$

The standard Gibbs energy of transfer of H_2O_2 across the water|1,2-DCE has been estimated to be close to that of H_2O being about 15.4 kJ mol^{-1} .^[30] Therefore, with $\left[E_{\text{O}_2/\text{H}_2\text{O}_2}^0 \right]_{\text{SHE}}^{\text{w}} = 0.695 \text{ V}$, one gets $\left[E_{\text{O}_2/\text{H}_2\text{O}_2}^0 \right]_{\text{SHE}}^{\text{DCE}} = 1.165 \text{ V}$ in 1,2-DCE. Similarly, the standard redox potentials for the redox couples $\text{O}_2/\text{H}_2\text{O}$ and $\text{H}_2\text{O}_2/\text{H}_2\text{O}$ can be estimated to be $\left[E_{\text{O}_2/\text{H}_2\text{O}}^0 \right]_{\text{SHE}}^{\text{DCE}} = 1.738 \text{ V}$ and $\left[E_{\text{H}_2\text{O}_2/\text{H}_2\text{O}}^0 \right]_{\text{SHE}}^{\text{DCE}} = 2.312 \text{ V}$, respectively.

The standard redox potentials of various O₂ reduction reactions are summarized in Table 4.3. It is clear that O₂ reduction to O₂^{•-} in 1,2-DCE will be more difficult than in an aqueous medium. Indeed, the reaction creates an anion that is less solvated than in water. In contrast, all the proton-coupled oxygen reduction reactions are favored in an organic phase, because of the elimination of charges. For instance, O₂ reduction to O₂^{•-} by DMFc in 1,2-DCE is largely unfavored, whereas in the presence of proton the O₂ reduction is significantly accelerated on the thermodynamic background.

Table 4.3: Calculated standard redox potentials of various O₂ reduction reactions, and those of the proton reduction reaction are also compared.

Reaction	$[E^0]_{\text{SHE}}^{\text{w}} / \text{V}$	$[E^0]_{\text{SHE}}^{\text{DCE}} / \text{V}$
$\text{H}^+(\text{s}) + e^- \rightarrow \frac{1}{2}\text{H}_2(\text{g})$	0	0.550
$\text{O}_2(\text{g}) + e^- \rightarrow \text{O}_2^{\bullet-}(\text{s})$	-0.330	-0.600
$\text{O}_2(\text{g}) + 2\text{H}^+(\text{s}) + 2e^- \rightarrow \text{H}_2\text{O}_2(\text{s})$	0.695	1.165
$\text{O}_2(\text{g}) + 4\text{H}^+(\text{s}) + 4e^- \rightarrow 2\text{H}_2\text{O}(\text{s})$	1.229	1.738
$\text{H}_2\text{O}_2(\text{s}) + 2\text{H}^+(\text{s}) + 2e^- \rightarrow \text{H}_2\text{O}(\text{s})$	1.763	2.312

4.5 Cyclic voltammetric measurements at a platinum microdisc electrode

Formation of the DMFc⁺ ion was also confirmed by the cyclic voltammetric response of a platinum microdisc electrode (diameter: 25 μm) in the organic phase, as illustrated in Figure 4.5. After 4 h of reaction, a steady-state current wave, which consists of a larger cathodic steady-state current (I_{SC}) and a smaller anodic steady-state current (I_{SA}), is observed at the

same potential as for DMFc in 1,2-DCE. As DMFc and DMFc⁺ ion have about the same diffusion coefficient, the percentage of DMFc oxidized can be calculated from the ratio I_{SC} / I_{SS} to be 74%, that is, a resulting concentration of 3.7 mM. Furthermore, the sum of the magnitudes of I_{SC} and I_{SA} is very close to that of freshly prepared 5 mM DMFc in 1,2-DCE (I_{SS}), as can be seen from Figure 4.5. This voltammetric result provides two indications. First, DMFc is oxidized to the DMFc⁺ cation, which stays in the 1,2-DCE phase. This coincides with the full line shown in Figure 4.1 in that the transfer of DMFc⁺ ion from 1,2-DCE to water only occurs at negative Galvani potential differences.

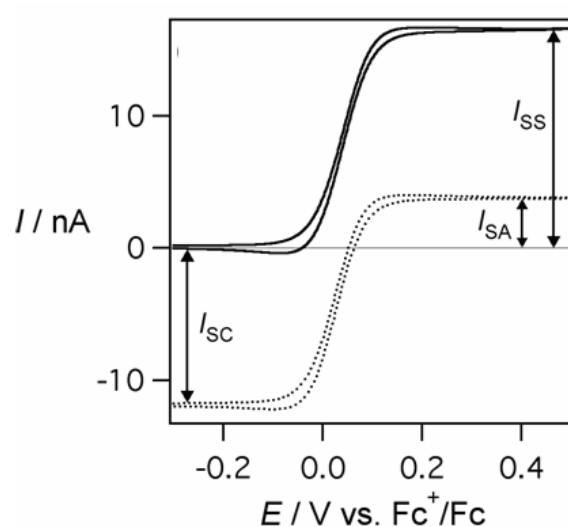


Figure 4.5: CVs obtained with a 25- μm Pt microelectrode of freshly prepared 5 mM DMFc (full line) and the 1,2-DCE phase after 4 h of the two-phase reaction (dotted line).

Mass spectrometric measurements were carried out for the 1,2-DCE phase containing 5 mM DMFc and 5 mM BATB on an LCT time of flight mass spectrometer combining with an electrospray ionization source before and after running 2 hours of two-phase reaction with an aqueous phase containing 5 mM H₂SO₄ and 5 mM LiTB. The 1,2-DCE solutions were diluted by CH₃CN by 1000 times prior to MS measurements. Second, it indicates that both DMFc and the DMFc⁺ cation are stable over the course of the two-phase reaction and that no decomposition takes place. This was also confirmed by mass spectrometric measurements in Figures 4.6 and 4.7. The mass spectra do not display any peaks for iron ions or a free cyclopentadienyl ring.

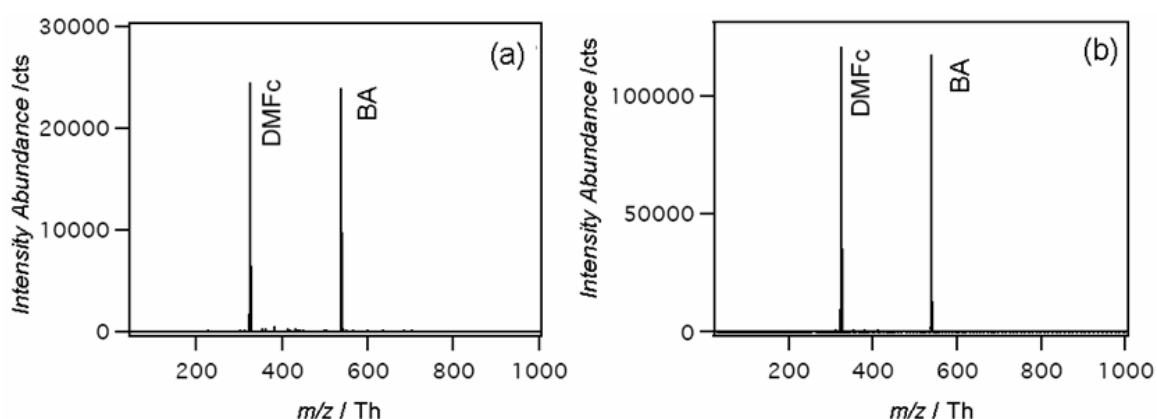


Figure 4.6: Full range mass spectra obtained (a) freshly prepared 5 mM DMFc and (b) and the 1,2-DCE phase after the two-phase reaction in a positive ionization mode.

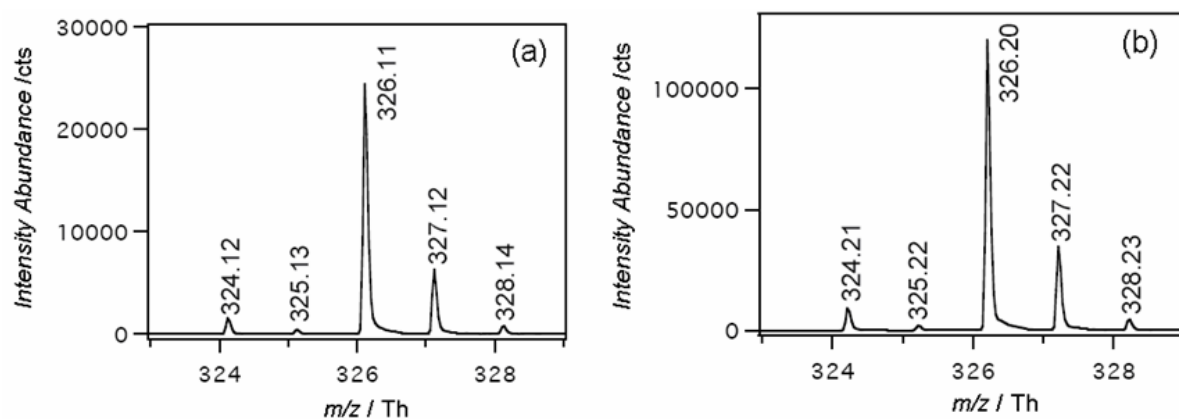


Figure 4.7: Magnified mass spectra of DMFc shown in Figure 4.6.

4.6 Titrating the aqueous phases with sodium iodide (NaI)

The isolated aqueous solution was titrated with NaI to detect the formation of H_2O_2 . Thus, 29.98 mg (corresponding to 0.1M, a large excess) of NaI was added to 2 mL of the solution and, as shown in Figure 4.8(b) the solution changed from colorless to pale yellow (flask 2). Adding NaI to an aqueous solution containing 5 mM LiTB and 5 mM H_2SO_4 in a controlled titration did not lead to any color change within the present experimental time scale, thus confirming the presence of H_2O_2 in the aqueous solution. H_2O_2 is a strong oxidant that can oxidize I^- to I_3^- , which can be visualized by adding starch to give a red-brown color (flask 3). I_3^- can be also detected by UV-Visible spectroscopy, as shown in Figure 4.8. Taking a ϵ_{max}

value of $2.76 \times 10^4 \text{ M}^{-1} \text{ cm}^{-1}$,^[31] the concentration of I_3^- can be calculated to be 0.070 ± 0.003 mM, which corresponds to that of H_2O_2 formed.

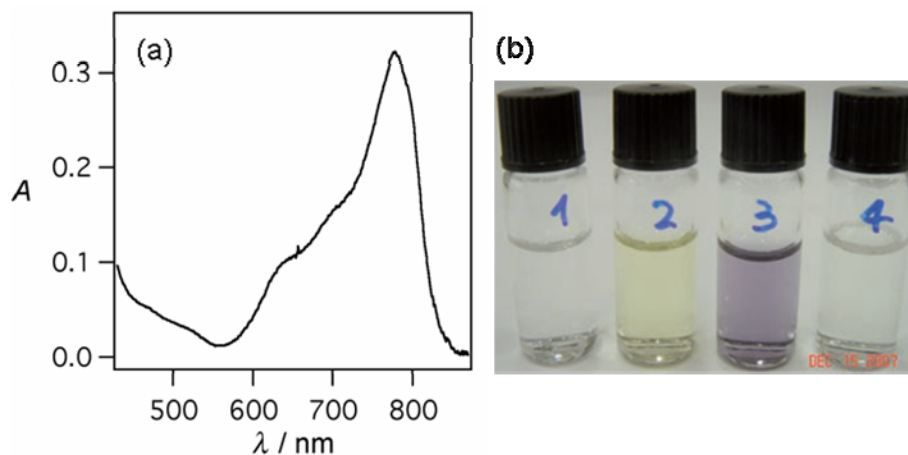


Figure 4.8: UV-Visible spectra of the (a) 1,2-DCE and (b) water phase; flask 1: water phase after 1 h of the two-phase reaction; flask 2: flask 1+0.1M NaI; flask 3: flask 2+starch; flask 4: 5 mM LiTB+5 mM H_2SO_4 +0.1M NaI + starch.

The partition coefficient for the extraction of H_2O_2 into water was examined by performing a titration measurement of the H_2O_2 partition between water and 1,2-DCE using NaI. This experiment reveals that the transfer of the H_2O_2 initially present in water to 1,2-DCE is negligible (Figure 4.9). H_2O_2 transfer between water and 1,2-DCE has been measured by taking equal volume of water and 1,2-DCE stirring for 10 minutes and waiting 30 minutes for separation of the two phases (Solution1), the aqueous phase was then separated. Solution 2 was freshly prepared aqueous solution containing 0.1 mM H_2O_2 and 5 mM H_2SO_4 . To solutions 1 and 2 excess amount of NaI was added. After waiting 60 minutes, the UV-Visible spectra of these of two solutions were measured.

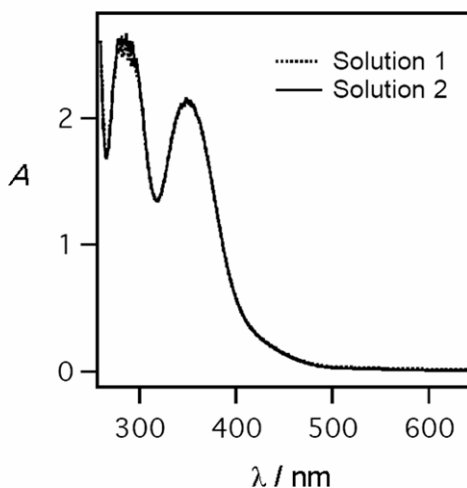


Figure 4.9: UV-Visible measurement on the transfer of H_2O_2 between water and 1,2-DCE by adding NaI to. Solution 1: aqueous phase after stirring for 10 minutes in contact with 1,2-DCE, Solution 2: freshly aqueous solution containing $0.1 \text{ mM H}_2\text{O}_2$ and $5 \text{ mM H}_2\text{SO}_4$.

Reduction of H_2O_2 by DMFc and/or decomposition must therefore account for the low quantities observed. H_2O_2 is a strong oxidant in acidic solution and it can readily oxidize DMFc to DMFc^+ .^[32] H_2O_2 can also decompose in a reaction that is catalyzed by most transition metals and their compounds.^[6] The rate of reaction is controlled by the Galvani potential difference across the interface, which has been determined chemically using various salts with a common ion. The resulting concentration of H_2O_2 has been measured and shows a yield of 20% with respect to the concentration of the reducing agent (DMFc).

4.7 Proton transfer by DMFc

Figure 4.10(a) compares the cyclic voltammograms in the absence (dotted line) and presence (full line) of 5 mM DMFc in 1,2-DCE at a water|1,2-DCE interface under aerobic conditions. Dissolving DMFc in 1,2-DCE results in clearly three new features with respect to the blank one: (i) an irreversible positive current on the positive potential regime (Signal I), (ii) a positive current offset in the middle of the potential window (Signal II, that can be more clearly observed when using LiCl as the aqueous supporting electrolyte as shown in Figure 4.10(b), Figure 4.11 and 4.12), and (iii) a current wave in the negative potential range with a formal potential of $\Delta_0^w \phi = -0.26 \text{ V}$ (Signal III).

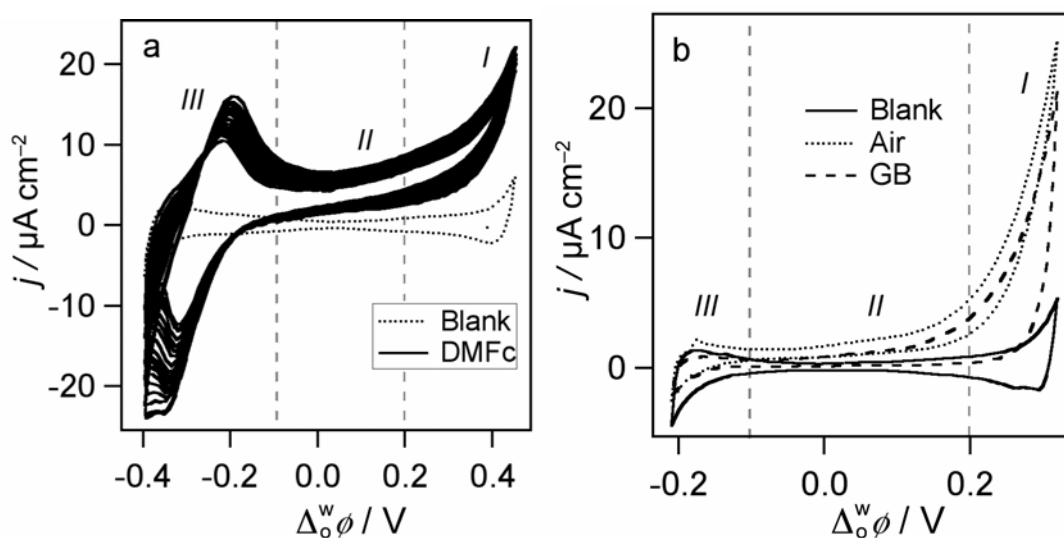


Figure 4.10: (a) CVs obtained with Cell 1 in the absence ($x = 0$, dotted line) and presence (full line, $x = 5, 20$ scans) of DMFc in 1,2-DCE. The scan rate was 50 mV s^{-1} ; (b) CVs obtained with Cell 2 in the absence ($p = 0, q = 100$, full line) and presence ($p = 5, q = 100$) of DMFc under air (dotted line) and oxygen free (dashed line) condition. The scan rate was 25 mV s^{-1} .

As shown in Figure 4.10(b), Signal *I* is independent of the presence of oxygen and therefore of subsequent chemical reactions that were published to yield H_2 under anaerobic conditions^[11] and H_2O_2 in aerated solutions.^[33, 34] Indeed, the two curves are identical if the offset current of Signal *II* is subtracted. Signal *III* displayed in Figure 4.10(a) is associated with the transfer of DMFc^+ across the water|1,2-DCE interface produced either subsequent chemical reactions (similar data for anaerobic conditions). The Gibbs energy of transfer for DMFc^+ obtained from the mid-peak potential value is equal to 25.1 kJ mol^{-1} . Therefore, any Galvani potential difference more positive than -0.26 V is enough to keep DMFc^+ in the organic phase, for example to hinder its reaction with H_2O_2 in water. As reported previously a ferrocenium cation can be a Fenton reagent that reacts with H_2O_2 to form OH^\bullet in water.^[35] On the other hand, as it was shown in Figure 4.10(a) that upon successive cycles the current magnitude of Signal *I* does not change significantly whilst that of Signal *III* increases continuously. This fact indicates that when cycling the potential to the positive side where Signal *I* is observed more and more DMFc^+ is produced by the subsequent chemical reactions, thus leading to the increment of DMFc^+ transfer current. The CVs compared in Figure 4.10(b) therefore indicate, that both proton and oxygen reduction reactions are initiated by the

same step, which is likely to be the assisted proton transfer (APT) or proton-coupled electron transfer (PCET) by DMFc across the water | 1,2-DCE interface:



This is supported by the pH dependence of Signal I, which shifts with the aqueous pH by approximately 60 mV/pH (Figure 4.11), in accordance to the Nernst equation for the ion transfer process occurring at the liquid|liquid interface. Essentially, this step corresponds to the protonation of DMFc but occurs heterogeneously in the present biphasic system, which gives rise to the experimentally observed electrical current, *i.e.* Signal I, with the four-electrode methodology at the liquid|liquid interface. Indeed, it is well known that ferrocene compounds can be protonated either on the iron or on the cyclopentadienyl ring (Cp) or on both via an agostic position bridging iron and Cp.^[36]

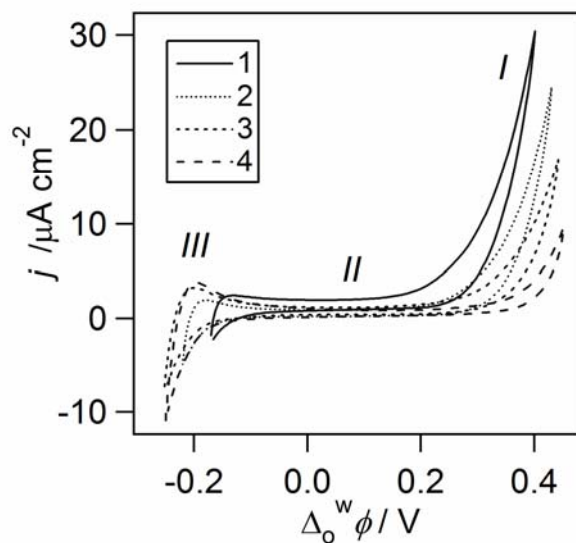


Figure 4.11: CVs obtained with Cell 2 in the presence of DMFc in 1,2-DCE ($p = 5$) at various pH. The pH was adjusted by HCl. The scan rate was 50 mV s^{-1} .

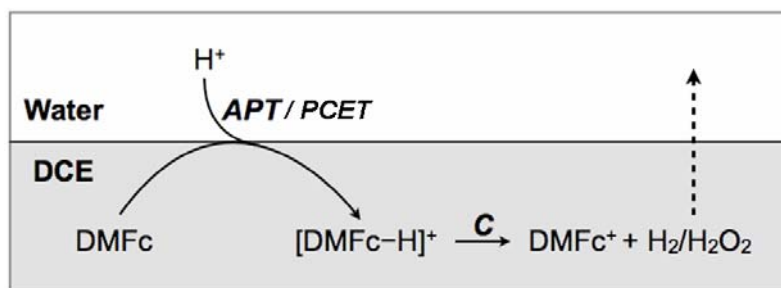
In addition, the current magnitude decreases with increasing the aqueous pH, which is due to a lower concentration of proton in water at a higher pH and the proton diffusion starts to be a controlling factor. Also, at a higher pH the transfer of Li^+ will take place prior to that of

proton at the positive potential limit, since the formal ion transfer potentials of proton and lithium across the water|1,2-DCE interface are $\Delta_o^w \phi_{H^+}^0 = 0.549$ V and $\Delta_o^w \phi_{Li^+}^0 = 0.591$ V, respectively.^[37]

4.8 Oxygen reduction in aerobic conditions

In aerobic conditions, the generation of hydrogen peroxide (H₂O₂) has been verified by redox titration with sodium iodide^[33] and scanning electrochemical microscopy.^[34] Quantitative analysis of the reaction products after a two-phase reaction controlled by a common ion, as reported previously, the yield of H₂O₂ with respect to the amount of DMFc⁺ is about 38%.^[33] One of possible sources of the extra DMFc⁺ might be generated by the further reaction of produced H₂O₂ with DMFc as reported previously.^[38] Indeed, H₂O₂ in 1,2-DCE is an extremely strong oxidant with a standard redox potential of 2.312 V as calculated in Section 4.4. In this sense, from a viewpoint of H₂O₂ production a key advantage of the present biphasic system is to allow a very efficient collection of H₂O₂ by separating DMFc/DMFc⁺ and H₂O₂ with a liquid junction between two adjacent phases, blocking effectively their further reactions.^[33] Indeed, in the industrial Riedl-Pfleiderer process H₂O₂ formed by the autooxidation of 2-ethyl-9,10-dihydroxyanthracene in a hydrophobic solvent (called the working solution) is also separated by an aqueous extraction.^[39] Moreover, at the polarizable water|1,2-DCE interface the separation of DMFc⁺ and H₂O₂ is reinforced by controlling the interfacial polarization either with an external voltage or with the partition of an ion. O₂ reduction by ferrocene derivatives in organic media in the presence of an acid, such as carboxylic acids (trichloroacetic and trifluoroacetic acids)^[19, 20] and perchloric acid,^[38, 40] has been known for many years, although the reaction mechanism is yet unresolved. For example, the initial reaction step has ever been assigned to be the protonation of ferrocene^[20, 36, 41-43], which leads to tilting of the rings and thus facilitates the binding of O₂ at Fe atom.^[20] Considering that insertion of triplet O₂ is spin-forbidden, Fomin has proposed that an intermediate hydrogen-bonded structure of O₂ sandwiched between two protonated ferrocenes is formed and thus H₂O₂ is generated by concerted breakdown of two Fe-H and formation of two H-O bonds.^[32] Preliminary density function theoretical (DFT) computations support the hypothesis that triplet molecular oxygen O₂ approaches Fe-H directly via a delocalized triplet (diradical) transition state [DMFc⁺·H·OO·]⁺ to yield H₂O₂ finally. Based on the experimental

results and theoretical considerations, a reaction pathway illustrated in Scheme 4.1 was proposed here for O₂/proton reduction by DMFc at the water|1,2-DCE interface.



Scheme 4.1: Mechanism of O₂ and proton reduction by DMFc at the water/1,2-DCE interface.

APT represents the assisted proton transfer across the water|1,2-DCE interface by DMFc and *C* is the following O₂/proton reduction reaction. *C* can be simply considered as an irreversible chemical reaction responsible for the absence of backward proton transfer (proton transfer back to water from 1,2-DCE). In this case, Scheme 4.1 is similar to an *EC* type reaction at the conventional electrode|solution interface. The *APT* or *PCET* step is equivalent to *E*, which is followed by the irreversible O₂/proton reduction reaction in 1,2-DCE designated *C*. Here *C* is a homogeneous reaction and does not involve any charge flux across the water|1,2-DCE interface.

4.9 DMFc partition and Signal II

One remaining issue associated with the present experimental system is the current offset in the middle of the potential window, *i.e.* Signal II in Figure 4.10, which is almost constant and potential-independent and can be clearly observed in Figures 4.11 and 4.12(a). The current offset starts from the electrochemical wave of DMFc⁺ from water to 1,2-DCE, and its positive sign suggests that it corresponds to a positive charge transfer from the aqueous to organic phase. Moreover, the magnitude of this current offset linearly increases with increasing DMFc concentration in 1,2-DCE (Figure 4.12(b)).

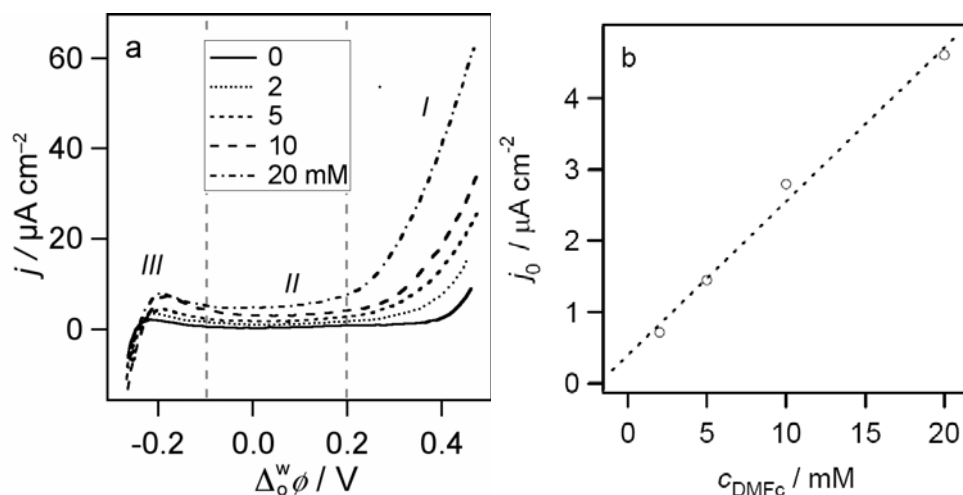


Figure 4.12: (a) Linear scan voltammogram obtained with Cell 2 at various concentrations of DMFc in 1,2-DCE ($p = 0, 2, 5, 10$ and 20 , $\text{pH } 2$). The scan started from the left at a rate of 20 mV s^{-1} ; (b) Dependence of the electrical current at 0 V on the DMFc concentration.

To unravel its origin, a biphasic test without electrochemical control was first performed, in which a concentrated 1,2-DCE solution containing 50 mM DMFc was put in contact with an acidic aqueous solution ($\text{pH } 2$ adjusted by HCl) in a volume ratio of $5:2$ (v/v, 1,2-DCE|Water). Apparently, the aqueous phase turned greener with time, as shown in Figure 4.13.

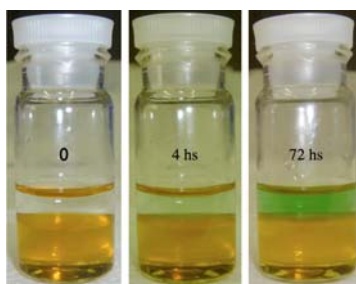


Figure 4.13: Illustration of a biphasic test without electrochemical control: a 5 ml of 1,2-DCE solution containing 50 mM DMFc was put in contact with a 2 ml aqueous solution ($\text{pH } 2$, adjusted by HCl).

UV-Visible spectroscopic measurement (Figure 4.14) revealed the formation of DMFc^+ in water with a characteristic absorption band at 779 nm , which grows continuously with time. Because the interface is not polarized and the 1,2-DCE phase is ion-free, the transfer of ions

including protons from water to 1,2-DCE can only occur in the presence of a very lipophilic counter ion. The production of DMFc^+ in water therefore most probably proceeds by the partition of DMFc from 1,2-DCE to water followed by oxidation with O_2 on the aqueous side of the interface, as illustrated by Scheme 4.2.

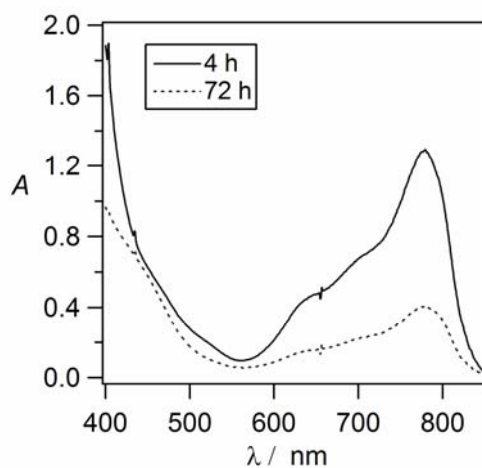
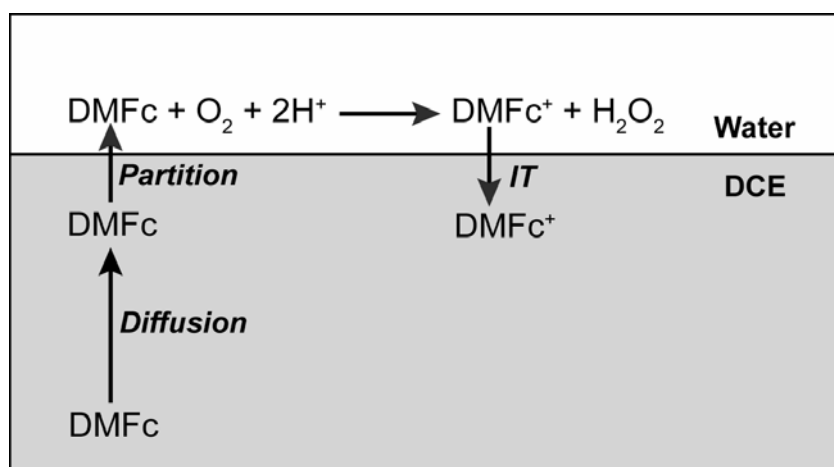


Figure 4.14: UV-Visible spectrum of the aqueous solution after the biphasic test shown in Figure 4.13 (the top solution in the right flask).

Furthermore, the transfer of thus formed DMFc^+ from water to 1,2-DCE, that is the *IT* (ion transfer) step in Scheme 4.2, gives rise to the positive current offset observed in the CV under the electrochemical polarization.



Scheme 4.2: Mechanism of partition of DMFc and reaction with O_2 in water.

Indeed, previous investigations have found that the electron transfer between ferrocene and hexacyanoferrate(III) at the liquid|liquid interface occurs by the same route, partitioning of ferrocene to water and reaction with hexacyanoferrate(III) homogenously on the aqueous side of the interface.^[44] Considering that oxygen is more soluble in 1,2-DCE than in water, oxygen reduction by DMFc on the aqueous side of the interface is likely to be accompanied by oxygen transfer from 1,2-DCE and by transfer from the surrounding air atmosphere.^[28, 45-47] Considering Scheme 4.2, the current offset is the steady state diffusion current due to DMFc⁺ transfer back from water, following the partition of DMFc from the organic phase and H₂O₂ production on the aqueous phase of the interface. Thus, if one assumes the aqueous reaction between DMFc and O₂/H⁺ to be fast, the production of DMFc⁺ in water is controlled by the rate of arrival of DMFc from the bulk organic phase to the interface. As a matter of fact, the steady state diffusion current increases monotonically with the DMFc concentration, indicating that the reaction is not limited by oxygen and proton supply. Accordingly, the sustained production of DMFc⁺ on the aqueous side of the interface can be envisaged as a diffusion–limited reaction, as follows:

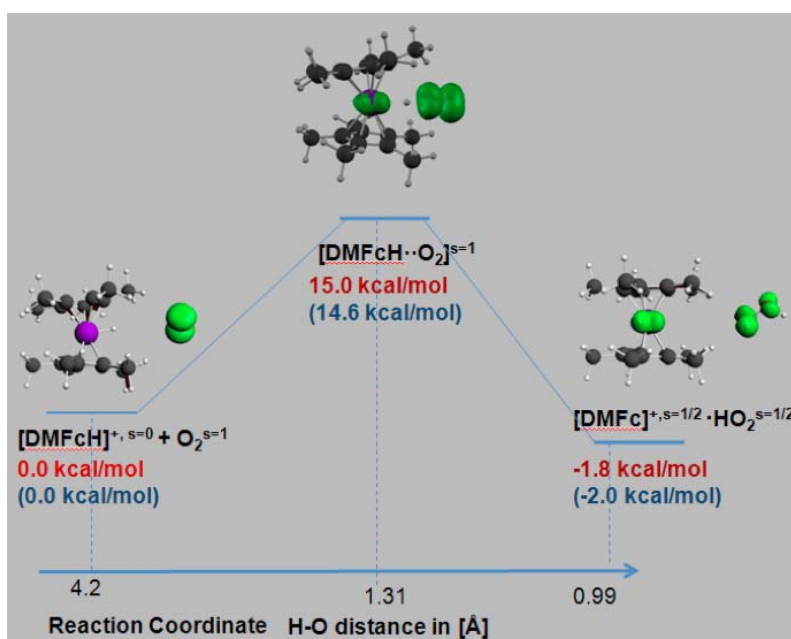
$$j = -D_{\text{DMFc}}^{\circ} \frac{c_{\text{DMFc}}^{\circ, \infty} - c_{\text{DMFc}}^{\circ, 0}}{\delta} \approx -D_{\text{DMFc}}^{\circ} \frac{c_{\text{DMFc}}^{\circ, \infty}}{\delta} \quad (4.21)$$

Where δ represents the diffusion layer thickness in the organic phase and D the diffusion coefficient. Naturally, DMFc⁺ will be afterwards transferred across the interface, giving rise to the aforementioned steady–state current.

4.10 Mechanisms

In proton/oxygen reduction, the reaction proceeds via two steps: first a heterogeneous proton transfer facilitated by DMFc from the aqueous to the organic phase, followed by a homogenous proton/oxygen reduction in the organic phase. This points out that the initial step of proton/oxygen reduction by ferrocene and its derivatives is their protonation, which has been fully characterised by the liquid|liquid electrochemical protocols. However, how the following proton/oxygen reduction proceeds had remained unresolved.

DFT computations support a reaction pathway involving protonated DMFc, DMFcH^+ , as an intermediate species, which reacts with proton/oxygen to produce hydrogen/hydrogen peroxide. But DFT computations do not support the hypothesis that triplet molecular oxygen O_2 coordinates to the iron atom or inserts into the Fe-H bond through a spin-forbidden mechanism. Instead, O_2 approaches the activated hydride directly via a delocalized triplet (diradical) transition state $[\text{DMFc}\cdot\cdot\text{H}\cdot\cdot\text{OO}\cdot]^+$ (Scheme 4.3) with an activation barrier of 15 kcal mol^{-1} in the gas phase (14.6 kcal mol^{-1} in the solvent). This process leads to the formation of dexamethylferrocenium (DMFc^+) and a hydrogen peroxy radical. The generation of H_2O_2 from the latter is then expected to proceed rapidly. Note that other possible mechanistic routes occurring via either a superoxoiron $[\text{DMFc}-\text{O}_2]$ (*i.e.* protonation last) or a superoxide intermediate $[\text{DMFc}-\text{O}_2\text{H}]^+$ (*i.e.* insertion into the Fe-H bond) are all spin-forbidden. Computational investigations of these processes were found to have considerably higher activation barriers than the mechanism proposed.



Scheme 4.3: DFT computation on oxygen reduction by DMFc.

The interface functions as a proton pump driven by the Galvani potential difference and the reaction pathway can be expressed as:



4.11 Conclusions

In summary, we have shown that O_2 reduction by DMFc occurs in the absence of any noble metal catalysts at a polarized water|1,2-DCE interface. In the case of DMFc, it has been shown that oxygen reduction at the polarized water|1,2-DCE interface produces decamethylferrocenium (DMFc^+) and hydrogen peroxide (H_2O_2), on the basis of the two-phase reaction controlled by a common ion with post-reaction product analyses.

The reaction can be equivalent to an *EC* type mechanism at the conventional solid solution interface, with the assisted proton transfer by DMFc across the water|1,2-DCE interface equivalent to the *E* step. The following irreversible oxygen reduction reaction and/or proton reduction reaction involving protonated DMFc in 1,2-DCE represent the chemical step.

4.12 References

- [1] R. Boulatov, J. H. Zagal, F. Bedioui, J.-P. Dodelet, Eds, *N₄-Macrocyclic Metal Complexes* Springer, New York, **2006**.
- [2] I. Yamanaka, T. Onizawa, S. Takenaka, K. Otsuka, *Angewandte Chemie - International Edition* **2003**, *42*, 3653.
- [3] I. Yamanaka, T. Murayama, *Angewandte Chemie - International Edition* **2008**, *47*, 1900.
- [4] K. Otsuka, I. Yamanaka, *Electrochimica Acta* **1990**, *35*, 319.
- [5] W. Eul, A. Moeller, N. Steiner, *Kirk–Othmer Encyclopedia of Chemical Technology, Vol. 14*, 5th ed., Wiley, Hoboken, **2005**.
- [6] J. M. Campos-Martin, G. Blanco-Brieva, J. L. G. Fierro, *Angewandte Chemie - International Edition* **2006**, *45*, 6962.
- [7] W. R. Thiel, *Angewandte Chemie - International Edition* **1999**, *38*, 3157.
- [8] J. H. Zagal, M. A. Paez, J. F. Silva, *N₄-Macrocyclic Metal Complexes*, Springer, New York, **2006**.
- [9] A. Trojanek, V. Marecek, H. Janchenova, Z. Samec, *Electrochemistry Communications* **2007**, *9*, 2185.
- [10] R. Partovi-Nia, B. Su, F. Li, C. P. Gros, J. M. Barbe, Z. Samec, H. H. Girault, *Chemistry - A European Journal* **2009**, *15*, 2335.
- [11] I. Hatay, B. Su, F. Li, R. Partovi-Nia, H. Vrubel, X. Hu, M. Ersoz, H. H. Girault, *Angewandte Chemie International Edition* **2009**, *48*, 5139.
- [12] A. Trojanek, J. Langmaier, B. Su, H. H. Girault, Z. Samec, *Electrochemistry Communications* **2009**, *11*, 1940.
- [13] A. Sarapuu, K. Vaik, D. J. Schiffrin, K. Tammeveski, *Journal of Electroanalytical Chemistry* **2003**, *541*, 23.
- [14] K. Tammeveski, K. Kontturi, R. J. Nichols, R. J. Potter, D. J. Schiffrin, *Journal of Electroanalytical Chemistry* **2001**, *515*, 101.
- [15] F. Mirkhalaf, K. Tammeveski, D. J. Schiffrin, *Physical Chemistry Chemical Physics* **2004**, *6*, 1321.
- [16] K. Vaik, A. Sarapuu, K. Tammeveski, F. Mirkhalaf, D. J. Schiffrin, *Journal of Electroanalytical Chemistry* **2004**, *564*, 159.
- [17] K. Vaik, D. J. Schiffrin, K. Tammeveski, *Electrochemistry Communications* **2004**, *6*, 1.
- [18] J. R. T. J. Wass, E. Ahlberg, I. Panas, D. J. Schiffrin, *Physical Chemistry Chemical Physics* **2006**, *8*, 4189.
- [19] R. Prins, A. G. T. G. Kortbeek, *Journal of Organometallic Chemistry* **1971**, *33*, C33.
- [20] T. E. Bitterwolf, A. C. Ling, *Journal of Organometallic Chemistry* **1972**, *40*, C29.
- [21] J. Lubach, W. Drenth, *Recueil des Travaux Chimiques des Pays-Bas* **1973**, *92*, 586.
- [22] A. Sabela, V. Marecek, Z. Samec, R. Fuoco, *Electrochimica Acta* **1992**, *37*, 231.
- [23] H. Jensen, V. Devaud, J. Josserand, H. H. Girault, *Journal of Electroanalytical Chemistry* **2002**, *537*, 77.
- [24] T. Kakiuchi, *Analytical Chemistry* **1996**, *68*, 3658.
- [25] V. S. Markin, A. G. Volkov, *Journal of Physical Chemistry B* **2004**, *108*, 13807.
- [26] H. H. Girault, *Analytical and Physical Electrochemistry*, EPFL Press, Lausanne, **2004**.
- [27] N. Eugster, D. J. Fermin, H. H. Girault, *Journal of Physical Chemistry B* **2002**, *106*, 3428.

- [28] D. Pletcher, S. Sotiropoulos, *Journal of the Chemical Society, Faraday Transactions* **1995**, 91, 457.
- [29] P. Lyhring, A. Schumpe, *Journal of Chemical and Engineering Data* **1989**, 34, 250.
- [30] A. Trojanek, Z. Samec, *private communications*.
- [31] R. O. Rahn, M. I. Stefan, J. R. Bolton, E. Goren, P. S. Shaw, K. R. Lykke, *Photochemistry and Photobiology* **2003**, 78, 146.
- [32] V. M. Fomin, A. E. Shirokov, N. G. Polyakova, P. A. Smirnov, *Russian Journal of General Chemistry* **2007**, 77, 652.
- [33] B. Su, R. P. Nia, F. Li, M. Hojeij, M. Prudent, C. Corminboeuf, Z. Samec, H. H. Girault, *Angewandte Chemie International Edition* **2008**, 47, 4675.
- [34] F. Li, B. Su, F. C. Salazar, R. P. Nia, H. H. Girault, *Electrochemistry Communications* **2009**, 11, 473.
- [35] Z. Brusova, K. Stulik, V. Marecek, *Journal of Electroanalytical Chemistry* **2004**, 563, 277.
- [36] M. L. McKee, *Journal of the American Chemical Society* **1993**, 115, 2818.
- [37] T. Wandlowski, V. Marecek, Z. Samec, *Electrochimica Acta* **1990**, 35, 1173.
- [38] S. Fukuzumi, S. Mochizuki, T. Tanaka, *Inorganic Chemistry* **1989**, 28, 2459.
- [39] W. Eul, A. Moeller, N. Steiner, *Kirk-Othmer Encyclopedia of Chemical Technology*, John Wiley & Sons, Hoboken, **2005**.
- [40] S. Fukuzumi, K. Okamoto, C. P. Gros, R. Guilard, *Journal of the American Chemical Society* **2004**, 126, 10441.
- [41] M. Buhl, S. Grigoleit, *Organometallics* **2005**, 24, 1516.
- [42] V. M. Fomin, *Russian Journal of General Chemistry* **2007**, 77, 954.
- [43] M. Meot-Ner, *Journal of the American Chemical Society* **1989**, 111, 2830.
- [44] H. Hotta, S. Ichikawa, T. Sugihara, T. Osakai, *Journal of Physical Chemistry B* **2003**, 107, 9717.
- [45] A. Schumpe, W.-D. Deckwer, K. D. P. Nigam, *Canadian Journal of Chemical Engineering* **1989**, 67, 873.
- [46] A. L. Barker, J. V. Macpherson, C. J. Slevin, P. R. Unwin, *Journal of Physical Chemistry B* **1998**, 102, 1586.
- [47] C. J. Slevin, S. Ryley, D. J. Walton, P. R. Unwin, *Langmuir* **1998**, 14, X.

Chapter 5

Proton pump for oxygen reduction catalyzed by 5,10,15,20-tetraphenylporphyrinatocobalt(II)

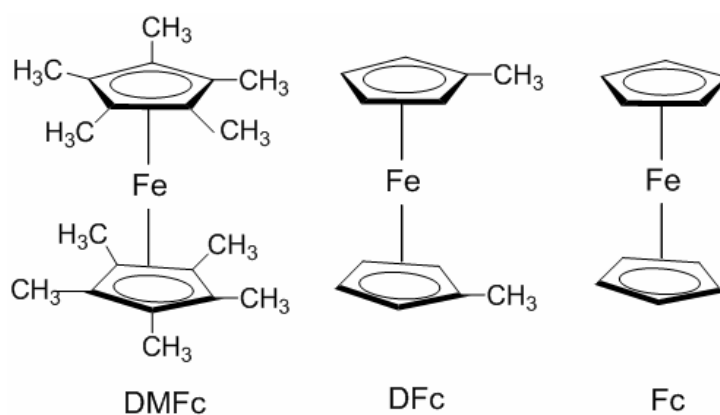
5.1 Introduction

Transition metal macrocyclic compounds, especially metalloporphyrins,^[1-4] form a major category of non-Pt catalysts for oxygen reduction. The electrochemical reduction of molecular oxygen is important especially for devices such as metal air batteries (*e.g.*, Zinc-Air batteries), fuel cells and air cathodes in many industrial electrocatalytic processes (*e.g.*, chlor-alkali cells). Cobalt porphyrins have been extensively studied because of their catalytic activity toward molecular oxygen (O_2) reduction reaction (ORR).^[3-26] The catalytic mechanism involves coordination of O_2 to the cobalt(II) centre, which allows electron delocalization from Co^{III} to bound O_2 to form a superoxide like adduct of $Co^{III}-O_2^{\cdot}$ or $Co^{III}-O_2^{\cdot}H^+$ in the presence of proton, followed by the reduction of the adduct either by an electrode or by a molecular electron donor.^[15-17] In most cases, monomeric cobalt porphyrins catalyze the electroreduction of O_2 to hydrogen peroxide H_2O_2 whereas dimeric cofacial cobalt porphyrins demonstrate the catalysis of four-electron reduction of O_2 to water.^[3, 4, 7, 12, 14, 17, 18, 26-29] Employing ferrocene derivatives as electron donors, O_2 reduction catalyzed by various cobalt porphyrins has been investigated by Fukuzumi *et al.* in organic media in the presence of $HClO_4$.^[15-17] In the reaction scheme, the steps of electron coordination to form a superoxide adduct and its reduction by ferrocene derivatives to produce H_2O_2/H_2O and Co^{III} are fast, and that of reducing Co^{III} by ferrocene derivatives is slow and rate limiting. Liquid|liquid interfaces offer the possibility to physically separate reactants, and to carry out interfacial reactions. Recently, O_2 reduction by DMFc at a polarized 1,2-DCE interface has been reported.^[25, 30-33] In this case, one reactant, namely protons, is located in the aqueous phase, whereas the second one, namely the electron donor, is located in the organic phase. We have shown in Chapter 4 that in this biphasic system the ORR probably proceeds through a proton

transfer from water to 1,2-DCE followed by O_2 reduction by DMFc in 1,2-DCE.^[30] H_2O_2 formed is then extracted to the adjacent water phase immediately after its generation in 1,2-DCE. The oxidation of DMFc to $DMFc^+$ has also been confirmed by UV-Visible spectrophotometric and electrochemical measurements. In the case of O_2 reduction by DMFc, different electrocatalysts, such as interfacially deposited platinum particles^[34] 5,10,15,20-tetraphenyl-21H,23H-porphyrin H_2TPP ,^[33,35] 5,10,15,20-tetraphenylporphyrinatocobalt(II) [Co(tp)]^[25] and cobalt porphine (CoP)^[36] have been studied at polarized water|1,2-DCE interfaces.

In this Chapter, we study the role of [Co(tp)] as a catalyst for a two electron reduction of O_2 by ferrocene (Fc) and its two derivatives, 1,1'-dimethylferrocene (DFc) and DMFc at the polarized water|1,2-DCE interface (Scheme 5.1).

The Voltammetric redox and diffusion coefficients are summarized in Table 5.1. The reaction was found to proceed by a catalytic mechanism similar to that proposed by Fukuzumi *et al.* for bulk reactions,^[16, 17] but in which the water|1,2-DCE interface essentially acts as a proton pump, allowing the control of the amount of protons in 1,2-DCE by the Galvani potential difference across the interface. Moreover, this biphasic system also allows for the very efficient collection of H_2O_2 by extraction immediately after its formation in 1,2-DCE to the adjacent water phase, thus decreasing the possibility of degradation and further reaction with ferrocene derivatives.



Scheme 5.1: Structure of ferrocene derivatives.

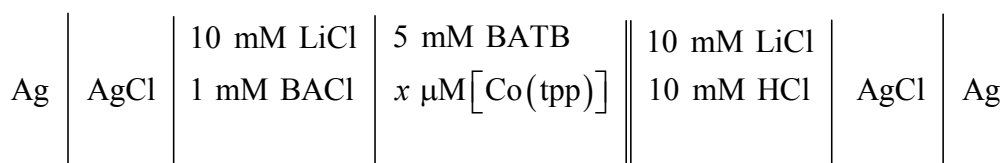
Table 5.1: Data refer to porphyrin and ferrocene derivatives with 5 mM BATB supporting electrolyte in dry 1,2-DCE at 20mVs⁻¹.

Concentration	E_1 vs SHE / V	E_2 vs SHE / V	E_3 vs SHE / V	D / cm ² s ⁻¹
[Co(tpp)], 50 μ M	0.94	1.4	1.9	5.4×10^{-6}
Fc, 5 mM	0.64	—	—	—
DFc, 5 mM	0.48	—	—	—
DMFc, 5 mM	0.034	—	—	—

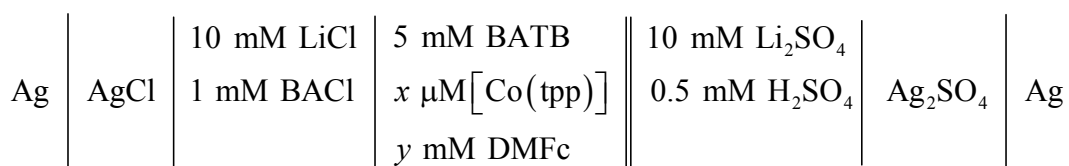
5.2 Electrochemical measurements

The cyclic voltammograms obtained at the water|1,2-DCE interface in the absence (dashed line) and presence (full line) of [Co(tpp)] (500 μ M) in 1,2-DCE, using LiCl (10 mM) and bis(triphenylphosphoranylidene)-ammonium tetrakis(pentafluorophenyl) borate (BATB, 5 mM) as the aqueous and organic supporting electrolytes, respectively, can be seen in Figure 5.1 (Cell 1 in Scheme 5.1). The aqueous pH was adjusted to 2 by the addition of HCl. The voltammetric response in the absence [Co(tpp)] is the classical potential window observed at the water|1,2-DCE interface. Adding [Co(tpp)] (500 μ M) in an oxygen bubbled solution of the organic phase shows significant Faradaic charge transfer reaction compared to the blank.^[33] The corresponding differential capacitance measurements revealed that adsorption of [Co(tpp)] at the interface occurs in the available potential window, as shown in Figure 5.2, the differential capacitance curve in the presence of [Co(tpp)] shows specific transfer/adsorption of [Co(tpp)] at the interface and manifests itself by perturbations of the differential capacitance.

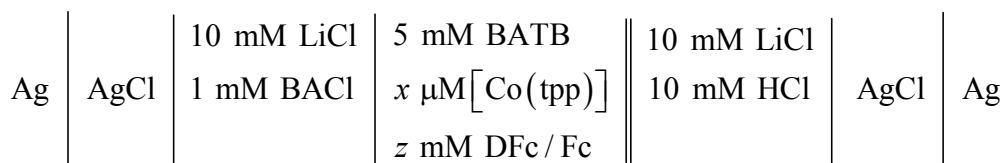
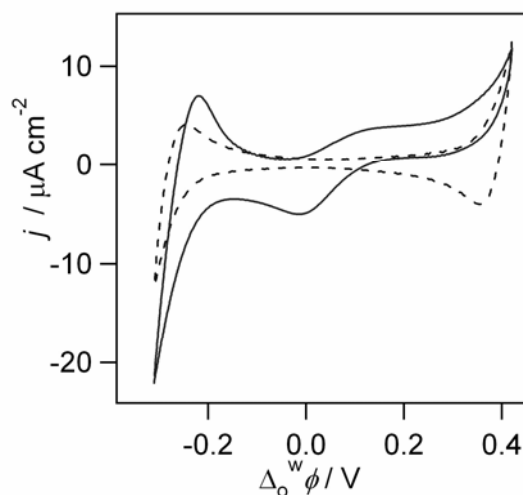
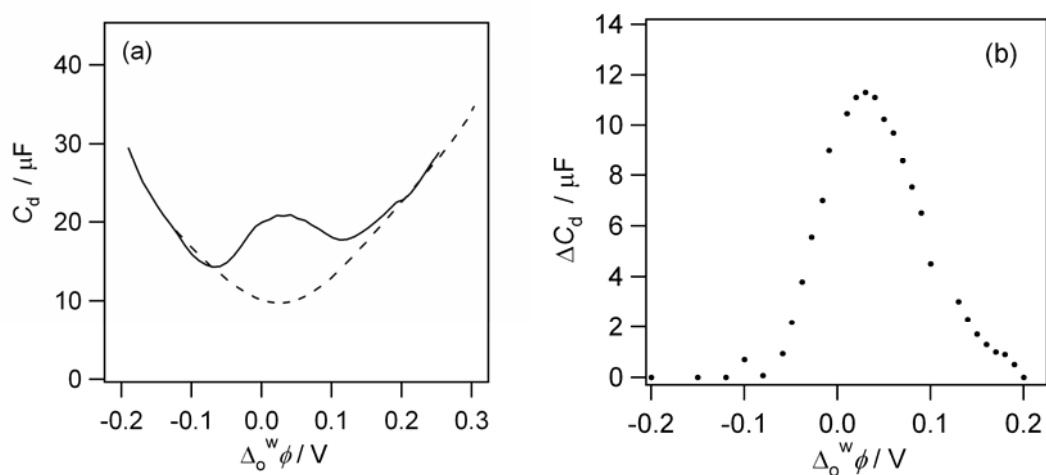
Cell 1



Cell 2



Cell 3

**Scheme 5.2:** Composition of electrochemical cells used.**Figure 5.1:** Cyclic voltammograms (50mVs^{-1}) Cell 1: in the absence ($x=0$, dashed line) and presence ($x=500$, full line) of $[\text{Co}(\text{tpp})]$ in 1,2-DCE.**Figure 5.2:** (a) differential capacitance and (b) alternating current (ac) voltammetry curves using Cell 1: in the absence ($x=0$, dashed line) and presence ($x=500$, full line) of $[\text{Co}(\text{tpp})]$ in 1,2-DCE.

The voltammetric responses of DMFc, DFc and Fc in the absence (dashed line) and the presence of [Co(tpp)] (full line) at the water|1,2-DCE interface are compared in Figure 5.3-5.5. In the presence of only DMFc in 1,2-DCE, a significant current increase (full line) relative to the blank (dotted line in Figure 5.1) can be observed at the positive potentials, as shown in Figure 5.3. This current response arises from proton transfer followed by O₂ reduction by DMFc, as previously reported.^[30] This reaction produces decamethylferrocenium (DMFc⁺) in 1,2-DCE, whose transfer across the water|1,2-DCE interface resulted in a current wave at the negative potential ($\Delta_o^w\phi_{1/2} = -0.26$ V). Further adding [Co(tpp)] in 1,2-DCE led to an increase in the current at the positive potentials, as well as an increase of the ion transfer current of DMFc⁺. These results mean that more DMFc⁺ was generated in the presence of [Co(tpp)], highlighting the catalytic role of [Co(tpp)] on the O₂ reduction by DMFc.

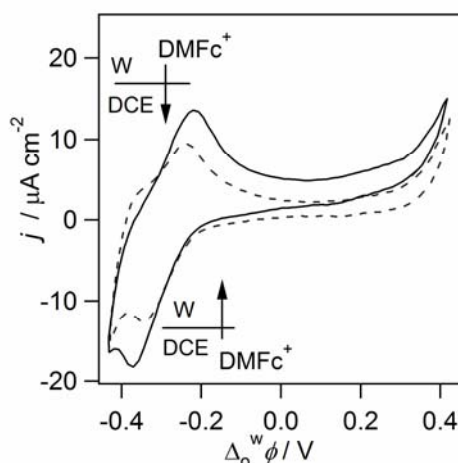


Figure 5.3: Cyclic voltammograms (50mVs^{-1}) using Cell 2: in the presence of only DMFc ($x=0$, $y=5$, dashed line) and both DMFc and [Co(tpp)] ($x=50$, $y=5$, full line).

For DFc and Fc (Figures 5.4 and 5.5) that are weaker reductants than DMFc, a small voltammetric wave was observed at a half-wave potential of -0.05 V and 0.04 V, respectively, when only DFc or Fc is present in 1,2-DCE. Each wave presents a peak-to-peak separation close to 60 mV and the peak current is linearly proportional to the square root of the scan rate.

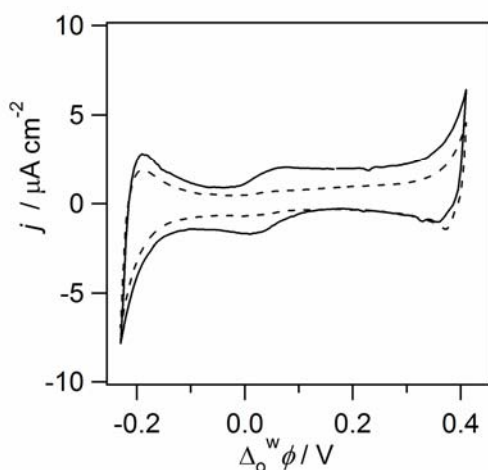


Figure 5.4: Cyclic voltammograms (50 mVs^{-1}) using Cell 3: in the presence of only Fc ($x=0, z=5$, dashed line) and both Fc and $[\text{Co}(\text{tpp})]$ ($x=50, z=5$, full line).

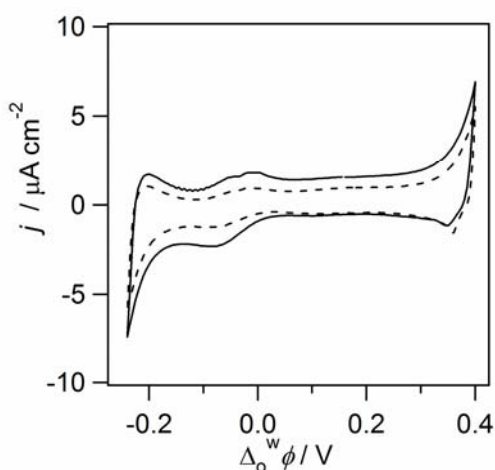


Figure 5.5: Cyclic voltammograms (50 mVs^{-1}) using Cell 3: in the presence of only DFc ($x=0, z=5$, dashed line) and both DFc and $[\text{Co}(\text{tpp})]$ ($x=50, z=5$, full line).

These results suggest that the two waves result from a monovalent ion transfer across the water|1,2-DCE interface, considering that no redox process could occur under the present experimental conditions. Therefore, they can be assigned to the ion transfer of DFc^+ and Fc^+ , formed slowly in the air-saturated solution. Similar to DMFc, if $[\text{Co}(\text{tpp})]$ is present the ion transfer currents of DFc^+ and Fc^+ increase remarkably, suggesting that more DFc^+ and Fc^+ are produced. It convincingly verifies the catalytic role of $[\text{Co}(\text{tpp})]$ on the O_2 reduction, since it

is known that DFc and Fc do not react with O₂ or react slowly, that is, days, in the presence of a strong acid.^[16, 17]

5.3 Shake flask experiments with Fc, DFc and DMFc

Shake flask experiment [Co(tpp)] catalyzed O₂ reductions by Fc, DFc and DMFc at a water|1,2-DCE interface at which the polarization was chemically controlled by a common ion, so called shake flask experiments, were performed as reported previously.^[30] Dissolving lithium tetrakis(pentafluorophenyl)borate (LiTB, 5 mM) and HCl (10 mM) in water and BATB (5 mM) in 1,2-DCE (water/DCE=1:1 in volume), the Galvani potential difference across the interface is fixed by the common ion TB⁻ at a potential 0.54 V.^[30, 37] At this potential, proton initially present in water will partition into 1,2-DCE, leading finally to a distribution of proton in two phases according to the Nernst equation. If only [Co(tpp)] is present in 1,2-DCE, a Soret band (λ_{\max} =427 nm) and a Q band (λ_{\max} =540 nm) are observed after the shake flask experiment, which demonstrates a bathochromic shift relative to those of a fresh [Co(tpp)] solution at 410 nm and 526 nm, as shown in Figure 5.6.

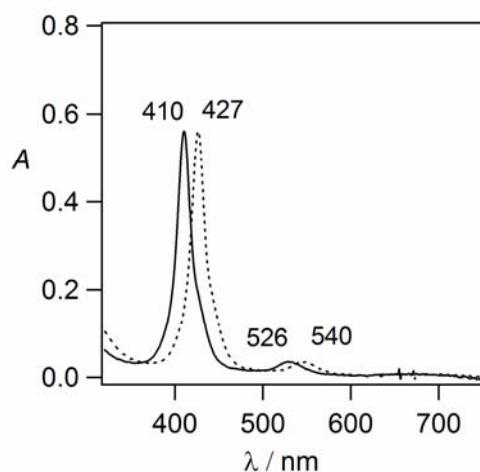


Figure 5.6: Absorption spectra of 1 μ M [Co(tpp)] in 1,2-DCE freshly prepared (full line) and after a shake flask experiment (dotted line).

This shift corresponds to proton facilitated oxygenation of [Co(tpp)] to form an adduct [$\{Co^{III}(tpp)^+-O_2^-\}$].^[16, 17, 38] As a control experiment, O₂ reduction by DMFc, DFc and Fc in the absence [Co(tpp)] was also performed in Figures 5.7 ,5.8 and 5.8. O₂ reduction by Fc and DFc occurs as evidenced by the detection of Fc⁺ at 620 nm and DFc⁺ at 652 nm, respectively,

as shown in Figures 5.8 and 5.9. However, the reaction proceeds rather slowly and it takes several hours to observe the evolution of Fc^+ and DFc^+ absorption bands. In contrast, O_2 reduction by DMFc is much faster, as demonstrated in Figure 5.7, and in tens of minutes all of the DMFc is consumed. The difference in O_2 reduction ability for Fc, DFc and DMFc is in agreement with that previously reported.^[16, 17]

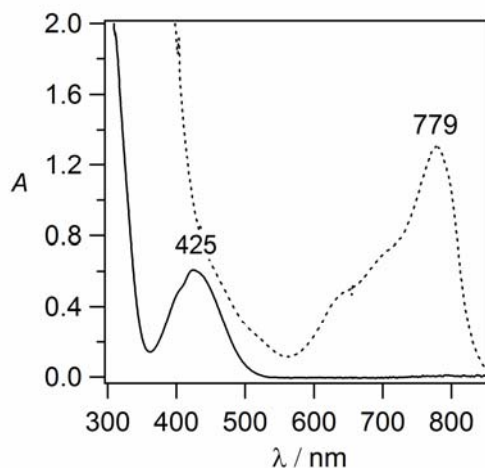


Figure 5.7: Absorption spectra of 5 mM DMFc in 1,2-DCE freshly prepared (full line) and after shake flask experiments (dotted line) for DMFc (30 minutes).

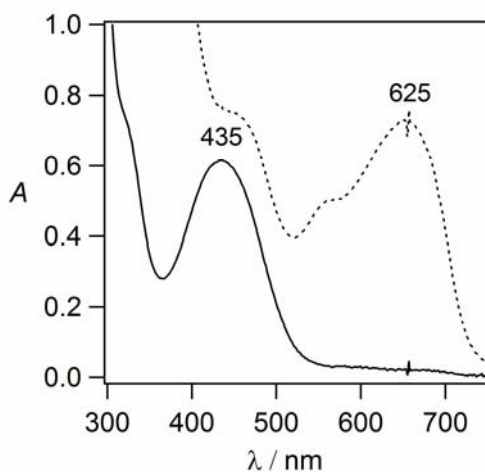


Figure 5.8: Absorption spectra of 5 mM DFc in 1,2-DCE freshly prepared (full line) and after shake flask experiments (dotted line) for DFc (24 hours).

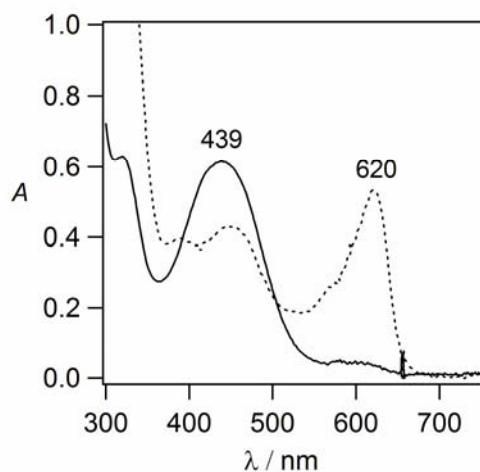


Figure 5.9: Absorption spectra of 5 mM Fc in 1,2-DCE freshly prepared (full line) and after shake flask experiments (dotted line) for Fc (24 hours).

Upon an addition of [Co(tp)], the rise of the absorption bands at 779, 652 and 620 nm, corresponding to DMFc^+ , DFc^+ and Fc^+ , respectively, could be immediately observed, as displayed in Figure 5.10.

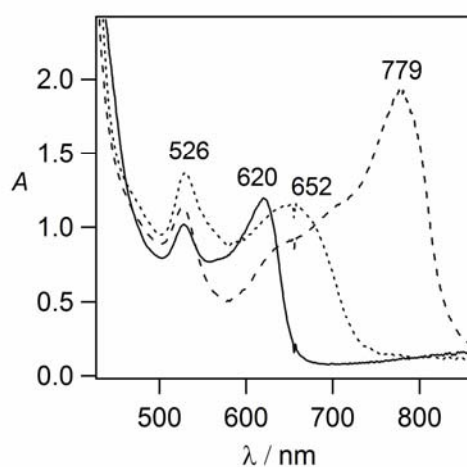


Figure 5.10: Absorption spectra of the 1,2-DCE phase after 30 minutes of shake flask experiments in presence of 50 μM [Co(tp)] with 5 mM DMFc (dashed line), DFc (dotted line) and Fc (full line).

A time profile of the formation of Fc^+ in the absence and presence of [Co(tp)] (compared in Figure 5.11) shows that the oxidation of Fc is much faster in the presence of [Co(tp)].

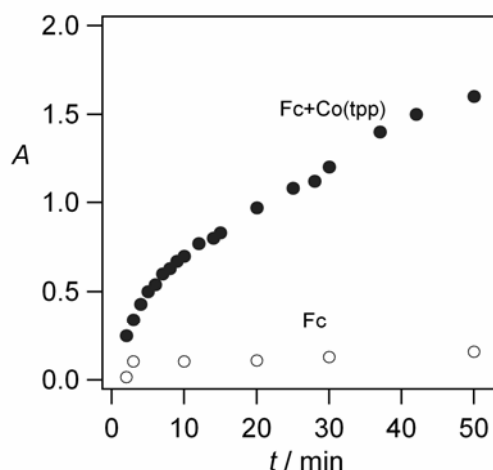


Figure 5.11: Time profile of the formation of Fc^+ in the absence (\circ) and presence (\bullet) of $50\mu M [Co(tp)]$ in 1,2-DCE during the shake flask experiments.

These results suggest that $[Co(tp)]$ has a catalytic role in the O_2 reduction by ferrocene compounds. As for the top aqueous phase, excess NaI (equivalent to 0.1M) was added and UV-Visible spectroscopic measurements revealed the absorption characteristics of I_3^- ($\lambda_{max}=287, 352$ nm), as shown in Figure 5.12. The detection of I_3^- confirms the production of H_2O_2 in the shake flask experiment, since H_2O_2 is a strong oxidant that can oxidize I^- to I_3^- .^[17, 30] One more point should be mentioned is that in the shake flask experiments, the Q band of $[Co(tp)]$ ($\lambda_{max}=526$ nm) was observed for all three ferrocene compounds, whereas that of $[Co(tp)]^+$ ($\lambda_{max}=540$ nm) was not, as shown in Figure 5.10. This result suggests the reduction of $[Co(tp)]^+$ by Fc and its two derivatives.

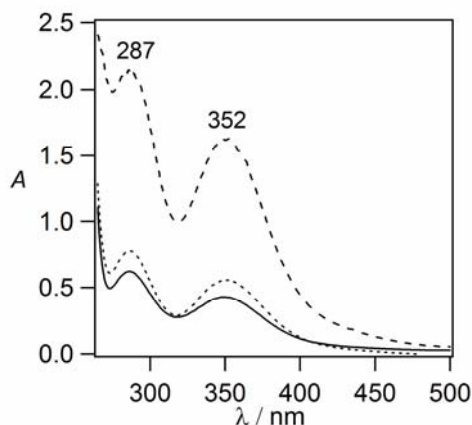
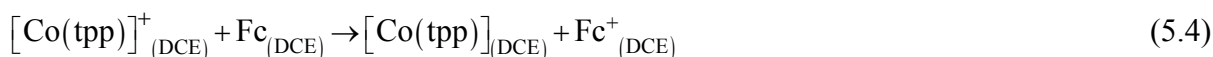
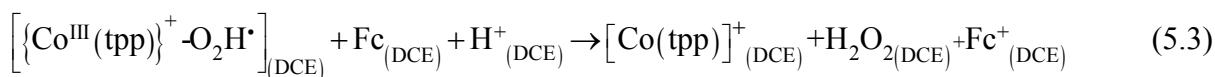
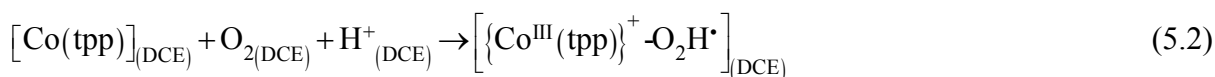


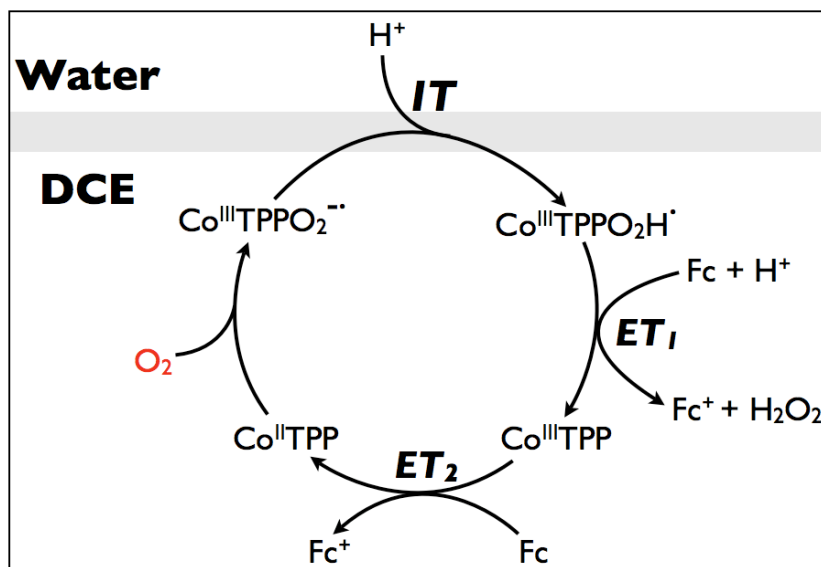
Figure 5.12: Absorption spectra of the aqueous phase after treated with excess NaI after 30 minutes of shake flask experiments in presence of 50 μM [Co(tpp)] with 5 mM DMFc (dashed line), DFc (dotted line) and Fc (full line).

5.4 Mechanisms

Based on above experimental results, it can be concluded that two-electron reduction of O₂ to H₂O₂ by DMFc, DFc and Fc, could be effectively catalyzed by [Co(tpp)]. This is in agreement with a conclusion that made previously that monomeric cobalt porphyrins only catalyze two-electron reduction of O₂.^[16, 17] One of advantages of the present system is that the liquid|liquid interface acts as a proton pump, controlled by the interfacial Galvani potential difference, driving the proton transfer from water to 1,2-DCE. The transfer of proton could be favoured by [$\{Co^{III}(tpp)^+ - O_2^-\}$] to form [$\{Co^{III}(tpp)^+ - O_2H^\bullet\}$], followed by its reduction by ferrocene derivatives to generate H₂O₂ and regeneration of [Co(tpp)] from [Co^{III}(tpp)]⁺ by ferrocene derivatives, see Equations (5.1)–(5.4):



This reaction chain leads to a reaction cycle displayed in Scheme 5.4, which is very similar to that proposed by Fukuzumi *et al.* for the homogeneously $[\text{Co}(\text{tpp})]$ catalyzed O_2 reduction by ferrocene derivatives.^[16, 17]



Scheme 5.4: Reaction scheme of the proton pump controlled by the Galvani potential difference for $[\text{Co}(\text{tpp})]$ catalyzed oxygen reduction by ferrocene compounds. IT =ion transfer, ET =electron transfer.

As proven by the quantity of H_2O_2 generated by DMFc, DFc and Fc, which follows an order of $\text{DMFc} > \text{DFc} > \text{Fc}$ with a molar ratio of 4:1.3:1 (Figure 5.12); the reduction of $[\text{Co}^{\text{III}}(\text{tpp})]^+$ by DMFc, DFc or Fc is the rate limiting step.

However, it should be mentioned that the reaction rate is in part controlled by the mass transport of proton across the water|1,2-DCE interface [Equation(5.1)]. Shake flask experiments indicated that the rate of formation of ferrocenium derivatives was dependent on the Galvani potential difference tuned by using various common ions.

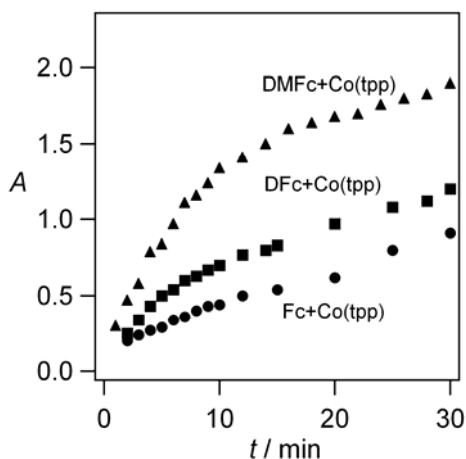


Figure 5.13: Time profile of the formation of Fc^+ , DFc^+ and $DMFc^+$ in presence $50\mu M$ $[Co(tp)]$ in 1,2-DCE during the shake flask experiments.

5.5 Conclusion

The interface essentially acts as a proton pump controlled by the Galvani potential difference across the interface, driving the proton transfer from water to 1,2-DCE, which is followed by $[Co(tp)]$ catalyzed O_2 reduction by Fc, DFc and DMFc to produce H_2O_2 . The catalytic mechanism is similar to that proposed by Fukuzumi *et al.* for bulk reactions.^[16, 17] This interfacial system favours the collection of H_2O_2 , by extraction immediately after its formation in 1,2-DCE to the adjacent water phase, thus preventing degradation and further reaction with ferrocene derivatives, which for bulk systems usually leads to an overall reaction stoichiometry higher than 2.^[16, 33]

5.6 References

- [1] B. Wang, *Journal of Power Sources* **2005**, *152*, 1.
- [2] H. Liu, L. Zhang, J. Zhang, D. Ghosh, J. Jung, B. W. Downing, E. Whitemore, *Journal of Power Sources* **2006**, *161*, 743.
- [3] J. P. Collman, P. Denisevich, Y. Konai, M. Marrocco, C. Koval, F. C. Anson, *Journal of the American Chemical Society* **1980**, *102*, 6027.
- [4] C. J. Chang, Y. Deng, C. Shi, C. K. Chang, F. C. Anson, D. G. Nocera, *Chemical Communications* **2000**, 1355.
- [5] J. H. Zagal, M. A. Paez, J. F. Silva, in *N4-Macrocyclic Metal Complexes (Eds.: J. H. Zagal, F. Bedioui, J.-P. Dodelet)*, Springer, New York, **2006**.
- [6] B. Steiger, C. Shi, F. C. Anson, *Inorganic Chemistry* **1993**, *32*, 2107.
- [7] B. Steiger, F. C. Anson, *Inorganic Chemistry* **2000**, *39*, 4579.
- [8] C. Shi, B. Steiger, M. Yuasa, F. C. Anson, *Inorganic Chemistry* **1997**, *36*, 4294.
- [9] I. Bhugun, F. C. Anson, *Inorganic Chemistry* **1996**, *35*, 7253.
- [10] D. A. Buttry, F. C. Anson, *Journal of the American Chemical Society* **1984**, *106*, 59.
- [11] J. P. Collman, N. H. Hendricks, C. R. Leidner, E. Ngameni, M. L'Her, *Inorganic Chemistry* **1988**, *27*, 387.
- [12] J. P. Collman, M. Marrocco, P. Denisevich, C. Koval, F. C. Anson, *Journal of Electroanalytical Chemistry* **1979**, *101*, 117.
- [13] R. R. Durand Jr, F. C. Anson, *Journal of Electroanalytical Chemistry* **1982**, *134*, 273.
- [14] R. R. Durand Jr, C. S. Bencosme, J. P. Collman, F. C. Anson, *Journal of the American Chemical Society* **1983**, *105*, 2710.
- [15] S. Fukuzumi, S. Mochizuki, T. Tanaka, *Chemical Letters* **1989**, 27
- [16] S. Fukuzumi, S. Mochizuki, T. Tanaka, *Inorganic Chemistry* **1989**, *28*, 2459.
- [17] S. Fukuzumi, K. Okamoto, C. P. Gros, R. Guilard, *Journal of the American Chemical Society* **2004**, *126*, 10441.
- [18] Y. L. Mest, C. Inisan, A. Laouenan, M. L'Her, J. Talarmin, M. E. Khalifa, J. Y. Saillard, *Journal of the American Chemical Society* **1997**, *119*, 6095.
- [19] C. Shi, F. C. Anson, *Inorganic Chemistry* **1992**, *31*, 5078.
- [20] C. Shi, F. C. Anson, *Inorganica Chimica Acta* **1994**, *225*, 215.
- [21] C. Shi, F. C. Anson, *Electrochimica Acta* **1994**, *39*, 1613.
- [22] C. Shi, F. C. Anson, *Inorganic Chemistry* **1996**, *35*, 7928.
- [23] B. Steiger, F. C. Anson, *Inorganic Chemistry* **1997**, *36*, 4138
- [24] E. Song, C. Shi, F. C. Anson, *Langmuir* **1998**, *14*, 4315.
- [25] A. Trojanek, V. Marecek, H. Janchenova, Z. Samec, *Electrochemistry Communications* **2007**, *9*, 2185.
- [26] J. E. Hutchison, T. A. Postlethwaite, C. H. Chen, K. W. Hathcock, R. S. Ingram, W. Ou, R. W. Linton, R. W. Murray, D. A. Tyvoll, L. L. Chng, J. P. Collman, *Langmuir* **1997**, *13*, 2143.
- [27] F. C. Anson, C. Shi, B. Steiger, *Accounts of Chemical Research* **1997**, *30*, 437.
- [28] C. J. Chang, Z. H. Loh, C. Shi, F. C. Anson, D. G. Nocera, *Journal of the American Chemical Society* **2004**, *126*, 10013.
- [29] R. R. Durand Jr, J. P. Collman, F. C. Anson, *Journal of Electroanalytical Chemistry* **1983**, *151*, 289.
- [30] B. Su, R. P. Nia, F. Li, M. Hojeij, M. Prudent, C. Corminboeuf, Z. Samec, H. H. Girault, *Angewandte. Chemie* **2008**, *47*, 4675.
- [31] V. J. Cunnane, G. Geblewicz, D. J. Schiffrin, *Electrochimica Acta* **1995**, *40*, 3005.
- [32] A. Trojanek, J. Langmaier, Z. Samec, *Electrochemistry Communications* **2006**, *8*, 475.

- [33] A. Trojanek, J. Sebera, S. Zalis, J.-M. Barbe, B. Su, H. H. Girault, Z. Samec, *unpublished results*.
- [34] A. Trojanek, J. Langmaier, Z. Samec, *Electrochemistry Communications* **2006**, 8, 475.
- [35] A. Trojanek, J. Langmaier, B. Su, H. H. Girault, Z. Samec, *Electrochemistry Communications* **2009**, 11, 1940.
- [36] I. Hatay, B. Su, F. Li, M. A. Mendez, T. Khoury, C. P. Gros, J. M. Barbe, M. Ersoz, Z. Samec, H. H. Girault, *Journal of the American Chemical Society* **2009**, 131, 13453.
- [37] T. Wandlowski, V. Marecek, Z. Samec, *Electrochimica Acta* **1990**, 35, 1173.
- [38] R. D. Jones, D. A. Summerville, F. Basolo, *Chemical Reviews* **1979**, 79, 139.

Chapter 6

Cobalt(II) Octaethylporphyrin catalysis for dioxygen reduction at liquid | liquid interfaces

6.1 Introduction

Oxygen reduction reaction is a spin-forbidden process, which is kinetically slow at ambient temperature unless a catalyst is present. Number of metalloporphyrins have been chemically synthesized ^[1-3] and their catalytic activity has been investigated extensively using the modified electrode methodology^[4-15] or using molecular electron donors, such as Fc and its derivatives, in homogeneous solutions.^[16-18] Reduction of O₂ by Fc in acidic solutions proceeds rather slowly, and the presence of catalytic amount of metalloporphyrins can significantly accelerate the reaction rate.^[18-21]

Another way to study the catalytic properties of different porphyrins as showed in Chapter 4 and 5 is to study oxygen reduction at polarised liquid|liquid interfaces. Indeed, such interfaces can be polarised *i.e.* the potential difference between the two phases can be controlled and furthermore they offer the possibility to physically separate reactants, such as the protons in water and the electron donors in the organic phase to carry out interfacial proton-coupled electron transfer reactions.

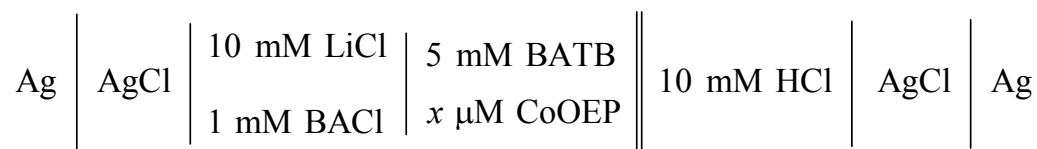
Electrochemistry at liquid|liquid interfaces is a new type of bio-inspired electrochemistry. Indeed, the electrochemical control of ITIES provides a very efficient method to control the rates of either proton or electron transfer across the interface that are both potential dependent. On the other hand, ORR is a proton-coupled electron transfer (*PCET*) reaction. When studying ORR on a solid electrode, one measures by amperometry the electron transfer rate but it is not possible to control the proton transfer step by controlling the electrode potential. Electrochemistry at a liquid|liquid interface, has manifested recently itself as a unique approach to study *PCET* reaction with the possibility of locating protons in the aqueous phase and electron donors in the organic phase.^[22]

In this Chapter, proton-coupled oxygen reduction by Fc involving cobalt porphyrin catalyst, 2,3,7,8,12,13,17,18-Octaethyl-porphyrin cobalt(II) (CoOEP), at a polarized water|1,2-DCE interface is reported. CoOEP serves as a redox catalyst like conventional cobalt porphyrins, activating on O₂ reduction via coordination with the cobalt(II) (Co^{II}) center by the formation of a superoxide structure. The present system provides an example of molecular electrocatalysis for oxygen reduction; molecular catalyst is a molecule like in homogeneous catalysis and electrocatalysis because the ORR depends on the applied Galvani potential difference between the two phases.

6.2 Interfacial electron transfer

Figure 6.1(a) shows the cyclic voltammogram of the base electrolyte, HCl in water and BATB in 1,2-DCE.

Cell 1



From the voltammogram in Figure 6.1, two signals were observed on the forward scan, with wave (A) and the other signal was observed on the reverse sweep, peak (B).

The first plateau (wave A) could correspond to a catalytic current from the presence of both, protons and [(Co-O₂)-OEP]. It is also clear that the magnitude of this signal is strongly dependant on the concentration of the porphyrin but not on the pH.

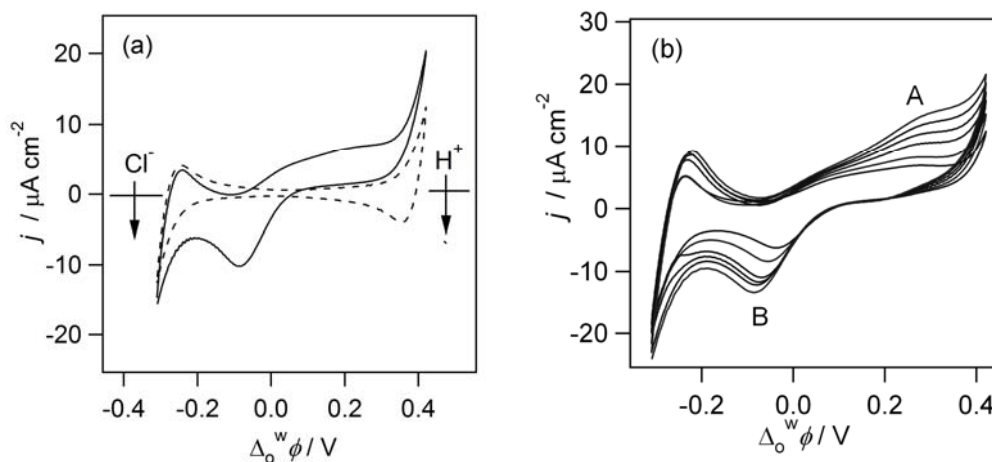


Figure 6.1: Cyclic voltammograms (50 mV s^{-1}) curves obtained using Cell 1(a) in the absence ($x=0$, dashed line) and presence ($x=200$, full line) of CoOEP in 1,2-DCE (b) at various scan rate: 0.02, 0.03, 0.05, 0.064, 0.08 and 100 mV s^{-1} .

This also indicates that the reaction might be limited by the diffusion and further adsorption of $\text{Co}^{\text{II}}\text{OEP}$ from the bulk solution to the interface. The positive current signal at the end of potential window corresponds to a proton-coupled electron transfer (*PCET*) reaction, in which proton transfer and electron transfer are tightly coupled. *PCET* reaction that depends on the interfacial polarization, *i.e.* on the potential difference applied between the two phases.

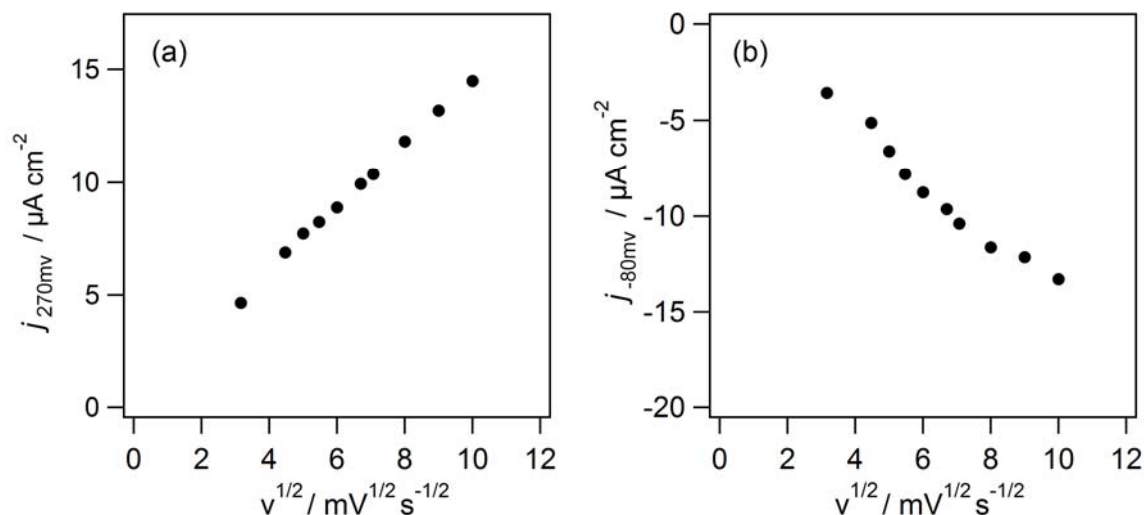


Figure 6.2: The relationship between the current of (a) forward and (b) return peak as a function of square root of scan rate.

The voltammetric response in Figure 6.1(b) shows typical CVs at the ITIES containing CoOEP in the organic phase and illustrates the influence of the scan rate, v , on forward (A) wave and reverse (B) peak current. The forward wave current (A) in Figure 6.2(a) was found proportional to the square root of scan rate, according to Randles-Sevcik equation^[23] indicating a semi-linear diffusion controlled process.

Adsorption/transfer characteristic of CoOEP at water|1,2-DCE was studied by differential capacitance measurements (Figure 6.3) and perturbation of interfacial capacitance observed (in presence of faradic current). Specific transfer/adsorption of CoOEP at the interface manifests itself by an increase of the differential capacitance. The symmetrical potential dependence of the capacitance around the zero charge was strongly affected the addition of CoOEP, suggesting that the porphyrin molecules are adsorbed at the molecular boundary between water and 1,2-DCE, introducing substantial changes in the potential distribution across the interface.

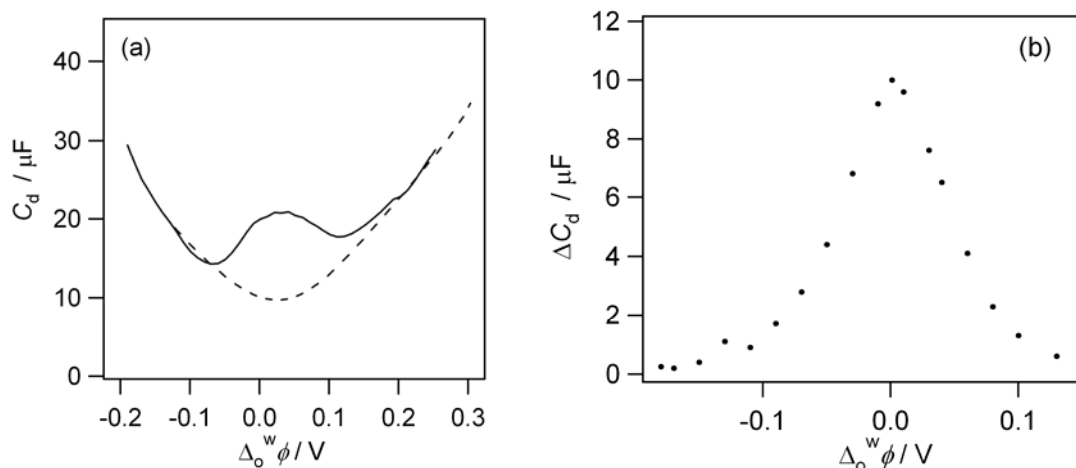


Figure 6.3: (a) differential capacitance and (b) ac voltammetry curves using Cell 1: in the absence ($x=0$, dashed line) and presence ($x=200$, full line) of CoOEP in 1,2-DCE.

Cyclic voltammograms of CoOEP at various acidic pH values as shown in Figure 6.4. The wave potential shifts 60mV/pH toward higher potential value when the pH in the aqueous phase increases. This shift confirms the implication of a proton. It is also interesting to notice that the positive current is rather constant and not affected by the pH, whereas the reverse peak appears larger at high pH values.

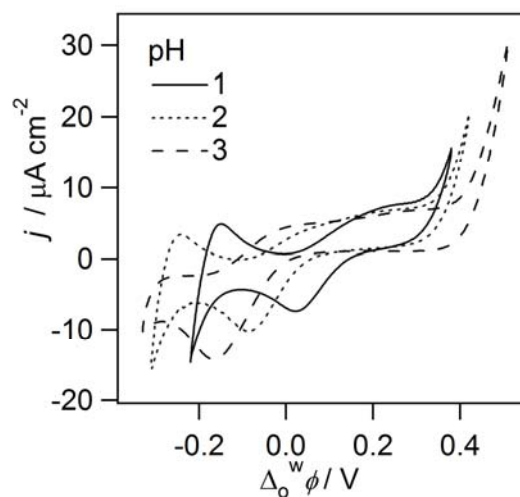


Figure 6.4: CVs obtained (50 mV/s) at a water/1,2-DCE interface with cell 1 when ($x = 200$) at different pH.

The effect of CoOEP concentration on the signal (A) was studied in Figure 6.5. The required amount of CoOEP and 5mM BATB solution was directly added to the organic phase to adjust the desired CoOEP concentration and the transfer was then measured by cyclic voltammetry. The measured peak currents also linearly increase with the CoOEP concentration. This

confirms that the ion transfer reaction limited by the diffusion of CoOEP species in the organic phase.

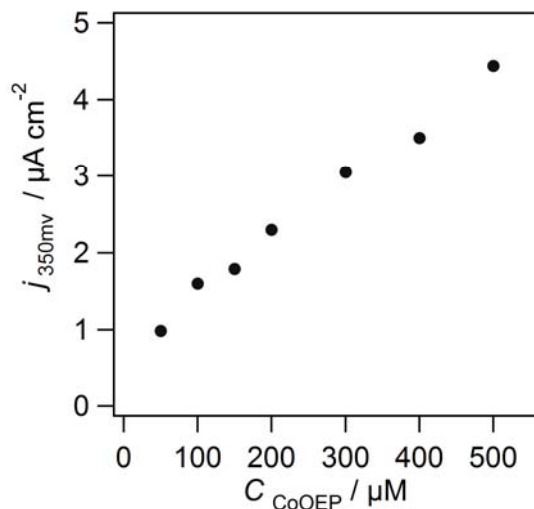


Figure 6.5: Linear dependence of the irreversible current at 350 mV on the CoOEP concentration at a water/1,2-DCE interface with Cell 1 in various concentrations of CoOEP.

The irreversible current wave as shown in Figure 6.6 enhanced under oxygen-saturated conditions compare to nitrogen-saturated, thereby producing more [(Co-O₂)-OEP]. This voltammetric data undoubtedly shows that this irreversible wave results from the combined presence of CoOEP and O₂.

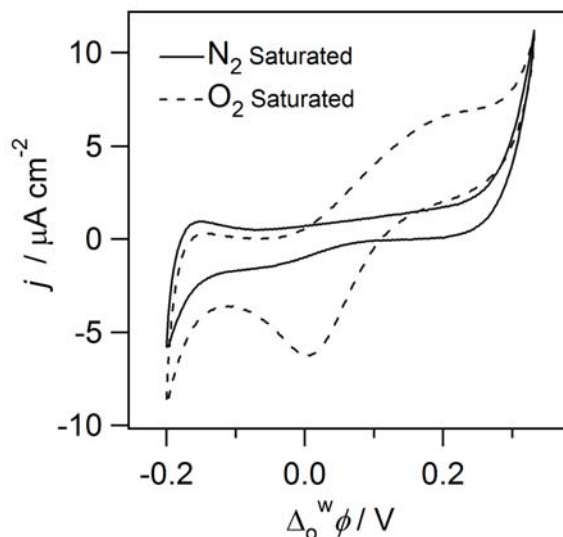


Figure 6.6: CVs obtained at a water/1,2-DCE interface using cell 1 with $x=200$ under N₂-saturated (full line) and O₂-saturated (dashed line) conditions.

The irreversible current depends on the oxygen concentration, and it is also directly proportional to the CoOEP concentration when O₂ and protons are in excess. CoOEP

catalyzed O_2 reductions at a water|1,2-DCE interface at which the polarization was chemically controlled by a common ion, so called shake flask experiments, were performed as reported previously.^[24]

6.3 Two-phase reactions controlled by common ion

Two-phase reactions were performed by 1,2-DCE solution containing 5 mM BATB and 200 μ M CoOEP in contact with an aqueous solution containing 5 mM LiTB and 10 mM HCl in a small flask. The Galvani potential difference across the water|1,2-DCE interface was polarized at a very positive value of 0.54 V by two salts, LiTB and BATB, having a common anion of TB^- . At such potential values, protons can be transferred from water to 1,2-DCE and the aqueous TB^- ions act as a proton pump dragging with them as they transfer to the organic phase. As shown in Figure 6.7 after 30 minutes stirring of the reaction flask, the two phases were separated from each other and were analyzed. When only CoOEP was present, the colour and UV-Visible spectrum of 1,2-DCE phase changed, indicating that the reaction took place, and a red shift of both Soret ($\lambda_{max}=390$ nm) and Q bands ($\lambda_{max}=515, 550$ nm) were observed.^[25-28] Its UV-Visible spectrum, which is ascribed to the oxygenation of $[Co^{II}(OEP)]$ by the formation of superoxide adduct considered formally as $[(Co^{III}-O_2)-OEP]$ at $\lambda_{max}=409$ nm, 523 and 557 nm, as shown in Figure 6.8.

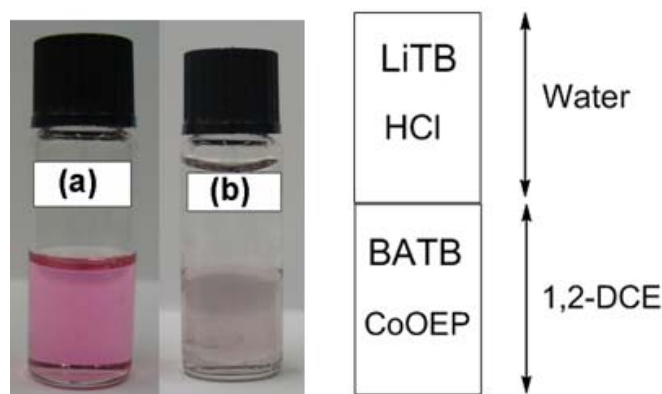


Figure 6.7: Two-phase reaction controlled by TB^- partition (a) before (b) after 30 minutes shaking: the top aqueous phase containing 5 mM LiTB + 10 mM HCl; the bottom 1,2-DCE phase contained 5 mM BATB + 200 μ M CoOEP in the flask.

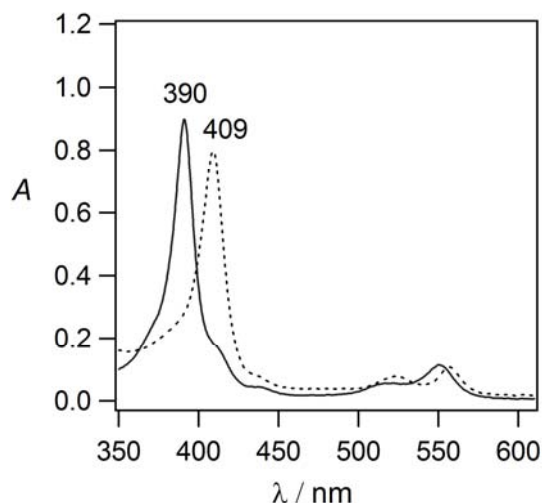


Figure 6.8: Absorption spectra of 5 μM CoOEP in 1,2-DCE freshly prepared (full line) and after a shake flask experiment (dotted line).

The isolated aqueous solution was titrated with NaI to detect the formation of H_2O_2 . Thus, 0.1M of NaI was added to 2 mL of the solution and, the solution changed from colourless to pale yellow. Adding NaI to an aqueous solution containing 5 mM LiTB and 10mM HCl in a controlled titration did not lead to any colour change within the present experimental time scale, thus confirming the presence of H_2O_2 in the aqueous solution. I_3^- can be also detected by UV-Visible spectroscopy, as shown in Figure 6.9 (sharp absorption band at $\lambda_{\text{max}} = 287, 352$ nm). Taking a ϵ_{max} value of $2.76 \times 10^4 \text{ M}^{-1} \cdot \text{cm}^{-1}$,^[29] the concentration of I_3^- can be calculated to be 0.023 mM.

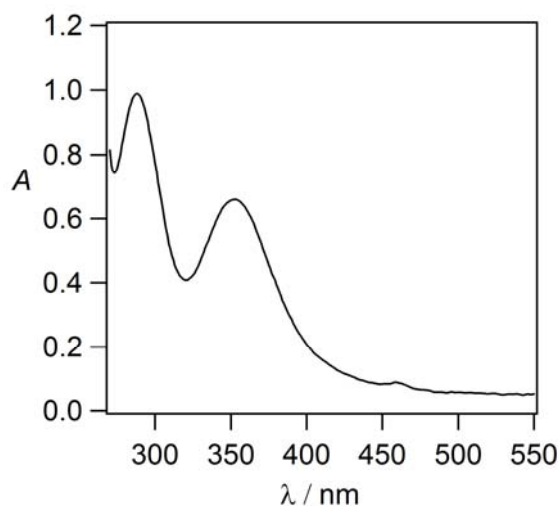


Figure 6.9: Absorption spectra of the aqueous phase after treated with excess NaI after 30 minutes of shake flask experiments in presence of 200 μM CoOEP.

A time profile of the formation of H_2O_2 in the presence of CoOEP in the case of TB^- at two pH value was observed in Figure 6.10, which shows that production of H_2O_2 occurs more in acidic water.

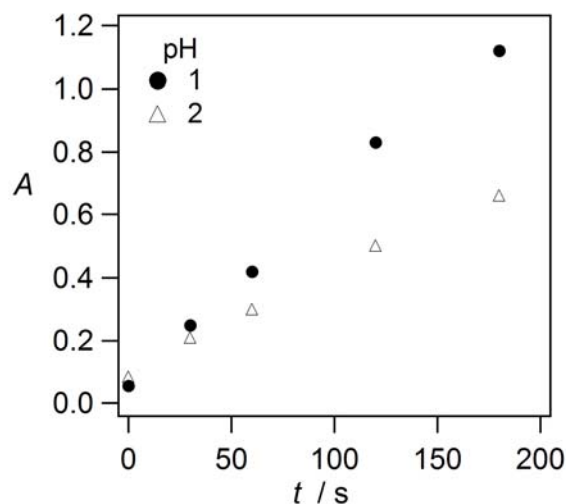


Figure 6.10: Time profile of the formation of H_2O_2 during the shake flask experiments after 30 minutes of shake flask experiments by TB common ion in presence of $200 \mu\text{M}$ CoOEP.

As demonstrated in Figure 6.10, titration of the aqueous solutions by excess NaI suggested that the amount of H_2O_2 produced decreases with increasing the aqueous pH, which is due to a lower concentration of proton in water at a higher pH and the proton diffusion starts to be a controlling factor for oxygen reduction reaction.

Based on above experimental results, it can be concluded that two-electron reduction of O_2 to H_2O_2 catalyzed by CoOEP. Complexation of Co^{II} could occur with O_2 to form $\text{Co}^{\text{III}}\text{O}_2^{\cdot}$. This complex that adsorbs at the interface with the oxygen pointing to the aqueous phase. At low pH complex likes to protonate and produce $\text{Co}^{\text{III}}\text{-O}_2\text{H}^+$. From Table 6.1, we know the redox potential of CoOEP is 0.69 V, which is close to the redox potential of ferrocene (0.64 V). Thus, CoOEP play a similar role as the ferrocene, $[\text{Co}^{\text{III}}\text{-O}_2\text{H}]^+$ is reduced by CoOEP. The hydroperoxide is attacked by protons to give H_2O_2 . The reaction mechanism is in agreement with a conclusion that made previously by Osakai for the interfacial electron transfer (ET) reaction by simulation of cyclic voltammograms at water | oil interface.^[30]

Table 6.1: Data refer to 50 μM of porphyrins with 5mM BATB supporting electrolyte in dry 1,2-DCE a 20mVs^{-1}

Concentration (50 μM)	E_1 vs SHE / V	E_2 vs SHE / V	E_3 vs SHE / V	D / cm^2s^{-1}
CoOEP	0.69	1.23	1.83	—

6.4 CoOEP catalyzed oxygen reduction by Fc

Figure 6.11 compares the CVs obtained under different experimental conditions. First, in the presence of only Fc in 1,2-DCE under aerobic conditions a small voltammetric wave with a half-wave potential at $\Delta_o^w \phi_{1/2} = 0$ V was observed, which corresponds to the transfer of ferrocenium (Fc^+) produced by a slow oxidation of Fc in air and in solution.^[22, 31]

Cell 2

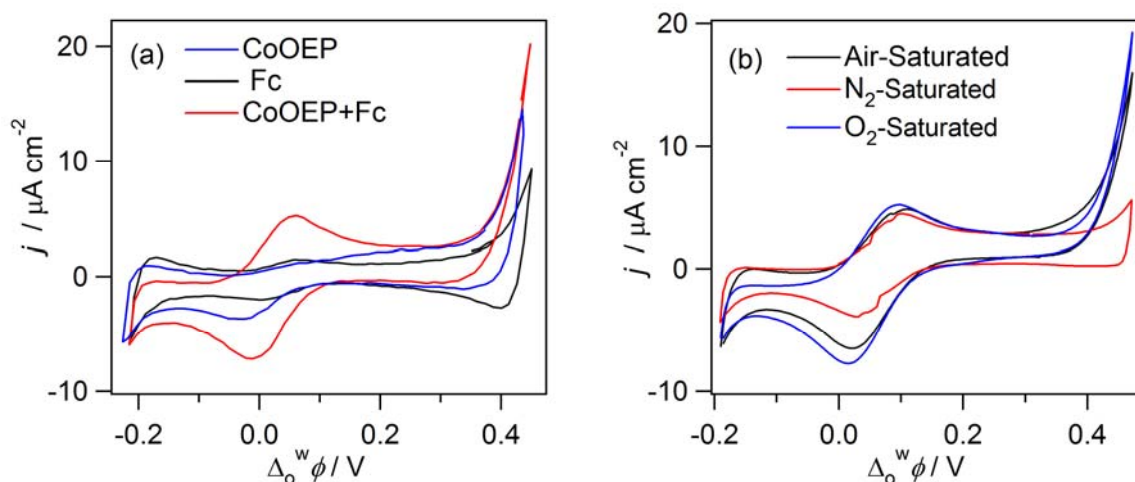
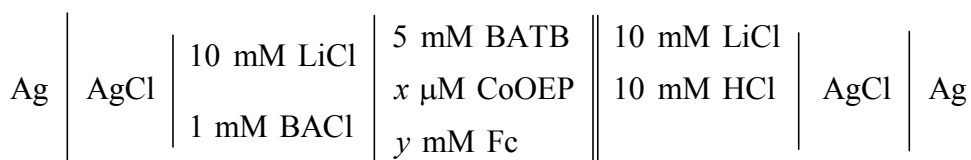


Figure 6.11: (a) Cyclic voltammetry obtained at a water/1,2-DCE interface with cell 2: $x = 50$ and $y = 0$ (blue line), $x = 0$ and $y = 5$ (black line) and $x = 50$ and $y = 5$ (red line); (b) Same with $x = 50$ and $y = 5$ under air-saturated (black line), N_2 -saturated (red line) and O_2 -saturated (blue line) conditions.

However, when both Fc and CoOEP were dissolved in 1,2-DCE, an irreversible positive current signal appeared in the positive potential range. A control experiment under anaerobic conditions showed that this current signal did not appear (red line in Figure 6.11(b)). These facts suggest that CoOEP, O_2 and Fc must be present at the same time to observe this signal.

Therefore, similar to that observed with cobalt porphine,^[22] this irreversible current signal corresponds to a proton-coupled oxygen reduction process catalyzed by CoOEP. This process produces Fc^+ , thus accounting for the significant increment of the Fc^+ transfer current wave located at 0 V as shown in Figure 6.11(a). In fact, when cycling the potential to the positive values repeatedly more Fc^+ will be produced, leading to a continuous increase of the Fc^+ transfer current.

The reduction of O_2 by Fc was also proved by shake flask experiments performed as reported previously.^[22] The Galvani potential difference across the water|1,2-DCE interface was polarized at a very positive value by two salts, LiTB and BATB. Results of the shake flask experiments are shown in Figure 6.12.

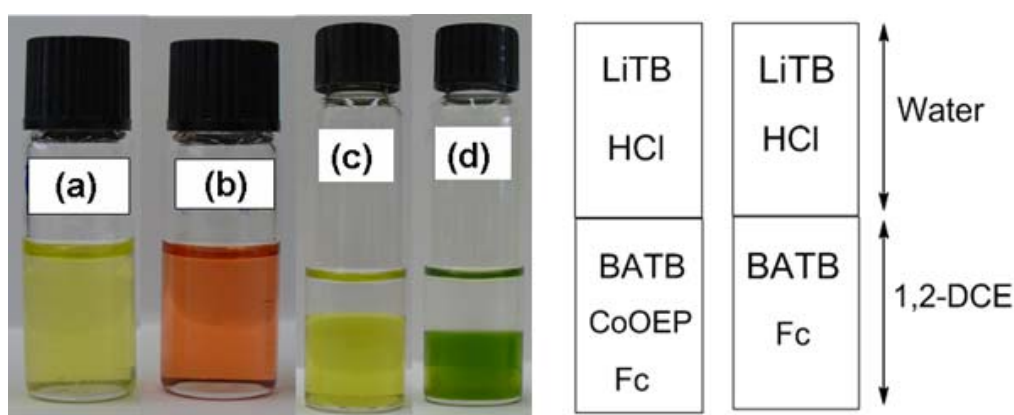


Figure 6.12: Photographs of two phase reactions. The composition of top aqueous phase is the same for two flasks: 5 mM LiTB + 10 mM HCl and 1,2-DCE phase contains (a) fresh solution of 5 mM Fc + 5 mM BATB (b) fresh solution of 5 mM Fc + 50 μM CoOEP + 5 mM BATB (c) 5 mM Fc + 5 mM BATB after contacting with the water solution (d) 5 mM Fc + 50 μM CoOEP + 5 mM BATB after contacting with the water solution.

As shown in Figure 6.12, 10 mM HCl was present in water in two flasks, and the 1,2-DCE phase contained only 5 mM Fc in flask (a), 50 μM CoOEP and 5 mM Fc in flask (b). It was observed that the 1,2-DCE phase in flask (b) changed its colour from orange to dark green immediately (flask (d)) after being put in contact with the water solution. In contrast, the 1,2-DCE phase in flask (a) remained the same (c). The two phases were then separated from each other for further spectroscopic and colorimetric tests.

First, UV-Visible spectra of the separated 1,2-DCE solutions were measured, as shown in Figure 6.13(a). The formation of Fc^+ in the 1,2-DCE solution from flask (d) was revealed and the absorption band with a maximum at 620 nm represents its signature (blue dotted).

The colour change is thus due to the oxidation of Fc to Fc^+ and the colour of 1,2-DCE phase in the flask (d) reflects a mixed colour of green Fc^+ and orange CoOEP. In contrast, in the

presence of Fc only in 1,2-DCE (flask (c)) no Fc^+ was detected, because no change in colour and in the absorption spectrum (dotted black compared to full black) was observed. As for the isolated aqueous solutions from three flasks, excess NaI equivalent to 0.1 M was added. It was observed that the one from flask (d) changed from colourless to yellow as illustrated in Figure 6.13(b).

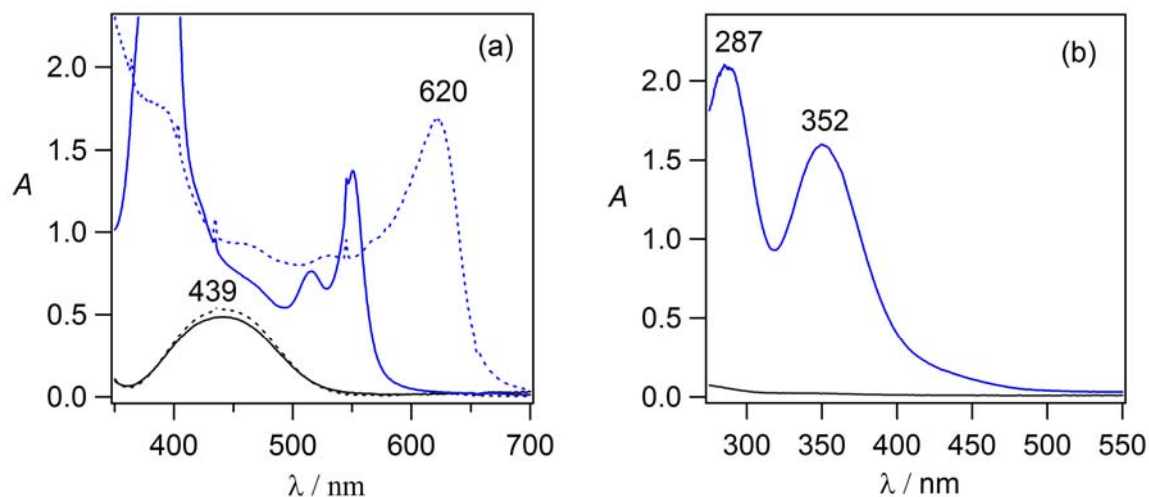


Figure 6.13: (a) Absorption spectra of the 1,2-DCE phases shown in Figure 6.12: flask a (full black), flask b (full blue), flask c (dotted black) and flask d (dotted blue) (b) UV-Visible spectra of the aqueous solutions flask c (black line) and flask d (blue line) after 30 minutes shake flask experiment.

As shown previously, this colour change can be due to the presence of H_2O_2 in the solution. In contrast, no H_2O_2 was detected at all in the aqueous solutions from flask (c). Above experimental facts clearly demonstrated that H_2O_2 and Fc^+ were produced in water and 1,2-DCE, respectively, only when both Fc and CoOEP were present (flask (b)). The concentration of I_3^- can be calculated to be 0.058 mM.

A time profile of the formation of Fc^+ in the absence and presence of CoOEP shows that the oxidation of Fc is much faster in the presence of CoOEP and the reaction rate for TB^- is higher than TMA^+ , which suggests that the heterogeneous reduction of H_2O_2 located in acidic water by Fc in 1,2-DCE does not occur. Upon an addition of CoOEP, the rise of the absorption bands at 620 nm, corresponding to Fc^+ , could be immediately observed, as displayed in Figure 6.14. These results indicated that the rate of formation of ferrocenium was dependent on the Galvani potential difference tuned by using various common ions and CoOEP plays a catalytic role in the O_2 reduction by ferrocene compounds.

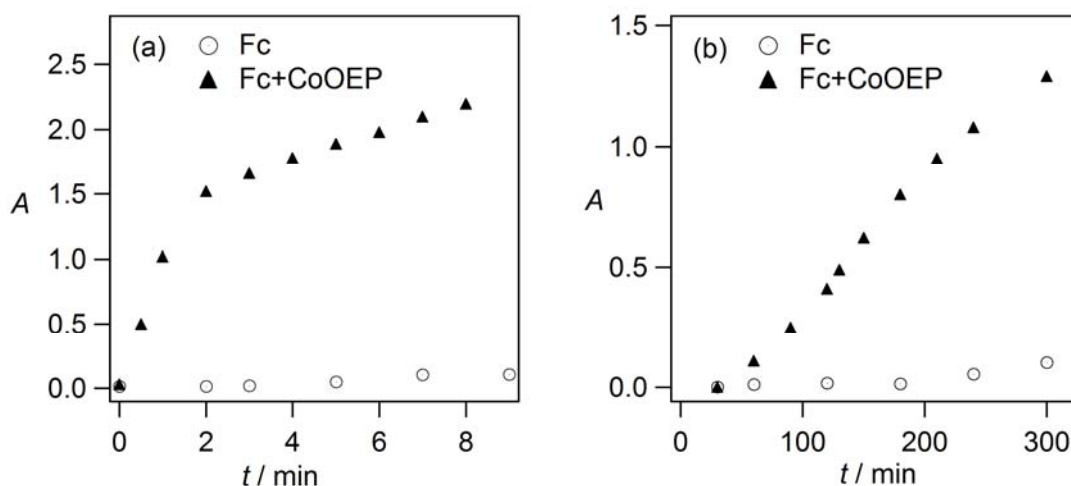


Figure 6.14: Time profile of the formation of Fc^+ in the absence (\circ) and presence (\blacktriangle) of $50 \mu\text{M}$ CoOEP in 1,2-DCE during the shake flask experiments with (a) TB and (b) TMA as a common ion.

A control cyclic voltammetry measurement also proved that in the available potential window no reaction takes place between Fc in 1,2-DCE and H_2O_2 in acidic aqueous phase, as shown in Figure 6.15. Therefore, the irreversible current wave in Figure 6.11(a) corresponds to an interfacial proton-coupled oxygen reduction process, where the electron and proton transfer occur concomitantly.

Cell 3

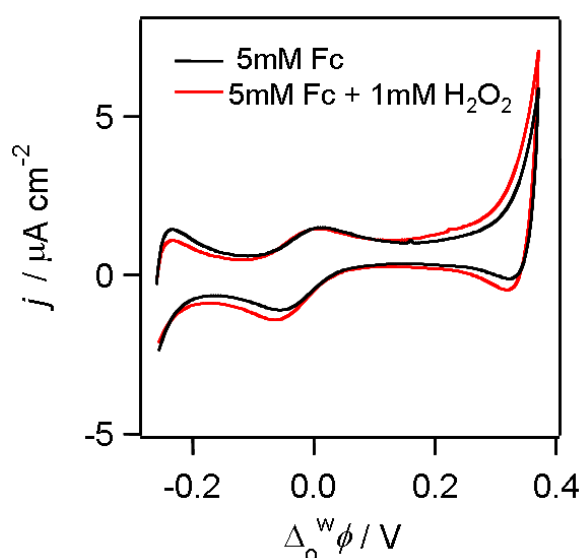
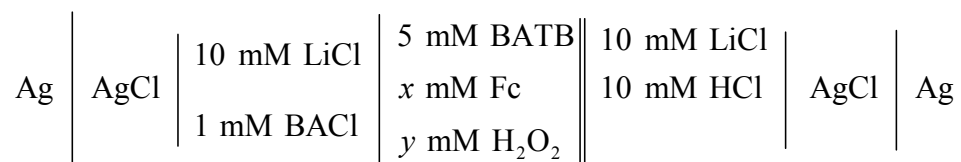


Figure 6.15: CVs obtained at a water/1,2-DCE interface with cell 3 illustrated in Scheme 1: $x = 5$ and $y = 0$ (black line) and $x = 5$ and $y = 1$ (red line).

6.5 CoOEP catalyzed oxygen reduction by DMFc

The voltammetric responses of DMFc in the absence (black line) and the presence of CoOEP (red line) at the water|1,2-DCE interface are compared in Figure 6.16 under aerobic and anaerobic conditions (Cell 4). Dissolving DMFc in 1,2-DCE results an irreversible positive current on the positive potential regime. This current response arises from O₂ reduction by DMFc, as previously reported.^[24]

Cell 4

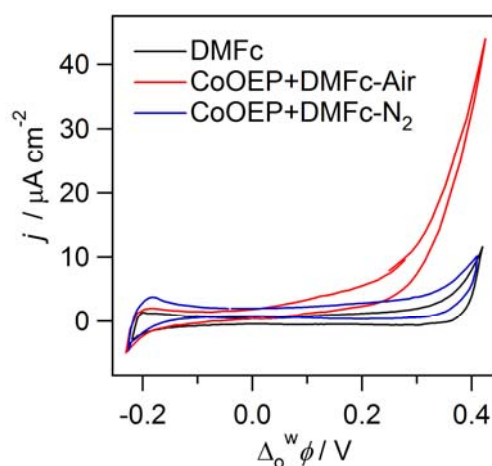
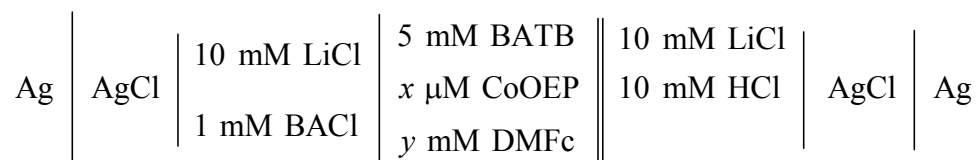


Figure 6.16: Cyclic voltammetry obtained at a water/1,2-DCE interface with cell 4: $x = 0$ and $y = 5$ (black line), $x = 50$ and $y = 5$ (red line) under air-saturated and $x = 50$ and $y = 5$ (blue line) under N₂-saturated condition.

When CoOEP and DMFc were both present, a large irreversible positive current wave was observed at positive potentials. Figure 6.16 clearly shows that the irreversible current wave disappears under anaerobic conditions and is enhanced under oxygen-saturated conditions. This voltammetric data undoubtedly shows that this irreversible wave results from the combined presence of CoOEP, DMFc and O₂.

In the following, two-phase reactions were performed. Typically, a 1,2-DCE solution containing 5 mM TMATB and 5 mM DMFc/50 μM CoOEP was put in contact with an aqueous solution containing 5 mM TMAcI and 10 mM HCl in a small flask. In this case, the Galvani potential difference between the two phases resulting from the distribution of all the ions is dominated by the partition of the common ion, here TMA⁺ anion. With such a choice of electrolyte, this distribution Galvani potential difference can be calculated knowing the

respective Gibbs energy of transfer of the different ionic species and is found to be equal to 0.16 V. After a few minutes stirring of the reaction flask, the two phases were separated from each other and were analyzed. As shown in Figure 6.17, when only DMFc was present (a), the colour and UV-Visible spectrum of 1,2-DCE phase did change to green indicating that reaction took place in flask (c).

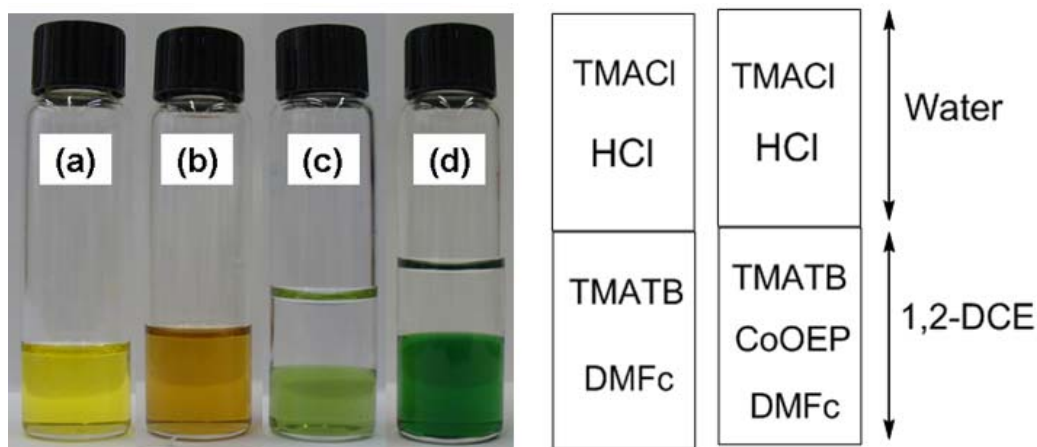


Figure 6.17: Photographs of two phase reactions. The composition of top aqueous phase is the same for two flasks: 5 mM TMACl + 10 mM HCl and 1,2-DCE phase contains (a) fresh solution of 5 mM DMFc+5 mM TMATB (b) fresh solution of 5 mM DMFc + 50 μ M CoOEP + 5 mM TMATB (c) 5 mM DMFc +5 mM TMATB after contacting with the water solution (d) 5 mM DMFc + 50 μ M CoOEP + 5 mM TMATB after contacting with the water solution.

In the presence of both DMFc and CoOEP (b) the colour of 1,2-DCE solution changed instantaneously upon contacting with the aqueous solution, and the final colour (d) indicates a mixture of DMFc⁺ and CoOEP. In the UV-visible spectrum, a strong absorption band at 779 nm due to DMFc⁺ was observed in Figure 6.18 that suggests that all DMFc was oxidized to DMFc⁺. By titrating the aqueous phases with sodium iodide, hydrogen peroxide was detected in the aqueous phase of both flask (c) and d (Figure 6.18 (b)). The H₂O₂ amount detected in flask (c) and (d) were 0.004 and 0.067 mM, respectively. Figure 6.18 undoubtedly confirms the occurrence of an oxygen reduction reaction catalyzed by CoOEP in this biphasic system. Moreover, both voltammetric and two-phase reaction data (Figures 6.16 & 6.18) clearly show that this catalytic oxygen reduction reaction requires the concomitant presence of H⁺, CoOEP, DMFc and O₂ at positive Galvani potential differences fixed either with a potentiostat (Figure 6.16) or chemically by salt distribution (Figure 6.18).

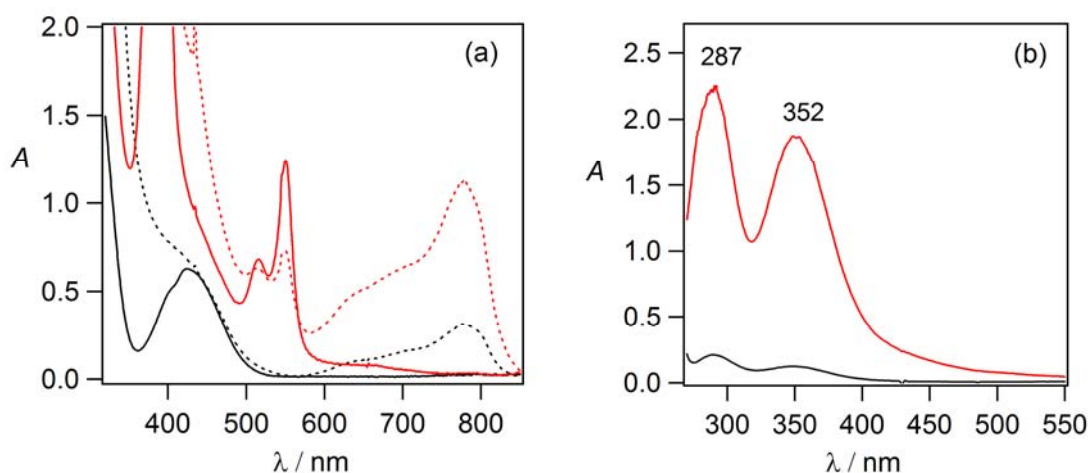
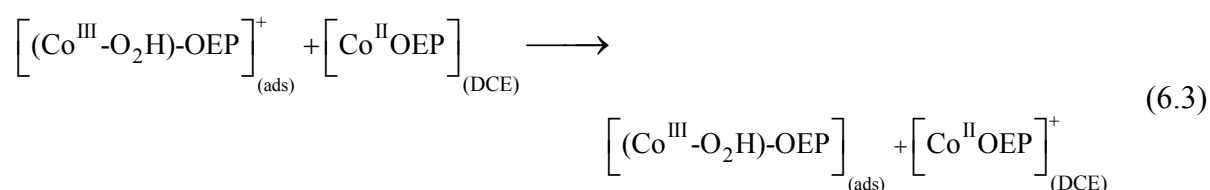
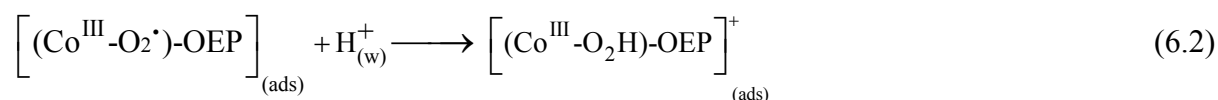
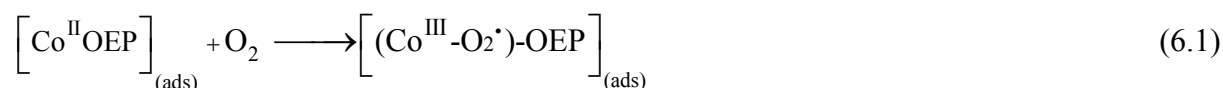


Figure 6.18: (a) Absorption spectra of the 1,2-DCE phases shown in Figure 6.17: flask a (full black), flask b (full red), flask c (dotted black) and flask d (dotted red) (b) UV-Visible spectra of the aqueous solutions flask c (black line) and flask d (red line) after 20 minutes shake flask experiment.

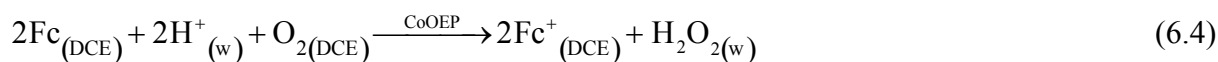
As reported previously by Fukuzimi *et al.* in a homogenous organic system, O_2 reduction by Fc derivatives in the presence of an organic soluble acid proceeds rather slowly but can be significantly accelerated in the presence of cobalt porphyrins as the catalyst.^[16, 17] In bulk phases, the reaction proceeds by a *PCET* reaction with electron transfer from Fc to O_2 and proton transfer from an organic soluble acid to O_2 . The catalysis originates from the formation of a superoxide-like intermediate, in which an electron partially delocalizes from porphyrin to O_2 . In the present biphasic system, the proton-coupled oxygen reduction by Fc occurs also interfacially as observed by voltammetry, with protons from the aqueous phase and electron donors from 1,2-DCE.

6.6 Mechanism

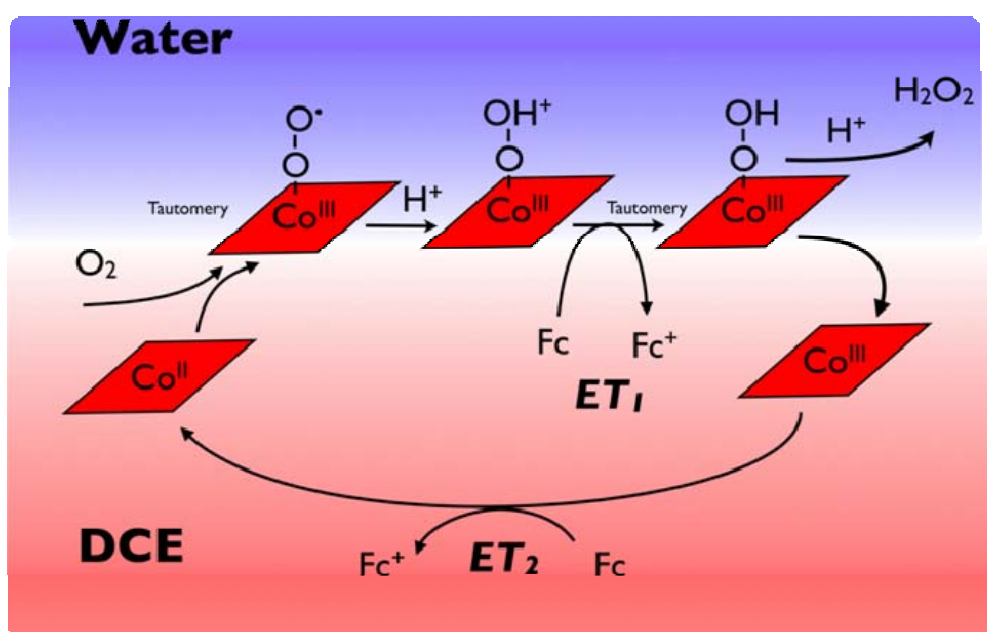
A mechanism is as follows:



An overall reaction of oxygen reduction with Fc catalyzed by CoOEP is:



A corresponding reaction Scheme 6.1 involving the adsorption of (Co-O₂)OEP, proton-coupled oxygen reduction and regeneration of CoOEP⁺ by Fc. These steps can be expressed as follows:



Scheme 6.1: Catalysis mechanism

6.7 Conclusions

In summary, we have shown that O₂ reduction by CoOEP occurs at a water|1,2-DCE polarized interface. CoOEP serves as a catalyst like conventional monomeric cobalt porphyrins, activating O₂ for the reduction to H₂O₂. Oxygen reduction by Fc has been investigated as well. Reduction of O₂ to H₂O₂ by using a weak (Fc) and strong (DMFc) reductant could be effectively catalyzed by CoOEP. Two-phase reactions with the Galvani potential difference between the two phases controlled by a common ion partition were performed, which not only proved the catalytic activation of CoOEP on O₂ reduction but also suggested a two-electron reduction pathway to produce H₂O₂. The voltammetry at soft

interfaces is a very powerful tool to study proton coupled electron transfer reactions of biological interest such as the interfacial reduction of oxygen catalysed by a metallic porphyrine. As in biosystems, the reactants can be phased separated, the protons in the aqueous phase and the electron donors in the organic phase. This work is to the best of our knowledge the first voltammetric study of an electrocatalytic reaction at a soft interface, where the rate of the catalytic reaction is controlled by the interfacial polarization, *i.e.* by the applied potential difference.

6.8 References

- [1] J. P. Collman, R. Boulatov, C. J. Sunderland, L. Fu, *Chemical Reviews* **2004**, *104*, 561.
- [2] E. Kim, E. E. Chufan, K. Kamaraj, K. D. Karlin, *Chemical Reviews* **2004**, *104*, 1077.
- [3] J. H. Zagal, M. A. Paez, J. F. I. Silva, J. H. Zagal, F. Bedioui, J.-P. Dodelet, Eds, *N4-Macrocyclic Metal Complexes*, Springer, New York, **2006**.
- [4] F. C. Anson, C. Shi, B. Steiger, *Accounts of Chemical Research* **1997**, *30*, 437.
- [5] C. J. Chang, Y. Deng, C. Shi, C. K. Chang, F. C. Anson, D. G. Nocera, *Chemical Communications* **2000**, 1355.
- [6] C. J. Chang, Z. H. Loh, C. Shi, F. C. Anson, D. G. Nocera, *Journal of the American Chemical Society* **2004**, *126*, 10013.
- [7] J. P. Collman, *Accounts of Chemical Research* **1977**, *10*, 265.
- [8] J. P. Collman, L. L. Chng, D. A. Tyvoll, *Inorganic Chemistry* **1995**, *34*, 1311.
- [9] J. P. Collman, P. Denisevich, Y. Konai, M. Marrocco, C. Koval, F. C. Anson, *Journal of the American Chemical Society* **1980**, *102*, 6027.
- [10] J. P. Collman, L. Fu, P. C. Herrmann, X. Zhang, *Science* **1997**, *275*, 949.
- [11] J. P. Collman, J. E. Hutchison, M. A. Lopez, A. Tabard, R. Guilard, W. K. Seok, J. A. Ibers, M. L'Her, *Journal of the American Chemical Society* **1992**, *114*, 9869.
- [12] J. P. Collman, M. Marrocco, P. Denisevich, C. Koval, F. C. Anson, *Journal of Electroanalytical Chemistry* **1979**, *101*, 117.
- [13] Y. Deng, C. J. Chang, D. G. Nocera, *Journal of the American Chemical Society* **2000**, *122*, 410.
- [14] C. Shi, B. Steiger, M. Yuasa, F. C. Anson, *Inorganic Chemistry* **1997**, *36*, 4294.
- [15] J. P. Collman, P. S. Wagenknecht, J. E. Hutchison, *Angewandte Chemie - International Edition in English* **1994**, *33*, 1537.
- [16] S. Fukuzumi, S. Mochizuki, T. Tanaka, *Inorganic Chemistry* **1989**, *28*, 2459.
- [17] S. Fukuzumi, K. Okamoto, C. P. Gros, R. Guilard, *Journal of the American Chemical Society* **2004**, *126*, 10441.
- [18] T. E. Bitterwolf, A. C. Ling, *Journal of Organometallic Chemistry* **1972**, *40*, C29.
- [19] R. Prins, A. G. T. G. Kortbeek, *Journal of Organometallic Chemistry* **1971**, *33*, C33.
- [20] V. M. Fomin, *Russian Journal of General Chemistry* **2007**, *77*, 954.
- [21] V. M. Fomin, A. E. Shirokov, N. G. Polyakova, P. A. Smirnov, *Russian Journal of General Chemistry* **2007**, *77*, 652.
- [22] I. Hatay, B. Su, F. Li, M. Mendez, T. Khoury, C. P. Gros, J. M. Barbe, M. Ersoz, Z. Samec, H. H. Girault, *Journal of American Chemical Society* **2009**, *131*, 13453.
- [23] A. J. Bard, L. R. Faulkner, *Electrochemical Methods: Fundamentals and Applications*, Wiley, New York, **2001**.
- [24] B. Su, R. P. Nia, F. Li, M. Hojeij, M. Prudent, C. Corminboeuf, Z. Samec, H. H. Girault, *Angewandte Chemie - International Edition* **2008**, *47*, 4675.
- [25] A. Salehi, W. A. Oertling, G. T. Babcock, C. K. Chang, *Journal of the American Chemical Society* **1986**, *108*, 5630.
- [26] Z. Gasyna, M. J. Stillman, *Inorganic Chemistry* **1990**, *29*, 5101.
- [27] C. Shi, F. C. Anson, *Inorganic Chemistry* **2001**, *40*, 5829.
- [28] E. Schmidt, H. Zhang, C. K. Chang, G. T. Babcock, W. A. Oertling, *Journal of the American Chemical Society* **1996**, *118*, 2954.
- [29] R. O. Rahn, M. I. Stefan, J. R. Bolton, E. Goren, P. S. Shaw, K. R. Lykke, *Photochemistry and Photobiology* **2003**, *78*, 146.
- [30] H. Hotta, S. Ichikawa, T. Sugihara, T. Osakai, *Journal of Physical Chemistry B* **2003**, *107*, 9717.

- [31] R. Partovi-Nia, B. Su, F. Li, C. P. Gros, J. M. Barbe, Z. Samec, H. H. Girault, *Chemistry - A European Journal* **2009**, *15*, 2335.

Chapter 7

Assisted proton transfer by free-base porphyrin and catalyzed oxygen reduction at polarized interface

7.1 Introduction

The protonation of the porphyrin macrocycle has been extensively studied.^[1, 2] Indeed, diprotonation of the porphyrin core has important effects on the static and dynamic photophysical properties when compared to their free-base parents. Some of these effects, such as those derived from increased symmetry, are analogous to those that occur upon formation of a corresponding metal derivative. Additionally, relative to the parent free-bases, the diacids exhibit broadened optical bands, increased spacing between absorption and emission maxima. All these effects are in particular enhanced in H₂TPP diacids.^[3]

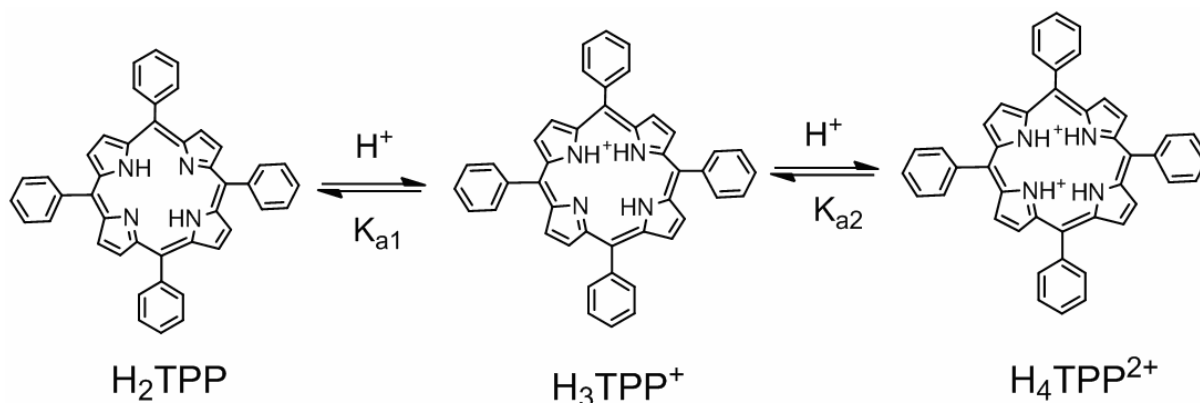
In free-base porphyrins the symmetry of the macrocycles is lowered from D_{4h} to D_{2h} due to the presence of the pyrrole protons. Porphyrin diacids typically have nonplanar structures with mainly saddle-type distortions of the porphyrin core, as revealed by X-ray crystallography.^[4-7] The deviations from planarity for diacids bearing meso-phenyl rings, such as H₂TPP diacids, approach in magnitude those seen in peripherally crowded porphyrins, such as free-base octaethyltetraphenylporphyrin (H₂OETPP)^[8], dodecaphenylporphyrin (H₂DPP).^[9] The porphyrin diacids is usually the chromophore of the protonated form and monocations can be obtained under special experimental conditions. Alsoph *et al.* have reported the protonation of porphyrin in 60% glacial acetic acid and 40% acetone.^[10] They observed four, three, and two Q bands for the free-base, monoprotated and biprotated porphyrins, respectively. Voltammetry at liquid|liquid interfaces is a very useful to study the protonation of molecules not soluble in water as pioneered by Hofmanova *et al.*^[11] In recent years, the transfer of H⁺ ion facilitated by ion carriers or extractants has been studied extensively in the literature.^[12-15] Homolka *et al.* investigated proton transfer across the (W|NB) interface assisted by a series of amines with an aromatic ring, discussed the dependence of the transfer

process on the structure of the proton acceptors and obtained the kinetic and thermodynamic parameters of the process.^[12, 13] Additionally, the transfer mechanism of protonated 1,10-phenanthroline and its derivatives between the aqueous phase and 1,2-DCE phase was elucidated by Yoshida and Freiser using current scanning polarography at an ascending water electrode.^[14] The transfer behaviour of protonated acridine across the W|NB interface has been studied by Liu and Wang^[15] using chronopotentiometry with linear current scanning, polarography with the electrolyte dropping electrode^[16, 17] and cyclic voltammetry.^[18, 19] Ion transfer voltammetry at the ITIES has now become a well-established method to study the acid-base properties of molecules dissolved in an organic phase in contact with an aqueous electrolyte. As shown by Reymond *et al.* for the study of therapeutic molecules, this methodology allows the determination of pK values, and the drawing of ionic partition diagrams.^[20-22] The transfer behavior of H^+ ion facilitated by porphyrins, which play an important role in metabolism in the biological body, has been reported previously.^[23] The effects of the more hydrophobic free-base 5,10,15,20-meso-tetraphenylporphyrin (H_2TPP) and its first transition-metal coordination compounds (MTPP) on the H^+ ion transfer across the W|NB interface were investigated.^[23] The kinetic of electron and proton transfer was investigated at micro-and macroscopic interfaces.^[24] In this Chapter we present a simple methodology to illustrate the existence of monoacid and diacid of tetraphenylporphyrin based on ion-transfer voltammetry and its catalytic effect for oxygen reduction at the polarized water|1,2-DCE interface and organic pK values are also estimated.

7.2 Visible absorption spectroscopic titration of H_2TPP with trifluoroacetic acid

The acid-base behavior of porphyrins has been widely studied in the last 60 years largely because of the strong influence of the protonation state on their structural and photophysical properties.^[4, 25, 26] This behavior depends, among other factors, on peripheral substitution, nature of the titrating acid or base, and dielectric constant of the solvent.^[27-33] The tetrapyrrole ring of a free-base porphyrins contains two tertiary nitrogen atoms, which allows the gain of protons to form a monoacid and a diacid, as illustrated for the free-base H_2TPP in Scheme 7.1, while the monoprotonated species has not been usually detected.^[4, 27, 29, 34-37] In a few

cases, the existence of these monoacid species was pointed out only by the lack of isobestic points in UV-Visible titrations or through kinetic experiments.^[38-48]



Scheme 7.1: Protonation of H_2TPP to form monoacid and diacid.

Diprotonation of porphyrin can be achieved in the presence of strong acids, such as trifluoroacetic acid (TFA), to give the porphyrin dication.^[49] In the diacid adducts, there appears to be close interactions between the diprotonated porphyrin and the conjugate bases of two acid molecules, such as hydrogen bonding to the central nitrogens.^[4, 6, 7] For example, the tetraphenylporphyrin diacid formed by reaction of H_2TPP and CF_3COOH is best represented as $[\text{H}_4\text{TPP}](\text{CF}_3\text{COO})_2$, which will be denoted $\text{H}_4\text{TPP}^{2+}$. The free-base porphyrin has a brownish-red color, which upon protonation gives way to the deep emerald green color of the porphyrin dication (Figure 7.1). Tautomerism in free-base porphyrins, as well as the nature of conjugate acids of porphyrin have been studied, and it was concluded that the most stable tautomer form has the structure of free-base porphyrin.^[37]

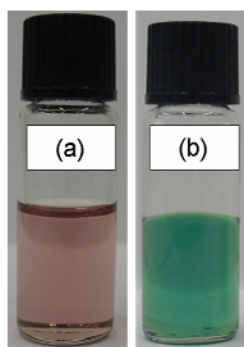


Figure 7.1: Titration of H_2TPP with TFA (a) at the beginning and (b) after protonation.

We have investigated the protonation of the H_2TPP to provide H_4TPP^{2+} in 1,2-DCE. Titration of H_2TPP in 1,2-DCE with TFA was performed and a typical spectral overlay is shown in Figure 7.2. With added TFA the H_2TPP absorbance at 416 nm diminishes to yield a H_4TPP^{2+} at 437 nm. The H_4TPP^{2+} absorption spectrum is red shifted from its position in neutral H_2TPP . By titrating H_2TPP usually one isosbestic point due to H_2TPP and H_4TPP^{2+} is observed and the diprotonated species appears stable under the conditions, whereas the intermediate H_3TPP^+ could not be clearly detected.^[25] To the best of our knowledge, only the monoacid derivative of a H_2TPP has been reported and characterized in 1,2-DCE solution by titration of H_2TPP with HTB.^[50] The existence of H_3TPP^+ , as well as pK_{a1} and pK_{a2} values has been reported in a few cases, one of which is based on the ion-transfer voltammetry at a polarized water|NB interface.^[23, 37, 40, 51]

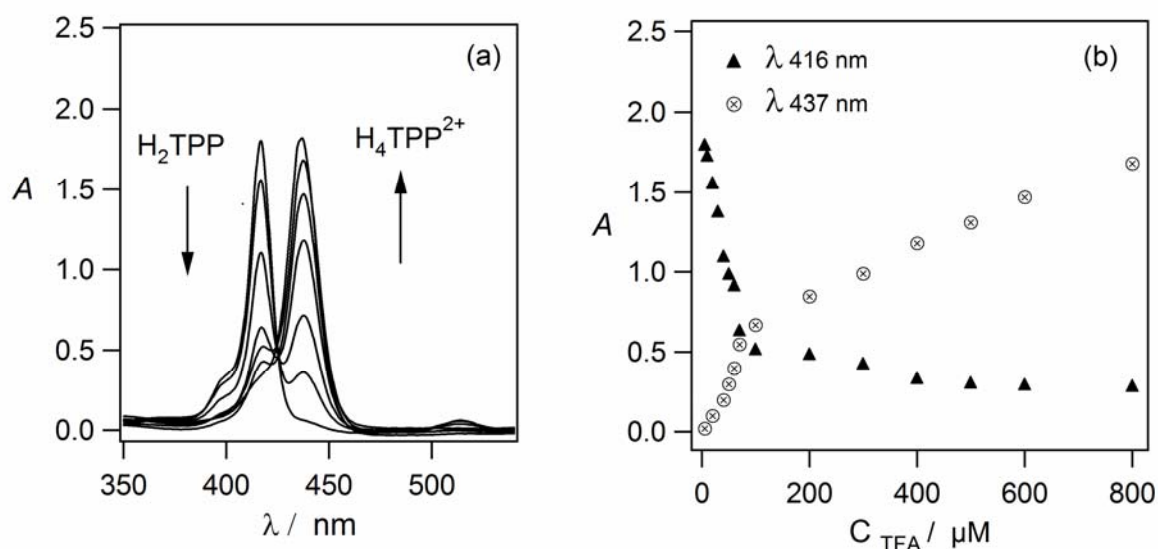


Figure 7.2: Repetitive spectral scan of $3\mu M H_2TPP$ in the titration with TFA in 1,2-DCE. (a) the arrows indicate the band direction upon addition of TFA (b) change in absorbance with concentration of TFA for selected band at 416 nm is for H_2TPP and that at 437 nm is for H_4TPP^{2+} .

7.3 Proton transfer across the water|1,2-DCE interface

7.3.1 Shake flask experiment

Shake flask experiment of H_2TPP were performed at a water|1,2-DCE interface and the polarization was chemically controlled by a common ion. Dissolving lithium tetrakis-

(pentafluorophenyl)borate (LiTB, 5 mM) and HCl (10 mM) in water and BATB (5 mM) in 1,2-DCE (water/DCE=2:2 in volume), the Galvani potential difference across the interface is fixed by the common ion TB^- at a potential 0.54 V. At this potential, proton initially present in water will partition into 1,2-DCE, leading finally to a distribution of proton in two phases according to the Nernst equation. If only H_2TPP is present in 1,2-DCE, a Soret band ($\lambda_{max}=437$ nm) is observed after the shake flask experiment, which demonstrates a bathochromic shift relative to the fresh H_2TPP solution at 416, as shown in Figure 7.3. This shift corresponds to proton facilitated of H_2TPP to form an adduct H_4TPP^{2+} .

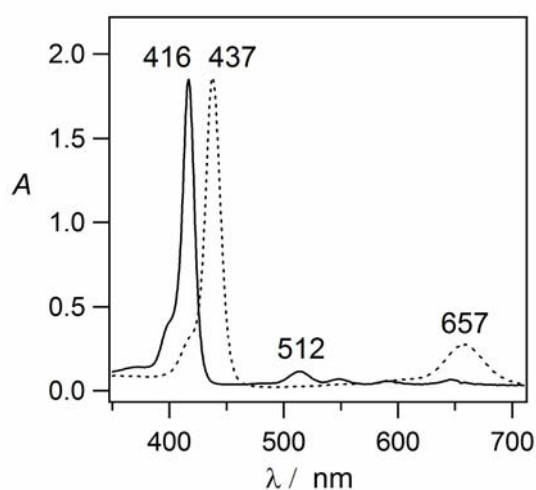


Figure 7.3: Absorption spectra of $3\mu M$ H_2TPP in 1,2-DCE freshly prepared (full line) and after shake flask experiments for 30 minutes (dotted line).

7.3.2 Voltammetric behaviour

The Voltammetric redox and diffusion coefficients is summarized in Table 7.1. Herein, using this simple methodology, we illustrate the existence of H_3TPP^+ in 1,2-DCE, pK_{a1} and pK_{a2} values are also estimated.

Table 7.1: Data refer to $50\mu M$ of porphyrin with $5mM$ BATB supporting electrolyte in dry 1,2-DCE a $20mVs^{-1}$

Concentration ($50\mu M$)	E_1 vs SHE / V	E_2 vs SHE / V	E_3 vs SHE / V	D / cm^2s^{-1}
H_2TPP	1.35	1.7	—	4.1×10^{-6}

An ITIES is formed when a water solution containing hydrophilic ions is put in contact with an organic solution containing lipophilic ions. Electrochemical polarization supplied by an external voltage can give a polarisable potential window. The potential dependence for ion transfer across the interface follows a Nernst equation. By using LiCl and HCl as the aqueous electrolytes and BATB as the lipophilic electrolyte in 1,2-DCE (Cell 1), a potential window ranging from -0.2 V to 0.4 V can be obtained, as shown by the dotted line in Figure 7.4(a).

Cell 1

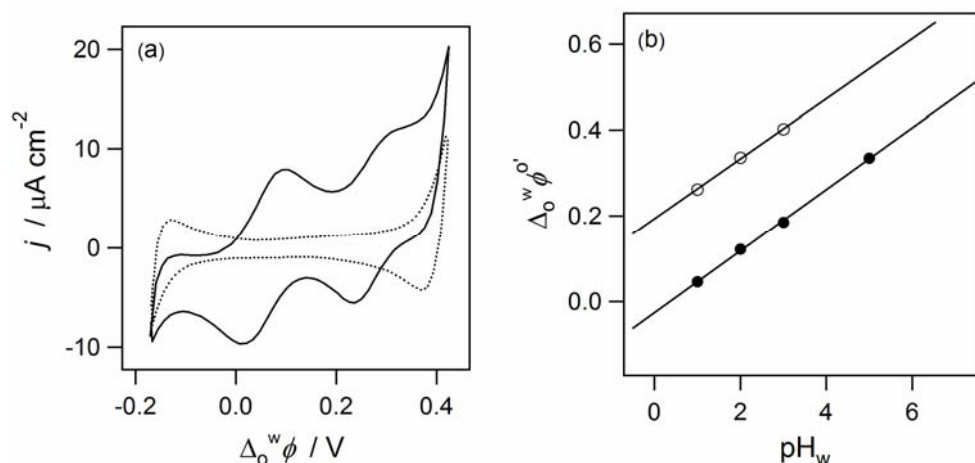
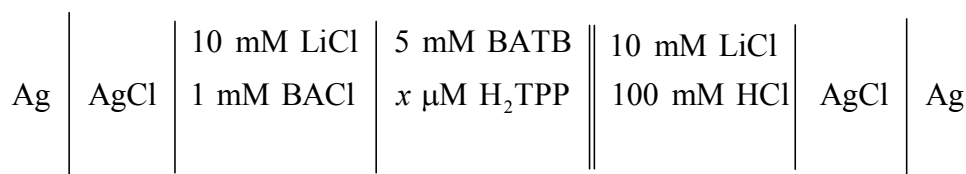


Figure 7.4: (a) Cyclic voltammograms (25mVs^{-1}) using Cell 1: in the absence ($x=0$, dotted line) and presence ($x=50$, full line) of H_2TPP in 1,2-DCE (b) pH dependence of the half-wave potentials of the two waves.

This window is determined by the transfer of H^+ and Cl^- from water to 1,2-DCE at positive and negative potentials, respectively. With the help of an ionophore present in 1,2-DCE that can complex with H^+ , the transfer of H^+ will be facilitated and a wave will appear in the middle of the potential window. Stated in another way, H^+ will transfer at less positive potentials in this case, due to the presence of a proton acceptor in the organic phase. This phenomenon is usually called facilitated ion transfer reaction (or Transfer by Interfacial Complexation, TIC)^[52] and the shift of the transfer potential provides information on the complexation constant between the ionophore and H^+ .

By dissolving 50 μM H_2TPP in a 1,2-DCE solution containing a BATB in contact with an acidic aqueous solution, two waves can be observed in the cyclic voltammogram, as illustrated by the full line in Figure 7.4(a). The two waves, featuring the same current magnitude, lie at 0.046 V ($\Delta_o^w\phi_1$) and 0.262 V ($\Delta_o^w\phi_2$), respectively. First of all, the peak-to-peak potential separations for the two waves are approximately 60 mV, which complies with the conditions for a reversible transfer of a singly charged ion. The maximum peak currents are in good agreement with the Randles-Sevcik equation as shown by the linear dependence on the square root of scan rate as shown in Figure 7.5, indicating that both waves originate from diffusion-controlled reactions.

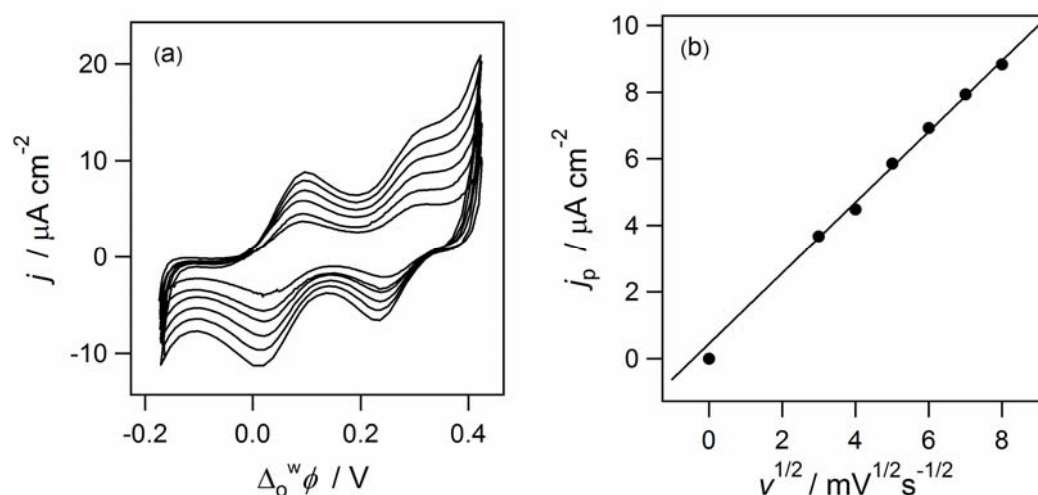


Figure 7.5: (a) CVs at various scan rates (9, 16, 25, 49 and 64 mV/s from inner to outer) using Cell 1(x=50) of H_2TPP in 1,2-DCE (b) The first anodic peak current as a function of the square root of the scan rate.

The measured peak currents also linearly increase with the H_2TPP concentration in the range 50 μM to 200 μM (Figure 7.6). This confirms that the ion transfer reactions are limited^[13] by the diffusion of H_2TPP species in the organic phase. Indeed, the proton concentration in water is in excess compared with that of H_2TPP in 1,2-DCE. Furthermore, the two waves shift with the acidity of aqueous phase by approximately 60 mV/pH, as illustrated in Figure 7.4(b), confirming that both waves correspond to a facilitated proton transfer reaction.

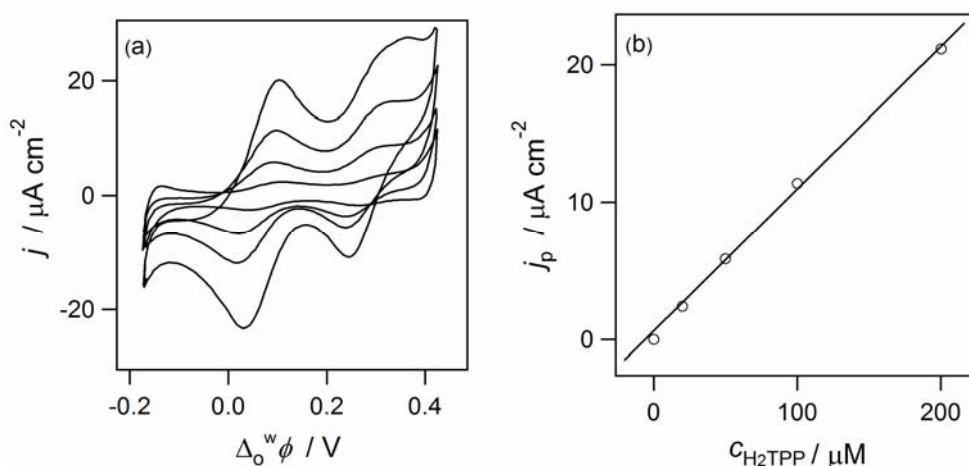


Figure 7.6: (a) CVs (25 mV/s) at various concentrations of H_2TPP in 1,2-DCE using Cell 1 (x: 20, 50, 100 and 200 μM , from inner to outer): of H_2TPP in 1,2-DCE (b) The first anodic peak current as a function of H_2TPP concentration.

7.4 Mechanism of H^+ ion transfer facilitated by H_2TPP

As illustrated in Figure 7.4(a), the first wave represents the transfer of a proton from water to 1,2-DCE facilitated by H_2TPP that in fact is the first protonation of H_2TPP to form the monoacid H_3TPP^+ in 1,2-DCE, and the second one represents the facilitated transfer of a second proton by H_3TPP^+ . These two processes can be expressed as:



The facilitated transfer of H^+ in the presence of H_2TPP and H_3TPP^+ is occurring at lower potentials than that of H^+ alone. In addition, considering the two processes represent a 1 : 1 complexation reaction controlled by the diffusion of the porphyrin species in the organic phase, K_{a1} and K_{a2} can be estimated by exploring the pH dependence of the apparent transfer potential according to the following equation^[53]:

$$\Delta_0^w \phi_{LH^+}^{1/2} = \Delta_0^w \phi_{H^+}^{0'} + \frac{RT}{2F} \ln \left(\frac{D_L}{D_{LH^+}} \right) - \frac{2.303RT}{F} pK_a^{DCE} + \frac{2.303RT}{F} pH^w \quad (7.3)$$

Where $\Delta_o^w \phi_{LH^+}^{1/2}$ is the half-wave transfer potential of the respective facilitated proton transfers. $\Delta_o^w \phi_{H^+}^{0'}$ is the formal transfer potential for the transfer of H^+ . D_L and D_{LH^+} ($L = H_2TPP$, H_3TPP^+) represent the diffusion coefficients of the proton acceptor ligand and its protonated form, and for simplicity it can be assumed that $D_L \approx D_{LH^+}$. pH^w is the aqueous pH. The relationship between $\Delta_o^w \phi$ and the pH^w is found to be linear, and the intercept allows the determination of the pK_a in the organic phase. K_a^{DCE} is defined by:

$$K_a^{DCE} = \frac{a_L^{DCE} a_{H^+}^{DCE}}{a_{LH^+}^{DCE}} \quad (7.4)$$

Doing so, as shown in Figure 7.4(b), pK_{a1}^{DCE} and pK_{a2}^{DCE} (Equations 7.5 and 7.6) here are found to be equal to 9.8 and 6.0, which show that both H_3TPP^+ and H_4TPP^{2+} are very weak acids in 1,2-DCE.

$$K_{a1}^{DCE} = \frac{a_{H_2TPP}^{DCE} a_{H^+}^{DCE}}{a_{H_3TPP^+}^{DCE}} \quad (7.5)$$

$$K_{a2}^{DCE} = \frac{a_{H_3TPP^+}^{DCE} a_{H^+}^{DCE}}{a_{H_4TPP^{2+}}^{DCE}} \quad (7.6)$$

Meanwhile, it suggests that both H_2TPP and H_3TPP^+ are weak bases, having a small affinity for proton. It is worthwhile to mention that the proton activity in 1,2-DCE is very small and the lack of hydrogen bonds in 1,2-DCE prevents the stabilization of the protonated species and favours the presence of neutral or low charges species.

7.5 Ionic partition diagram

Ionic partition diagrams have proved to be a rather useful representation of thermodynamic equilibria involving ionisable species in biphasic liquid systems. The method consists in representing the domains of predominance of the various species as a function of applied potential and aqueous pH. The construction of the partition diagram of an ionisable solute

follows the well-known potential versus pH diagrams developed by Pourbaix^[54] in order to study the corrosion of metals in acidic and alkaline solutions under oxidative or reductive conditions.

7.5.1 The case of a lipophilic monobasic compound

For a lipophilic monobasic compound B partitioning between two immiscible phases, the first boundary line (line 1 Figure 7.7) corresponds to the equiconcentration of the two charged species BH^{+w} and BH^{+o} , as defined by the Nernst equation for ion transfer which reduces to (7.8):

$$\Delta_o^w \phi = \Delta_o^w \phi_i^0 + \frac{RT}{z_i F} \ln \left(\frac{a_i^o}{a_i^w} \right) \quad (7.7)$$

$$\Delta_o^w \phi = \Delta_o^w \phi_{BH^+}^0 \quad (7.8)$$

Where $\Delta_o^w \phi_{BH^+}^0$ is the standard transfer potential of cation BH^+ . Two other boundaries have to be considered in the next step. The interfacial acidic/basic equilibrium between the charged species in the aqueous phase and the neutral species in the organic phase corresponds to the reaction:



The acidity constant in water can be expressed as a function of pH, the standard partition coefficient of B ($P_B^0 = a_B^o / a_B^w$), and the ratio $a_B^o / a_{BH^+}^w$

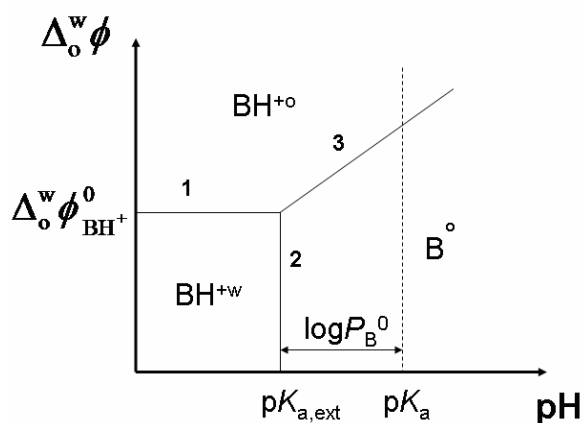


Figure 7.7: Theoretical ionic partition diagram for a lipophilic base (equiconcentration convention). The dotted line shows the value of the aqueous dissociation constant.

$$K_a^w = \frac{a_B^w a_{H^+}^w}{a_{BH^+}^w} = \frac{a_B^o}{a_{BH^+}^w} \cdot \frac{a_{H^+}^w}{P_B^0} \quad (7.10)$$

or

$$pK_a^w = -\log\left(\frac{a_B^o}{a_{BH^+}^w}\right) + \text{pH} + \log P_B^0 \quad (7.11)$$

At low concentrations where activity coefficients can be neglected, the boundary line corresponding to equal concentrations of aqueous BH^{+w} and neutral base in the organic phase B^o (line 2 Figure 7.7) is then given by:

$$\text{pH} = pK_a^w - \log P_B^0 \quad (7.12)$$

This pH value can be considered as the extraction acidity constant $pK_{a,\text{ext}}$, since when using an aqueous acid to extract a neutral base from the organic phase, it is necessary to use a stronger acid than suggested by the aqueous bulk pK_a^w value. Indeed, $pK_{a,\text{ext}}$ is lower than pK_a^w by one unit of pK_a per unit of $\log P_B^0$. The boundary between BH^{+o} and B^o (line 3 Figure 7.7) is similarly defined by developing the ratio $a_{BH^+}^o/a_B^o$ from the partition coefficients of the neutral and the Nernst equation (7.7) for BH^+ which reads:

$$\Delta_o^w \phi = \Delta_o^w \phi_{\text{BH}^+}^0 + \frac{2.3RT}{F} \log \left(\frac{a_{\text{BH}^+}^o}{a_{\text{BH}^+}^w} \right) = \Delta_o^w \phi_{\text{BH}^+}^0 + \frac{2.3RT}{F} \log P_{\text{BH}^+} \quad (7.13)$$

The partition coefficient P_{BH^+} is a function of the Galvani potential difference, itself established by the partition coefficient of all the other ionic species present in the biphasic system at equilibrium or imposed by the electrochemical setup when dealing with voltammetric experiments. Thus, by substitution of equations (7.10) and (7.13) can be rewritten as:

$$\Delta_o^w \phi = \Delta_o^w \phi_{\text{BH}^+}^0 + \frac{2.3RT}{F} \log \left(\frac{a_{\text{BH}^+}^o}{a_{\text{B}}^o} \right) + \frac{2.3RT}{F} \log \frac{P_{\text{B}}^0 K_a^w}{a_{\text{H}^+}^w} \quad (7.14)$$

For dilute solutions, the boundary line between the neutral B^0 and the charged species BH^{+0} in the organic phase is given by:

$$\Delta_o^w \phi = \Delta_o^w \phi_{\text{BH}^+}^0 + \frac{2.3RT}{F} (\log P_{\text{B}}^0 - \text{p}K_a^w) + \frac{2.3RT}{F} \text{pH} \quad (7.15)$$

Again, this boundary line is pH dependent. Finally, the corresponding ionic partition diagram can be established as presented in Figure 7.7. This Figure shows that the more lipophilic the neutral base B, the smaller the predominance area of BH^+ in water and the larger the predominance area of B in the organic phase.

7.5.2 Calculation of the boundary lines

7.5.2.1 Partition equilibria between the two phases

As the boundary lines represent the locus where the concentrations of two contiguous species are equal, the Nernst equations can be used directly to determine the evolution of the potential with pH for the partition of each ionic species between the two phases:

Line $\text{H}_3\text{TPP}^{+0}/\text{H}_3\text{TPP}^{+w}$:



$$\Delta_o^w \phi = \Delta_o^w \phi_{\text{H}_3\text{TPP}^+}^0 + \frac{RT}{F} \ln \left(\frac{a_{\text{H}_3\text{TPP}^+}^{\text{o}}}{a_{\text{H}_3\text{TPP}^+}^{\text{w}}} \right) \quad (7.17)$$

Starting from the Nernst equation for the proton,

$$\Delta_o^w \phi = \Delta_o^w \phi_{\text{H}^+}^0 + \frac{RT}{F} \ln \left(\frac{a_{\text{H}^+}^{\text{o}}}{a_{\text{H}^+}^{\text{w}}} \right) = \Delta_o^w \phi_{\text{H}^+}^0 + \frac{RT}{F} \ln \left(\frac{K_{\text{a}1}^{\text{o}} a_{\text{H}_3\text{TPP}^+}^{\text{o}} a_{\text{H}_2\text{TPP}}^{\text{w}}}{K_{\text{a}1}^{\text{w}} a_{\text{H}_3\text{TPP}^+}^{\text{w}} a_{\text{H}_2\text{TPP}}^{\text{o}}} \right) \quad (7.18)$$

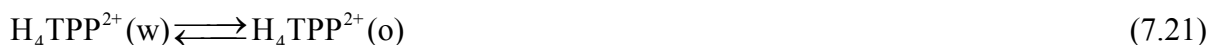
Such that

$$\Delta_o^w \phi_{\text{H}_3\text{TPP}^+}^0 = \Delta_o^w \phi_{\text{H}^+}^0 + \frac{RT}{F} \ln \left(\frac{K_{\text{a}1}^{\text{o}}}{K_{\text{a}1}^{\text{w}} P_{\text{H}_2\text{TPP}}^0} \right) \quad (7.19)$$

$$P_{\text{H}_2\text{TPP}}^0 = \frac{a_{\text{H}_2\text{TPP}}^{\text{o}}}{a_{\text{H}_2\text{TPP}}^{\text{w}}} \quad (7.20)$$

To determine this horizontal line, we need to determine both $K_{\text{a}1}^{\text{w}}$ and $P_{\text{H}_2\text{TPP}}^0$.

Line $\text{H}_4\text{TPP}^{2+0}/\text{H}_4\text{TPP}^{2+w}$:



$$\Delta_o^w \phi = \Delta_o^w \phi_{\text{H}_4\text{TPP}^{2+}}^0 + \frac{RT}{F} \ln \left(\frac{a_{\text{H}_4\text{TPP}^{2+}}^{\text{o}}}{a_{\text{H}_4\text{TPP}^{2+}}^{\text{w}}} \right) \quad (7.22)$$

We start from the Nernst equation

$$\Delta_o^w \phi_{\text{H}_4\text{TPP}^{2+}}^0 = \Delta_o^w \phi_{\text{H}^+}^0 + \frac{RT}{2F} \ln \left(\frac{K_{a_1}^o K_{a_2}^o}{K_{a_1}^w K_{a_2}^w P_{\text{H}_2\text{TPP}}^0} \right) \quad (7.23)$$

To determine this horizontal line, we need to determine $K_{a_2}^w$.

Line $\text{H}_2\text{TPP}^0/\text{H}_3\text{TPP}^{+w}$: We start from the acidity constant

$$K_{a_1}^w = \frac{a_{\text{H}_2\text{TPP}}^w a_{\text{H}^+}^w}{a_{\text{H}_3\text{TPP}^+}^w} = \frac{a_{\text{H}_2\text{TPP}}^o a_{\text{H}^+}^w}{a_{\text{H}_3\text{TPP}^+}^w P_{\text{H}_2\text{TPP}}^0} \quad (7.24)$$

The vertical borderline is

$$\text{pH} = \text{p}K_{a_1}^w - \log P_{\text{H}_2\text{TPP}}^0 \quad (7.25)$$

Line $\text{H}_3\text{TPP}^{+o}/\text{H}_4\text{TPP}^{+w}$: We start from the Nernst equation for the mono-acid

$$\Delta_o^w \phi = \Delta_o^w \phi_{\text{H}_3\text{TPP}^+}^0 + \frac{RT}{F} \ln \left(\frac{a_{\text{H}_3\text{TPP}^+}^o}{a_{\text{H}_3\text{TPP}^+}^w} \right) = \Delta_o^w \phi_{\text{H}_3\text{TPP}^+}^0 + \frac{RT}{F} \ln \left(\frac{a_{\text{H}_3\text{TPP}^+}^o a_{\text{H}^+}^w}{K_{a_2}^w a_{\text{H}_4\text{TPP}^{2+}}^w} \right) \quad (7.26)$$

The borderline is

$$\Delta_o^w \phi = \Delta_o^w \phi_{\text{H}_3\text{TPP}^+}^0 - \frac{RT}{F} \ln K_{a_2}^w - 0.06\text{pH} \quad (7.27)$$

Line $\text{H}_2\text{TPP}^0/\text{H}_2\text{TPP}^w$:



$$\Delta_o^w \phi = \Delta_o^w \phi_{\text{H}_2\text{TPP}}^0 + \frac{RT}{F} \ln \left(\frac{a_{\text{H}_2\text{TPP}}^o}{a_{\text{H}_2\text{TPP}}^w} \right) \quad (7.29)$$

Where it should be noted for memory that the logarithmic term on the right hand side of these three relationships represents the partition coefficient of each ionic species. When the aqueous and organic concentrations of a given species are equal, equations 7.17, 7.22 and 7.29 become independent of pH, and reduce to trivial relationships:

$$\Delta_o^w \phi = \Delta_o^w \phi_i^0 \quad (7.30)$$

This results in three boundary lines parallel to the pH axis with an ordinate equal to the formal transfer potential of the respective ion. These segments are limited by the various (de)protonation equilibria which delimit the boundaries between two ions differing in electrical charge.

7.5.2.2 Equilibria in the aqueous phase

Using the thermodynamic definition of the dissociation constants K_a^w and neglecting the logarithm of the ratios of the activity coefficients, the acid-base equilibria in the aqueous phase may be written as follows:



$$\log \left(\frac{a_{H_3TPP^+}^w}{a_{H_4TPP^{2+}}^w} \right) = \text{pH} - \text{p}K_{a_2}^w \quad (7.32)$$



$$\log \left(\frac{a_{H_2TPP}^w}{a_{H_3TPP^+}^w} \right) = \text{pH} - \text{p}K_{a_1}^w \quad (7.34)$$

Line H_3TPP^{+w}/H_4TPP^{2+w} :

$$K_{a_2}^w = \frac{a_{H_3TPP^+}^w a_{H^+}^w}{a_{H_4TPP^{2+}}^w} \quad (7.35)$$

The borderline is simply

$$pH = pK_{a_2}^w \quad (7.36)$$

Line H_2TPP^w/H_3TPP^{+w} :

$$K_{a_1}^w = \frac{a_{H_2TPP}^w a_{H^+}^w}{a_{H_3TPP^+}^w} \quad (7.37)$$

The borderline is simple

$$pH = pK_{a_1}^w \quad (7.38)$$

When the left-hand side of equations (7.32) and (7.34) is zero, the concentrations of the various species in each equation are equal, and we simply get:

$$pH = pK_{a_j}^w \quad (7.39)$$

Where $j= 1,2$. Consequently, equation (7.32) define two additional boundary lines which are parallel to the ordinate axis and independent of $\Delta_o^w \phi$.

7.5.2.3 Equilibria in the organic phase

The acid-base equilibria in the organic phase depend: (a) on the same equilibria as in the aqueous phase, (b) on the partition coefficient of the neutral species, (c) on the partition coefficients of the ionic species, and (d) on the proton concentration in the organic phase.

Therefore, using the Nernst equation for the proton can be used to express any concentration ratio as a function of pH. With eight species as in present case, the art of drawing ionic partition diagrams then consists in foreseeing which boundaries have a physical meaning.

Line $\text{H}_2\text{TPP}^0/\text{H}_3\text{TPP}^{+0}$: We start from the Nernst equation for the proton

$$\Delta_o^w \phi = \Delta_o^w \phi_{\text{H}^+}^0 + \frac{RT}{F} \ln \left(\frac{a_{\text{H}^+}^o}{a_{\text{H}^+}^w} \right) \quad (7.40)$$

And we define the dissociation constant

$$K_{a_1}^o = \frac{a_{\text{H}_2\text{TPP}}^o a_{\text{H}^+}^o}{a_{\text{H}_3\text{TPP}^+}^o} \quad (7.41)$$

By substitution, we obtain

$$\Delta_o^w \phi = \Delta_o^w \phi_{\text{H}^+}^0 + \frac{RT}{F} \ln \left(\frac{K_{a_1}^o}{a_{\text{H}^+}^w} \right) + \frac{RT}{F} \ln \left(\frac{a_{\text{H}_3\text{TPP}^+}^o}{a_{\text{H}_2\text{TPP}}^o} \right) \quad (7.42)$$

The last term is equal to zero at the half-wave potential, so that we can calculate $K_{a_1}^o$, and a value of $\text{p}K_{a_1}^o=9.8$ has been determined. The borderline of the partition diagram is then

$$\Delta_o^w \phi = \Delta_o^w \phi_{\text{H}^+}^0 + \frac{RT}{F} \ln K_{a_1}^o + 0.06\text{pH} = \Delta_o^w \phi_{\text{H}^+}^0 - 0.06\text{p}K_{a_1}^o + 0.06\text{pH} \quad (7.43)$$

Line $\text{H}_3\text{TPP}^{+0}/\text{H}_4\text{TPP}^{2+0}$: Again, we start from the Nernst equation for the proton transfer and we define the second acidity constant

$$K_{a_2}^o = \frac{a_{\text{H}_3\text{TPP}^+}^o a_{\text{H}^+}^o}{a_{\text{H}_4\text{TPP}^{2+}}^o} \quad (7.44)$$

By substitution, we obtain

$$\Delta_o^w \phi = \Delta_o^w \phi_{H^+}^0 + \frac{RT}{F} \ln \left(\frac{K_{a_2}^o}{a_{H^+}^w} \right) + \frac{RT}{F} \ln \left(\frac{a_{H_4TPP^{2+}}^o}{a_{H_3TPP^+}^o} \right) \quad (7.45)$$

Again, the last term is equal to zero at the half-wave potential, so that we can calculate $K_{a_2}^o$, and a value of $pK_{a_2}^o=6.0$ has been determined. The borderline of the partition diagram is then

$$\Delta_o^w \phi = \Delta_o^w \phi_{H^+}^0 + \frac{RT}{F} \ln K_{a_2}^o + 0.06pH = \Delta_o^w \phi_{H^+}^0 - 0.06pK_{a_2}^o + 0.06pH \quad (7.46)$$

7.5.3 Born solvation model

The acidity constant in the two phases are related by

$$K_{a_1}^w = K_{a_1}^o \frac{P_{H_3TPP^+}^0}{P_{H^+}^0 P_{H_2TPP}^0} \quad (7.47)$$

The standard partition coefficient is by defined

$$\ln P_i^0 = -\frac{\mu_i^{0,o} - \mu_i^{0,w}}{RT} = -\frac{\Delta G_{tr,i}^{0,w \rightarrow o}}{RT} = -\frac{z_i F}{RT} \Delta_o^w \phi_i^0 \quad (7.48)$$

According to the Born solvation model, the Gibbs energy of solvation, ΔG_{IS} is the sum of a term for the neutral species and one for the contribution of the charge given by:^[55]

$$\Delta G_{IS} = -\frac{z^2 e^2 N_A}{8\pi \epsilon_0 r_{ion}} \left(1 - \frac{1}{\epsilon_r} \right) \quad (7.49)$$

Where e is the charge of the proton, N_A is the Avogadro number, r is the molecular radius, ϵ_r is the dielectric constant, z is the charge number and ϵ_0 is the vacuum permittivity.

For the H_2TPP/H_3TPP^+ , we have

$$\ln P_{\text{H}_3\text{TPP}^+}^0 = -\frac{\Delta G_{\text{tr},\text{H}_3\text{TPP}^+}^{0,\text{w}\rightarrow\text{o}}}{RT} = -\frac{\Delta G_{\text{tr},\text{H}_2\text{TPP}}^{0,\text{w}\rightarrow\text{o}}}{RT} + \frac{\Delta G_{\text{IS}}^{\text{w}} - \Delta G_{\text{IS}}^{\text{o}}}{RT} =$$

$$\ln P_{\text{H}_2\text{TPP}}^0 + \frac{e^2 N_{\text{A}}}{8\pi\epsilon_0 r_{\text{ion}} RT} \left(\frac{1}{\epsilon_{\text{r}}^{\text{w}}} - \frac{1}{\epsilon_{\text{r}}^{\text{o}}} \right) \quad (7.50)$$

Or

$$\ln \left(\frac{P_{\text{H}_3\text{TPP}^+}^0}{P_{\text{H}_2\text{TPP}}^0} \right) = \frac{e^2 N_{\text{A}}}{8\pi\epsilon_0 r_{\text{ion}} RT} \left(\frac{1}{\epsilon_{\text{r}}^{\text{w}}} - \frac{1}{\epsilon_{\text{r}}^{\text{o}}} \right) = -4.86 \quad (7.51)$$

i.e. a shift of -12 kJmol^{-1} for a radius of 0.5nm.

$$\ln P_{\text{H}_3\text{TPP}^+}^0 = -\frac{F\Delta_{\text{o}}^{\text{w}}\phi_{\text{H}_3\text{TPP}^+}^0}{RT} = -\frac{F\Delta_{\text{o}}^{\text{w}}\phi_{\text{H}^+}^0}{RT} - \ln \left(\frac{K_{\text{a}_1}^{\text{o}}}{K_{\text{a}_1}^{\text{w}} P_{\text{H}_2\text{TPP}}^0} \right) \quad (7.52)$$

Or

$$\log \left(\frac{P_{\text{H}_3\text{TPP}^+}^0}{P_{\text{H}_2\text{TPP}}^0} \right) = \frac{e^2 N_{\text{A}}}{8\pi\epsilon_0 r_{\text{ion}} RT \ln 10} \left(\frac{1}{\epsilon_{\text{r}}^{\text{w}}} - \frac{1}{\epsilon_{\text{r}}^{\text{o}}} \right) = \log P_{\text{H}^+}^0 + \text{p}K_{\text{a}_1}^{\text{o}} - \text{p}K_{\text{a}_1}^{\text{w}} \quad (7.53)$$

So we can calculate $K_{\text{a}_1}^{\text{w}}$. With $P_{\text{H}^+}^0 = 5 \times 10^{-10}$, we have $\text{p}K_{\text{a}_1}^{\text{w}} = 2.1 - 9.4 + 9.8 = 2.5$.

For the $\text{H}_2\text{TPP}/\text{H}_4\text{TPP}^{2+}$, we have similarly

$$\ln \left(\frac{P_{\text{H}_4\text{TPP}^{2+}}^0}{P_{\text{H}_2\text{TPP}}^0} \right) = \frac{4e^2 N_{\text{A}}}{8\pi\epsilon_0 r_{\text{ion}} RT} \left(\frac{1}{\epsilon_{\text{r}}^{\text{w}}} - \frac{1}{\epsilon_{\text{r}}^{\text{o}}} \right) \quad (7.54)$$

Which represents a shift of -48 kJmol^{-1} for a radius of 0.5nm.

By subtraction, we have

$$\ln \left(\frac{P_{\text{H}_4\text{TPP}^{2+}}^0}{P_{\text{H}_3\text{TPP}^+}^0} \right) = \frac{3e^2 N_A}{8\pi\epsilon_0 r_{\text{ion}} RT} \left(\frac{1}{\epsilon_r^w} - \frac{1}{\epsilon_r^o} \right) = \frac{F}{RT} \left[\Delta_o^w \phi_{\text{H}_3\text{TPP}^+}^0 - 2\Delta_o^w \phi_{\text{H}_4\text{TPP}^{2+}}^0 \right] \quad (7.55)$$

Using the Nernst equation for the mono- and the diacid

$$\log \left(\frac{P_{\text{H}_4\text{TPP}^{2+}}^0}{P_{\text{H}_3\text{TPP}^+}^0} \right) = \ln P_{\text{H}^+}^0 + \ln \left(\frac{K_{a_2}^w}{K_{a_2}^o} \right) \quad (7.56)$$

Or

$$\frac{3e^2 N_A \ln 10}{8\pi\epsilon_0 r_{\text{ion}} RT} \left(\frac{1}{\epsilon_r^w} - \frac{1}{\epsilon_r^o} \right) = \log P_{\text{H}^+}^0 + \text{p}K_{a_2}^o - \text{p}K_{a_2}^w \quad (7.57)$$

So we can calculate $K_{a_2}^w$. With $P_{\text{H}^+}^0 = 5 \times 10^{-10}$, we have $\text{p}K_{a_2}^w = 6.3 - 9.4 + 6 = 2.9$.

Since $\text{p}K_{a_2}^w > \text{p}K_{a_1}^w$, we can conclude that the monoacid does not exist in water. The difference between the two horizontal lines is

$$\Delta_o^w \phi_{\text{H}_4\text{TPP}^{2+}}^0 - \Delta_o^w \phi_{\text{H}_3\text{TPP}^+}^0 = \frac{RT}{2F} \ln \left(\frac{K_{a_1}^w K_{a_2}^o P_{\text{H}_2\text{TPP}}^0}{K_{a_1}^o K_{a_2}^w} \right) \quad (7.58)$$

$\text{H}_2\text{TPP}^0/\text{H}_3\text{TPP}^{+o}$	$\Delta_o^w \phi = 0.55 - 0.06 \cdot 9.8 + 0.06\text{pH} = -0.04 + 0.06\text{pH}$
$\text{H}_3\text{TPP}^{+o}/\text{H}_4\text{TPP}^{2+o}$	$\Delta_o^w \phi = 0.55 - 0.06 \cdot 6 + 0.06\text{pH} = 0.19 + 0.06\text{pH}$
$\text{H}_3\text{TPP}^{+w}/\text{H}_4\text{TPP}^{2+w}$	$\text{pH} = \text{p}K_{a_2}^w = 2.9$

$H_3TPP^{+o} / H_3TPP^{+w}$	$\Delta_o^w \phi_{H_3TPP^+}^0 = 0.55 + 0.06 \cdot (2.5 - 6 - 9.8) = -0.25V$
$H_4TPP^{2+o} / H_4TPP^{2+w}$	$\Delta_o^w \phi_{H_4TPP^{2+}}^0 = 0.55 + 0.03 \cdot (2.5 + 2.9 - 6 - 9.8 - 6) = 0.06$
$H_2TPP^{+o} / H_3TPP^{+w}$	$pH = 2.5 - 6 = -3.5$
$H_3TPP^{+o} / H_4TPP^{2+w}$	$\Delta_o^w \phi = -0.25 + 0.06 \cdot 2.9 - 0.06pH = -0.76 - 0.06pH$
$H_2TPP^{+o} / H_4TPP^{2+w}$	$pH = \frac{1}{2}(2.5 + 2.9 - 6) = -0.3$

For the last case $H_2TPP^{+o} / H_4TPP^{2+w}$ considering that the second pK_a is more positive than the first one, the aqueous mono-acid doesn't have a zone of existence. We can therefore calculate the borderline between H_2TPP and H_4TPP^{2+} .

$$K_{a_1}^w K_{a_2}^w = \frac{a_{H_2TPP}^w (a_{H^+}^w)^2}{a_{H_4TPP^{2+}}^w} = \frac{a_{H_2TPP}^o (a_{H^+}^w)^2}{a_{H_4TPP^{2+}}^w P_{H_2TPP}^0} \quad (7.59)$$

and the border line reads

$$pH = \frac{1}{2} (pK_{a_1}^w + pK_{a_2}^w - \log P_{H_2TPP}^0) \quad (7.60)$$

The same method is used to deduce the other boundary lines from the Nernst equations expressed for each ionic species and from the definition of acid-base dissociation constants, and these lines are the geometric locus delimiting the domain of predominance of each species involved. It is straightforward to express these boundary lines numerically and to

calculate their and points.^[20] The results obtained are displayed in Figure 7.8 which shows the ionic partition diagram of H₂TPP at water|1,2-DCE.

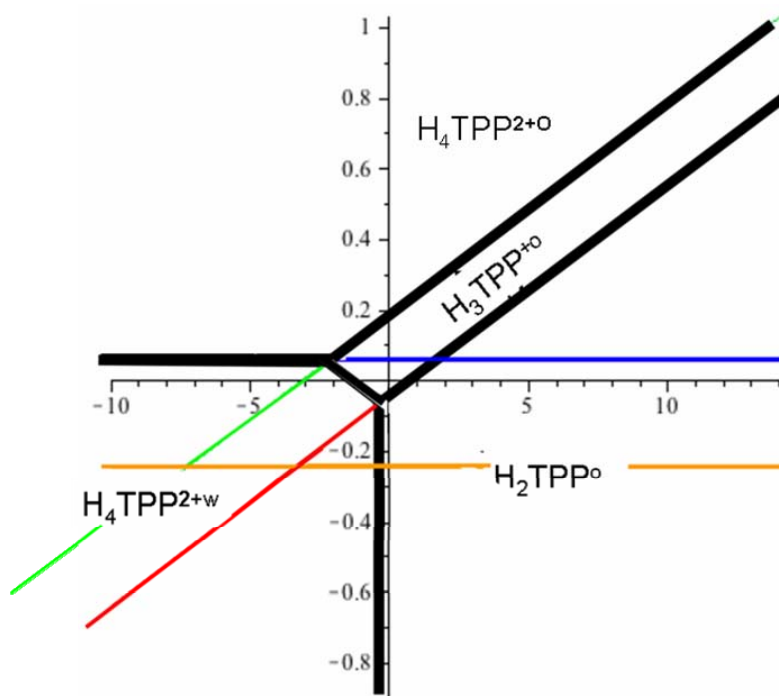
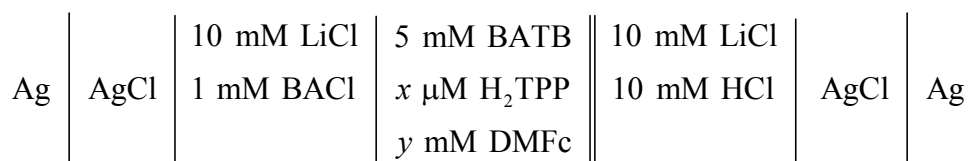


Figure 7.8: Ionic partition diagram of H₂TPP at water/1,2-DCE

7.6 H₂TPP catalyzed oxygen reduction by DMFc

As I have shown in Chapter 4 O₂ reduction leads to generation of H₂O₂ in acidified biphasic water|1,2-DCE system in presence of DMFc. In the presence of 50 μM H₂TPP in the 1,2-DCE phase, and in the absence of DMFc, cyclic voltammogram exhibits two current peaks in Figure 7.4(a) which correspond to the successive transfer of two protons from water to 1,2-DCE facilitated by the association with H₂TPP and H₃TPP⁺.^[56] In the presence of both DMFc and H₂TPP in 1,2-DCE (Cell 2), cyclic voltammogram exhibits slowly increasing positive current in the range 0.04 V < Δ₀^wφ < 0.47 V as shown in Figure 7.9.

Cell 2



The positive current can be ascribed to the proton-coupled reduction of O_2 with DMFc yielding $DMFc^+$.^[57] Cyclic voltammogram shows a remarkable enhancement of both the positive current in the potential range of the first and second proton transfer step. However, after removing dissolved oxygen from both solutions by argon purging, cyclic voltammogram of H_2TPP is recovered (Figure 7.9, full line). As shown in Figure 7.10 with the increasing pH of the aqueous phase, both catalytic waves shift positively by ca. 60 mV/pH. The same shift was reported in Figure 7.4(b) for the voltammetric peaks of the facilitated proton transfer.^[56]

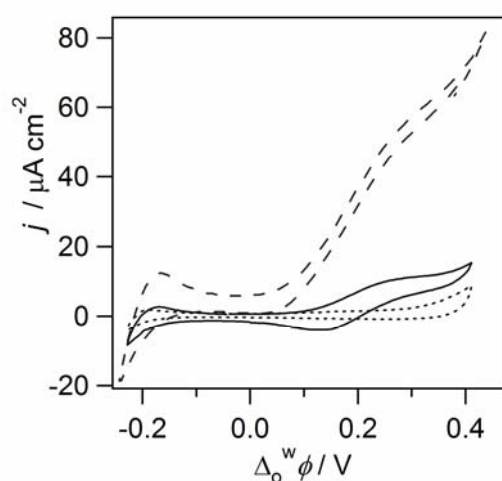


Figure 7.9: Cyclic voltammograms ($50mVs^{-1}$) using Cell 2: in the absence ($x=0, y=5$, dotted line) and presence of H_2TPP ($x=50, y=5$, dashed line) with the deaerated solutions ($x=50, y=5$, full line).

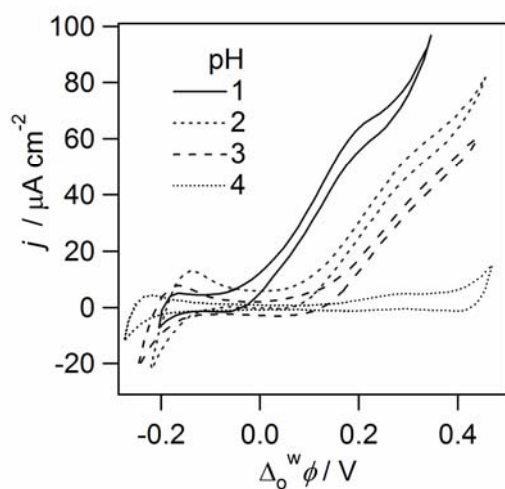
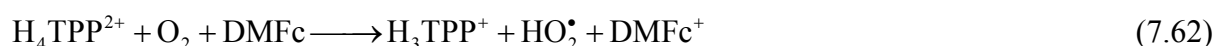


Figure 7.10: CVs obtained at a water/1,2-DCE interface with cell 2 when ($x=50, y=5$) at different pH.

The catalytic current is associated with the protonated forms of H₂TPP, the concentration of which at a constant potential decreases with the increasing pH. CV behavior thus points to the regeneration of H₂TPP and H₃TPP⁺ (or H₂TPP) in two homogeneous electron transfer (*ET*) reactions in 1,2-DCE involving DMFc, O₂ and H₃TPP⁺ or H₄TPP²⁺, which follow the first and second H⁺ ion transfer (*IT*), such as

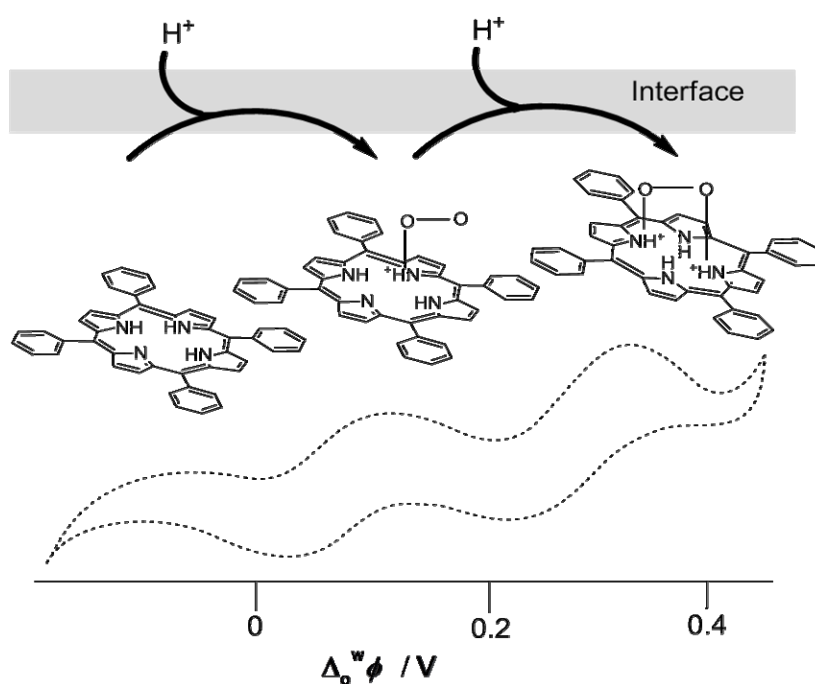


Using the classical electrochemical terminology, each of the two *IT-ET* sequences above is equivalent to the catalytic *EC* reaction scheme involving an electron transfer at electrode (*E*) followed by a chemical reaction (*C*) regenerating starting material.^[58-60]

The effects of the DMFc and H₂TPP concentrations and absence of O₂ in the system investigated by Samec *et al.* The results are consistent with the mechanism involving the reversible formation of an adduct between monoacid or diacid and the molecular oxygen that is followed by the irreversible electron transfer from DMFc^[61], *e.g.* for the reaction (7.61),



From DFT calculations^[62] point to the formation of weak adducts H₃TPP⁺-O₂ and H₄TPP²⁺-O₂, where the molecular oxygen is bound to the protonated nitrogen atoms of two opposite pyrrole rings with the stabilization energy of ca. 0.1 eV (Scheme 7.2).



Scheme 7.2: Illustration of interfacial formation of H_3TPP^+ and H_4TPP^{2+} .

To further study this catalytic process, we have used two-phase reactions to investigate the role of H_2TPP and to identify the reaction products. Here, we have used TB^- to form by extraction the organic acid HTB . The 1,2-DCE phase contains only 5 mM DMFc and 50 μ M H_2TPP and 10 mM HCl was present in the top aqueous phase. After adding the water phase, the color of 1,2-DCE phase change from orange to green (Figure 7.11).

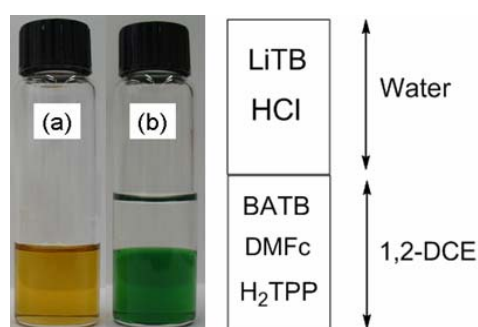


Figure 7.11: (a) Two-phase reaction controlled by TB^- partition before (a) and after (b) contact with aqueous phase containing 5 mM LiTB + 10 mM HCl; the bottom 1,2-DCE phase.

Moreover, the experiment performed in absence of oxygen showed that the 1,2-DCE solution containing DMFc and H_2TPP did not change its color. In the presence of both DMFc and

H₂TPP in 1,2-DCE phase, the formation of DMFc⁺ clearly can be observed, as shown by the red curve in Figure 7.12, characteristic of an absorption band with a maximum at 779nm. The formation of DMFc⁺ in the presence of only DMFc in 1,2-DCE phase observed less than DMFc in presence of H₂TPP (Figure 7.12(b)).

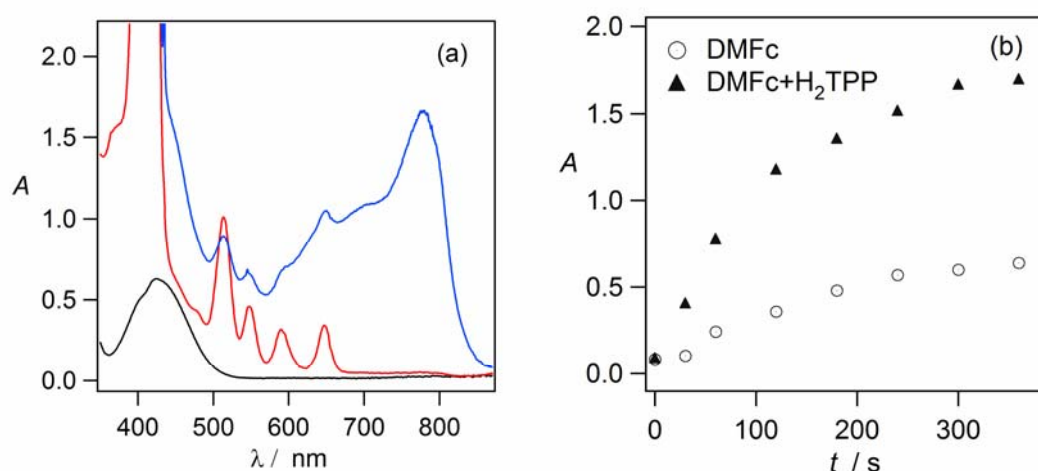


Figure 7.12: UV-Visible spectra of the 1,2-DCE (a) freshly prepared 5 mM DMFc (black line) freshly prepared 50 μM H₂TPP (red line) after 5 minutes two-phase reaction 5 mM DMFc+50 μM H₂TPP (blue line) (b) time profile of the formation of DMFc⁺ in the absence (○) and presence (▲) of 50 μM H₂TPP in 1,2-DCE during the shake flask experiments with TB as a common ion.

After separation of the two phases, the UV-Visible spectra of 1,2-DCE phases were measured and the aqueous phases were titrated with NaI. Addition of sodium iodide (NaI) to different aqueous phases was used to detect hydrogen peroxide by formation of I₃⁻, displaying two absorption bands at 287 and 352 nm as shown in Figure 7.13. Rather slow reduction of molecular oxygen by DMFc at the polarized water|1,2-DCE interface proceeds remarkably faster in the presence of tetraphenylporphyrin monoacid (H₃TPP⁺) and diacid (H₄TPP²⁺), which are formed in 1,2-DCE by the successive transfer of two protons from the acidified aqueous phase. A mechanism is proposed, which includes the formation of adduct between H₃TPP⁺ or H₄TPP²⁺ and O₂ that is followed by electron transfer from DMFc to the adduct leading to the observed production of DMFc⁺ and the regeneration of H₂TPP or H₃TPP⁺, respectively.

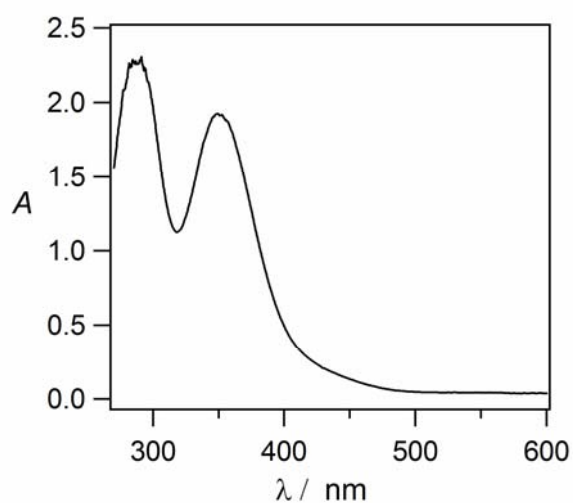
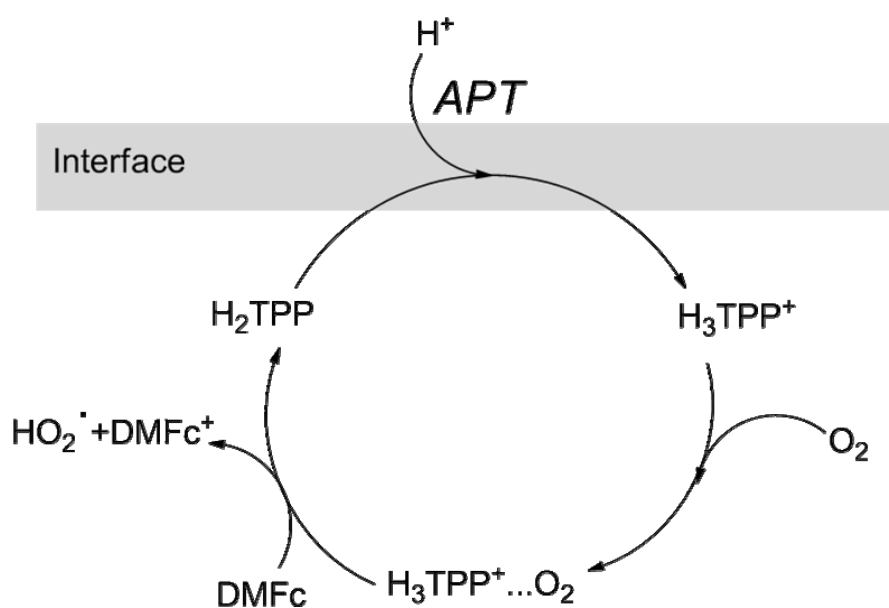


Figure 7.13: UV-Visible spectra of the aqueous phases separated after being treated with excess NaI.



Scheme 7.3: Mechanism of O_2 reduction with DMFc catalyzed by H_2TPP .

7.7 Conclusions

In conclusion, the protonation of H_2TPP in 1,2-DCE solution have been widely investigated by visible absorption spectroscopy. We present a simple methodology to illustrate the existence of H_3TPP^+ in 1,2-DCE, based on ion transfer voltammetry at the water|1,2-DCE

interface. H_2TPP can assist the H^+ ion transfer across the interface. The transfer process is reversible and diffusion-controlled. K_{a1} and K_{a2} values can be accurately determined. The catalytic activation of the protonated forms of a H_2TPP , on the molecular oxygen reduction by DMFc has been investigated at the polarized water|1,2-DCE interface.

7.8 References

- [1] J. Simplicio, *Biochemistry* **1972**, *11*, 2525.
- [2] S. Mazumdar, O. K. Medhi, N. Kannadaguili, S. Mitra, *Journal of the Chemical Society, Dalton Transactions* **1989**, 1003.
- [3] V. S. Chirvony, A. Van Hoek, V. A. Galievsky, I. V. Sazanovich, T. J. Schaafsma, D. Holten, *Journal of Physical Chemistry B* **2000**, *104*, 9909.
- [4] A. Stone, E. B. Fleischer, *Journal of the American Chemical Society* **1968**, *90*, 2735.
- [5] W. S. Sheldrick, *Journal of the Chemical Society, Perkin Transactions 2* **1976**, 453.
- [6] E. Cetinkaya, A. W. Johnson, M. F. Lappert, G. M. McLaughlin, K. W. Muir, *Journal of the Chemical Society, Dalton Transactions* **1974**, 1236.
- [7] B. Cheng, O. Q. Munro, H. M. Marques, W. R. Scheidt, *Journal of the American Chemical Society* **1997**, *119*, 10732.
- [8] L. D. Sparks, C. J. Medforth, M. S. Park, J. R. Chamberlain, M. R. Ondrias, M. O. Senge, K. M. Smith, J. A. Shelntt, *Journal of the American Chemical Society* **1993**, *115*, 581.
- [9] C. J. Medforth, M. O. Senge, K. M. Smith, L. D. Sparks, J. A. Shelntt, *Journal of the American Chemical Society* **1992**, *114*, 9859.
- [10] A. H. Corwin, A. B. Chivvis, R. W. Poor, D. G. Whitten, E. W. Baker, *Journal of the American Chemical Society* **1968**, *90*, 6577.
- [11] A. HofmanovÅi, L. Q. Hung, W. Khalil, *Journal of Electroanalytical Chemistry* **1982**, *135*, 257.
- [12] N. Kozlov Yu, J. Koryta, *Analytical Letters* **1983**, *16*, 255.
- [13] E. Wang, Y. Liu, *Journal of Electroanalytical Chemistry* **1986**, *214*, 459.
- [14] Z. Yoshida, H. Freisher, *Journal of Electroanalytical Chemistry* **1984**, *162*, 307.
- [15] Y. Liu, E. Wang, *Journal of Electroanalytical Chemistry* **1987**, *234*, 85.
- [16] J. Koryta, P. Vanysek, M. Brezina, *Journal of Electroanalytical Chemistry* **1976**, *67*, 263.
- [17] J. Koryta, P. Vanysek, M. Brezina, *Journal of Electroanalytical Chemistry* **1977**, *75*, 211.
- [18] Z. Samec, V. Marecek, J. Koryta, M. W. Khalil, *Journal of Electroanalytical Chemistry* **1977**, *83*, 393.
- [19] Z. Samec, V. Marecek, J. Weber, *Journal of Electroanalytical Chemistry* **1979**, *100*, 841.
- [20] F. Reymond, G. Steyaert, P. A. Carrupt, B. Testa, H. Girault, *Journal of the American Chemical Society* **1996**, *118*, 11951.
- [21] F. Reymond, G. Steyaert, P. A. Carrupt, B. Testa, H. H. Girault, *Helvetica Chimica Acta* **1996**, *79*, 101.
- [22] F. Reymond, G. Steyaert, A. Pagliara, P. A. Carrupt, B. Testa, H. Girault, *Helvetica Chimica Acta* **1996**, *79*, 1651.
- [23] X. H. Xia, W. D. Su, S. M. Zhou, *Journal of Electroanalytical Chemistry* **1992**, *324*, 59.
- [24] M. G. Kuzmin, I. V. Soboleva, N. A. Kotov, *Analytical Sciences* **1999**, *15*, 3.
- [25] S. Aronoff, C. A. Weast, *Journal of Organic Chemistry* **1941**, *6*, 550.
- [26] P. Hambright, *The Porphyrin Handbook*, eds., K. M. Kadish, K. M. Smith, R. Guilard, **2000**.
- [27] E. B. Fleischer, L. E. Webb, *Journal of Physical Chemistry* **1963**, *67*, 1131.
- [28] M. Meot-Ner, A. D. Adler, *Journal of the American Chemical Society* **1975**, *97*, 5107.

- [29] R. Karaman, T. C. Bruice, *Inorganic Chemistry* **1992**, *31*, 2455.
- [30] G. De Luca, A. Romeo, L. M. Scolaro, *Journal of Physical Chemistry B* **2005**, *109*, 7149.
- [31] G. De Luca, A. Romeo, L. M. Scolaro, *Journal of Physical Chemistry B* **2006**, *110*, 7309.
- [32] G. De Luca, A. Romeo, L. M. Scolaro, *Journal of Physical Chemistry B* **2006**, *110*, 14135.
- [33] J. L. Garate-Morales, F. S. Tham, C. A. Reed, *Inorganic Chemistry* **2007**, *46*, 1514.
- [34] R. I. Walter, *Journal of the American Chemical Society* **1953**, *75*, 3860.
- [35] P. Hambright, E. B. Fleischer, *Inorganic Chemistry* **1970**, *9*, 1757.
- [36] R. J. Abraham, G. E. Hawkes, K. M. Smith, *Tetrahedron Letters* **1974**, *15*, 71.
- [37] O. Almarsson, A. Blasko, T. C. Bruice, *Tetrahedron* **1993**, *49*, 10239.
- [38] D. C. Barber, R. A. Freitag-Beeston, D. G. Whitten, *Journal of Physical Chemistry* **1991**, *95*, 4074.
- [39] S. Aronoff, M. Calvin, *Journal of Organic Chemistry* **1943**, *8*, 205.
- [40] S. Aronoff, *Journal of Physical Chemistry* **1958**, *62*, 428.
- [41] R. F. Pasternack, P. R. Huber, P. Boyd, G. Engasser, L. Francesconi, E. Gibbs, P. Fasella, G. C. Venturo, L. D. C. Hinds, *Journal of the American Chemical Society* **1972**, *94*, 4511.
- [42] H. Baker, P. Hambright, L. Wagner, *Journal of the American Chemical Society* **1973**, *95*, 5942.
- [43] D. K. Lavalley, A. E. Gebala, *Inorganic Chemistry* **1974**, *13*, 2004.
- [44] F. Hibbert, K. P. P. Hunte, *Journal of the Chemical Society, Chemical Communications* **1975**, 728.
- [45] R. F. Pasternack, N. Sutin, D. H. Turner, *Journal of the American Chemical Society* **1976**, *98*, 1908.
- [46] F. Hibbert, K. P. P. Hunte, *Journal of the Chemical Society, Perkin Transactions 2* **1977**, 1624.
- [47] A. H. Jackson, *The Porphyrins, Vol. 1*, Academic Press, New York, **1978**.
- [48] D. C. Barber, T. E. Woodhouse, D. G. Whitten, *Journal of Physical Chemistry* **1992**, *96*, 5106.
- [49] *Porphyrins and Metalloporphyrins*, Elsevier, Amsterdam, **1975**.
- [50] I. Hatay, PhD thesis, Selcuk University (Turkey), **2010**.
- [51] G. De Luca, A. Romeo, L. M. Scolaro, G. Ricciardi, A. Rosa, *Inorganic Chemistry* **2007**, *46*, 5979.
- [52] Y. Shao, M. D. Osborne, H. H. Girault, *Journal of Electroanalytical Chemistry* **1991**, *318*, 101.
- [53] H. Matsuda, Y. Yamada, K. Kanamori, Y. Kudo, Y. Takeda, *Bull. Chem. Soc. Jpn* **1991**, *64*, 1497.
- [54] M. Pourbaix, *Atlas d'Equilibres Electrochimiques*, Paris, **1963**.
- [55] B. Moyer, Y. Sun, *Ion exchange and solvent extraction, Vol. 13*, New York, **1997**.
- [56] B. Su, F. Li, R. Partovi-Nia, C. Gros, J. M. Barbe, Z. Samec, H. H. Girault, *Angewandte chimie* **2008**, 5037.
- [57] V. J. Cunnane, G. Geblewicz, D. J. Schiffrin, *Electrochimica Acta* **1995**, *40*, 3005.
- [58] A. J. Bard, L. R. Faulkner, *Electrochemical Methods: Fundamentals and Applications*, John Wiley and Sons, New York, **1980**.
- [59] J. M. Saveant, E. Vianello, *Electrochimica Acta* **1965**, *10*, 905.
- [60] R. S. Nicholson, I. Shain, *Analytical Chemistry* **1964**, *36*, 706.

- [61] A. Trojanek, J. Langmaier, B. Su, H. H. Girault, Z. Samec, *Electrochemistry Communications* **2009**, *11*, 1940.
- [62] J. Sebera, S. Zalis, A. Trojanek, Z. Samec, *in preparation*.

Chapter 8

Protonation and catalytic role of free-base octaethyl porphyrin for oxygen reduction across the water|1,2-DCE interface

8.1 Introduction

The porphyrins and related compounds have intensively been studied for several decades due to their significance in biological and technological areas.^[1] It is well known that, under acidic conditions, the free-base porphyrins are capable of combining two additional hydrogens on the central nitrogen atoms to form N-protonated diacids.^[2-6] As many metal-incorporation reactions require an acidic condition, the porphyrin diacids may play an important role in the syntheses of metalloporphyrins.^[7] Porphyrin diacids have been found to exhibit perturbed photophysical properties compared to their neutral parent compounds.^[8-11] Moreover, porphyrin diacids typically have nonplanar macrocycles due to the steric hindrance and electrostatic repulsion of the central hydrogen atoms.^[8, 9] Therefore, the porphyrin diacids provide unique examples to study the influence of nonplanarity on the chemical and physical properties of porphyrin macrocycles.^[12, 13] Nonplanar conformations of porphyrins and related compounds are known important for their possible functions in photosynthetic reaction center, bacteriochlorophyll a protein and heme proteins.^[14-16] Rosa *et al.* studied the effects of core saddling, meso-phenyl twisting, and counter ions on the optical properties of the meso-tetraphenylporphyrin diacid (H_4TPP^{2+}).^[17] Cheng *et al.* carried out a study on a series of porphyrin diacids; they evaluated the effect of peripheral substituents on the molecule's flexibility.^[18]

It has been shown that the strong interaction of the systems of the phenyl groups and the porphyrin ring leads to the red-shift of the Q and B bands and the hyperchromicity of the Q-bands in the diacids. Avilov *et al.* investigated the photophysical properties of a series of porphyrin diacids with DFT.^[19]

Among the porphyrins, octaethylporphyrin (OEP) received more attention due to its symmetric structure and excellent solubility in organic solvents. Li *et al.* carried out DFT

calculations on the structure and spectroscopies of H_4OEP^{2+} .^[20] Chirvony *et al.* examined the photophysical properties of octaethylporphyrin diacid.^[8] They found that it exhibited a number of perturbed properties relative to its free base form.

In this Chapter, we present electrochemical and spectroscopic measurements of the di-protonated form of 2,3,7,8,12,13,17,18-octaethyl-21H,23Hporphine (H_2OEP) on ion-transfer voltammetry and its catalytic effect for oxygen reduction at the polarized water|1,2-DCE interface.

8.2 Ion-transfer voltammetry

Electrochemical measurements at the water|1,2-DCE interface were carried out so as to characterize the protonation of the H_2OEP .

By dissolving H_2OEP in a 1,2-DCE solution containing a lipophilic salt (BATB) in contact with an acidic aqueous solution LiCl and HCl (Cell 1), only one wave can be observed in the cyclic voltammogram, as illustrated by the full line in Figure 8.1.

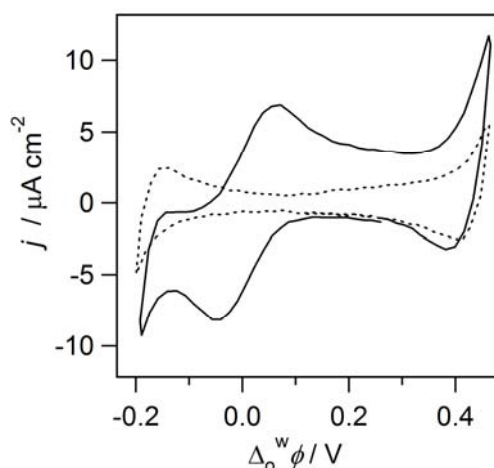
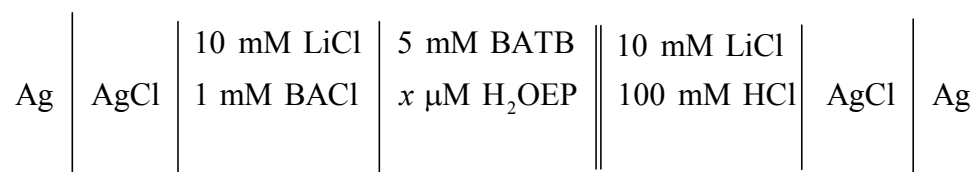
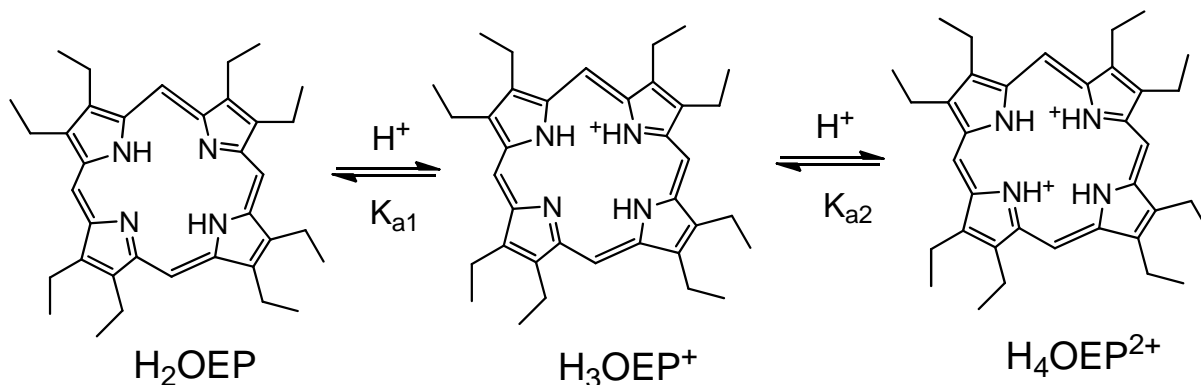


Figure 8.1: (a) Cyclic voltammograms ($50mVs^{-1}$) using Cell 1: in the absence ($x=0$, dotted line) and presence ($x=50$, full line) of H_2OEP in 1,2-DCE.

While the tetrapyrrole ring of a free-base porphyrins contains two tertiary nitrogen atoms, which allows the gain of protons to form a monoacid and a diacid, as illustrated for the free-base H_2OEP in Scheme 8.1.

Cell 1





Scheme 8.1: Protonation of H_2OEP to form monoacid and diacid.

Proton transfer reactions can be presented as follows,



The simplest case is that where both ion transfer reactions are rapid. We consider the cyclic voltammetric behavior for this situation. The appearance of the voltammogram depends ^[21], K_{a1} and K_{a2} , and the spacing between them,

$$\Delta E^0 = pK_{a2} - pK_{a1} \quad (8.3)$$

Whenever protonation reactions take place, one must consider the possibility of a disproportionation/comproportionation equilibrium, which is not our case.



$$K_{disp} = \frac{[H_2OEP][H_4OEP^{2+}]}{[H_3OEP^+]^2} \quad (8.5)$$

The extent of the reaction, as measured by the equilibrium constant K_{disp} is governed by ΔE^0 :

$$(RT/F) \ln K_{disp} = \Delta E^0 = pK_{a2} - pK_{a1} \quad (8.6)$$

Computations of cyclic voltammograms were carried out using DigiSim (version 3.03b, distributed by Bioanalytical Systems, Inc., 2701 Kent Ave., West Lafayette, IN 47906), the variation of the current as a function of potential are shown in Figure 8.2.

In general the nature of the i - E curve depends on $\Delta E^0 (=pK_{a2} - pK_{a1})$. Calculated cyclic voltammograms for different values of ΔE^0 in a system with two one-protonation steps are shown in Figure 8.2.

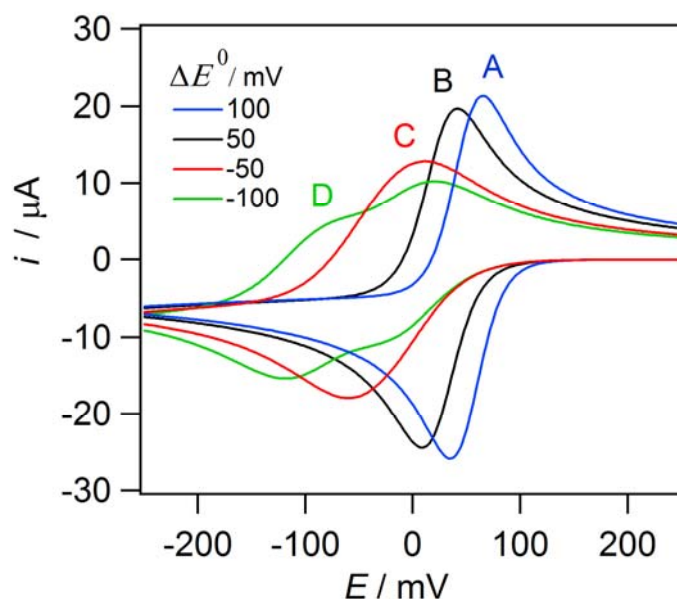


Figure 8.2: DigiSim simulation of the proposed reaction mechanism for the case where $x=5$, $T=298.2\text{ K}$, area 1 cm^2 and $D=1.0 \times 10^{-5}\text{ cm}^2\text{ s}^{-1}$ for all species.

When $\Delta E^0 > 100\text{ mV}$, the second protonation occurs much more easily than the first, and one observes a single wave with characteristics of two-proton transfer ($\text{H}_2\text{OEP} + 2\text{H}^+ \rightarrow \text{H}_4\text{OEP}^{2+}$) (i.e., $\Delta E_p = 29\text{ mV}$). However, simultaneous transfer of two protons are very unlikely. As ΔE^0 decreases, the individual waves are merged into a broad single wave until ΔE^0 reaches about -100 mV . If pK_{a1} and pK_{a2} are well separated, with $pK_{a1} > pK_{a2}$ (i.e., H_2OEP protonated before H_3OEP^+) then two separate waves are observed.

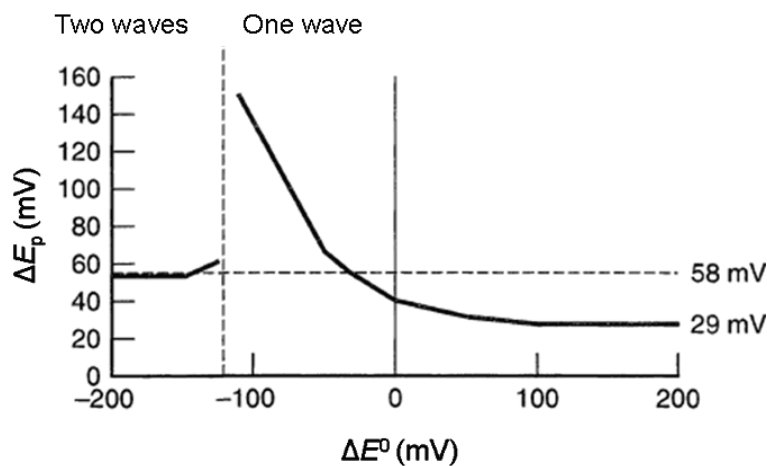


Figure 8.3: ΔE_p vs ΔE^0 the discontinuity at negative values of ΔE^0 occurs when two waves are resolved.

The two waves become resolvable at $\Delta E^0 = -200$ mV, where each wave takes on the characteristics of a one-proton transfer (*i.e.*, $\Delta E_p = 58$ mV). In Figure 8.3 the variation of the peak current function and the peak splitting between the cathodic and anodic reversal waves (ΔE_p) at 25°C are summarized.^[22]

In the case of H₂OEP K_{a1} and K_{a2} are close to each other as shown C in Figure 8.2, $\Delta E^0 < 0$ first and second protonation occur at the same pH value. The separation between the forward and backward peaks in Figure 8.1 is 65 mV. This value is in agreement with the theoretical consideration (Figure 8.3) and simulation result.

In The magnitude of this current wave does not change with the acidity of the aqueous phase showing that the current is limited by the diffusion of H₂OEP in the organic phase, whereas the wave continuously moves to positive potentials with the half-wave potential shifting by approximately 60 mV/pH, as displayed in Figure 8.4. These data indicate that the voltammetric wave corresponds to the assisted transfer of proton from water to 1,2-DCE by H₂OEP.

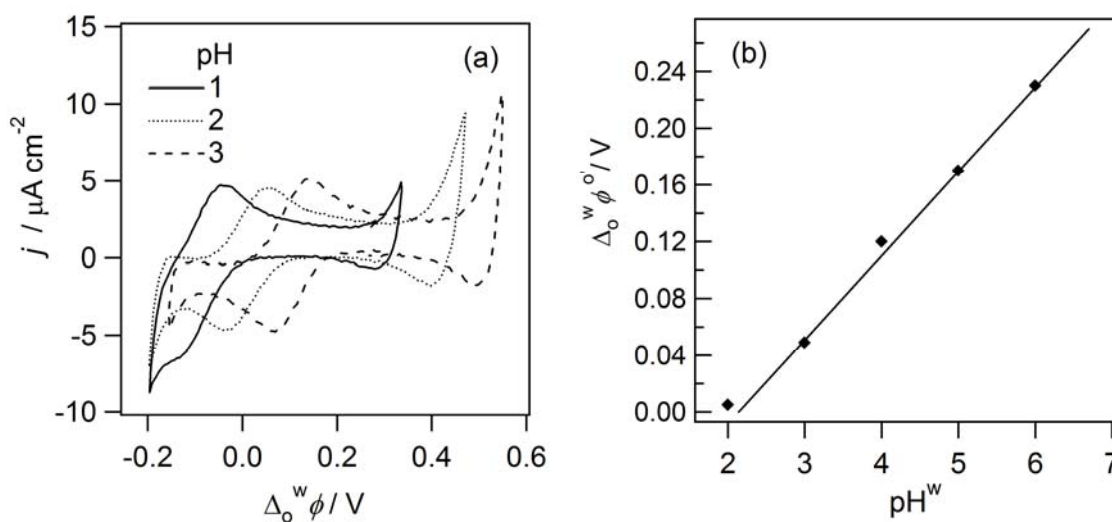


Figure 8.4: (a) Cyclic voltammograms in the presence of H₂OEP (Cell 1, $x=50$) in 1,2-DCE at different pH values, scan rate 50mV s^{-1} (b) pH dependence of the half-wave potentials.

Indeed, the voltammetric current displays a linear dependence on the square root of the sweep rate (Figure 8.5). It indicates that the H⁺ facilitated H₂OEP transfer process at the big interface is a diffusion limited process.

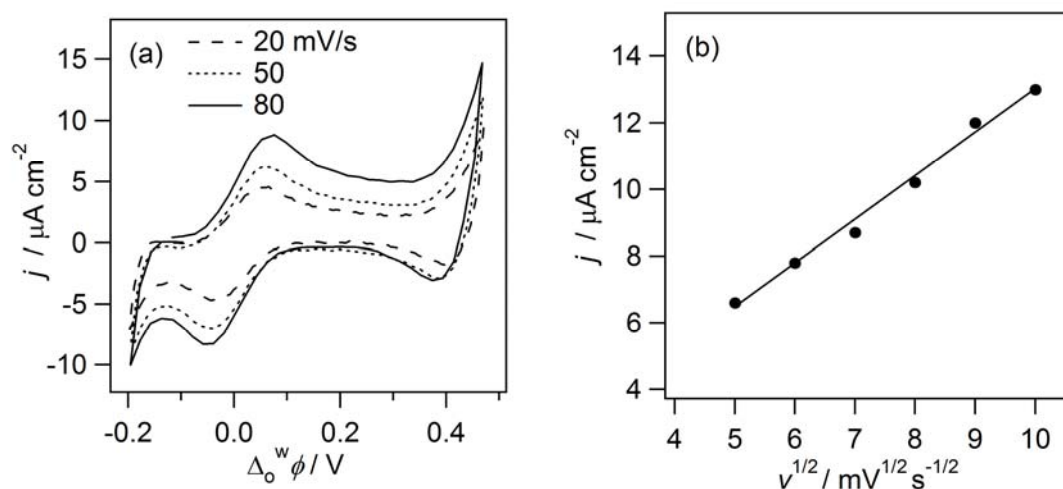


Figure 8.5: (a) CVs at various scan using Cell 1($x=50$) of H₂OEP in 1,2-DCE (b) The anodic peak current as a function of the square root of the scan rate.

Effects of the concentrations of H₂OEP from voltammograms are shown in Figure 8.6. The height of the anodic peak is proportional to the H₂OEP concentration. Proton transfer facilitated by H₂OEP are observed with varying the concentration of H₂OEP.

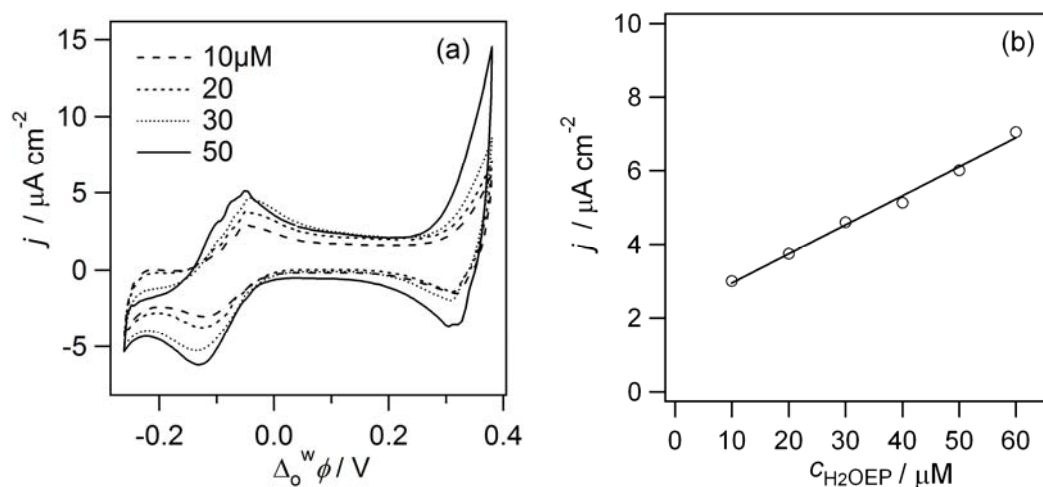


Figure 8.6: (a) CVs at various concentration of H₂OEP in 1,2-DCE using Cell 1 (b) relationship between the anodic peak current as a function of concentration.

Moreover, ion-transfer voltammetry allows the estimation of dissociation constant of the diacid by exploring the dependence of $\Delta_0^w \phi_{H_4OEP^{2+}}^0$ on the acidity of aqueous phase according to the following equation:

$$\Delta_0^w \phi = \Delta_0^w \phi_{H^+}^{0'} + \frac{RT}{F} \ln \left(\frac{c_{H^+}^o}{c_{H^+}^w} \right) \quad (8.7)$$

$$K_{app} = K_{a1} K_{a2} \quad (8.8)$$

$$\Delta_o^w \phi_{\text{H}_4\text{OEP}^{2+}} = \Delta_o^w \phi_{\text{H}^+}^{0'} + \frac{RT}{2F} \ln K_{\text{app}} + \frac{2.303RT}{F} \text{pH}^w \quad (8.9)$$

where $\Delta_o^w \phi_{\text{H}^+}^{0'}$ is the formal transfer potential for the transfer of H^+ , pH^w is the aqueous pH and K_{app} is the apparent dissociation constant of $\text{H}_4\text{OEP}^{2+}$ in 1,2-DCE. As shown in Figure 8.4, the relationship between $\Delta_o^w \phi_{\text{H}_4\text{OEP}^{2+}}$ and the pH^w is found to be linear with a slope of 60 mV, and the $\text{p}K_{\text{app}}$ value was determined to be equal to 11.2.

8.3 Spectrophotometric titration

Nonplanar distortions of the porphyrin core are realized by the addition of two protons to the tertiary nitrogens of the porphyrin core to form the diacid $\text{H}_4\text{OEP}^{2+}$. Such diprotonation can be achieved in organic solvents by the addition of acid, trifluoroacetic acid (TFA). In the diacid adducts, there appears to be close interactions between the diprotonated porphyrin and the conjugate bases of two acid molecules (Figure 8.7), such as hydrogen bonding to the central nitrogens.^[2, 18, 23]

The octaethylporphyrin diacid formed by reaction of H_2OEP and CF_3COOH is best represented as $[\text{H}_4\text{OEP}](\text{CF}_3\text{COO})_2$, which will be denoted $\text{H}_4\text{OEP}^{2+}$. Porphyrin diacids typically have nonplanar structures with mainly saddle type distortions, as revealed by X-ray crystallography, although other structures can be realized depending, for example, on the acid reagent used.^[8, 24] The spectrophotometric titration of H_2OEP with an organic soluble acid, TFA, was performed in 1,2-DCE.

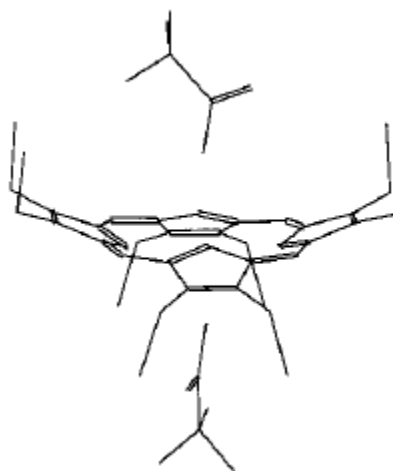


Figure 8.7: Structures of $\text{H}_4\text{OEP}^{2+}$ including the two CF_3COO species from the acid reagents that are hydrogen-bonded to the central nitrogens and seen in the X-ray structures.^[18]

The UV-Visible absorption spectra of H₂OEP and its diacid H₄OEP²⁺ in 1,2-DCE are shown in Figure 8.8. Neutral H₂OEP displays a Soret band at 395 nm and four bands in the visible region at 498, 531, 564 and 619 nm, similar to the reported ones. In the diprotonated form, as is well-documented,^[6] the visible spectral region is dominated by two major bands at 547 and 590 nm with a weaker band at 568 nm, which appears as a shoulder to the main peak at 547 nm. The spectral simplification from H₂OEP to the diacid H₄OEP²⁺ is a result of the approach towards square symmetry (*i.e.*, D_{4h}) in the diacid when protons are added to the pyrrole nitrogen atoms.

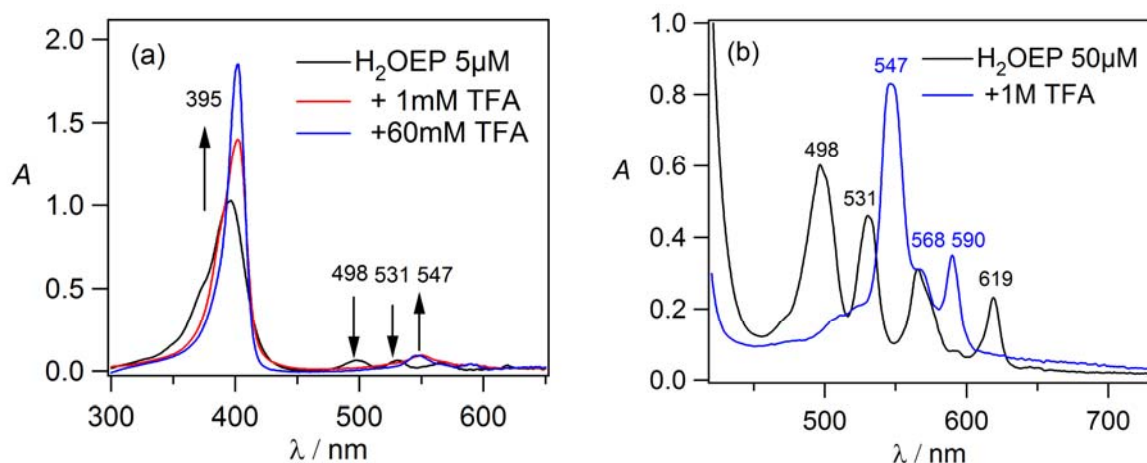


Figure 8.8: Spectrophotometric titration of (a) 5 μM (b) 50 μM H₂OEP in 1,2-DCE by TFA.

Figure 8.8(a) illustrate adding TFA to a H₂OEP solution led to a slight decrease and red-shift (from 395 nm to 401 nm) of the Soret band and the appearance of three new Q bands that increase with increasing TFA concentration.

The color of 1,2-DCE phases is shown in the inset of Figure 8.9(a) before addition of the aqueous phase. After adding TFA, the color change of the 1,2-DCE from pink to violet is indicative of the protonation of H₂OEP. These experimental results are indeed similar to those observed previously for a free base tetraphenylporphyrin. As reported previously, in the case of 5,10,15,20-tetraphenylporphyrin (H₂TPP) it was possible to observe the two successive protonations of two tertiary nitrogen atoms with dissociation constants of 1.6×10^{-10} and 1.0×10^{-6} for H₃TPP⁺ and H₄TPP²⁺ by ion-transfer voltammetry.^[25]

Therefore, what is observed in the ion-transfer voltammetry corresponds to the successive protonation of the tertiary nitrogen atoms to form the diacid H₄OEP²⁺. It should be mentioned that H₃OEP⁺ was not clearly detected in the course of the spectrophotometric titration by TFA.

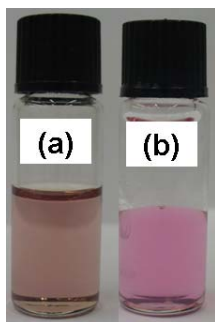


Figure 8.9: Titration of H_2OEP with TFA (a) at the beginning (b) after protonation.

8.4 H_4OEP^{2+} catalyzed oxygen reduction by DMFc

The voltammetric responses of DMFc in the absence (dashed line) and the presence of H_2OEP (full line) at the water|1,2-DCE interface are compared in Figure 8.10.

Cell 2

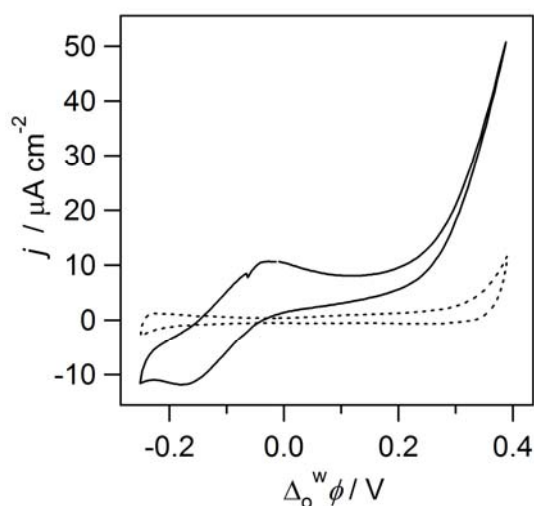
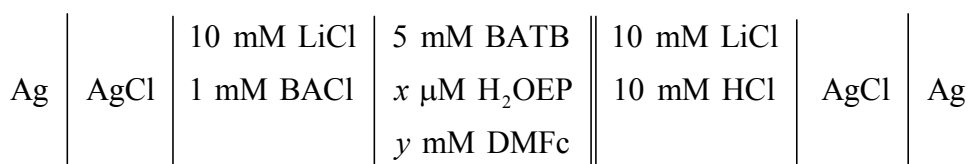


Figure 8.10: Cyclic voltammograms (50 mVs^{-1}) using Cell 2: in the absence ($x=0$, $y=5$, dotted line) and presence ($x=50$, $y=5$, full line) of H_2OEP .

In the presence of only DMFc in 1,2-DCE, a significant current can be observed at the positive potentials, as shown in Chapter 4. This current response arises from proton transfer followed by O_2 reduction by DMFc, as previously reported.^[26]

Figure 8.10 compares the cyclic voltammograms in the presence of only DMFc (dotted line) and in the presence of both DMFc and H₂OEP (full line). When H₂OEP and DMFc were both present, a large irreversible positive current wave was observed at positive potentials, *i.e.* a wave without a signal on the return scan. This positive current signal originating from a proton-coupled electron transfer (*PCET*) reaction, in which proton transfer and electron transfer are tightly coupled. *PCET* reaction that depends on the interfacial polarization, *i.e.* on the potential difference applied between the two phases.

As we showed in Chapter 7 after removing dissolved oxygen from both solutions by argon purging, cyclic voltammogram of H₂OEP is recovered. Although H₂OEP is a free base porphyrin, it exhibits a catalytic behavior similar to that of cobalt tetraphenylporphyrin [Co(tpp)] toward oxygen reduction by DMFc.^[27]

This process is equivalent to a catalytic *EC* reaction scheme in the classical electrode|solution electrochemistry, involving an electron transfer reaction (*E*) at the electrode|solution interface followed by a chemical reaction (*C*) in the solution regenerating the starting reactant. Here, the assisted proton transfer (*APT*) step represents a Faradaic process with an ionic flux across the interface, thus being equivalent to the *E* step. The oxygen reduction reaction involving H₄OEP²⁺, DMFc and O₂ is the following *C* step to produce H₂O₂ and regenerate the catalyst H₂OEP.

8.5 Shake flask experiments

To further study this catalytic process, we have used two-phase reactions to investigate the role of H₄OEP²⁺ and to identify the reaction products. A chemical way to drive aqueous protons to the organic phase is to add a very lipophilic anion to the aqueous phase. Here, we have used TB⁻ and TMA⁺ as a common ion.

As illustrated in Figure 8.11, 10 mM HCl and LiTB were present in the top aqueous phase flask and the 1,2-DCE phase contains 5 mM DMFc +50 μM H₂OEP+5 mM BATB in Figure 8.11(a). After adding the water phase for 5 minutes, the color of the 1,2-DCE phase in flask (a) change from yellow to green. After separation of the two phases, the UV-Visible spectra of 1,2-DCE phases were measured and the aqueous phases were titrated with NaI.

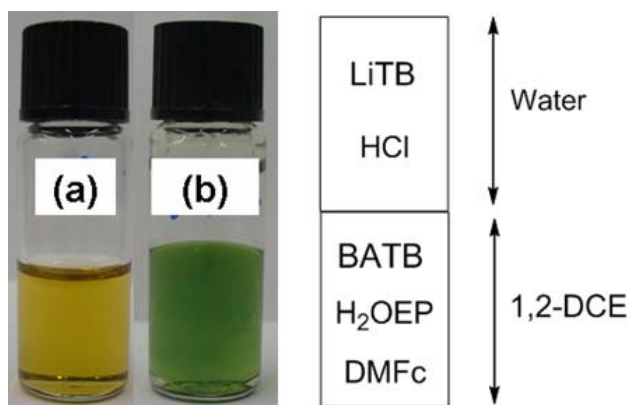


Figure 8.11: Photographs of two phase reactions. The composition of top aqueous phase is 10mM HCl+5mM LiTB: (a) fresh solution of 5 mM DMFc + 50 μ M H₂OEP + 5 mM BATB (b) 5 mM DMFc + 50 μ M H₂OEP+ 5 mM BATB after contacting with the water solution .

In the presence of both DMFc and H₂OEP in 1,2-DCE phase, the formation of DMFc⁺ clearly can be observed, as shown by the dotted line in Figure 8.12(a), characteristic of an absorption band with a maximum at 779 nm. When only H₂OEP is present in 1,2-DCE phase, the protonation of H₂OEP to form H₄OEP²⁺ can be observed clearly from the UV-Visible spectrum, shifting of Soret band and Q bands (Figure 8.8).

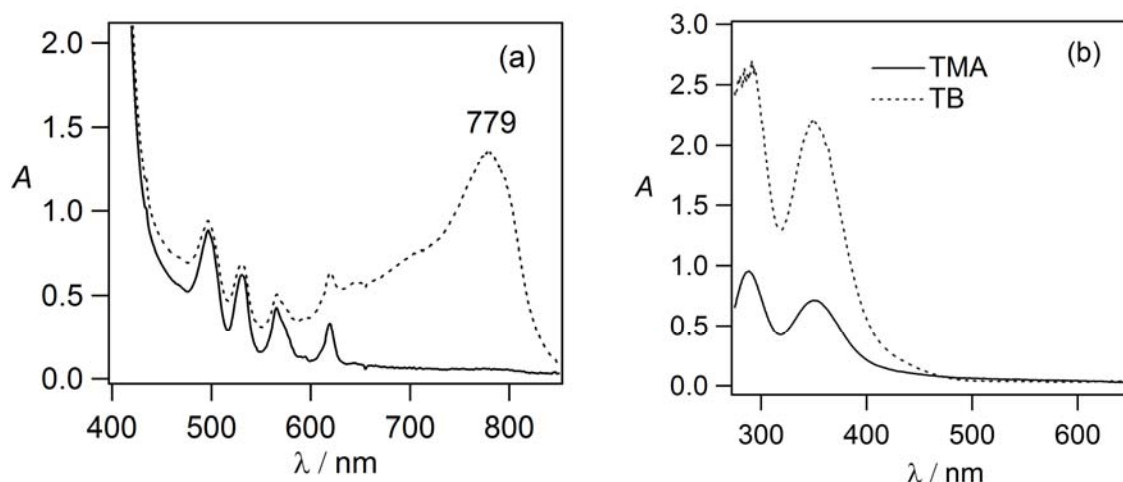


Figure 8.12: (a) Absorption spectra of the 1,2-DCE phases shown in Figure 8.9: flask a (full line), flask b (dotted line) (b) UV-Visible spectra of the aqueous solutions flask b, TMA common ion after 30 minutes shake flask experiment (full line) and TB common ion after 5 minutes two-phase reaction (dotted line).

Addition of sodium iodide (NaI) to different aqueous phases was used to detect hydrogen peroxide by formation of I₃⁻, displaying two absorption bands at 287 and 352 nm as shown in Figure 8.12(b) for two common ions TMA and TB. The H₂O₂ amount detected in the case of TMA and TB were 0.025 and 0.08 mM, respectively.

Figure 8.12(b) illustrates the influence of the Galvani potential difference on this two-phase reaction when employing different common ions. The Galvani potential difference at the water|1,2-DCE interface is set at 0.54 V and 0.160 V by the ions TB^- , TMA^+ , respectively. It is clear from the color change, as well as the UV-Visible spectra (Figure 8.12(b)), that the reaction rate follows the order $TB^- > TMA^+$. The reaction is very fast when TB^- is used as the common ion. The colour change of the 1,2-DCE solution from yellow to green after 5 minutes at the interfacial region upon contact of the aqueous solution with the 1,2-DCE solution, thereby indicating that the O_2 reduction by DMFc occurs at the interface.

It has been shown that oxygen reduction at the polarized water|1,2-DCE interface produces $DMFc^+$ and H_2O_2 , on the basis of the two-phase reaction controlled by a common ion.

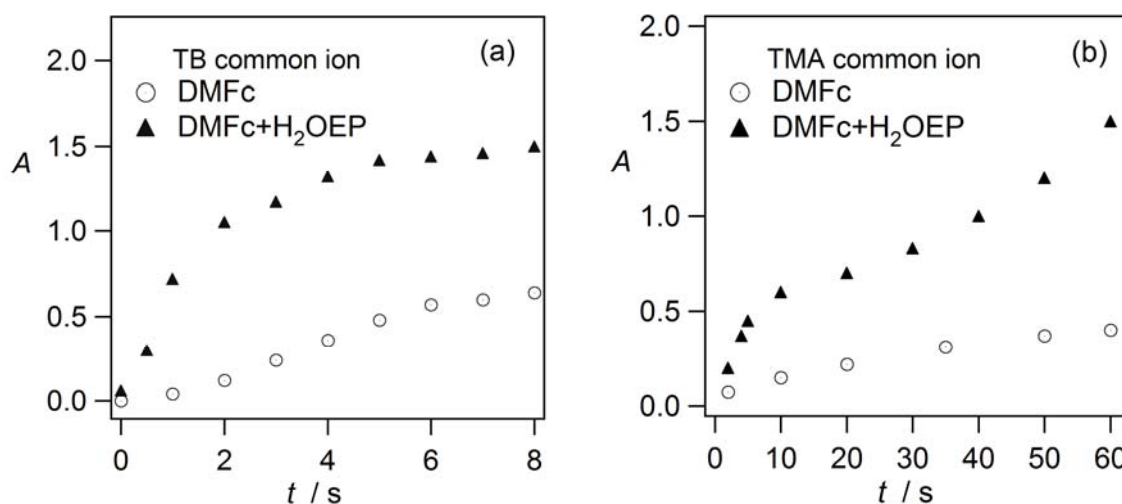


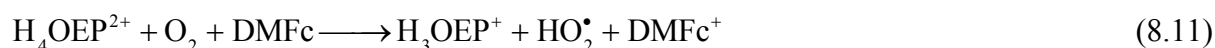
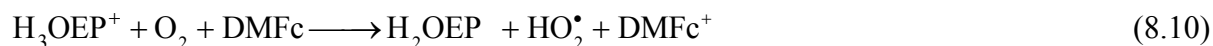
Figure 8.13: Time profile of the formation of $DMFc^+$ in the absence (○) and presence (▲) of $50 \mu M H_2OEP$ in 1,2-DCE during the shake flask experiments (a) TB and (b) TMA as a common ion.

A time profile of the formation of $DMFc^+$ in the absence and presence of H_2OEP shows that the oxidation of DMFc is much faster in the presence of H_2OEP and the reaction rate for TB^- (Figure 8.13(a)) is higher than TMA^+ (Figure 8.13(b)). Upon an addition of H_2OEP , the rise of the absorption bands at 779 nm, corresponding to $DMFc^+$, could be observed, as displayed in Figure 8.13. These results indicated that the rate of formation of decamethylferrocenium was dependent on the Galvani potential difference tuned by using various common ions and H_2OEP plays a catalytic role in the O_2 reduction by DMFc.

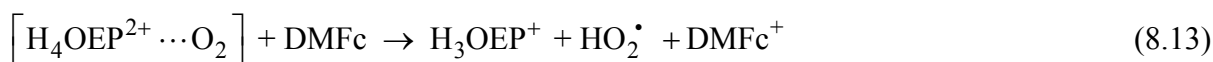
8.6 Mechanisms

All the data presented there above demonstrate unambiguously that H_4OEP^{2+} can promote oxygen reduction by DMFc. Samec *et al.* investigated the reversible formation of an adduct

between monoacid or diacid and the molecular oxygen by DFT calculation.^[28] The mechanism is very similar to that proposed by Samec *et al.* for H₂TPP catalyzed O₂ reduction by DMFc.^[28] The formation of weak adducts H₃OEP⁺-O₂ and H₄OEP²⁺-O₂, where the molecular oxygen is bound to the protonated nitrogen atoms of two opposite pyrrole rings, *e.g.* for the reaction (8.7),



The mechanistic routes involving a proton-coupled electron transfer as shown below (8.9) are currently under investigation.



The generation of hydrogen peroxide from the formed hydroperoxyl radical, HO₂[•], is expected to proceed rapidly.

8.7 Conclusions

Protonation of free base porphyrin, 2,3,7,8,12,13,17,18-octaethyl-21H,23Hporphine (H₂OEP) has been studied by cyclic voltammetry and spectrophotometric method. The acidity constants *K*_{a1} and *K*_{a2} are very close to each other, only one peak can be seen. Two protonation peaks occur at the same pH and combine to make one peak at 0.04 V. The cyclic voltammogram shape and peak separation of experimental results is in good agreement with computational results. The titration of H₂OEP with an organic soluble acid, was studied in 1,2-DCE and formation of H₂OEP diacid (H₄OEP²⁺) confirmed by UV-Visible. H₄OEP²⁺ can bind to oxygen, and the complex in the organic phase can easily be reduced by DMFc to produce hydrogen peroxide as studied by two-phase reactions with the Galvani potential difference between the two phases being controlled by the partition of a common ion. The catalytic activation of the protonated forms H₂OEP on the molecular oxygen reduction by decamethylferrocene has been investigated at the polarized 1,2-DCE interface.

8.8 References

- [1] D. Dolphin, *The Porphyrins, Vol. 1-7*, Academic press, New York, **1978**.
- [2] A. Stone, E. B. Fleischer, *Journal of the American Chemical Society* **1968**, *90*, 2735.
- [3] W. S. Sheldrick, *Journal of the Chemical Society, Perkin Transactions 2* **1976**, 453.
- [4] T. Ema, M. O. Senge, N. Y. Nelson, H. Ogoshi, K. M. Smith, *Angewandte Chemie-International Edition in English* **1994**, *33*, 1879.
- [5] A. T. Gradyushko, V. N. Knyukshto, K. N. Solovev, M. P. Tsvirko, *Journal of Applied Spectroscopy* **1975**, *23*, 1205.
- [6] H. Ogoshi, E. Watanabe, Z. Yoshida, *Tetrahedron* **1973**, *29*, 3241.
- [7] B. F. Burnham, J. J. Zuckerman, *Journal of the American Chemical Society* **1970**, *92*, 1547.
- [8] V. S. Chirvony, A. Van Hoek, V. A. Galievsky, I. V. Sazanovich, T. J. Schaafsma, D. Holten, *Journal of Physical Chemistry B* **2000**, *104*, 9909.
- [9] G. A. Schick, M. R. O'Grady, R. K. Tiwari, *Journal of Physical Chemistry* **1993**, *97*, 1339.
- [10] R. F. Pasternack, K. F. Schaefer, P. Hambright, *Inorganic Chemistry* **1994**, *33*, 2062.
- [11] J. M. Ribo, J. Crusats, F. Sagues, J. Claret, R. Rubires, *Science* **2001**, *292*, 2063.
- [12] B. Shah, B. Shears, P. Hambright, *Inorganic Chemistry* **1971**, *10*, 1828.
- [13] R. Khosropour, P. Hambright, *Journal of the Chemical Society, Chemical Communications* **1972**, *0*, 13.
- [14] J. Deisenhofer, H. Michel, *Angewandte Chemie - International Edition in English* **1989**, *28*, 829.
- [15] D. E. Tronrud, M. F. Schmid, B. W. Matthews, *Journal of Molecular Biology* **1986**, *188*, 443.
- [16] J. Deisenhofer, H. Michel, *Science* **1989**, *245*, 1463.
- [17] A. Rosa, G. Ricciardi, E. J. Baerends, A. Romeo, L. M. Scolaro, *Journal of Physical Chemistry A* **2003**, *107*, 11468.
- [18] B. Cheng, O. Q. Munro, H. M. Marques, W. R. Scheidt, *Journal of the American Chemical Society* **1997**, *119*, 10732.
- [19] I. V. Avilov, A. Y. Panarin, V. S. Chirvony, *Chemical Physics Letters* **2004**, *389*, 352.
- [20] Z. Y. Li, H. L. Wang, T. T. Lu, T. J. He, F. C. Liu, D. M. Chen, *Spectrochimica Acta - Part A: Molecular and Biomolecular Spectroscopy* **2007**, *67*, 1382.
- [21] D. S. Polcyn, I. Shain, *Analytical Chemistry* **1966**, *38*, 370.
- [22] A. J. Bard, L. R. Faulkner, *Electrochemical methods; Fundamentals and Applications*, John Wiley and sons, New York, **2001**.
- [23] H. H. Thanga, A. L. Verma, *New Journal of Chemistry* **2002**, *26*, 342.
- [24] A. Singh, L. W. Johnson, *Spectrochimica Acta - Part A: Molecular and Biomolecular Spectroscopy* **2006**, *64*, 761.
- [25] B. Su, F. Li, R. Partovi-Nia, C. Gros, J. M. Barbe, Z. Samec, H. H. Girault, *Chemical Communications* **2008**, 5037.
- [26] B. Su, R. P. Nia, F. Li, M. Hojeij, M. Prudent, C. Corminboeuf, Z. Samec, H. H. Girault, *Angewandte Chemie - International Edition* **2008**, *47*, 4675.
- [27] R. Partovi-Nia, B. Su, F. Li, C. P. Gros, J. M. Barbe, Z. Samec, H. H. Girault, *Chemistry - A European Journal* **2009**, *15*, 2335.
- [28] A. Trojanek, J. Langmaier, B. Su, H. H. Girault, Z. Samec, *Electrochemistry Communications* **2009**, *11*, 1940.

Chapter 9

Summary

In this work, a novel electrocatalytic approach has been studied for oxygen reduction based on molecular catalysts at soft interface such as a liquid | liquid interface. The objective of this project is the design of a novel class of molecular catalysis for the electroreduction of oxygen at water | 1,2-DCE interface.

First of all, the oxygen reduction by DMFc has been proved in the absence of any noble metal catalysts at a polarized water|1,2-DCE interface. Electrochemical results point to a mechanism similar to the *EC* type reaction at the conventional electrode/solution interface, the protonation of DMFc occurs heterogeneously to the formation of DMFc-H⁺ in the present biphasic system. We present an electrochemical method for producing H₂O₂ at a soft molecular interface rather than at a solid electrode. This approach relies on controlling the interfacial Galvani potential difference between two immiscible phases to allow the reduction of O₂ to H₂O₂. The electrochemical method used for the study of ORR reaction and rate of reaction is controlled by the Galvani potential difference across the interface, which has been determined chemically using various salts with a common ion.

[Co(tpp)] and CoOEP catalyzed O₂ reduction by ferrocene derivatives at the polarized water|1,2-DCE interface. This study demonstrates the oxidation of Fc derivatives is much faster in the presence of cobalt porphyrins.

Furthermore, the proton transfer facilitated by H₂TPP has been demonstrated. The first protonation of H₂TPP to form the monoacid H₃TPP⁺ in 1,2-DCE represents the transfer of a proton from water to 1,2-DCE and the second protonation represents the facilitated transfer of a second proton by H₃TPP⁺. These results show a simple methodology to illustrate the existence of H₃TPP⁺ in 1,2-DCE, based on ion transfer voltammetry at the water|1,2-DCE interface. It has been conclusively demonstrated that cyclic voltammetry is a relevant technique to explore the partition of ionic species of H₂TPP in the water | 1,2-DCE solvent system. It allows the evaluation of thermodynamic quantities with determination of ionic partition of H₂TPP. Rather slow reduction of molecular oxygen by DMFc at the polarized water | 1,2-DCE interface proceeds remarkably faster in the presence of monoacid (H₃TPP⁺)

and diacid ($\text{H}_4\text{TPP}^{2+}$), which are formed in 1,2-DCE. A mechanism is proposed, which includes the formation of adduct between H_3TPP^+ or $\text{H}_4\text{TPP}^{2+}$ and O_2 that is followed by electron transfer from DMFc to the adduct leading to the observed production of DMFc^+ and the regeneration of H_2TPP or H_3TPP^+ , respectively.

Finally, the protonation of H_2OEP has been studied by cyclic voltammetry and spectrophotometric method. From ion-transfer voltammetry only one peak appears. This was related to the fact the two protonation peaks combine to make one peak, the cyclic voltammogram shape and peak separation of experimental results is in good agreement with computational results. The reaction mechanism clearly explained by theoretical model and confirmed by computational consideration which is in a good agreement with the experimental results. Protonated octaethylporphyrin can catalyze ORR reaction by DMFc to produce hydrogen peroxide.

Curriculum Vitae

Personal

Name: Raheleh Partovi Nia

Date of Birth: 11th Jun 1979

Place of Birth: Mashhad, Iran

Nationality: Iranian

Education

- **March. 2006 – January 2010:** PhD student

Laboratoire d'Electrochimie Physique et Analytique, Ecole Polytechnique Fédérale de Lausanne, Switzerland.

Thesis: Electrocatalysis at liquid | liquid interfaces

Advisor: Prof. Hubert Girault

- **September 2003 – February 2005:** Master of Science

Shiraz University, Shiraz, Iran

Thesis: Application of chemometric methods in simultaneous determination of some pharmaceuticals and inorganic anions

Advisor: Prof. Afsaneh Safavi

- **September 1999 – July 2003:** Bachelor of Applied Chemistry

Ferdowsi University of Mashhad, Mashhad, Iran

Teaching Assistantships

- **Doctoral assistant**, Analytical chemistry laboratory in high performance liquid chromatography (HPLC), 5 semesters, EPFL, (2006-2009).
- **Assistant**, Analytical chemistry laboratory in electrochemistry, 2 semesters, Shiraz University, Iran, (2004-2005).
- **Assistant**, General chemistry laboratory, 2 semesters, Shiraz University, Iran, (2003-2004).

Skills and Abilities

- **Analytical/ Instrumental:** Spectro-Electro chemical methods and Instruments; SECM, Photo-Electro Chemistry, Laser Excimer, He-Ne Laser, Femtosecond Laser, Self Assembly Multilayer Thin Films, Spectrofluorometer, Absorption Spectrometer (UV-Vis-NIR), HPLC.
- **Computer Abilities:** Experienced in Windows Environments, Experienced in Microsoft Office: Word, Power Point, Chemistry Drawing Software: Chem Draw, Corel Draw, Math Type, Endnote and Excel, Matlab, Pascal, Igor.
- **Language Abilities:** Able to communicate in English Fluently, Able to communicate in French Fluently, Able to communicate in Persian (Farsi) as the mother language, Acquainted with Esperanto

HONORS

Top Ranks in National MSc Entrance Examination among nearly 7000 students of Chemistry: 74th Rank in Analytical Chemistry , 82nd Rank in Applied Chemistry, 100th in Organic Chemistry, 116th in Inorganic Chemistry, 121st in Physical Chemistry.

Scientific publications

- B Su, R Partovi Nia, F Li, M Hojeij, M Prudent, C Corminboeuf, Z Samec, and H H. Girault. H₂O₂ generation by decamethylferrocene at a liquid-liquid interface. In *Angewandte Chemie, International Edition*, volume 47, number 25, pages 4675-4678, 2008.
- B Su, F Li, R Partovi Nia, C Gros, J-M Barbe, Z Samec and H H Girault. Evidence of tetraphenylporphyrin monoacids by ion-transfer voltammetry at polarized liquid-liquid interfaces. *Chem. Commun.*, 2008, 5037 – 5038.
- R Partovi-Nia, B Su, F Li, C Gros, J-M Barbe, Z Samec and H H. Girault. Proton pump for O₂ reduction catalyzed by 5,10,15,20-tetraphenylporphyrinatocobalt(II) CoTPP. *Chemistry - A European Journal* 15 (10), 2335-2340.
- F Li, B Su, F C Salazar, R Partovi-Nia and H H Girault. Detection of hydrogen peroxide produced at a liquid-liquid interface using scanning electrochemical microscopy. *Electrochemistry Communications* 11 (2), 473-476.
- I Hatay , B Su, F Li, R Partovi-Nia , H Vrubel, X Hu, M Ersoz, H H Girault. Hydrogen evolution at liquid-liquid interfaces. *Angewandte Chemie - International Edition* 48 (28), 5139-5142.
- B Su, I Hatay, F Li, R Partovi-Nia, Z Samec, M Ersoz and H H. Girault. Oxygen and proton reduction by decamethylferrocene at liquid-liquid interfaces accepted in *Journal of Electroanalytical Chemistry*.
- R Partovi-Nia, B Su, C Gros, J-M Barbe, Z Samec and H H. Girault. Cobalt(II) octaethylporphyrin catalysis for dioxygen reduction at liquid-liquid interfaces *in preparation*.
- R Partovi-Nia, C Gros, J-M Barbe, Z Samec and H H. Girault. O₂ reduction catalyzed by free base octaethylporphyrin at biphasic system *in preparation*.

Presentation and Posters

- R Partovi-Nia, B Su, H H Girault. Molecular catalysis for oxygen reduction at liquid-liquid interface. SCS Swiss chemical society fall meeting, Zurich, Switzerland, September 2008.
- R Partovi-Nia, B Su, F Li, H H Girault. Proton Pump for Oxygen Reduction Catalyzed by 5, 10, 15, 20 tetraphenylporphyrinatocobalt (II). The 60th Annual Meeting of the International Society of Electrochemistry, Beijing, China, August 2009.